



IPICYT

**INSTITUTO POTOSINO DE INVESTIGACIÓN
CIENTÍFICA Y TECNOLÓGICA, A.C.**

POSGRADO EN CIENCIAS APLICADAS

**Synthesis, characterization and photocatalytic performance
of zinc oxide structured nanocomposites for the treatment of
endocrine disrupting compounds in water**

Tesis que presenta

Alma Berenice Jasso Salcedo

Para obtener el grado de

Doctora en Ciencias Aplicadas

En la opción de

Ciencias Ambientales

Director de la Tesis:

Dr. Vladimir Alonso Escobar Barrios

San Luis Potosí, S.L.P., México, Agosto de 2014



Constancia de aprobación de la tesis

La tesis "*Synthesis, characterization and photocatalytic performance of zinc oxide structured nanocomposites for the treatment of endocrine disrupting compounds in water*" presentada para obtener el Grado de Doctora en Ciencias Aplicadas en la opción de Ciencias Ambientales fue elaborada por **Alma Berenice Jasso Salcedo** y aprobada el **veintinueve de agosto de dos mil catorce** por los suscritos, designados por el Colegio de Profesores de la División de Ciencias Ambientales del Instituto Potosino de Investigación Científica y Tecnológica, A.C.

Dr. Vladimir Alonso Escobar Barrios
Director de la tesis

Dr. José René Rangel Méndez
Miembro del Comité Tutorial

Dr. Luis Felipe Cházaro Ruiz
Miembro del Comité Tutorial

Dra. Alma Gabriela Palestina Escobedo
Miembro del Comité Tutorial

Dra. Sandrine Hoppe
Miembro del Comité Tutorial

Dr. Fernando Pla
Miembro del Comité Tutorial



Créditos Institucionales

Esta tesis fue elaborada en la División de Ciencias Ambientales del Instituto Potosino de Investigación Científica y Tecnológica, A.C., bajo la dirección del Dr. Vladimir Alonso Escobar Barrios.

Durante la realización del trabajo el autor recibió la beca académica del Consejo Nacional de Ciencia y Tecnología (No. 211830) y del Instituto Potosino de Investigación Científica y Tecnológica, A. C.

La autora recibió el apoyo para asistencia a congresos de la División de Ciencias Ambientales para la divulgación de resultados del trabajo de tesis.

La autora recibió beca ECOS-NORD México-Francia M11P02, 2013 para la realización de experimentos en el Laboratoire de Chimie Physique de la Universidad Paris Sud en Francia.

La autora recibió la beca del Programa de Cooperación de Posgrado México-Francia del Consejo Nacional de Ciencia y Tecnología (PCP004-12, 2012-2014) para la realización de estancias doctorales en Laboratoire Réactions et Genie des Procédés de la Universidad de Lorraine en Francia.



Instituto Potosino de Investigación Científica y Tecnológica, A.C.

Acta de Examen de Grado

El Secretario Académico del Instituto Potosino de Investigación Científica y Tecnológica, A.C., certifica que en el Acta 027 del Libro Primero de Actas de Exámenes de Grado del Programa de Doctorado en Ciencias Aplicadas en la opción de Ciencias Ambientales está asentado lo siguiente:

En la ciudad de San Luis Potosí a los 29 días del mes de agosto del año 2014, se reunió a las 10:00 horas en las instalaciones del Instituto Potosino de Investigación Científica y Tecnológica, A.C., el Jurado integrado por:

Dr. José René Rangel Méndez	Presidente	IPICYT
Dra. Alma Gabriela Palestino Escobedo	Secretario	UASLP
Dr. Fernand Pla	Sinodal externo	Univ-Lorraine
Dr. José Elías Pérez López	Sinodal externo	UASLP
Dr. Juan Martínez Vega	Sinodal externo	Univ-Toulouse
Dra. Sandrine Hoppe	Sinodal externo	Univ-Lorraine
Dr. Vladimir Alonso Escobar Barrios	Sinodal	IPICYT

a fin de efectuar el examen, que para obtener el Grado de:

DOCTORA EN CIENCIAS APLICADAS
EN LA OPCION DE CIENCIAS AMBIENTALES

sustentó la C.

Alma Berenice Jasso Salcedo

sobre la Tesis intitulada:

Synthesis, characterization and photocatalytic performance of zinc oxide structured nanocomposites for the treatment of endocrine disrupting compounds in water

que se desarrolló bajo la dirección de

Dr. Vladimir Alonso Escobar Barrios

El Jurado, después de deliberar, determinó

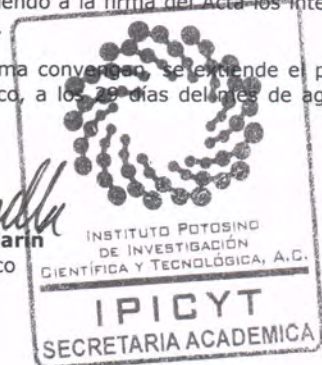
APROBARLA

Dándose por terminado el acto a las 13:00 horas, procediendo a la firma del Acta los integrantes del Jurado. Dando fe el Secretario Académico del Instituto.

A petición de la interesada y para los fines que a la misma convenga, se extiende el presente documento en la ciudad de San Luis Potosí, S.L.P., México, a los 29 días del mes de agosto de 2014.

Mtra. Ivonne Lizette Cuevas Vélez
Jefa del Departamento del Posgrado

Dr. Marcial Bomilla Marín
Secretario Académico



Dedicatorias

A Raúl Loera Valencia por motivarnos a seguir en este camino.

A toda mi hermosa familia, muy especialmente mi mamá Josefina quien me ha apoyado desde el principio.

El tiempo es lo mas valioso que un hombre puede gastar

(Time is the most valuable thing a man can spend)

Acknowledgements

I specially want to thank Vladimir Escobar-Barríos, Fernand Pla, Sandrine Hoppe, Dimitrios Meimaroglou, Mauricio Camargo for their invaluable mentorship and committed work in this international collaboration.

Thanks also to Gabriela Palestino, René Rangel Mendez, Hynd Remita, Juan Martínez Vega and Elías Pérez López for their advices to improve this research work.

We acknowledge the access to the facilities of the national laboratories LINAN and LANBAMA at the IPICYT, especially to the technicians of Environmental Sciences department.

My most certain acknowledgements to the University of Lorraine for hosting me in this joint program.

Table of contents

Constancia de aprobación de la tesis.....	ii
Créditos Institucionales	iii
Acta de examen	iv
Dedicatorias	v
Acknowledgements	vi
Table of contents.....	vii
List of Tables	xi
List of Figures.....	xiii
Abbreviations.....	xviii
Resumen	xix
Abstract	xxi
Introduction.....	1
Main problems to be solved.....	6
Hypotheses	8
Objectives.....	9
Scope of research	10
1 Chapter 1. ZnO AND ITS NANOCOMPOSITES FOR HETEROGENEOUS PHOTOCATALYSIS: THE STATE OF THE ART.....	12
1.1 Surface chemistry of the photocatalyst.....	13
1.2 ZnO properties.....	17
1.2.1 Crystal structure.....	17
1.2.1 Electronic and optical properties	19
1.3 ZnO modification for photocatalytic performance improvement.....	21
1.3.1 Reducing size: Nanoparticles.....	21
1.3.2 ZnO surface modification by metals.....	23
1.3.3 ZnO–polymer composites	24
1.4 ZnO as photocatalyst applied	29
1.4.1 Factors affecting the photocatalytic process	29
1.4.2 Kinetics and reaction rate normalization	30
2 Chapter 2. EXPERIMENTAL TECHNIQUES.....	34
2.1 REAGENTS.....	34
2.1.1 Synthesis of Ag/ZnO	34
2.1.2 Synthesis of Ag/ZnO-poly(acrylic acid) nanocomposites	34
2.1.3 Photocatalytic performance.....	35
2.2 EXPERIMENTAL SETUP.....	37
2.2.1 Functionalization system.....	37
2.2.2 Polymerization reactor	38

2.2.3	Photocatalysis system.....	39
2.3	CHARACTERIZATION TECHNIQUES.....	42
2.4	EXPERIMENTAL DESIGN, MODELLING & OPTIMIZATION	45
3	Chapter 3. SYNTHESIS OF Ag/ZnO PHOTOCATALYST: STARTEGY USING PREFORMED AgNPs	47
3.1	BACKGROUND.....	48
3.2	EXPERIMENTAL METHODOLOGY.....	49
3.2.1	Preparation of Ag/ZnO photocatalyst.....	49
3.2.1.1	Photodeposition method.....	50
3.2.1.2	Impregnation method.....	50
3.2.1.3	Nomenclature	50
3.2.2	Sample preparation for characterization	50
3.2.2.1	Inductively Coupled plasma optical emission spectroscopy	50
3.2.2.2	X-Ray diffraction.....	50
3.2.2.3	Scanning and transmission electron microscopy.....	51
3.2.2.4	Nitrogen adsorption-desorption	51
3.2.2.5	Fourier transform infrared spectroscopy.....	51
3.2.2.6	UV-Vis spectroscopy	51
3.3	RESULTS AND DISCUSSION	52
3.3.1	Mechanism of functionalization by preformed nanoparticles.....	52
3.3.2	Effect of synthesis conditions on structural and textural properties.....	56
3.3.3	Effect of synthesis conditions on optical properties.....	66
3.4	CONCLUSION.....	68
4	Chapter 4. SYNTHESIS OF Ag/ZnO-POLY(ACRYLIC ACID) NANOCOMPOSITES	69
4.1	BACKGROUND.....	69
4.2	EXPERIMENTAL METODOLOGY	72
4.2.1	Photocatalyst surface modification.....	72
4.2.2	Synthesis of poly(acrylic acid) hydrogels	72
4.2.3	Synthesis of photocatalyst/poly(acrylic acid) composite.....	73
4.2.4	Sample preparation for characterization	74
4.2.4.1	Inductively Coupled plasma optical emission spectroscopy	74
4.2.4.2	Scanning electron microscopy.....	74
4.2.4.3	Fourier transform infrared spectroscopy.....	75
4.2.4.4	X-Ray diffraction.....	75
4.2.4.5	Thermogravimetric analysis.....	75
4.2.4.6	Contact angle	75
4.3	RESULTS AND DISCUSSION	76
4.3.1	Mechanism of functionalization and composites synthesis	76

4.3.2	Chemical interaction between Ag/ZnO photocatalyst and the matrix in the nanocomposite.....	78
4.3.3	Structural and textural properties of the Ag/ZnO-poly(acrylic acid) nanocomposite.....	80
4.3.4	Wettability of the Ag/ZnO-poly(acrylic acid) composite	85
4.3.5	Effect of Ag/ZnO photocatalyst on thermal properties of the composite	86
4.3.6	Ag/ZnO-poly(acrylic acid) nanocomposite structure photostability	90
4.4	CONCLUSION.....	92
5	Chapter 5. PHOTOCATALYTIC ACTIVITY ON DEGRADATION OF ENDOCRINE DISRUPTOR, EMERGENT COMPOUNDS AND DYES	93
5.1	BACKGROUND.....	94
5.1.1	Bisphenol-A.....	94
5.1.2	Triclosan	95
5.1.3	Rhodamine B	96
5.2	EXPERIMENTAL METHODOLOGY.....	97
5.2.1	Part 1. Ag/ZnO photocatalyst	97
5.2.2	Part 2. Ag/ZnO-poly(acrylic acid) nanocomposites	98
5.3	RESULTS AND DISCUSSION	100
5.3.1	Part 1. Photocatalytic activity of Ag/ZnO	100
5.3.1.1	Bisphenol-A degradation	100
5.3.1.1.1	Effect of functionalization method.....	100
5.3.1.1.2	Effect of the wavelength	103
5.3.1.1.3	Effect of pH.....	105
5.3.1.1.4	Effect of the dose of photocatalyst.....	111
5.3.1.2	Triclosan degradation	112
5.3.1.3	Rhodamine-B degradation.....	113
5.3.2	Part 2. Ag/ZnO-poly(acrylic acid) composites for bisphenol-A degradation	117
5.4	CONCLUSION.....	121
6	Chapter 6. MODELING AND OPTIMIZATION OF THE PHOTOCATALYTIC PROCESS	122
6.1	BACKGROUND.....	122
6.1.1	Main problems to be solved	122
6.1.2	Modeling tools ANN and RSM	124
6.1.3	Photocatalytic process modeling: state of art.....	126
6.2	METHODOLOGY	129
6.2.1	Define input/output parameters.....	130
6.2.1.1	Functionalization of ZnO – Model A.....	130

6.2.1.2	Photocatalytic activity: apparent rate constant – Model B	130
6.2.2	Experimental design.....	132
6.2.2.1	Full factorial	132
6.2.2.2	Central composite design	132
6.2.3	Mathematical tools for model and optimization	136
6.2.3.1	Response surface methodology	136
6.2.3.2	Artificial neural networks.....	136
6.2.3.3	Evolutionary algorithm for optimization.....	137
6.3	RESULTS AND DISCUSSION	140
6.3.1	Preliminary experiments.....	140
6.3.2	Modeling step.....	142
6.3.2.1	Functionalization of ZnO-Model A	142
6.3.2.1.1	RSM modeling of ZnO functionalization-Model A	142
6.3.2.1.2	ANN modeling of ZnO functionalization – Model A.....	145
6.3.2.1.3	Comparison of RSM and ANN models	147
6.3.2.2	Photocatalytic activity: apparent rate constant-Model B	148
6.3.3	Optimization step	150
6.4	CONCLUSION.....	153
7	Chapter 7. GENERAL CONCLUSION	155
7.1	Recall to the objectives.....	155
7.2	General conclusions	156
7.3	Final remarks.....	160
7.4	Challenges and recomendations	161
7.5	SCIENTIFIC PRODUCTS	165
7.5.1	List of publications	165
7.5.2	Extended abstracts	166
7.5.3	Attendance at conferences	166
8	REFERENCES	168
9	SUPPORTING INFORMATION.....	177
9.1	Appendix A	177
9.2	Appendix B	179
9.3	Appendix C.....	180
9.4	Appendix D.....	183

List of Tables

Table 1.1. Materials used as matrices on nanoparticle/polymer nanocomposites.	27
Table 2.1. Specifications of the reagents used for the synthesis of Ag/ZnO.	35
Table 2.2. Specifications of the reagents used for the polymerization processes.	35
Table 2.3. Specifications of the reagents used for the photocatalytic activity evaluation.	36
Table 2.4. Complementary materials for polymerization process.	39
Table 2.5. Specifications of the UV lamps in the photoreactors.	39
Table 2.6. Specifications of the analytical techniques.	43
Table 3.1. Physicochemical properties of Ag/ZnO photocatalyst.	59
Table 4.1. Photocatalytic degradation of dyes by photocatalyst-polymer composites.	71
Table 4.2. Composition of the solution used in polymerization.	73
Table 4.3. Operating conditions used for the synthesis of Ag/ZnO-poly(acrylic acid) composites.	74
Table 4.4. Thermogravimetric analysis of Ag/ZnO-PAA composites in air atmosphere.	88
Table 5.1. Experimental conditions used to evaluate Ag/ZnO photocatalytic activity.	98
Table 6.1. Experimental range of the independent variables on the 2 ³ factorial design.	132
Table 6.2. Experimental range of the independent variables on the CCD design.	132
Table 6.3. Experimental data of the functionalization of ZnO with AgNPs by the photodeposition method of CCD design.	133
Table 6.4. Experimental data of the functionalization of ZnO with AgNPs by the impregnation method of CCD design.	134

Table 6.5. Experimental data of the photocatalytic degradation of bisphenol-A.....	135
Table 6.6. Estimated regression coefficients and p -values of the factorial fit.....	141
Table 6.7. ANOVA test of the quadratic model for the response Y_2	144
Table 6.8. Estimated regression coefficients and p -values of the quadratic model for the response Y_2	144
Table 6.9. Comparison of the predictive capacity of the models for the functionalization of ZnO.....	148
Table 6.10. Structure and R^2 optimum values of ANN model of k_{app}	149
Table 6.11. Optimal conditions for bisphenol-A degradation.....	151
Table 6.12. Optimal conditions for the target amount AgNPs.	151
Table 6.13. Optimal conditions for bisphenol-A degradation at fixed wavelength.	152
Table 6.14. Optimal conditions for the target amount AgNPs.	152

List of Figures

- Figure 1** Number of papers published on photocatalysis per year in the period 1991-2014 using Web of Science database by keywords “photocatalysis AND degradation” (yellow bar), “photocatalysis AND ZnO” (pink bar) and “photocatalysis AND degradation AND ZnO” (blue bar). 5
- Figure 1.1.** Representation of the global photocatalytic mechanism of an endocrine disrupting compound on ZnO surface involving seven basic steps. Scale time of nanoseconds. 14
- Figure 1.2.** Schematic representation of the photocatalytic mechanism of ZnO where a) the photon energy greater than the bandgap energy is adsorbed by ZnO and generates electron-hole pairs, b) the photoexcited charge carriers spate and migrate to the surface, and c) adsorbed species are reduced and oxidized by the photogenerated electrons and holes, respectively. (A/A⁻: acceptor species, D/D⁺ donor species). 14
- Figure 1.3.** Life time of the reactive species in the photocatalytic process (Figure original from Fujishima *et al.*,2008). 17
- Figure 1.4.** ZnO unit cell showing (001), (100) and (101) planes (a, b, c) and the ball-stick model of ZnO crystals (d, e) (Modified from Chu *et al.*, 2009). 18
- Figure 1.5.** SEM photograph of the commercial ZnO nanoparticles (VP AdNano ZnO 20DW, Degussa Co.) used in this thesis. The different morphologies include rods, tetrapods with both pyramidal and round tips. 20
- Figure 2.1.** Photograph of the photoreactor Q200 for the functionalization of ZnO by the photodeposition method. 37
- Figure 2.2.** Scheme of the polymerization reactor setup. 38
- Figure 2.3.** Photograph of the photoreactor 3UV. 40
- Figure 2.4.** Photograph of the photoreactor Oriel. 40
- Figure 2.5.** Photograph of the photoreactor Vilber. 41
- Figure 2.6.** Scheme of the characterization techniques described in Table 2.6. 42
- Figure 2.7.** Scheme of the experimental design, model and optimization tools used to study the synthesis of Ag/ZnO photocatalyst and their photocatalytic behavior. Abbreviations CCD: central composite design, RSM: response surface methodology, ANN: artificial neural network, EA: evolutionary

algorithm, ANOVA: analysis of variance, MSE: mean squared error, R^2 : correlation value. The x_i and w_j , where $i=3$ and $j=4$ are input factors, Y_1 , Y_2 and Z_1 are the response.	46
Figure 3.1. Representation of AgNPs stabilized in alkanethiol surfactant.	53
Figure 3.2. Mechanism for functionalization of ZnO with silver nanoparticles by photodeposition method (A) and impregnation method (B).	55
Figure 3.3. XRD pattern of 1%w/w Ag/ZnO obtained by photodeposition (PD) and impregnation (IMP) methods (A). ZnO unit cell showing (100) and (101) planes that lead the grow of nanorod with pyramidal tip (B). Zoom of Ag/ZnO XRD spectra showing the peaks shift (C) due to the insertion of Ag in ZnO crystallite (D).	57
Figure 3.4. TEM images of stabilized AgNPs (A, B) and 1%w/w Ag/ZnO photocatalyst prepared by the photodeposition method (C, E: high-magnification) and impregnation method (D). Frequency histograms of AgNPs size before (B, $n=106$) and after (F, $n=40$) functionalization of ZnO.	61
Figure 3.5. N_2 adsorption-desorption isotherm of 1% w/w Ag/ZnO photocatalyst prepared by the photodeposition (PD) and impregnation (IMP) method.	63
Figure 3.6. FTIR spectra (A) and TEM image (B) of stabilized AgNPs. EDX elemental analysis (C) corresponds to the squared area in B.	64
Figure 3.7. FTIR spectra of pure ZnO, AgNPs and 1%w/w Ag/ZnO.	65
Figure 3.8. UV-Vis spectra of pure ZnO and 1%w/w Ag/ZnO.	67
Figure 4.1. Representation of the mechanism of Ag/ZnO silanization with GLYMO (A) and the Ag/ZnO-poly(acrylic acid) composite synthesis (B).	77
Figure 4.2. FTIR spectra of pure and surface silanized Ag/ZnO photocatalyst.	79
Figure 4.3. FTIR spectra of pure poly(acrylic acid) hydrogels and Ag/ZnO-poly(acrylic acid) nanocomposites. PAA: poly(acrylic acid).	79
Figure 4.4. SEM images of the synthesized swollen crosslinked poly(acrylic acid).	81
Figure 4.5. SEM images of swollen Ag/ZnO-poly(acrylic acid) nanocomposites. Low magnification (A, B) and high magnification (C, D).	82

Figure 4.6. Elemental distribution maps of SEM-EDX for the 8% Ag/ZnO-poly(acrylic acid) nanocomposites.	83
Figure 4.7. XRD pattern of poly(acrylic acid), Ag/ZnO and 8% Ag/ZnO-poly(acrylic acid) composites.	84
Figure 4.8. Images of water droplet on (A) 8% Ag/ZnO-poly(acrylic acid) nanocomposite (contact angle= $117.8 \pm 2.51^\circ$) and (B) pure ZnO photocatalyst (contact angle= $135 \pm 3.65^\circ$) placed on a glass slide.	85
Figure 4.9. TGA curve of silanized Ag/ZnO, pure PAA and Ag/ZnO-PAA nanocomposites.	89
Figure 4.10. FTIR (A) and TGA spectra (B) of Ag/ZnO-poly(acrylic acid) composite under 8 h of UV irradiation exposure.	91
Figure 5.1. Linear plot $Y=mx + b$ to obtain the kinetics parameters (k_{app} and n).	100
Figure 5.2. (A) Photocatalytic activity of 1%w/w Ag/ZnO and (B) surface area normalized rate constant of bisphenol-A degradation (test conditions: BPA=10 mg/L, photocatalyst= 1 g/L, pH=10.5, reaction time of 120 min for $\lambda=302$ nm).	101
Figure 5.3. Schematic representation of the photocatalytic mechanism of Ag/ZnO where a) the photon energy greater than the bandgap energy is adsorbed by ZnO and generates electron-hole pairs, b) the photoexcited charge carriers spate and migrate to the surface, c) the photoexcited electrons are sink into the silver metal bond and d) adsorbed species are reduced and oxidized by the photogenerated electrons and holes, respectively. (A/A ⁻ : acceptor species, D/D ⁺ donor species).	103
Figure 5.4. Normalized concentration of bisphenol-A at different wavelength using ZnO and Ag/ZnO photocatalyst (test conditions: BPA=10 mg/L, photocatalyst= 1 g/L, pH=10.5, reaction time of 120 min for $\lambda=254, 302, 365$ nm, and 180 min for $\lambda>450$ nm).	105
Figure 5.5. Normalized concentration of bisphenol-A at different pH using ZnO (test conditions: BPA=10 mg/L, photocatalyst= 1 g/L, $\lambda=302$ nm, reaction time=120 min).	107
Figure 5.6. Species distribution curve of a solution containing ZnO.	107
Figure 5.7. Normalized concentration of bisphenol-A at different conditions of pH control using pure ZnO and Ag/ZnO-IMP11 photocatalysts (test conditions: BPA=10 mg/L, photocatalyst= 1 g/L, $\lambda=302$ nm, pH=10.5).	109

Figure 5.8. Time evolution of byproducts profile in time detected by HPLC during bisphenol-A degradation under uncontrolled pH (A) and controlled pH (B). RT: retention time (min) recorded in the chromatogram (see Appendix C). Test conditions: BPA=10 mg/L, photocatalyst= 1 g/L, λ =302 nm, pH=10.5.	110
Figure 5.9. Normalized concentration of bisphenol-A at different doses of Ag/ZnO-IMP11 photocatalyst (test conditions: BPA=10 mg/L, λ =302 nm, pH=10.5, reaction time=120 min).	111
Figure 5.10. Normalized concentration of triclosan in function of time using pure ZnO and Ag/ZnO photocatalysts (test conditions: triclosan=20 mg/L, λ =302 nm, pH=8.6, photocatalyst= 0.5 g/L).	113
Figure 5.11. Normalized concentration of rhodamine-B in function of time using pure ZnO and Ag/ZnO photocatalysts (test conditions: rhodamine-B=47 mg/L, λ =254 nm, photocatalyst= 1 g/L).	115
Figure 5.12. Normalized concentration of rhodamine-B in function of time using pure ZnO and Ag/ZnO photocatalysts (test conditions: rhodamine-B =47 mg/L, λ >455 nm, photocatalyst= 1 g/L).	115
Figure 5.13. Photocatalytic performance in the degradation of bisphenol-A using pure Ag/ZnO-GLYMO photocatalyst and Ag/ZnO-poly(acrylic acid) composites (A) and overall photodegradation performance after two cycles of 8 h (B) (test conditions: bisphenol-A =10 mg/L, λ =365 nm, pH=10.5).	118
Figure 6.1. Number of papers published on photocatalysis per year in the period 1991-2014 using Web of Science database. Research results by keywords “photocatalysis AND response surface methodology” (yellow bar), “photocatalysis AND artificial neural network” (pink bar) and “photocatalysis AND response surface methodology AND artificial neural network” (blue bar).	129
Figure 6.2. Linear plot $Y=mx + b$ to obtain the kinetics parameters (k_{app} and n).	131
Figure 6.3. Scheme of the experimental design, model and optimization setting used to study the synthesis of Ag/ZnO photocatalyst and their photocatalytic behavior. The abbreviations FE: functionalization efficiency, CCD: central composite design, RSM: response surface methodology, ANN: artificial neural network, MSE: mean square error, EA: evolutionary algorithm.	139
Figure 6.4. Pareto chart of the standardized effects on the functionalization of ZnO by the (A) photodeposition and (B) impregnation method.	141

Figure 6.5. 3D surface plot of the effect of actual amount AgNPs and pH on the response of the RSM model of the functionalization of ZnO by the (A) photodeposition and (B) impregnation method. 145

Figure 6.6. Plot of the experimental data against predicted data by ANN model for Y_2 actual amount AgNPs response prepared by the (A) photodeposition and (B) impregnation methods. 146

Figure 6.7 Plot of the experimental data against predicted data by ANN model for apparent rate constant (k_{app}) of the bisphenol-A degradation using Ag/ZnO photocatalysts obtained by the (A) photodeposition and (B) impregnation methods. 149

Abbreviations

ANN	Artificial neural network
ANOVA	Analysis of variance
CB	Conduction band
CCD	Central composite design
EA	Evolutionary algorithm
E_g	Band gap energy
k_{app}	Apparent rate constant
MAE	Mean absolute error
MLP	Multi-layered perception
MSE	Mean squared error
NHE	Normal hydrogen electrode
PAA	Poly(acrylic acid)
pH PZC	pH of point zero charge
R^2	Correlation coefficient value
RSM	Response surface methodology
VB	Valence band

Resumen

SÍNTESIS, CARACTERIZACIÓN Y ACTIVIDAD FOTOCATALÍTICA DE NANOCOMPOSITOS CON BASE EN ÓXIDO DE ZINC PARA LA DEGRADACIÓN DE COMPUESTOS DISRUPTORES ENDÓCRINOS EN AGUA

El ZnO es un material no tóxico de bajo costo con un interesante potencial fotocatalítico en la degradación de contaminantes en medio acuoso. Sin embargo, su aplicación se encuentra limitada por su baja eficiencia, fotocorrosión y el costo energético de su recuperación.

Este trabajo tiene como objetivo incrementar la actividad fotocatalítica en la degradación de compuestos disruptores endócrinos a través de la funcionalización de ZnO con nanopartículas de plata. Además el desarrollo de un método para la inmovilización del fotocatalizador modificado, Ag/ZnO, en una matriz polimérica proyectando su uso en sistemas de tratamiento continuo de agua.

Los resultados demuestran que el método de fotodeposición promueve la distribución homogénea de nanopartículas de plata. El incremento en los parámetros de red indican la inserción de iones Ag^+ en la estructura cristalina del ZnO dando lugar a una fuerte interacción química entre las nanopartículas de plata y ZnO. Adicionalmente, la presencia de grupos hidroxilo, OH^- , y el incremento en la absorción de luz visible promovió la degradación fotocatalítica bisfenol A, triclosan y rodamina B de manera más eficiente.

Los resultados de degradación del bisfenol A a 302 nm por el fotocatalizador Ag/ZnO muestran una constante de velocidad aparente (k_{app}) 3.7 veces mayor al valor obtenido por ZnO: $k_{\text{app}} = 0.01929 \text{ min}^{-1} \text{ m}^{-2}$. Además, la degradación de bisfenol A (25%, 3h), triclosan (35%, 2h) y rodamina B (95%, 2h) en condiciones de luz visible se traduce en el potencial del catalizador de ser activado con luz solar.

Por otra parte, las nanopartículas de fotocatalizador Ag/ZnO fueron inmovilizadas en una matriz de poli(ácido acrílico) entrecruzado. La superficie de las partículas fue previamente modificada por un agente acoplante (GLYMO®) que permitió (i) la dispersión y anclaje por esterificación de las nanopartículas en la matriz poliacrílica en formación y (ii) promover la cristalización y estabilidad térmica del polímero.

Los nanocompositos Ag/ZnO-poli(ácido acrílico) mostraron una eficiencia fotocatalítica en la degradación de bisfenol A comparable a la obtenida por el fotocatalizador Ag/ZnO puro, además de que dicha actividad se mantuvo en dos ciclos consecutivos (47% y 64%, para 1er y 2do ciclo, respectivamente). De manera tal que el nanocomposito generado en ésta tesis doctoral tiene el potencial de ser utilizado en el tratamiento continuo de agua contaminada con compuestos disruptores endócrinos.

En el contexto de la catálisis heterogénea, el establecimiento de relaciones entre la actividad y propiedades de los catalizadores es particularmente difícil a causa de los numerosos parámetros operacionales que están involucrados. Considerando esta premisa, la metodología de superficie de respuesta (MSR) y las redes neurales artificiales (RNA) se utilizaron en la construcción de modelos que reflejan la influencia de los parámetros del proceso en la síntesis de Ag/ZnO y la constante de velocidad aparente de la degradación de bisfenol A. Los modelos RNA acoplados al algoritmo evolucionario mostraron mayor capacidad predictiva y permitieron identificar las condiciones óptimas de síntesis del catalizador y actividad fotocatalítica. La optimización mostró que un bajo contenido de plata (~0.35-0.5 % w/w) y un pH alcalino durante la funcionalización de ZnO y la degradación de bisfenol A maximizan el valor de k_{app} .

La aplicación de las herramientas matemáticas al estudio de las relaciones estructura-desempeño en el contexto de fotocatalisis representa una importante contribución de esta tesis al estudio de un problema no trivial.

PALABRAS CLAVE : Ag/ZnO, composito polimérico, fotocatalisis, bisfenol A, red neuronal artificial, metodología de superficie de respuesta.

Abstract

SYNTHESIS, CHARACTERIZATION AND PHOTOCATALYTIC PERFORMANCE OF ZINC OXIDE STRUCTURED NANOCOMPOSITES FOR THE TREATMENT OF ENDOCRINE DISRUPTING COMPOUNDS IN WATER

ZnO is a non-toxic catalyst of low cost with interesting photocatalytic potential, particularly for the degradation of water contaminants. However, its application has not been much developed because of its poor efficiency, its photocorrosion and energetic cost of recovery.

Therefore, the main objectives of this research was to improve the efficiency of ZnO for the degradation of endocrine disrupting compounds and propose a method for the immobilization of the photocatalyst projecting a continuous water treatment process.

The first step consisted in the design of a new photocatalytic system by functionalizing ZnO nanoagglomerates with silver nanoparticles (Ag/ZnO). The results showed that photodeposition method promotes a homogeneous distribution of AgNPs on ZnO surface. Moreover, the increment in lattice parameters suggests the insertion of Ag⁺ ions into the crystalline structure of ZnO and strong interactions between AgNPs and ZnO. In addition, hydroxyl surface content and the improved absorption under visible light allowed the enhancement in the photodegradation efficiency of bisphenol-A, triclosan and rhodamine-B.

The obtained Ag/ZnO photocatalyst showed higher apparent rate constant (k_{app}) for the degradation of bisphenol-A at 302 nm: $k_{app}=0.01929 \text{ min}^{-1} \text{ m}^{-2}$, which is 3.7 times the value for pure ZnO. Degradation of bisphenol-A (25%, 3h), triclosan (35%, 2h) and rhodamine-B (95%, 2h) was successfully carried out under visible light which is an important achievement in case of solar light use.

On the other hand, to overcome aggregation problems, Ag/ZnO photocatalyst was immobilized owing to their incorporation in a cross-linked poly(acrylic acid) matrix. The surface of Ag/ZnO was previously modified, using a silane coupling agent: GLYMO® which allowed (i) dispersing and anchoring NPs on the polyacrylic matrix by formation of ester bonds, and (ii) promoting crystallization and thermal stability of the polymer.

The Ag/ZnO-poly(acrylic acid) nanocomposites were successfully tested on the degradation of bisphenol-A with an efficiency comparable to that of Ag-functionalized ZnO. Moreover, two successive cycles led to an overall degradation of 47% and 64%, for the 1st and 2nd cycles, respectively. The immobilization provides the potential use of the photocatalyst in continuous mode.

This thesis work demonstrated for the first time the potential of the nanocomposites based on ZnO for the degradation of endocrine disruptors in water.

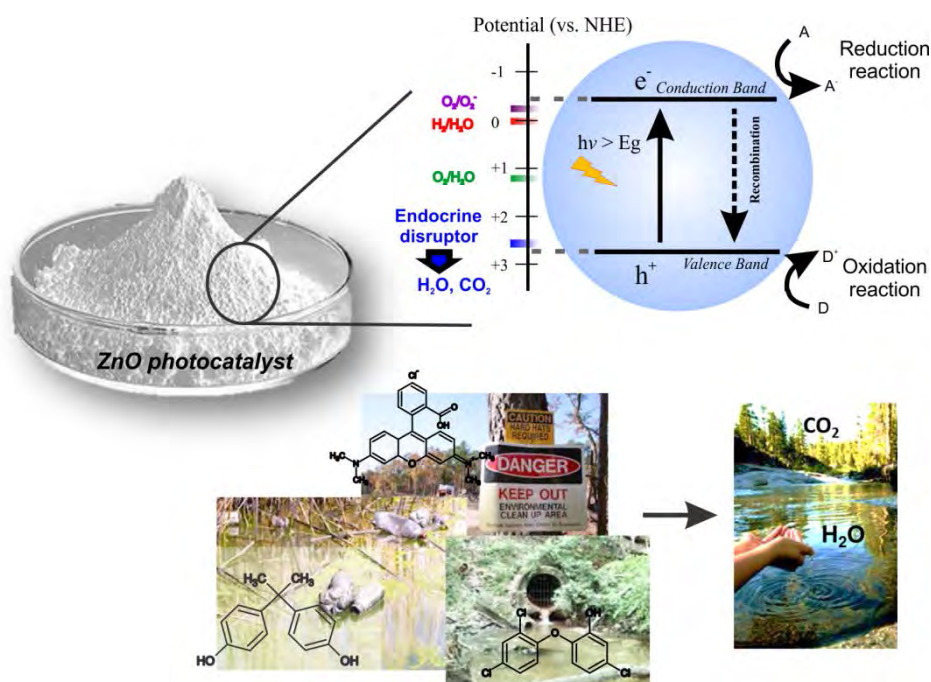
Nowadays, the challenge of understanding relationships between catalyst properties and performance in the context of heterogeneous catalysis is a hot topic. Indeed, catalysis processes are generally affected by many different operational parameters. This research explored the modeling of the operating parameters influencing the Ag-functionalization of ZnO and its photocatalytic performance using response surface methodology (RSM) and artificial neural network (ANN). The ANN models showed a better predictive capacity than RSM. Then the optimization showed that a low silver content (~ 0.35 - 0.5 %w/w) and an alkaline pH, during both functionalization of ZnO and photodegradation of bisphenol-A, maximized the k_{app} .

The mathematical tools used in this thesis represent an important contribution to systematically study structure-performance relationships, a non-trivial problem in photocatalysis.

KEY WORDS: Ag/ZnO, polymeric nanocomposite, photocatalysis, bisphenol-A, triclosan, artificial neural network, response surface methodology.

Introduction

This section shows the publishing statistics concerning the use of ZnO for degradation of organic compounds, which indicates its potential as the next generation photocatalyst in academia and in the industry. In the literature revision we detected key points of the process that motivate this research.



1. Photocatalysis generalities

Photocatalysis is a term describing a catalyst that uses photons as energy source to enhance the reaction rate of a chemical process until equilibrium is achieved. In this process the photons are generated and consumed.

This term first appeared in a publication of Fujishima *et al.* (1972) who described the photo-assisted electrolysis of water under irradiation of TiO₂ with photons of greater energy than the band gap of TiO₂. The concept of photocatalysis linked to environmental remediation was introduced by Carey *et al.* (1976) in a study on

photodechlorination. From that moment, the number of papers grew exponentially as shown by Rajeshwar (2011).

Photocatalysis is an area of intense research activity globally and the papers on the subject are represented in journals focused on catalysis, but also mainly in the literature for environmental remediation of air, water and soil (Web of Science v5.14). Chemists, physicists, material scientists, environmental scientists and engineer's contributions are fundamental to get better understanding of the field.

The evolution of knowledge of materials with photocatalytic potential can be described in terms of three generations as suggested by Rajeshwar (2011):

- The first generation (1975-1985), which is focused on studies on single crystals to understand the semiconductor-solution interface under UV irradiation.
- The second generation (1986-2000), which developed efforts on studies on polycrystalline thin films under visible light, dye sensitization and powder suspensions for photocatalytic degradation of dyes in waste streams.
- The third-generation (2000-today) which explored the use of nanostructured (nanotubes, nanowires, nanofibers) and quantum-sized semiconductors is explored. The development of semiconductor-conducting polymer composites and biomimetic architectures is giving a new basis to the engineered materials for photocatalysis.

TiO₂ has emerged as a model photocatalyst, and continues to dominate the literature because it is non-toxic (it is often included in pharmaceuticals), photo-stable, and low-cost. Few other semiconductors, as ZnO, can compete in terms of these three aspects. Among other advantages, ZnO have a high photonic efficiency, chemical stability, low toxicity and visible light sorption (Di Paola *et al.*, 2012; Sakthivel *et al.*, 2003). These properties will be discussed further in Chapter 1.

2. ZnO as photocatalyst: the state of the art

It seems important to take a look of the publishing statistics of ZnO as a semiconductor with the potential to become an important material for photocatalysis in the academy and industry. The literature search results carried out in the most important database of science: Web of Science are shown in [Figure 1](#). A total of 9003 papers regarding photocatalytic process for pollutants degradation are being registered over the period of 1991-2014. The number of publications increases exponentially since the 90's when the second generation of catalysts was first used for photocatalytic degradation of dyes. The 15% of those publications concern to ZnO as photocatalyst for degradation of organic compounds, while the other percentage concerns to the widely used catalyst in degradation studies: TiO₂. The progress made using ZnO as photocatalyst and the challenges in the photocatalytic degradation of organic compounds have been reviewed by Di Paola *et al.*, (2011). There an important effort in the development of a new variety of photocatalysts having the potential on environmental remediation, e.g. binary oxides (WO₃, iron oxides, CeO₂), ternary oxides (vanadates, Bi₂WO₆, AgMO₂ with M: Al, Ga, In) and quaternary oxides (Di Paola *et al.*, 2011).

The majority of papers using the keywords "photocatalysis AND ZnO AND degradation" in the Web of Science database are published in chemistry, material science and engineering fields, and only 20% publish in the research area of environmental sciences and water resources. Thus the synthesis and physicochemical characterization of ZnO materials still dominates the research field, while the water/air treatment applications are just starting.

Researchers from China, India and Iran made the major contribution to the study of ZnO as photocatalyst, while other countries like Brazil, South Korea, Japan, Italy, Spain, Germany, Mexico and France contribute with 20 papers each one since 1991. Indeed the international scientific community is encouraging the photocatalytic process using ZnO through organizing discussion symposia within

the catalysis conferences (i.e. International Conference on Catalysis (ICC), International Conference on Environmental Catalysis (ICEC), International Materials Research Congress (IMRC), Iberoamerican Congress of catalysis (CICat), European Congress on Catalysis (EUROPACAT)), and workshops dedicated to ZnO properties and environmental applications (see <http://www.mrs.org/iwzno-2014/>).

The number of papers regarding the silver modification of ZnO photocatalyst is low, barely reach 76 papers registered on the Web of Science database. However the number has increased exponentially since 2003 because of the significant enhancement of photocatalytic activity under visible light, a key progress in the design of solar-driven photocatalysts.

Regarding the synthesis of zinc oxide based composites, a total of 2965 papers using the keywords “polymer AND ZnO” were published between 1991 and 2014, most of them in the research area of material science, physic, chemistry and polymer, and only few focuses on environmental sciences.

A total of 520 papers contains the keywords “polymer AND photocatalysis”, most of them using titania and other metal oxides as photocatalyst. Until now only 15 to 27 papers discuss the ZnO modification with polymer in environmental photocatalysis. Short chain polymers (e.g. polyethylene glycol and polysaccharides) were employed as surface modifiers mainly to avoid photocorrosion. Just recently long-chain polymers become trending as effective matrices for both ZnO photocatalyst immobilization and photocorrosion inhibition.

The scarce literature in this area encourages this thesis to work in this novel field for apply ZnO modified with silver nanoparticles and its immobilization on poly(acrylic acid) as photocatalysts for water treatment, specifically for degradation of endocrine disruptor compounds.

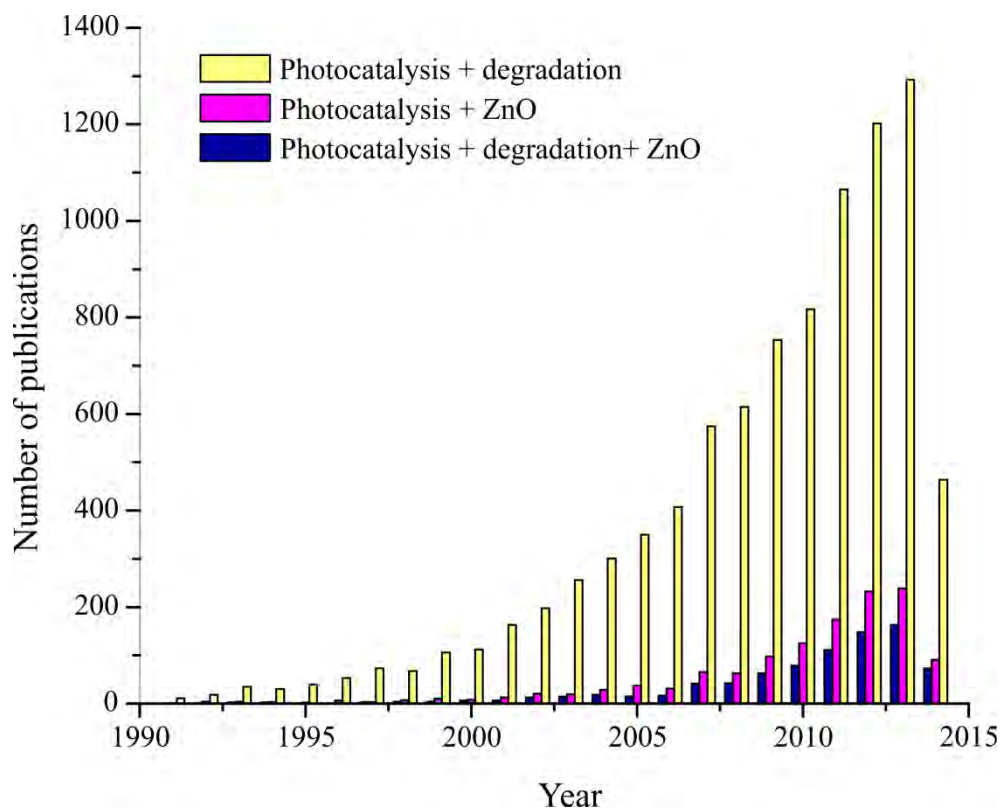


Figure 1 Number of papers published on photocatalysis per year in the period 1991-2014 using Web of Science database by keywords “photocatalysis AND degradation” (yellow bar), “photocatalysis AND ZnO” (pink bar) and “photocatalysis AND degradation AND ZnO” (blue bar).

Main problems to be solved

The first problem is related to the **low efficiency** of the photocatalysts under visible light conditions and to the efficient utilization of the photogenerated electron–hole pairs for photodegradation of pollutants. The photoactivation of ZnO requires UV light ($\lambda=385$ nm) which accounts for less than 3% of available sunlight energy. In addition, near-UV flux from indoor fluorescent light is three orders of magnitude less than sunlight, suggesting limited uses in ambient light applications. Thus high consumption of energy by UV sources increases the cost of the process.

Therefore, two aspects must be considered in order to improve the photocatalytic efficiency under visible light: the size reduction of the photocatalyst and the modification of its surface. The ZnO surface modification with metal particles changes the number of oxygen vacancies and surface defects improving the charges separation for more efficient photocatalytic processes.

This thesis will explore the use of silver nanoparticles as surface modifiers of ZnO nanoagglomerates with the aim of improve its photocatalytic activity under both UV and visible light over the degradation of endocrine disrupting compounds.

The synthesis of the ZnO photocatalyst and the photocatalytic activity are complex processes and thus difficult to model mechanistically. Therefore, the **correlation between structure and performance of a photocatalyst** is a non-trivial problem. In addition, the optimization of ZnO properties gains importance when the photocatalytic process is meant to be used at industrial scale and the cost (\$) is the decision rule to compete with TiO₂. Mathematical tools like the Response Surface Methodology (RSM) and Artificial Neural Networks (ANN) can perform multivariable analysis of the operational conditions. Those tools are useful in the modeling and optimization of the whole photocatalytic process (photocatalyst preparation and photocatalytic performance).

We propose *the modeling of the synthesis of ZnO modified with silver nanoparticles and its photocatalytic performance using ANN*. The connection between the two models made it possible to identify the optimal synthesis conditions that lead to a desired photocatalytic performance and assess structure-photocatalytic performance associations.

The second problem concerns **the agglomeration** of ZnO nanoparticles. It is well known that nanoparticles minimize their surface energy by forming agglomerates therefore losing the exceptional properties of nanoparticles such as high surface area and high number of active sites. In addition, the use powder catalyst results in other technical disadvantages like poor dispersion, energy costly stirring during the photocatalytic reaction and finally difficult separation of catalyst after the reaction, sometimes even producing a secondary pollution. In fact, the energy needed to separate the nano-sized catalytic particles is greater than that needed for micro-sized particles, therefore increasing the cost of the photocatalytic process.

Therefore, the catalyst immobilization in a matrix could make it possible to overcome those disadvantages and extend their use in continuous modes, at laboratory-scale or industrial scale.

In this thesis we explored the immobilization of the photocatalyst in a poly(acrylic acid) matrix. The photocatalytic degradation of endocrine disruptor compounds by the immobilized photocatalysts will be studied.

Hypotheses

- i. The functionalization of ZnO nanoagglomerates with silver nanoparticles, by impregnation and photodeposition methods will increase the photocatalytic degradation rate of organic water contaminants (bisphenol-A, triclosan, rhodamine-B), under UV and visible light, because of the retention of the reactive species (photoexcited electron) by the silver nanoparticles.
- ii. The surface modification of Ag/ZnO photocatalyst, using a silane coupling agent, will allow their dispersion and anchorage on a polyacrylic matrix through carboxylic groups.
- iii. The mathematical models of the experimental data of the Ag-functionalization of ZnO (model 1) and the photocatalytic degradation of bisphenol-A by Ag/ZnO (model 2) will be connected through the silver content variable in order to identify the optimal functionalization conditions that lead to a desired photocatalytic degradation of bisphenol-A.

Objectives

The aim of the thesis is to functionalize ZnO with silver nanoparticles to increase its potential as photocatalyst for treatment of water contaminated by endocrine disruptors, and test their immobilization in a poly(acrylic acid) matrix.

The specific objectives are listed here:

- I. The study of the influence of functionalization conditions (pH, silver amount, and reaction time) on structural, textural and optical properties of Ag/ZnO.
- II. The study of the influence of the photocatalysis parameters on the photocatalytic efficiency and reaction rates for the degradation of bisphenol-A, triclosan, rhodamine-B.
- III. Modeling and optimization of the Ag/ZnO synthesis and its photocatalytic activity on the degradation of bisphenol-A.
- IV. Immobilization of Ag/ZnO on the poly(acrylic acid) matrix and physicochemical characterization of the Ag/ZnO-poly(acrylic acid) nanocomposite.
- V. Evaluation of the feasibility of the nanocomposite for photodegradation of bisphenol-A.

Scope of research

The present thesis is comprised of six chapters.

Chapter 1 will provide the theoretical basis of the photocatalytic process, namely reactive species, lifetime and the surface chemistry of ZnO photocatalyst. The trends in ZnO modifications to improve the photocatalytic efficiency, specially using metals will be presented. The state of the art of ZnO based nanocomposites, and their synthesis approaches will then be revised to understand (i) the chemical interactions between the polymer and ZnO surface and (ii) how ZnO can be used to design new nanocomposites with high photocatalytic potential. Finally, the trends in normalization of the photocatalytic activity will be presented.

Chapter 2 will be divided in four parts. The first part lists the used reagents for the synthesis of Ag/ZnO and for their immobilization in a poly(acrylic acid) matrix, as well as their photocatalytic performance. Then, the used experimental setups and the analytical techniques used to study the properties of the samples synthesized will be described in the second and third part. Finally, the fourth part will resume the methodology to study the influence of both the synthesis operating conditions and the photocatalytic parameters on the catalytic efficiency using the two most popular methodologies to model and optimize the process: response surface methodology and artificial neural network coupled to evolutionary algorithm.

Chapter 3 will then provide the proposed mechanism for the functionalization of ZnO nanoagglomerates with silver nanoparticles using two methods: photodeposition and impregnation. The effect of the synthesis parameters: (i) on the structural, (ii) textural and (iii) optical properties of the nanoparticles will be studied.

Chapter 4 will then present a general overview of the state of the art on photocatalyst-polymer composites for photocatalytic degradation of water contaminants. Then the proposed approach and mechanism for the synthesis of Ag/ZnO-poly(acrylic acid) composites by the polymerization of the crosslinked poly(acrylic acid) in the presence of the modified photocatalyst will be described. The results of structural and textural characterization of the new designed composites will be also discussed.

In **Chapter 5** will be discussed the results of the photocatalytic efficiencies for the degradation of water contaminants, particularly endocrine disrupting compounds (i.e. bisphenol-A), emergent contaminants (i.e. triclosan) and dyes (i.e. rhodamine-B), under both UV and visible light. The results of photocatalytic performance are divided in two sections, one for Ag/ZnO photocatalyst and other for Ag/ZnO-poly(acrylic acid) composite.

Chapter 6 will concern the modeling and optimization of the photocatalytic process. The influence of (i) the parameters of Ag/ZnO synthesis (i.e. pH, silver concentration, and reaction time) and (ii) the photocatalysis parameters (e.g. contaminant concentration, catalyst concentration and pH) on the catalytic efficiency will be modeled and optimized using response surface methodology and artificial neural network coupled to evolutionary algorithm. An interesting approach will be proposed to correlate the synthesis operating conditions and photocatalytic performance for bisphenol-A, namely a two-step modeling on the basis of multi-layer back-propagating neural networks. Then, the results will be discussed taking into account the complexity of the research problem.

A general conclusion of the main results will finally be presented together with some recommendations to solve problems encountered during the development of this research, and perspectives.

1 Chapter 1. ZnO AND ITS NANOCOMPOSITES FOR HETEROGENEOUS PHOTOCATALYSIS: THE STATE OF THE ART

Zinc oxide (ZnO) nanoparticles (NPs) have emerged as semiconductor with a wide range of applications. For example, the recent use of ZnO in the health field for biotherapeutic applications due to their high degree of biocompatibility and optical emission on the visible range of the spectrum. These properties have been experienced on the treatment of cancer and other therapeutic applications.

However the understanding of the physical-chemical interaction with the most important biomolecules, namely DNA, proteins, etc., is still incomplete. Some studies of the chemical interaction of ZnO with nucleotide bases of DNA and RNA have been recently reported (Shewale *et al.*, 2011), since some other studies have shown that ZnO NPs induce significant changes in the DNA structure and their functionality. This matter is of big importance since the abuse in the use of ZnO nanoparticles and wrong wastes disposal could potentially affect the animal and human health.

Therefore, the environmental applications of ZnO NPs in water treatment, which is the case in this thesis, need to have in mind the human and wildlife safety concerns. Once stated the responsible use of ZnO NPs, we will proceed to inquire their environmental application on the water decontamination using solar irradiation.

1.1 Surface chemistry of the photocatalyst

In order to understand the photocatalytic process and the scientific problems to solve in this thesis, this section regards the surface chemistry of a photocatalyst, the basic concepts of the energy band theory, reactive species and lifetimes.

The global photocatalytic reaction occurs through the following steps (Figure 1.1):

- i. mass transfer of reactants from fluid bulk to the catalyst surface (external diffusion),
- ii. mass transfer of reactants from the catalyst surface into its pore structure (internal diffusion),
- iii. adsorption of reactants,
- iv. surface reaction,
- v. desorption of products,
- vi. mass transfer of products toward the pore structure of the catalyst to the surface, and
- vii. mass transfer of products from the catalyst surface to fluid bulk.

Specifically the photocatalysis involves redox reactions of organic or inorganic molecules induced by suitable light irradiation upon a semiconductor particle (i.e. ZnO). Thus, photocatalytic reactions (equivalent to step iv in Figure 1.1) can be described as follows:

- a) *photogeneration* of electron-hole pairs by exciting a semiconductor with radiation with suitable light energy;
- b) *separation* of electron-hole pairs by traps which have a trapping rate higher than the electron-hole recombination rate;
- c) *redox reaction* between the separated electrons and holes with adsorbed substrates.

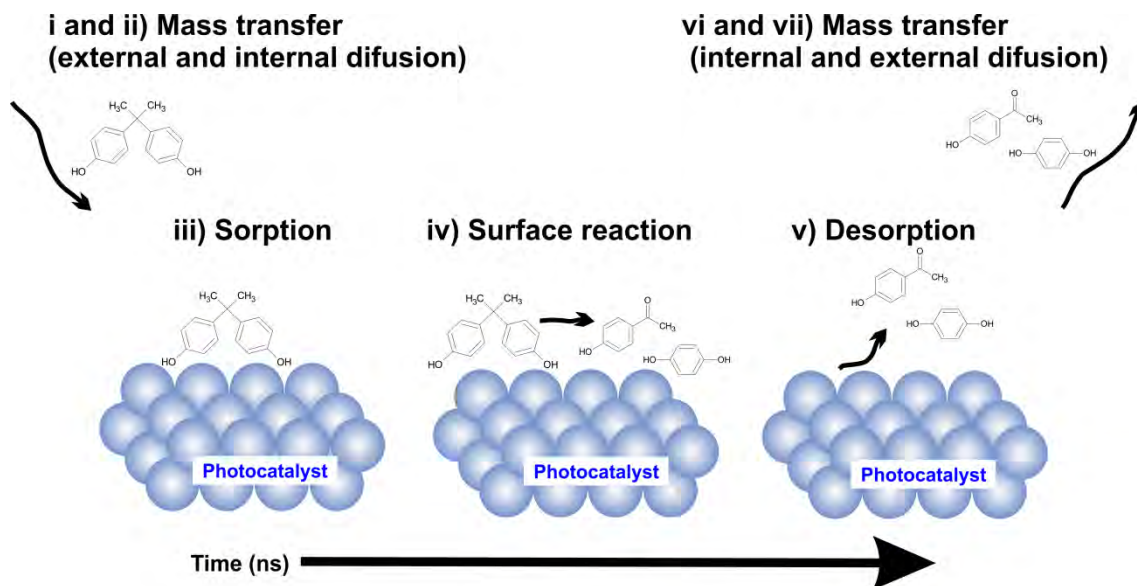


Figure 1.1. Representation of the global photocatalytic mechanism of an endocrine disrupting compound on ZnO surface involving seven basic steps. Scale time of nanoseconds.

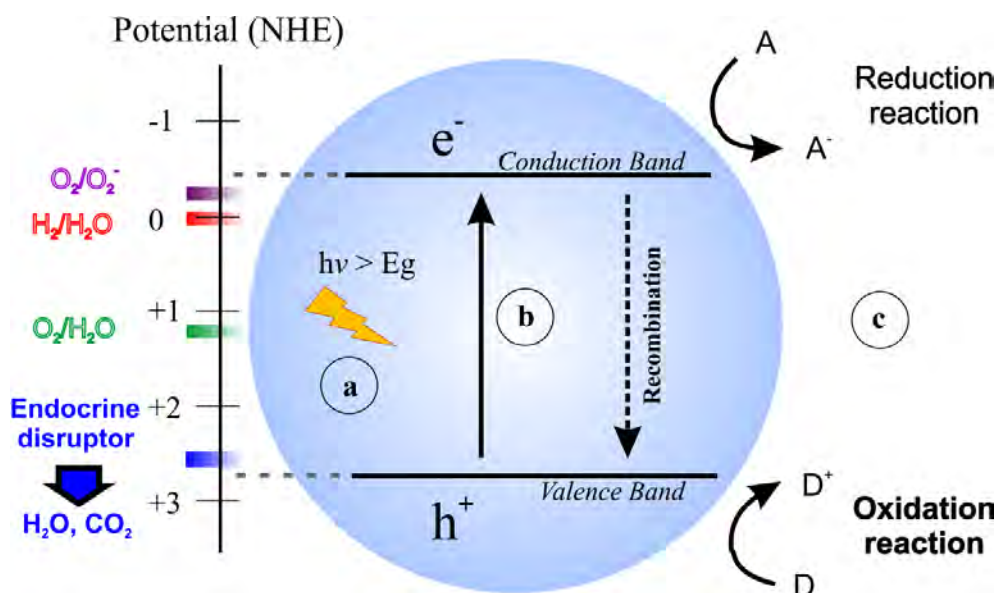


Figure 1.2. Schematic representation of the photocatalytic mechanism of ZnO where a) the photon energy greater than the bandgap energy is adsorbed by ZnO and generates electron-hole pairs, b) the photoexcited charge carriers spate and migrate to the surface, and c) adsorbed species are reduced and oxidized by the photogenerated electrons and holes, respectively. (A/A⁻: acceptor species, D/D⁺ donor species).

The absorption of photon energy at the surface of ZnO semiconductor particles can excite the solid semiconductor. The photoexcitation means a band-to-band electronic transition, moving an electron from the top most filled band (valence band, VB) to the closest empty band (conduction band, CB) (Figure 1.2). The difference between the energy level of these bands is known as *bandgap* energy (E_g).

In other words, light with energy higher than the bandgap energy will lead to electrons excitation, resulting in the formation of an electron-hole pair in the semiconductor (Equation 1.1):



where e^-_{CB} is an electron in the conduction band and h^+_{VB} is a positive hole in valence band.

The minimum wavelength of the incident radiation, that is required to promote an electron excitation depends upon the bandgap energy of the photocatalyst and is given by the simplified Planck equation (Equation 1.2):

$$E_g = 1240 / \lambda_{\text{min}} \quad (1.2)$$

where λ_{min} is the minimum wavelength (nm) of the incident radiation to induce photoexcitation of a semiconductor with a bandgap energy E_g (eV).

The electrons in the conduction band compete in three processes before returning to the ground state in the valence band:

- 1) radiative recombination (exciton emission),
- 2) trapping of the hole at the surface, and
- 3) trapping of the excited electron at the surface (non-radiative recombination) (Van Dijken *et al.*, 2000).

The state of the art

Usually a non-radiative recombination is considered to be the most important back draw and an unfavorable process for the aimed photocatalytic performance. Ideally, electrons and holes must be somehow separated to minimize the electron-hole recombination process. Trends in charge separation will be exposed in section 1.3 of this chapter.

The hole can be trapped by the electron at both the surface and the inner part of the particle, by tunneling in a deep trap (V_o^* center). The later process is less important when the particle size increases because then the two localized states are difficult to reach each other.

In resume, the function of the ZnO bulk lattice is to absorb the incident photons and generate excited electrons and holes. Then the surface catalytic active sites (excited electrons and holes) on the surface perform the catalytic reaction (redox reactions and chemical transformation of adsorbed species).

The photocatalytic processes occur on femtosecond to nanosecond time scales (Figure 1.3). Even when the reported lifetimes were obtained from a data collection for TiO₂ photocatalyst, it gives us an idea of time scale occurring photocatalytic reactions and charge recombination on ZnO photocatalysts.

Information of the photogenerated charge carriers, either free or trapped, can be obtained by various spectroscopic techniques and an extensive literature review focused on ZnO characterization is encouraged. Both trapped holes and electrons absorb light in the visible and near-infrared spectral regions whereas free electrons absorb light in the infrared or microwave regions. These absorptions allow to accurately measuring the time scale of photocatalytic processes by means of transient spectroscopies, such as absorption spectroscopy, diffuse reflectance spectroscopy, and time-resolved microwave conductivity (TRMC) measurements (Colbeau-Justin *et al.*, 2013; Fujishima *et al.*, 2008).

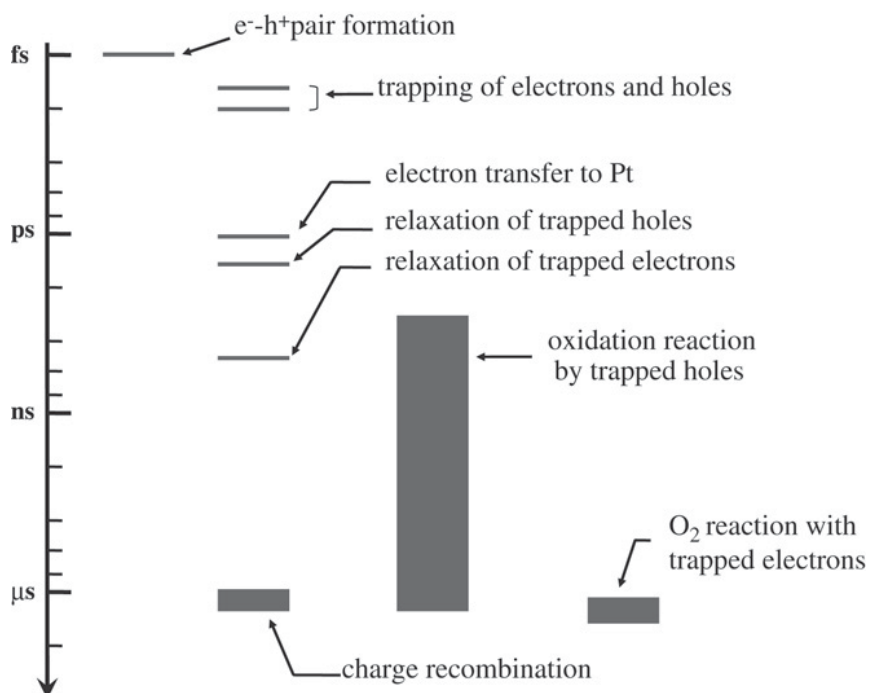


Figure 1.3. Life time of the reactive species in the photocatalytic process (Figure original from Fujishima *et al.*, 2008).

1.2 ZnO properties

1.2.1 Crystal structure

Zinc oxide is a II-VI group semiconductor with wurtzite structure with lattice parameters $a=0.3296$ nm and $c=0.52065$ nm. Zn^{2+} atoms are tetrahedrally coordinated with O^{2-} atoms stacked alternately along the c axis (Wang, ZL *et al.*, 2004), so that d-electrons of zinc are hybridized with 2p-electrons of oxygen.

Two kind of termination faces exist: the polar and nonpolar (Figure 1.4). The Zn^{2+} -terminated (001) face and O^{2-} -terminated ($00\bar{1}$) face are polar, while (10 $\bar{1}$ 0) face containing equal number of Zn and O atoms is the nonpolar face (Zhang *et al.* 2010). The positively Zn^{2+} -terminated (001) and negatively O^{2-} -terminated ($00\bar{1}$) polar faces have high energy surfaces that decrease as the crystal growths (Chu *et al.*, 2009; Huang *et al.*, 2014).

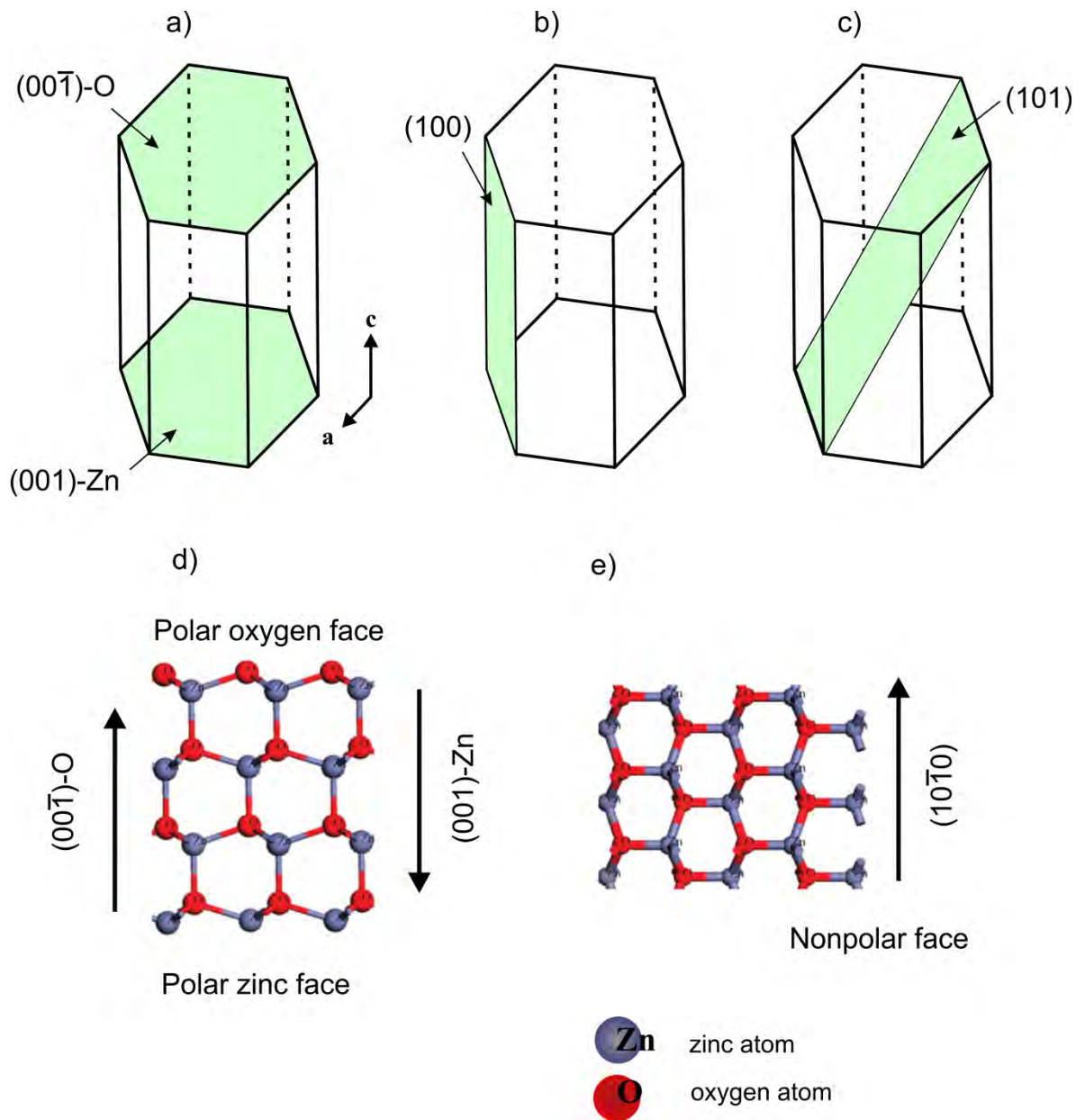


Figure 1.4. ZnO unit cell showing (001), (100) and (101) planes (a, b, c) and the ball-stick model of ZnO crystals (d, e) (Modified from Chu *et al.*, 2009).

Catalytic properties, chemical stability and surface electronic surface depend on ZnO polarity (Chu *et al.*, 2009; Zhang *et al.* 2010). An important phenomenon for photocatalysis such as the photocorrosion is increased by the O^{2-} -terminated ($00\bar{1}$) face. While the Zn^{2+} -terminated (001) face is less soluble, resistant to photocorrosion and shows the highest photocatalytic activity (Matsumoto *et al.*, 2009).

Capping agents or surfactants, such as CTAB, polymer and citrate ions, are often used to promote selective growth and velocity of crystal faces, finally this passivant materials are removed from the surface (Wilcoxon *et al.*, 2006). A recent strategy uses metal oxide nanoparticles, Bi_2WO_6 , as seeds to control the ZnO polar faces (Huang *et al.*, 2014). The most popular synthesis methods to obtain ZnO with polar faces are sol-gel (Zhang *et al.* 2010), chemical bath deposition (Huang *et al.*, 2014), hydrothermal growth and sputtering (Irzh *et al.*, 2009). The controlled synthesis of ZnO is remarkable since its photocatalytic properties are associated with polar faces as explained before (Huang *et al.*, 2014; Matsumoto *et al.*, 2009; Zhang, *et al.* 2010).

We must point out that ZnO raw material used in this thesis (provided by Degussa Co.) has a hexagonal cylinder shape with both pyramidal tip and round tip. The [Figure 1.5](#) shows other dominant nanoparticle morphology: tetrapods.

1.2.1 Electronic and optical properties

The electrical conductivity of ZnO is determined by the defects in the material. ZnO is intrinsically doped via oxygen vacancies and/or zinc interstitials spaces. Mostly ZnO exhibits n-type conductivity with electron concentration of 10^{17} cm^{-3} due to excess of zinc ions. The large exciton binding energy between 30 and 60 meV, allows efficient excitonic lasing mechanism to operate at room pressure and temperature. Therefore, ZnO in the form of films or pressed powders attract a great attention (Wang, ZL *et al.*, 2004).

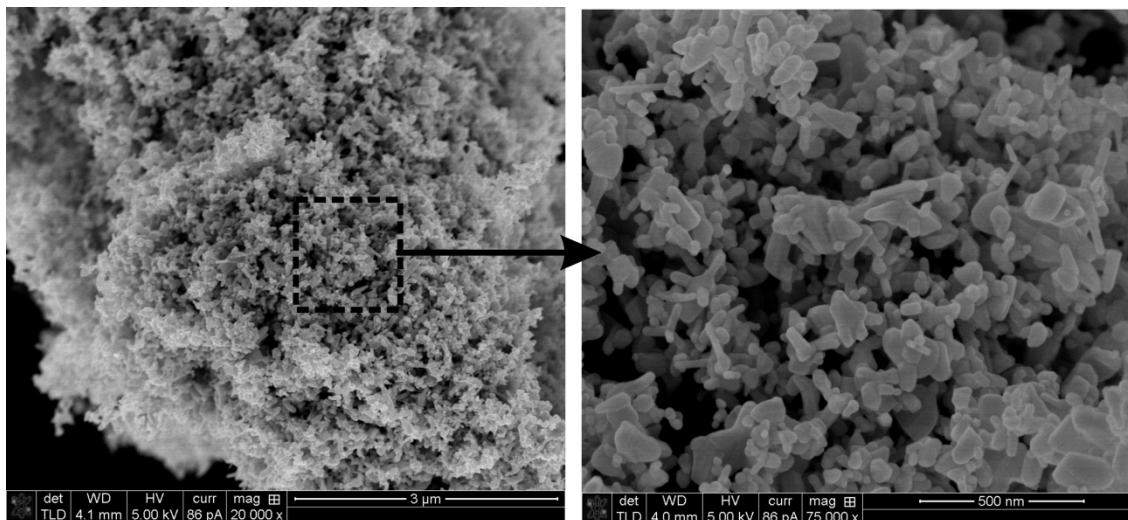


Figure 1.5. SEM photograph of the commercial ZnO nanoparticles (VP AdNano ZnO 20DW, Degussa Co.) used in this thesis. The different morphologies include rods, tetrapods with both pyramidal and round tips.

Another important property is the optical band gap energy (E_g). ZnO is a direct bandgap semiconductor with an E_g of 3.2 eV at room temperature. The bandgap energy of ZnO and titanium dioxide (TiO_2), the latter a well-known and extensively used photocatalyst, is basically the same (3.2 eV). However, the valence and conduction bands exhibit differences in electric potential; whose reported values are in the range of -0.45 to 2.75 eV vs. NHE and -0.1 to 3.1 eV vs. NHE, for ZnO and TiO_2 , respectively (Li, B *et al.*, 2011; Xiong *et al.*, 2010). Thus, due to the position of the valence band of ZnO, the photogenerated holes have strong enough oxidizing power to decompose most organic compounds.

Other piezoelectric properties are extensively studied by Wang, Z.L. *et al.* (2004) review, where it is suggested that ZnO could be the next most important nanomaterial after carbon nanotubes.

1.3 ZnO modification for photocatalytic performance improvement

Three trends in ZnO photocatalyst modification are followed in the development of the third generation of semiconductor materials.

- 1) First, the enhancement of the surface area by synthesis of nanostructured semiconductors materials. Specifically, the size-quantization effect causes significant changes in the optical band gap of the semiconductor.
- 2) The second consists in introducing states within the ZnO bandgap to absorb the visible light region by doping metals or non-metals into ZnO lattice.
- 3) The third trend is the development of semiconductor-conducting polymer composites which is giving a new basis to the engineered materials for photocatalysis.

All these improvements are only possible with the inclusion of nanotechnology, polymer chemistry and inorganic chemistry areas.

1.3.1 Reducing size: Nanoparticles

The improvement of the photocatalytic activity of ZnO under visible light irradiation is possible through the size reduction of the photocatalyst particles. ZnO nanostructures can be synthesized with many configurations controlling the growth kinetics, local growth-temperature and the chemical composition of the source materials. The use of capping agents is commonly used to decrease the particle size and maintain the size dispersion, and to obtain specific optical absorption profiles.

The synthesized nanostructures include nanorod, nanowires, nanocolumns, nanotubes, nanobelts, nanorings, nanoribbons, nanosheet networks, hollow micro- and nano-spheres, nanoflowers and nanocombs.

The state of the art

Several reviews are recommended in order to obtain detailed information about the synthesis methodologies and characterization of ZnO nanostructures (Fan *et al.*, 2005; Hahn, 2011; Wang, ZL, 2004a;2004b; Ye *et al.*, 2005). Those papers are focus on the ZnO properties for the field of biosensors, light-emitting diodes and photovoltaic cells, but easily can be extrapolated to photocatalytic materials.

Size reduction greatly affects the adsorption of reactants and reaction efficiency due to their increased surface to volume ratio and unique surface, optical and electronic properties (Shvalagin *et al.*, 2007). For example, Zhou *et al.* (2010) reported the superhydrophilicity and superhydrophobicity on ZnO micro- and nano-structures. It means that surface wettability of ZnO powders is regulated by their micro-nanostructures. This finding is significant for the applications of photocatalysis in aqueous solutions.

Furthermore, ZnO quantum dots (QDs) with several nanometers in diameter and large surface to volume ratio are receiving attention due to their quantum size effect, possessing more surface defects such as oxygen vacancies than the bulk ZnO materials. Zhang, L. *et al.* (2010) reported highly faceted prisms ZnO quantum dots of about 3-4 nm in diameter with polar faces and high crystallinity with enhanced photocatalytic activity. Most importantly, the presence of high proportion of polar surfaces is helpful to adsorb oxygen molecules and OH⁻ ions, resulting in a fastest production rate of H₂O₂ and OH[•] radicals, hence promoting photocatalytic reactions.

The relationship between the morphology, crystal growth habit, and photocatalytic properties of the ZnO QDs with several nanometers in diameter, remains as an interesting topic involving a non-trivial problem.

1.3.2 ZnO surface modification by metals

The rationale for ZnO modification with transition metals is based on three possible benefits, which are: a bandgap reduction, a charge separation in order to minimize the electron-hole recombination rate and the promotion of active defect sites on surface that function as reactive centers (Wei, S-H *et al.*, 2008; Yan *et al.*, 2006).

Since 2003 the authors have been study the positive role of metallic silver (Ag) nanoparticles on ZnO on improving the photocatalytic efficiency (Ahn *et al.*, 2006; Gao *et al.*, 2011; Georgekutty *et al.*, 2008; Patole *et al.*, 2006; Wang, J *et al.*, 2011). The evidence suggest that the Ag nanoparticles act as electron sinks and can trap the photogenerated electrons from the semiconductor and thus improve the separation efficiency of the photogenerated electrons and holes, hence improving the photocatalytic activity but also the photostability.

Silver also acts as an oxygen chemisorption site, which react with the photogenerated electrons to form reactive oxygen species. Thus silver facilitates the trapping of the photogenerated electrons and finally improves the photocatalytic activity. Moreover, silver can enhance the photocatalytic activity by creating a local electric field and the optical vibration of surface plasmon in silver can make a reasonable enhancement in this electric field (Georgekutty *et al.*, 2008).

However, one can add the photocorrosion inhibition by silver nanoparticles. The photocorrosion of ZnO is the main disadvantage for its use as photocatalyst at industrial scale. The photocorrosion process consists on the consumption of two holes for the dissolution of ZnO giving rise to the formation of Zn²⁺ ion and oxygen according to [Equation 1.3](#):



The state of the art

Xie, W. *et al.*, (2010) achieved a photostable ZnO since the surface defect sites were reduced after Ag loading, suggesting that the metallic silver is deposited on the defect sites, where the photocorrosion of ZnO occurs. Kawano, K. *et al.*, (2002) reported that Ag nucleation and photoreduction of Ag^+ ion on Zn^{2+} -terminated polar faces reduce the photocorrosion process. Furthermore, the strong interaction between water and Zn^{2+} -terminated polar face for water decomposition is reported, which in turn suppress the photocorrosion.

We must point out that the results are contradictory, and the visible light response by Ag-modified ZnO is not always accompanied by an improvement in the photocatalytic activity.

Doping with other member of the group-IB elements such Cu and Au (Yan, Y. *et al.*, 2006) have been tested but Ag is still the best candidate to improve ZnO photoactivity. Surface modification with nonmetal atoms like N, B and S (Marschall *et al.*, 2013; Patil *et al.*, 2011) is a recent topic but they will be not discussed in this thesis.

1.3.3 ZnO–polymer composites

The literature describing catalytic properties of supported TiO_2 is great in number, but the case of ZnO is less abundant. ZnO have been supported in natural polymers (cellulose substrates) or most widely on synthetic polymers.

Incorporating ZnO nanoparticles into polymeric matrices modify optical, mechanical and thermal properties. However, those properties are affected by both the dispersion of nanoparticles in the matrix and the interfacial interactions between them. Nanoparticle/polymer nanocomposites present the advantage of the high surface area of the nanoparticle and the mechanical strength of the polymer and often exhibit synergetic properties.

The nanoparticle can be incorporated into the matrix via three different approaches:

- 1) mixing of preformed nanoparticle and matrix,
- 2) synthesis of matrix in presence of nanoparticle, and
- 3) synthesis of nanoparticle inside the matrix.

From the wide range of nanocomposite applications (e.g. antibacterial, catalytic, sensing, electronic devices and energy production) this thesis will focus only on that for photocatalytic water treatment. However, this section will discuss the improvement on mechanical, thermal and optical properties of the matrix due to the incorporation of ZnO nanoparticles, the actual application and the potential application of such nanocomposites on photocatalysis. A list of recently reported ZnO-based nanocomposites is shown in [Table 1.1](#).

The most common strategy in the nanocomposites preparation is the *mixing* accompanied by energy source, radiation or heat, to promote the strong interaction between ZnO nanoparticles and the matrix (Abdolmaleki, A. *et al.*, 2011; Li, S.C. *et al.*, 2010; Ma, C.C.M. *et al.*, 2005; Mallakpour, S. *et al.*, 2012). It is important to mention that silane coupling agents were used in all cases to promote the chemical interaction between functional groups of the polymer chains and ZnO surface. The resulting material shows both enhanced thermal stability and improved UV-A absorbance. Their application in photocatalysis under solar irradiation is possible because of the enhanced UV-A sorption however, its catalytic activity is limited to the surface area exposed in the pellets of micrometer or millimeter size. It means that some part of the surface area and active sites of the ZnO catalyst are loosed in the inner part of the nanocomposite pellet. On the other hand, the mechanical resistance of the polymer matrix is very helpful on packing reactors for continuous treatment of water.

The state of the art

The second strategy concerns the *polymerization* of the matrix *in presence of ZnO*. The nanoparticles dispersion is affected by the operating conditions and polymerization method. For example, solid spherical particles wrapping ZnO nanoparticles were found in the ZnO/polyaniline composites when using THF as the oil phase in pickering emulsion polymerization (Jeng, J. *et al.*, 2008). Whereas that hollow composite particles with ZnO nanoparticles attached to the surface were found using toluene as oil phase using the same operating conditions. As mentioned before, thermal characteristics were improved and used as UV coatings (He, J. *et al.*, 2009; Jeng, J. *et al.*, 2008; Lu, N. *et al.*, 2007) due to the UV sorption properties of ZnO. Using the appropriated coupling and stabilizer agents, the ZnO nanoparticle size is maintained after the polymerization process keeping the properties of high surface area and UV sorption.

Finally, the synthesis of ZnO nanoparticles inside the matrix has been carried out through reduction of zinc salts. For example, the dip-coating method is a simple, quick (5 min) and versatile method to prepare films supporting ZnO particles. The catalyst can be supported on a wide variety of matrices (e.g. glass, poly(methyl methacrylate), polycarbonate, poly(acrylic acid), polypropylene, Nylon 6,6, etc.) showing different shape and crystallite orientation. For example ordered flower-like morphology of ZnO was formed over glass, but unordered rods of ZnO were found on polycarbonate, polypropylene and Nylon 6,6 (Irzh *et al.*, 2009). This is an important finding since the photocatalytic activity of ZnO has been recently associated with polar facets (Huang *et al.*, 2014; Zhang, Luyuan *et al.*, 2010).

Zhang *et al.* (2010) reported higher photocatalytic efficiency for ZnO quantum dots with Zn²⁺-terminated (001) and O²⁻-terminated (00⁻1) polar faces than non-polar faces. Specifically, Zn²⁺-terminated (001) faces have unsaturated oxygen coordination making easy adsorption of oxygen molecules and OH⁻ ions to produce H₂O₂ and free radicals like [•]OH and hence accelerate the photocatalytic reaction.

Table 1.1. Materials used as matrices on nanoparticle/polymer nanocomposites.

Nanoparticle (precursor, content)	Matrix	Synthesis technique (approach) ^a	Application	Observations	Reference
ZnO (4-12% w/w)	Poly(amide-imide)s	Ultrasonic radiation (1)	Biodegradable optical coating	Increase thermal stability Block UV-A irradiation.	(Mallakpour <i>et al.</i> , 2012)
ZnO (2-10% w/w)	Poly(ester-amide)	Ultrasonic radiation (1)	Surgical implants and drug delivery devices	Enhance of thermal stability, nanoparticles dispersed homogeneously	(Abdolmaleki <i>et al.</i> , 2011)
ZnO (5-30% w/w)	Polystyrene	Melt-blending (1)	Antistatic material	Reduce surface resistivity, improve flexural properties, increase glass transition temperature (T _g)	(Ma <i>et al.</i> , 2005)
ZnO (0.2-2% w/w)	High-density polyethylene	Melt-blending and hot compression-molding (1)	Antibacterial films	UV absorbance improved, increased tensile strength and elongation at break	(Li, SC <i>et al.</i> , 2010)
ZnO (86% w/w)	Polyaniline	Pickering emulsion polymerization (2)	pH regulation	Different morphologies depending nature of oil phase	(Jeng <i>et al.</i> , 2008)
ZnO (1-15% w/w)	Polyurethane acrylate	UV radiation-initiated polymerization (2)	Luminescent films for optical coating	Increase thermal stability, transparent films	(Lü <i>et al.</i> , 2007)

The state of the art

ZnO (0.5-3% w/w)	Polyethylene terephthalate	Polymerization (2)	UV-protections agent	Increase melting transition (T_m) and crystallization (T_c) temperature	(He <i>et al.</i> , 2009)
ZnO [Zn(NO ₃) ₂ , 4.33%]	Poly(acrylic acid)	Biomimetic synthesis on flexible plastic (3)	Ultrasensitive bioimaging with ZnO quantum-dots	Enhanced UV emission, transparent nanocomposites	(Zou <i>et al.</i> , 2009)
ZnO[(Zn(AC) ₂ , 0.05-0.13% w/w]	Glass, Poly(methyl methacrylate), Polycarbonate, Nylon 6,6.	Microwave assisted dip-coating (3)	Conducting films	Different orientation of crystallites on glass vs polymer surfaces	(Irzh <i>et al.</i> , 2009)
ZnO [Zn(AC) ₂ 2H ₂ O, 26-57%w/w]	Nanocellulose	Sol-gel method (3)	Antibacterial activity	Increase thermal properties, reduced band gap	(Azizi <i>et al.</i> , 2013)

^a Approach of nanoparticle incorporation into the matrix via: 1) mixing of preformed nanoparticle and matrix, 2) synthesis of matrix in presence of nanoparticle and 3) synthesis of nanoparticle inside the matrix

Therefore, the novel techniques reported for the preparation of films (Azizi, S. *et al.*, 2013, Irzh, A. *et al.*, 2009, Zou, S. *et al.*, 2009) could be useful for the development of engineered oriented photocatalyst films for efficient air or water treatment.

The case of ZnO/nanocellulose nanocomposites preparation deserves special attention. Nanocellulose acts as capping agent during ZnO NPs synthesis stabilizing the nanoparticle dispersion (Azizi *et al.*, 2013). The exceptional properties such hydrophilicity (water superadsorption), good mechanical strength, thermal resistance and the highest catalyst content (57% w/w) gives to the ZnO/nanocellulose nanocomposites the potential to be used as good photocatalysts for water treatment even when the authors have only tested this new material for antibacterial activity.

1.4 ZnO as photocatalyst applied

This section will expose the factors that affect the photocatalytic efficiency and the trends in normalized calculations.

1.4.1 Factors affecting the photocatalytic process

Photocatalysis involves redox reactions of organic or inorganic molecules, induced by suitable light irradiation upon a ZnO semiconductor. The catalytic reactions depend on the nature of the chemical interaction between liquid and the morphological and textural properties of ZnO. The governing factors on the photocatalytic reaction rate are associated with both the nature of the photocatalyst (e.g. crystal structure, morphology, pore size, surface area and metal content) and the liquid properties (e.g. pH, contaminant concentration, light intensity, wavelength of light and mass transport).

The state of the art

The pH of the solution is perhaps the most important factor in the photocatalytic process since it affects the surface charge of the photocatalyst as well as the ionization state of both the photocatalyst and the contaminant. Given the evidence that substrate degradation occurs on the photocatalyst surface, the effect of pH on contaminant ionization and adsorption process is an important factor to pay attention.

It is well known that contaminant adsorption is maximum near the zero point charge or isoelectric point, at which the photodegradation is also maximum (Daneshvar *et al.*, 2007). Specifically for ZnO it occurs around pH value of 9.0. On the other hand, alkaline solution media (high pH) is abundant on hydroxyl ions and subsequently on hydroxyl radicals ($\cdot\text{OH}$) that could increase the reaction rate.

Photocorrosion through self-oxidation (Equation 1.3) and dissolution are the main back draws for the photocatalytic process. The dissolution of ZnO occurs mainly in acidic pH (Equation 1.4) and less notably under strong alkaline environment (Equation 1.5).



In addition, reactions 1.4 and 1.5 compete with the formation of OH^\cdot radicals by decreasing the availability of holes for water oxidation or surface OH^- oxidation.

1.4.2 Kinetics and reaction rate normalization

This section present the normalization of the photocatalytic reaction rate proposed until now in order encouraging the standardization. We must point out that such normalization procedures have being mainly applied for photocatalytic splitting of water since the scientific community found transcendental the comparisons in the energy generation from H_2 . It does not represent a limitation for apply such

normalization system on the photocatalytic decontamination of water and even several journals encourage it.

Bangun and Adesina (1998) were the first in proposed the photocatalytic reaction rate, R_{rxn} , dependency on catalyst concentration as shows [Equation 1.6](#).

$$R_{rxn} = \frac{k_{app} C}{(1 + \alpha_{cat} C)^2} \quad (1.6)$$

where C is the catalyst concentration, k_{app} and α_{cat} are reaction parameters. This equation suggests that the optimum catalyst dosage is $1/\alpha_{cat}$. In fact, the photocatalyst dose widely used is of 1 g/L since the photocatalytic reactions are considered of pseudo-first order.

However, the comparison of the photocatalytic reaction rate between laboratories is not yet possible because the photocatalytic performance is subject to both i) physical, chemical and optical properties of the catalyst and ii) operational parameters (pH, contaminant concentration, light intensity, etc.) (Lam, S. *et al.*, 2012). Specifically, the photocatalytic activity of ZnO has been attributed to specific properties of the catalyst such as the size particle, surface area (Wang, J *et al.*, 2011), morphology (Li, D *et al.*, 2003), and crystal orientation (Kislov *et al.*, 2009).

The call to normalize the photocatalytic reaction rate was proposed four year ago to rank the photocatalysts reported by different laboratories (Maschmeyer *et al.*, 2010). The most common normalization method is the mass normalized turnover rate (TOR_m) because of the easy determination of product moles formed, by liquid chromatography or UV-Vis spectroscopy, and the mass of the photocatalyst used. TOR_m express the moles converted or produced per gram of photocatalyst per unit of time.

The state of the art

The photocatalytic activity normalized per surface area or number of surface sites allows establish relationships between the bulk properties and the photocatalyst structure characteristics. The surface area normalized turnover rate (TOR_s) express the molecules converted or produced per m^2 of photocatalyst per unit of time, while surface site normalized turnover frequency (TOF) is defined by the moles converted or produced per photoactive surface site of photocatalyst per unit of time. Note that TOF normalization can be determined from the surface characterization of the photocatalyst that provide the number of photoactive surface sites per gram. Turnover number (TON) expresses the moles converted or produced per photoactive surface site (number of initial OH-sites).

In order to obtain a deep knowledge of the normalized photoactivity on different systems (i.e. mono-phasic, multicomponent mono-phasic, biphasic and tri-phasic photocatalyst) the review of Wachs *et al.*, (2013) is recommended.

Other useful way to normalize the photoactivity is the apparent quantum efficiency (AQE) which depends on the incident photons and not on the real adsorbed ones, by the photocatalyst, to initiate the generation of electron-hole pairs. This normalization is useful for comparison only of experiences realized under the same illumination conditions.

Photocatalysis is a complex system since both the photocatalyst bulk and the surface sites contribute to the overall process. Thus, AQE still does not provide insights about the individual contributions of the photocatalyst bulk lattice (e.g., particle size, crystallinity, crystal form, among others) or photoactive surface sites (e.g., surface area, number of exposed photoactive sites, surface structure and polarity) to the overall photocatalysis process (Wachs *et al.*, 2013). Despite the efforts in normalize the reaction rate and photocatalytic activity, the scientific community still does not address a good enough structure-catalytic performance relationship.

In chapter 6 we will propose the standardization based on the metallic content of ZnO photocatalyst. It is well known that doping yields are lower than 100% (Gao *et al.*, 2011; Kim, M-R *et al.*, 2009; Zanella *et al.*, 2002), and even some authors do not report the process efficiency. So, the comparison between photocatalytic activities of metal modified ZnO photocatalysts is ambiguous because of the uncertain metal content on the photocatalyst. Certainly, the use of standardized measurements protocols by researches is critical for obtaining progress in environmental photocatalysis.

2 Chapter 2. EXPERIMENTAL TECHNIQUES

This chapter describes the reagents and devices used for the synthesis of Ag/ZnO nanoagglomerates, their immobilization in a poly(acrylic acid) matrix, and the study of their photocatalytic performance. A first part concerns the experimental setups and the analytical techniques to study the properties of the photocatalyst synthesized, while a second part is oriented on the experimental design and the mathematical models, namely response surface methodology and artificial neural network coupled to evolutionary algorithm, used to optimize the synthesis of Ag/ZnO and their photocatalytic efficiency.

2.1 REAGENTS

2.1.1 Synthesis of Ag/ZnO

The characteristics of the used reagent in this study for the functionalization of zinc oxide nanoagglomerates with silver nanoparticles are detailed in [Table 2.1](#). All the reagents were used as received. AgNPs solution is a non-commercial sample that was characterized and as result it has a silver concentration of 8×10^{-2} mol/L and particle size of 7 nm. We must point out that composition of the anionic surfactant is industrial secret; however FTIR characterization was done in order to propose a functionalization mechanism.

2.1.2 Synthesis of Ag/ZnO-poly(acrylic acid) nanocomposites

The details of chemicals used for the photocatalyst surface modification and polymerization of pure poly(acrylic acid) and composites are listed in [Table 2.2](#). All the reagents were used as received without any purification.

2.1.3 Photocatalytic performance

The reagents used to test the photocatalytic activity of the synthesized photocatalysts in this study are listed in Table 2.3. Stock solutions of bisphenol-A, triclosan, hydroquinone, 4-hydroxybenzaldehyde and 4'-hydroxyacetophenone were first prepared by dissolving the reagent in methanol followed by gradual dilution with deionized water to 100 mg/L in order to prepare standard solutions, in which the methanol concentration was about 0.30%(v/v).

Table 2.1. Specifications of the reagents used for the synthesis of Ag/ZnO.

Reactive name	Use	Code	Provider
Zinc oxide (ZnO)	Photocatalyst	VP AdNano ZnO 20DW, 1314-13-2	Degussa Co.
Silver nanoparticles, AgNPs (Stabilized)	Modifier of photocatalyst	AntiBac-Mx OM20030601907	CITD-Peñoles Mexico
Hydrochloric acid, HCl (38%)	Decrease pH	7647-01-0	Fermont
Sodium hydroxide, NaOH (98%)	Increase pH	1310-73-2	Fermont
Deionized water	Aqueous solvent	17.2 MΩcm	E-pure

Table 2.2. Specifications of the reagents used for the polymerization processes.

Reactive name	Use	Code	Provider
Acrylic acid, 99%	Monomer	79-10-7	Aldrich
2',2'-Azobis(2-methylpropanenitrile) or Vazo64 (AIBN)	Initiator	78-67-1	Dupont
Potassium persulfate, K ₂ S ₂ O ₈ , (KPS)	Initiator	7727-21-1	Aldrich
Sodium metabisulfite, NaHSO ₃ , (SMBS)	Initiator	7681-57-4	Aldrich
N, N'-Methylenebisacrylamide, (MBA) (97%)	Crosslinker	110-26-9	Afa Aesar
Sodium hydroxide, NaOH (98%)	Neutralization	1310-73-2	Aldrich
3-Glycidyloxypropyltrimethoxysilane, (GLYMO)	Coupling agent or surface modifier	2530-83-8	Dynasilan Evonik

Experimental section

Table 2.3. Specifications of the reagents used for the photocatalytic activity evaluation.

Reactive name	Use	Code	Provider
Bisphenol-A, [2,2-bis(4-hydroxyphenyl)propane], (BPA) (>99%)	New Model Contaminant	80-05-7	Aldrich
Irgasan or Triclosan (TCS) (>97% HPLC)	New Model Contaminant	3380-34-5	Aldrich
Rhodamine-B, (RB)	Model Contaminant	81-88-9	Fluka
Hydroquinone, (HQ) (>99% HPLC)	Standard ^a	123-31-9	Fluka
4-Hydroxybenzaldehyde (>95% HPLC)	Standard	123-08-0	Aldrich
4'-Hydroxyacetophenone (99%)	Standard	99-93-4	Aldrich
Acetonitrile (>99.8% HPLC)	Mobile phase	75-05-8	Aldrich
Methanol (>99% GC-FID)	Solvent	6756-1	Aldrich
TiO ₂ , P25	Photocatalyst of reference	13463-67-7	Degussa Co.
Deionized water	Mobile phase	18 MΩcm	E-pure

^a The concentration of the three standards was 1-50 mg/L.

2.2 EXPERIMENTAL SETUP

2.2.1 Functionalization system

The preparation of functionalized ZnO with AgNPs was carried out by two methods: Photodeposition and Impregnation. The experiments for both methods were carried out using a photoreactor Q200 provided by SevMexico comprising a UV lamp inside of a quartz tube (Figure 2.1). Note that the lamp was turned-off for the impregnation method.

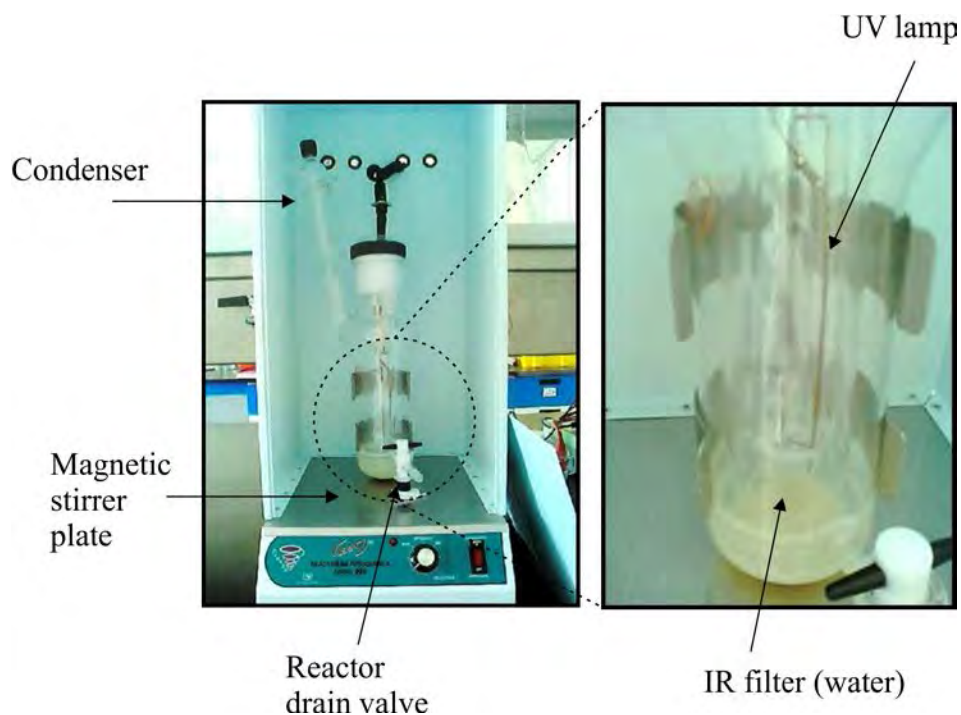


Figure 2.1. Photograph of the photoreactor Q200 for the functionalization of ZnO by the photodeposition method.

Experimental section

2.2.2 Polymerization reactor

A laboratory-scale polymerization reactor (250 ml) was used for the synthesis of poly(acrylic acid) and the Ag/ZnO-poly(acrylic acid) composite. It is made of Pyrex and is equipped with a condenser, a thermocouple, and oil bath (SilOil P20.275.50, Huber) which could be replaced with by a heating blanket (100A, Glas-Col). A nitrogen flow (15 mL/min) avoids oxygen entry during polymerization.

Complementary equipment comprises an ultrasonic processor for dispersion of the photocatalyst and a vacuum pump for bubbles removal before the polymerization step.

The reactor is schematized in [Figure 2.2](#) and the complementary equipment is described in [Table 2.4](#).

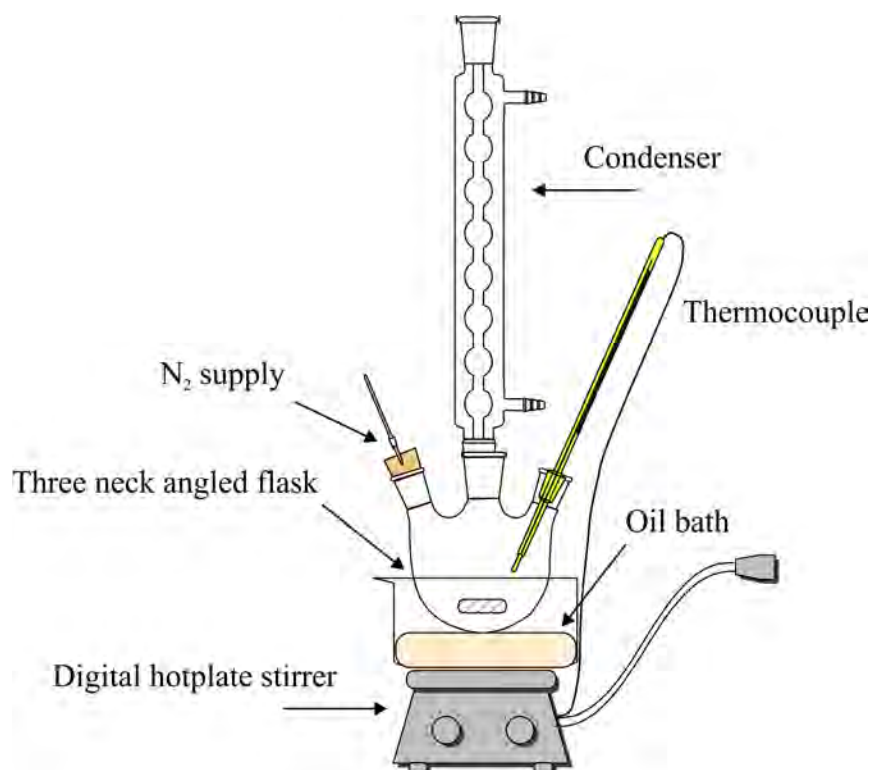


Figure 2.2. Scheme of the polymerization reactor setup.

Table 2.4. Complementary materials for polymerization process.

Apparatus	Use	Specifications	Code	Provider
Ultrasonic processor	Homogenization of photocatalyst	100 W, amplitude 55%, cycle 0.7 s, 1 h	UP200S UP50H	Hielscher Ultrasound Technology
Vacuum pump	Remove bubbles of the AgNPs/ZnO suspension	1.5 h	-	-
Digital hotplate stirrer and temperature regulating	Homogenization of reaction solution	68°C, 2 h 77°C, 1 h 400 rpm	SLR	Schott

2.2.3 Photocatalysis system

The photocatalytic activity experiments were carried out in the photoreactors of different configurations as shown in Figures 2.3 to 2.5. The specifications of the wavelength and light intensity are listed in Table 2.5. Multiple spots stirrer plate allows managing at least three runs in parallel.

Table 2.5. Specifications of the UV lamps in the photoreactors.

Photoreactor name	Use	Specifications	Code	Provider
Q200	Synthesis of Ag/ZnO	250 nm (3.4 mW/cm ²)	Q-200 (175 watt)	SevMexico
3UV	Photodegradation of bisphenol-A and triclosan	254, 302 and 365 nm (3.8, 2.8 and 0.97 mW/cm ² , respectively)	3UV-38(8 watt)	UVP Inc.
3UV	Photodegradation of bisphenol-A and triclosan	>450 nm (8 uW/cm ²)	F8T5/CW(8 watt)	Hampton Bay
Oriel	Photodegradation of rhodamine-B	254 nm, >455 nm ^a	XE (1000 watt)	Oriel
Vilber	Photodegradation of bisphenol-A using composites	365 nm (0.05 mW/cm ²)	Hg T-15L (15 watt)	Vilber

^a Glass filter to cut-off wavelength shorter than 455 nm (GG455, Schott AG). No information of intensity is available.

Experimental section

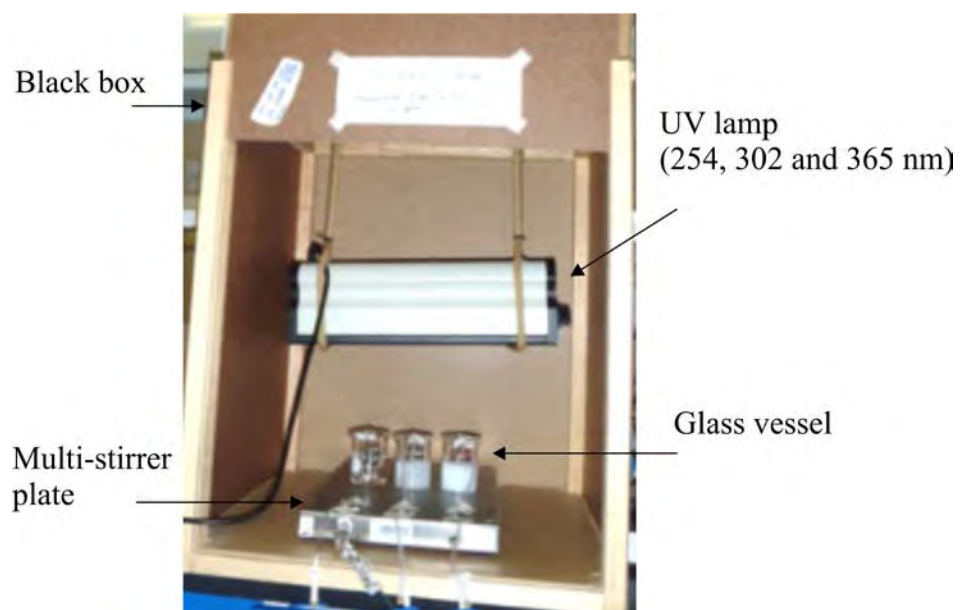


Figure 2.3. Photograph of the photoreactor 3UV.

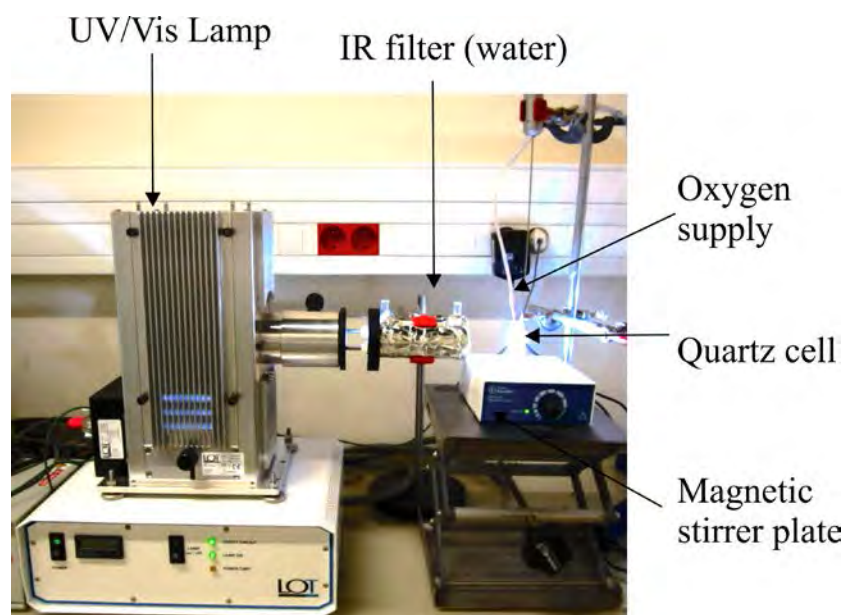


Figure 2.4. Photograph of the photoreactor Oriel.

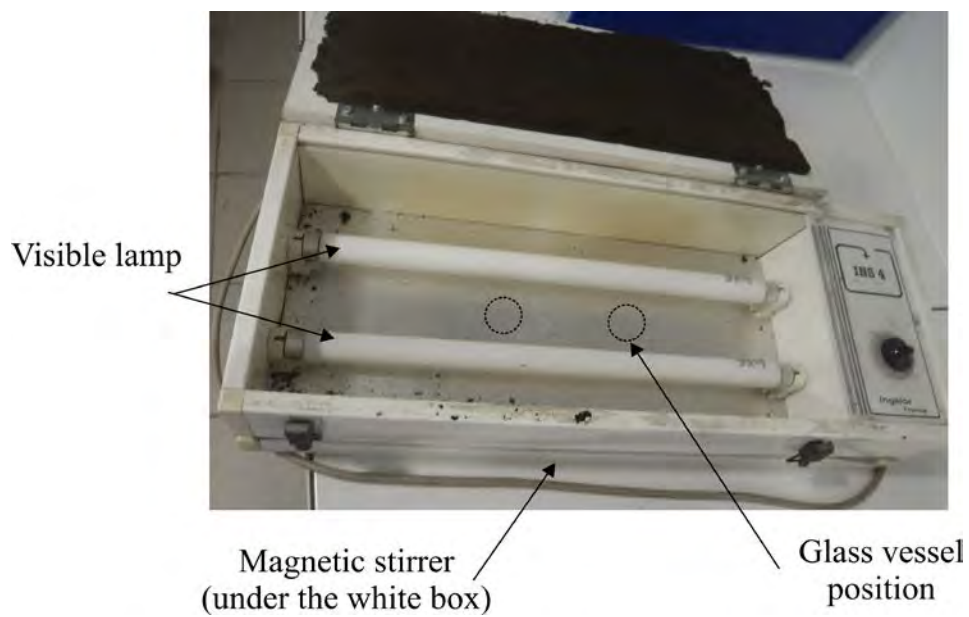


Figure 2.5. Photograph of the photoreactor Vilber.

2.3 CHARACTERIZATION TECHNIQUES

Figure 2.6 summarizes the analytical techniques to study the properties of the Ag/ZnO and Ag/ZnO-poly(acrylic acid) nanocomposites samples. A detailed description of each one is listed in Table 2.6. The samples preparation is described in the experimental section of the respective chapter.

Most of the analyses were realized in National Laboratories of IPICYT: National Biotechnology, Agricultural and Medical Laboratory (LANBAMA) and National Nanoscience and Nanotechnology Laboratory (LINAN). The other characterizations were carried out in the Laboratoire Réactions et Génie des Procédés (LRGP) of the Lorraine University.

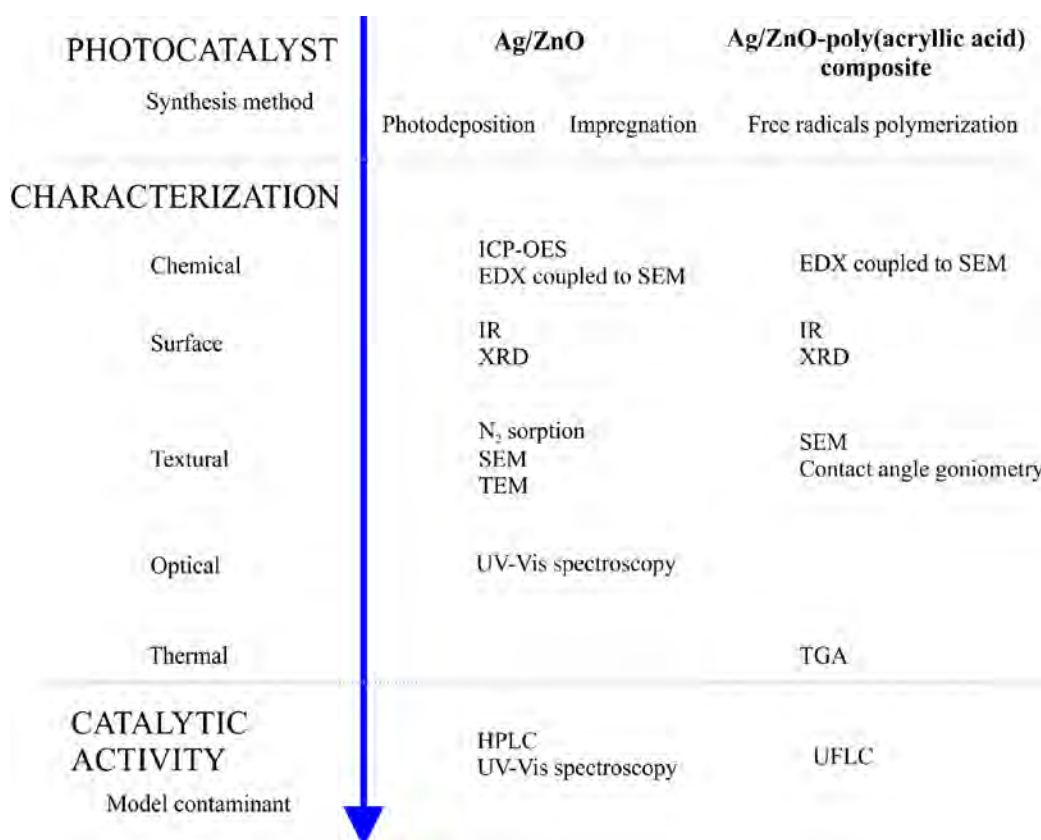


Figure 2.6. Scheme of the characterization techniques described in Table 2.6.

Table 2.6. Specifications of the analytical techniques.

Analytical technique (acronym)	Property measured	Specifications	Code	Provider
Inductively Coupled plasma optical emission spectroscopy (ICP-OES)	Ag and Zn quantification, % w/w	Ag (328.1 nm), Zn (213.9)	730-ES	Varian Inc.
X-Ray Diffraction (XRD)	Crystalline structure	20-80°, 0.02°/seg, CuK α , 35kV, 25 mA	BRUKER D8	Advance
Environmental scanning electron microscope (ESEM)	Surface properties, morphology, particle size, chemical composition by EDX	25kV, low vacuum 100-130 Pa	QUANTA 200	FEI
Scanning electron microscope (SEM)	Surface properties, morphology, particle size, chemical composition by EDX	5kV	HELIOS Nanolab 600	FEI
Transmission electron microscope (HR-TEM)	Surface properties, morphology, particle size, chemical composition by EDX	300 kV, STEM and EFTEM mode. Cu Grid, Lacey Formvar/carbon 300 mesh	Tecnai F-30 Cod. 01883	FEI Ted Pella
Nitrogen adsorption-desorption	Surface area, pore volume	N ₂ , 77 K	ASAP 2020	MICROMERITIC S
Fourier transform infrared spectroscopy by attenuated total	Chemical interactions, functional groups	500-4000 cm ⁻¹	Nicolet 6700	Thermo Scientific

Experimental section

reflectance (FTIR-ATR)		375-4000 cm ⁻¹	ALPHA-P	Bruker
Contact angle goniometry	Wetting properties, contact angle	Sessile drop	TL100	Attension
Thermogravimetric analyzer (TGA)	Thermal, properties (e.g. T ₅₀), chemical composition	N ₂ , 30 °C/min, 200-700 °C	TGA/DCS 1	Mettler Toledo
UV-Vis Spectroscopy	UV-light sorption on solid state (e.g. Band gap, surface plasmon of resonance)	300-600 nm, standard BaSO ₄ .	Varian Cary 4000 UV-Vis	Agilent Technologies
UV-Vis Spectroscopy	Rhodamine concentration	190-1000 nm	Uvikon 860	Kottron Instrumentals
High Performance Liquid Chromatography (HPLC)	Bisphenol-A and byproducts concentration	Fluorescence and diode detectors, column Synergy 4u Hydro-RP 250mm x 4.6mm, H ₂ O:acetonitrile 60%:40%	MOD 1200 SERIES	Agilent Technologies
Ultra Fast Liquid Chromatography (UFLC)	Bisphenol-A and byproducts concentration	Column Kinetex 2.6u C18 100A 50mm x 4.6mm, H ₂ O:acetonitrile 35%:65%.	Prominence UFLC	Shimadzu

2.4 EXPERIMENTAL DESIGN, MODELLING & OPTIMIZATION

The photocatalyst preparation is a complex process dependent on several factors that affect its properties and the photocatalytic performance. Therefore, it is important to select an appropriate experimental design and to develop a mathematical model able to predict and optimize the process.

In general, response surface methodology (RSM) and artificial neural network (ANN) provides mathematical relationships between the factors and the responses, even if it is unknown. In other words, ANN is able to obtain complex nonlinear, while RSM uses linear relationships to represent the process.

In this thesis, these two most popular methods were used to model and optimize the process parameters. This section describes the general methodology followed to study the functionalization of ZnO with silver nanoparticles (synthesis of Ag/ZnO photocatalyst) and its photocatalytic performance using RSM and ANN coupled to evolutionary algorithm (EA).

[Figure 2.7](#) describes the procedure and statistic tools employed in this thesis. Detailed information of the experimental designs, models, statistical analysis and optimization will be given in chapter 6.

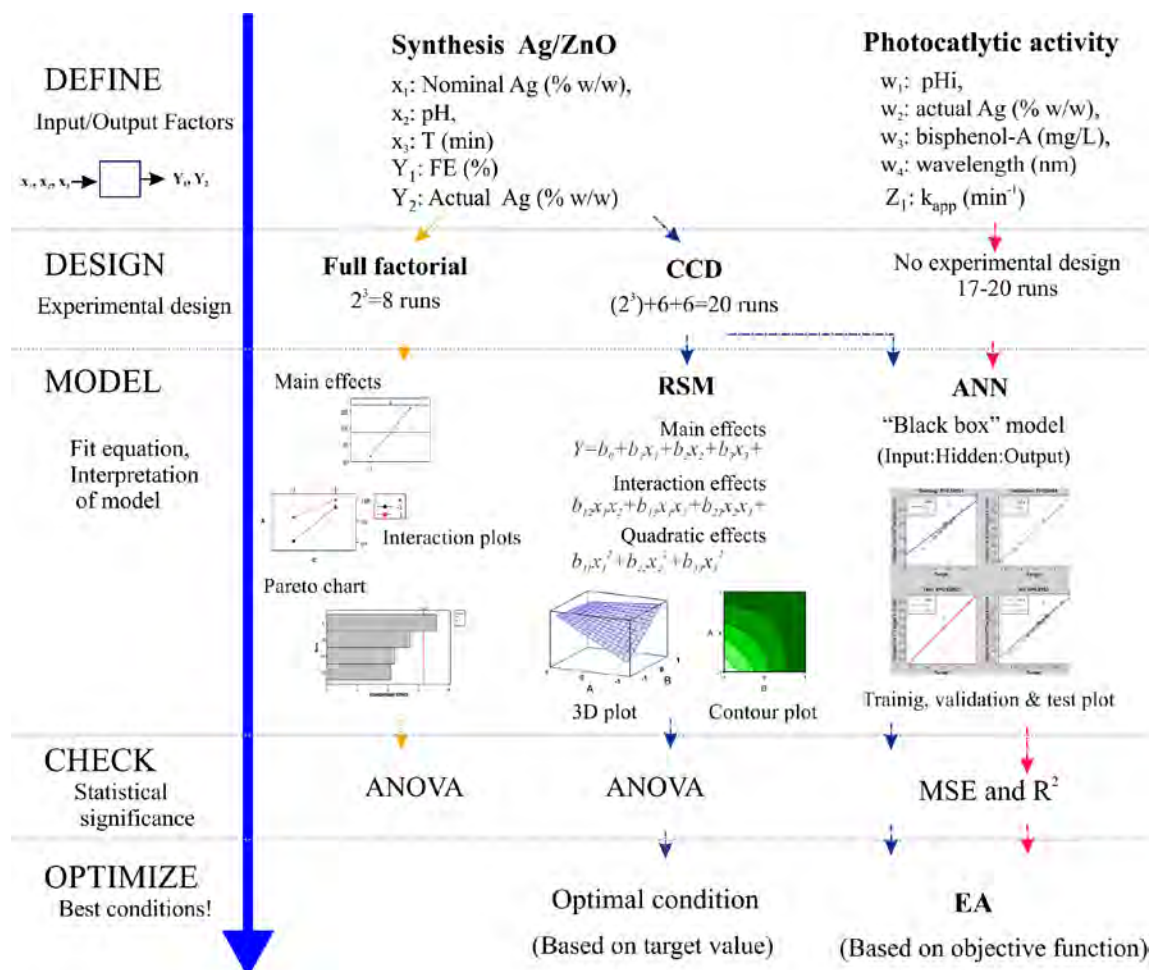


Figure 2.7. Scheme of the experimental design, model and optimization tools used to study the synthesis of Ag/ZnO photocatalyst and their photocatalytic behavior. Abbreviations CCD: central composite design, RSM: response surface methodology, ANN: artificial neural network, EA: evolutionary algorithm, ANOVA: analysis of variance, MSE: mean squared error, R^2 : correlation value. The x_i and w_j , where $i=3$ and $j=4$ are input factors, Y_1 , Y_2 and Z_1 are the response.

3 Chapter 3. SYNTHESIS OF Ag/ZnO PHOTOCATALYST: STRATEGY USING PREFORMED AgNPs

Nowadays, the challenge of understanding relationships between catalysts properties and performance in the context of heterogeneous catalysis is a hot topic. Indeed, catalysis processes are generally affected by many different operational parameters. This has encouraged us to study the structural, textural and optical properties of Ag/ZnO, which was prepared by two methods using stabilized and easy dispersible silver nanoparticles as an alternative approach for ZnO modification.

Chapter 3 concerns the description of the methods, namely *photodeposition* and *impregnation*, and mechanisms for the functionalization of zinc oxide nanoagglomerates with silver nanoparticles. The influence of the synthesis conditions (i.e. nominal amount of silver nanoparticles, pH and time) on structural, textural and optical properties of Ag/ZnO will be described.

This chapter was adapted from Effect of Ag, pH and time on preparation of Ag-functionalized zinc oxide nanoagglomerates as photocatalyst (2014). Journal of Catalysis (accepted) doi: 10.1016/j.jcat.2014.06.008.

3.1 BACKGROUND

Zinc oxide (ZnO) is a photocatalyst with adequate efficiency for the photodegradation of dissolved contaminants in aqueous solutions. It also has biomedical and antibacterial applications and has been used as sensing and piezoelectric devices due to semiconductor properties such as direct bandgap and large (60 meV) excitation binding energy (Gimenez *et al.*, 2010; Wang, Z. L *et al.*, 2004).

The characteristic bandgap of each material is related to the ease of charge transfer between the valence band and the conduction band, giving a photocatalytic capacity to the semiconductor. The goal of engineered semiconductors is to achieve a narrow bandgap in order to be photoactivated with lower energy radiation as visible light. The bandgap energy of ZnO and titanium dioxide (TiO₂), the latter being a well-known and extensively used photocatalyst, is basically the same (3.2 eV). However, the valence and conduction bands exhibit differences in electrical potential, whose reported values are in the range of -0.45 to 2.75 eV vs. NHE and -0.1 to 3.1 eV vs. NHE, for ZnO and TiO₂, respectively (Li, B *et al.*, 2011; Xiong *et al.*, 2010). This gives advantages to ZnO for catalyzing specific reduction reactions at lower potentials.

Other important advantages of ZnO are its photonic efficiency, its chemical stability, its null human cell toxicity (Reddy *et al.*, 2007) and low cost. Moreover, the optical and electronic properties of ZnO photocatalysts might be improved by controlling their surface area, particle size and shape, and polar/nonpolar surface orientation (Kislov *et al.*, 2009).

For all these reasons, nanometric ZnO can become a photocatalytic material with renewed applications for degradation of low concentrations of endocrine disruptors, pharmaceutical compounds and other emergent contaminants dissolved in aqueous solutions.

In addition, the surface modification of ZnO with nanosized Ag, has received attention, since it increases the half-life of both the charge carriers (Georgekutty *et al.*, 2008) (excited electrons and holes, e^*-h^+) in the ZnO surface after light absorption and the secondary active species generated (free radicals, i.e. $\bullet\text{OH}$). The metallic bond of Ag acts as a sink for photoexcited electrons, which reduces the recombination of the charge carriers in ZnO and increases the path length of the electrons and their sensitivity to visible light (Georgekutty *et al.*, 2008; Zheng *et al.*, 2007). Despite their importance, there are some subjects that need consideration: (i) deposition yield of Ag, since it is usually low (< 100%), (ii) distribution of Ag, which is not always homogeneous, and (iii) reaction condition optimization.

Recent developments in green synthesis of Ag nanoparticles using microorganisms (Narayanan *et al.*, 2010) or harmless reducing agents (Zhang, L *et al.*, 2003) have led to homogeneous size and specifically shaped nanoparticles with catalytic properties. Those findings open up the possibility of new Ag nanoparticle sources to be used as surface modifiers of photocatalytic materials such as ZnO. Also, the use of stabilized Ag nanoparticles makes feasible the use of green, simple, and low-cost methodologies for the functionalization of photocatalysts like ZnO without sacrificing size, shape, and catalytic properties in general.

3.2 EXPERIMENTAL METHODOLOGY

3.2.1 Preparation of Ag/ZnO photocatalyst

The Ag/ZnO photocatalyst was obtained by photodeposition (PD) and impregnation (IMP) methods as follows.

For both methods, a suspension containing ZnO and stabilized silver nanoparticles (AgNPs) was adjusted at desired initial pH values using 0.1N HCl and/or 0.5 N NaOH; the pH values were below and above the pH point of zero charge (pH_{PZC}) of ZnO nanoagglomerates ($\text{pH}_{\text{PZC}}=8.2$ see [Figure A.1, Appendix A](#)).

Ag/ZnO photocatalyst

The suspension was stirred during the certain irradiation time, and then the sample was submitted to centrifugation/re-dispersion cycles in distilled water and ethanol solutions several times in order to remove the non-attached AgNPs from ZnO surface.

The samples were then dried at 80°C for 8h and finally stored in the darkness.

3.2.1.1 Photodeposition method

The suspension (10 g/L ZnO) was irradiated using UV light of 254 nm on a Photoreactor Q-200.

3.2.1.2 Impregnation method

The suspension (25 g/L ZnO) was only mechanically mixed at room conditions. Finally the impregnated samples were dried and calcined at 300°C for 1h.

3.2.1.3 Nomenclature

The nomenclature used for the samples is as follows: x_1 Ag/ZnO-PD x_2 x_3 and x_1 Ag/ZnO-IMP x_2 x_3 , where x_1 is the nominal amount of AgNPs (0.1 to 5 % w/w), x_2 means the initial pH (7 to 11) and x_3 means reaction time (0.5 to 5h).

3.2.2 Sample preparation for characterization

3.2.2.1 Inductively Coupled plasma optical emission spectroscopy

For the elemental analysis, 0.01 g of sample was digested with 1 mL of HNO₃ 70%. The sample was diluted with deionized water and filtered (0.45 μm) prior analysis. Total zinc and silver concentrations were measured at 328.1 nm and 213.9 nm wavelength, respectively. The instruments were calibrated each time with standards ranged from 0.25 to 1.25 mg/L for silver and 1 to 5 mg/L for zinc.

3.2.2.2 X-Ray diffraction

For the X-ray analysis, the sample was dried prior analysis at 80 °C for 12 h. Approximately 0.5 g of powder sample was put on the sampler forming a thin layer. The sample could be recovered after the analysis (i.e. nondestructive analysis).

3.2.2.3 Scanning and transmission electron microscopy

Structural and textural properties of ZnO, AgNPs Silver and Ag/ZnO were studied by energy dispersive X-ray analysis (EDX) coupled to SEM microscope. The powder sample was deposited over a doubled-side carbon tape supported by an aluminum pin.

For the TEM observation on EF-TEM and STEM mode, a drop of a previously sonicated solution (Ag/ZnO: methanol) was placed on a TEM grid (Cu, 300 mesh, formvar/carbon film) and dried to air 48 h prior analysis.

3.2.2.4 Nitrogen adsorption-desorption

The sample was powdered and dried prior analyses, then approximately 0.13 g were used for the physisorption analysis under N₂ atmosphere at 77 K. Specific surface area was obtained by use of Brunauer-Emmett-Teller method.

3.2.2.5 Fourier transform infrared spectroscopy

For the chemical analysis, approximately 0.05 g of powder sample (or enough to cover the sampler) was placed on the diamond surface, pressed with the sample press device and collect the data. For liquid sample, a drop of liquid was used in similar way using a concave tip.

3.2.2.6 UV-Vis spectroscopy

UV-Vis absorbance spectra of Ag/ZnO and ZnO powders were obtained from the dry-pressed disk samples. BaSO₄ was used as standard and recorded from 300-600 nm.

3.3 RESULTS AND DISCUSSION

3.3.1 Mechanism of functionalization by preformed nanoparticles

The photocatalytic activity of Ag doped ZnO, has been recently attributed to the size of the nanoparticles (Wang, J *et al.*, 2011) and to the synthesis method (Zheng *et al.*, 2008), therefore making more challenging the comparison between studies result. However, should be considered that the differences in the photocatalytic efficiency are also related to the uncertain metal content in the photocatalyst. It is well known that doping yield is lower than 100% (Gao *et al.*, 2011; Kim, M-R *et al.*, 2009; Zanella *et al.*, 2002), and even some authors have not measured it.

In this thesis, we decided to determine the actual amount of AgNPs attached to ZnO surface in order to assess photocatalyst metal content -photocatalytic performance associations. We prepared Ag/ZnO photocatalyst by two methods: photodeposition and impregnation methods, using stabilized and easy dispersible silver nanoparticles as an alternative approach for ZnO modification.

It is well known that anionic surfactant promotes the dispersion of nanoparticles keeping their particle size intact (Salaün *et al.*, 2010; Salgueiriño-Maceira *et al.*, 2006; Song *et al.*, 2008). However, the experimental conditions like pH and nanoparticles concentration have a great influence on the dispersion stability as will explain.

Therefore, in this work we studied the effect of pH, silver concentration and reaction time on the attachment of AgNPs, stabilized in an alkanethiol surfactant, on ZnO surface. The proposed mechanisms of functionalization, affected by these parameters, are described as follows.

The alkanethiol surfactant, defined by FTIR characterization, is adsorbed to the silver nanoparticles surface via the sulfur atoms ($\text{COOH}-(\text{CH}_2)_n-\text{S}-\text{Ag}$). The resulting monolayer stabilizes the nanoparticles. The carboxylic acid tail groups in this monolayer show an acid-base behavior dependent on the pH. The pK_a of the carboxylic acid group is 4.0. When the pH is higher than 4.0, the carboxyl group is ionized (COO^-) enhancing the solubility due to the anionic center that promotes interactions with water and electrostatic repulsions between the stabilized nanoparticles (Figure 3.1).

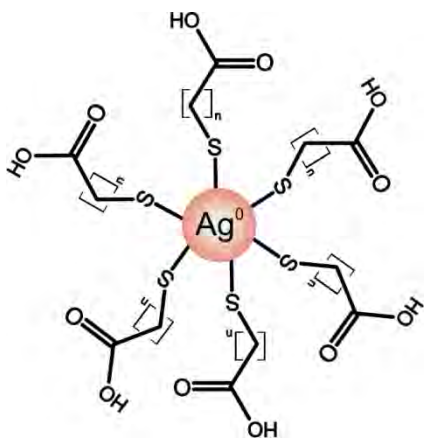


Figure 3.1. Representation of AgNPs stabilized in alkanethiol surfactant.

Figure 3.2A describes the mechanism of functionalization of ZnO by photodeposition method. The mechanism considers the stabilized AgNPs addition using the photogenerated electron-hole pairs (primary reactive species) and free radicals (secondary reactive species) on ZnO surface as follows:

- i. Once ZnO and AgNPs are placed together, the electrical double layer is shortened as reaction time increases.
- ii. Under UV light irradiation, the electron-hole pair diffuses to the ZnO surface to produce free radicals ($\cdot\text{OH}$, $^-\cdot\text{O}$),
- iii. Both primary and secondary reactive species promoted the decomposition of the surfactant, leading to AgNPs deposition.
- iv. The byproducts of surfactant decomposition and their accumulation decrease the pH values from 11 to 8 (Table A.2 of Appendix A).

Ag/ZnO photocatalyst

- v. In addition, formation of ionic silver (Ag^+) also takes place on the ZnO surface due to the direct oxidation of AgNPs (Ag^+/Ag^0 , +0.799 eV vs NHE) by holes (+2.75 eV, vs NHE). The insertion of ionic silver into the crystalline structure of ZnO occurs at the same time as they are reduced again to the zerovalent form (Ag^0) by photoexcited electrons. Such insertion of Ag^+ promote strong interaction between AgNPs and ZnO surface that enhance the electron transport, reduce recombination and improve the photocatalytic activity.
- vi. Finally, non-attached AgNPs are washed out at the end of the functionalization process.

Figure 3.2B describes the functionalization of ZnO by impregnation method. The mechanism is as follows:

- i. The electrical double layer between AgNPs and ZnO is reduced.
- ii. Under alkaline conditions non-ionized form of the surfactant ($\text{HOOC}-(\text{CH}_2)_n\text{-S-Ag}$) does not create electrical repulsion. If the interaction between AgNPs and ZnO surface are strong enough, the wash out of AgNPs could be avoided.
- iii. Besides, high concentrations of AgNPs tend to form silver clusters, as a way to minimize the surface energy, making difficult to reach ZnO surface and they are easily washed away.
- iv. Finally the surfactant is decomposed during the heating process (at 300°C) releasing AgNPs onto ZnO surface.

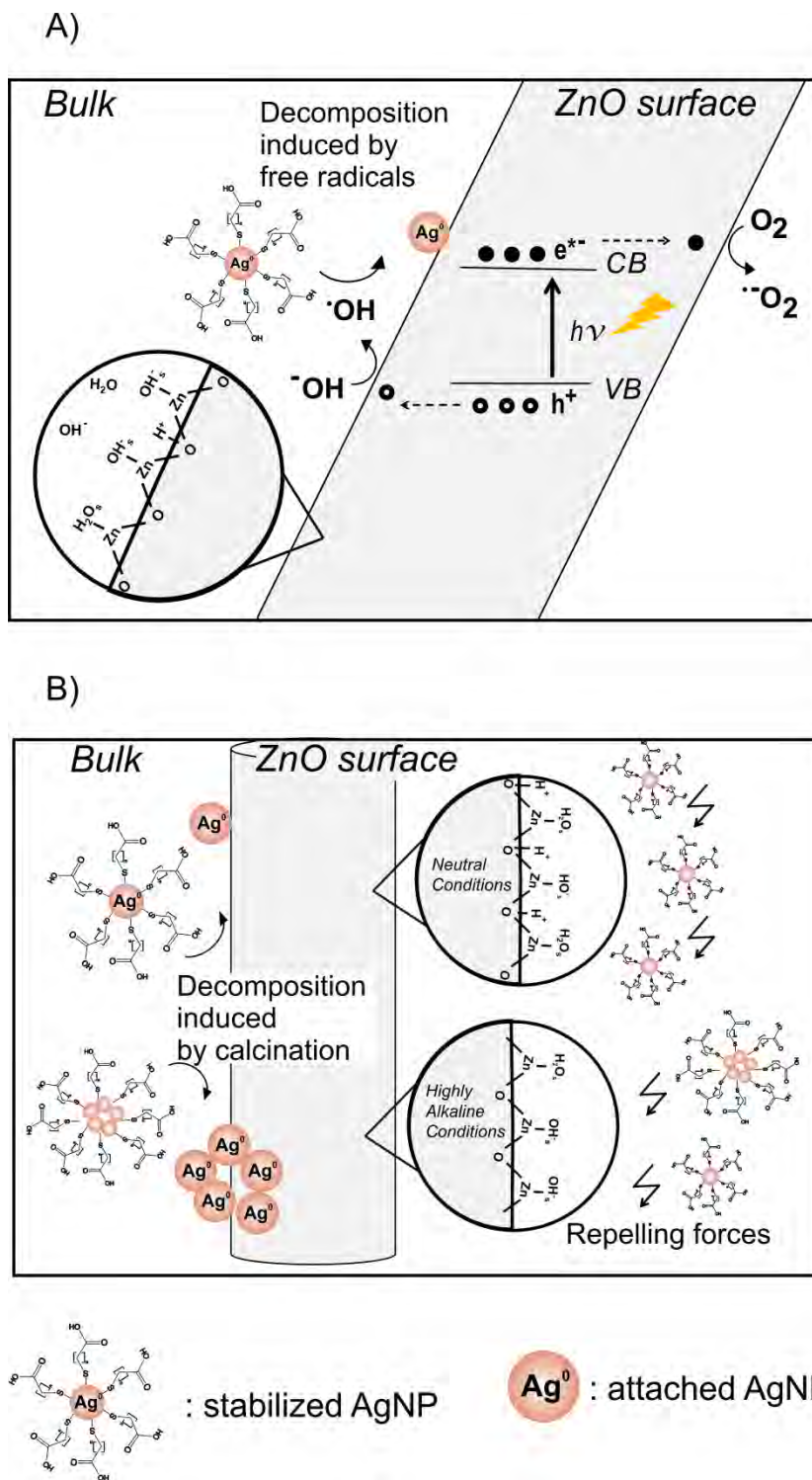


Figure 3.2. Mechanism for functionalization of ZnO with silver nanoparticles by photodeposition method (A) and impregnation method (B).

3.3.2 Effect of synthesis conditions on structural and textural properties

Figure 3.3A shows the X-ray diffraction pattern of Ag/ZnO obtained by photodeposition and impregnation. The diffraction pattern of ZnO shows peaks attributed to crystalline planes (100), (002), (101), (102), (110), (103), (112) and (201) corresponding to hexagonal wurtzite of zinc oxide (card JCPDS 36-1451). The diffraction pattern of the stabilized AgNPs solution exhibits the planes (111), (200) and (220) which matches to face-centered-cubic (fcc) crystal structure of silver (card JCPDS 04-0783). In the diffraction patterns of Ag/ZnO photocatalyst we observed the major plane (111) of metallic Ag, which confirms its presence on the ZnO surface, even when 1 % w/w AgNPs was added.

Figure 3.3A shows that impregnated photocatalyst keep the characteristic peaks of ZnO unchanged. The major plane (101) of ZnO crystallite indicates it's tend to grow along the c axis to form nanorods with both pyramidal tip and plane tip (Figure 3.3B), as corroborated by SEM images (Figure 1.5 and Figure 3.4). Such (101) orientation have been reported recently to show a unique reactivity over acetone and dyes (Angappane *et al.*, 2009; Chang *et al.*, 2013). It is interesting that (101) orientation could expose both the O²⁻-terminated and Zn²⁺-terminated polar faces with highest photocatalytic efficiency (Zhang *et al.*, 2010). Furthermore, Chang *et al.*, (2013) reported a strong binding and less aggregation of dye molecules over O²⁻-terminated face.

Regarding the photodeposited photocatalysts, Figure 3.3C shows a slight peak shift toward low angles and decreased peak intensity for samples with 1 % w/w AgNPs, while no change was detected at 0.1 % w/w AgNPs. Chu *et al.*, (2009) reported the alteration of ZnO microtubules due to acidic pH, which causes a reduction of peaks intensity. The evidence in this work suggest that such changes of ZnO crystalline structure to the insertion of silver nanoparticles by UV irradiation power.

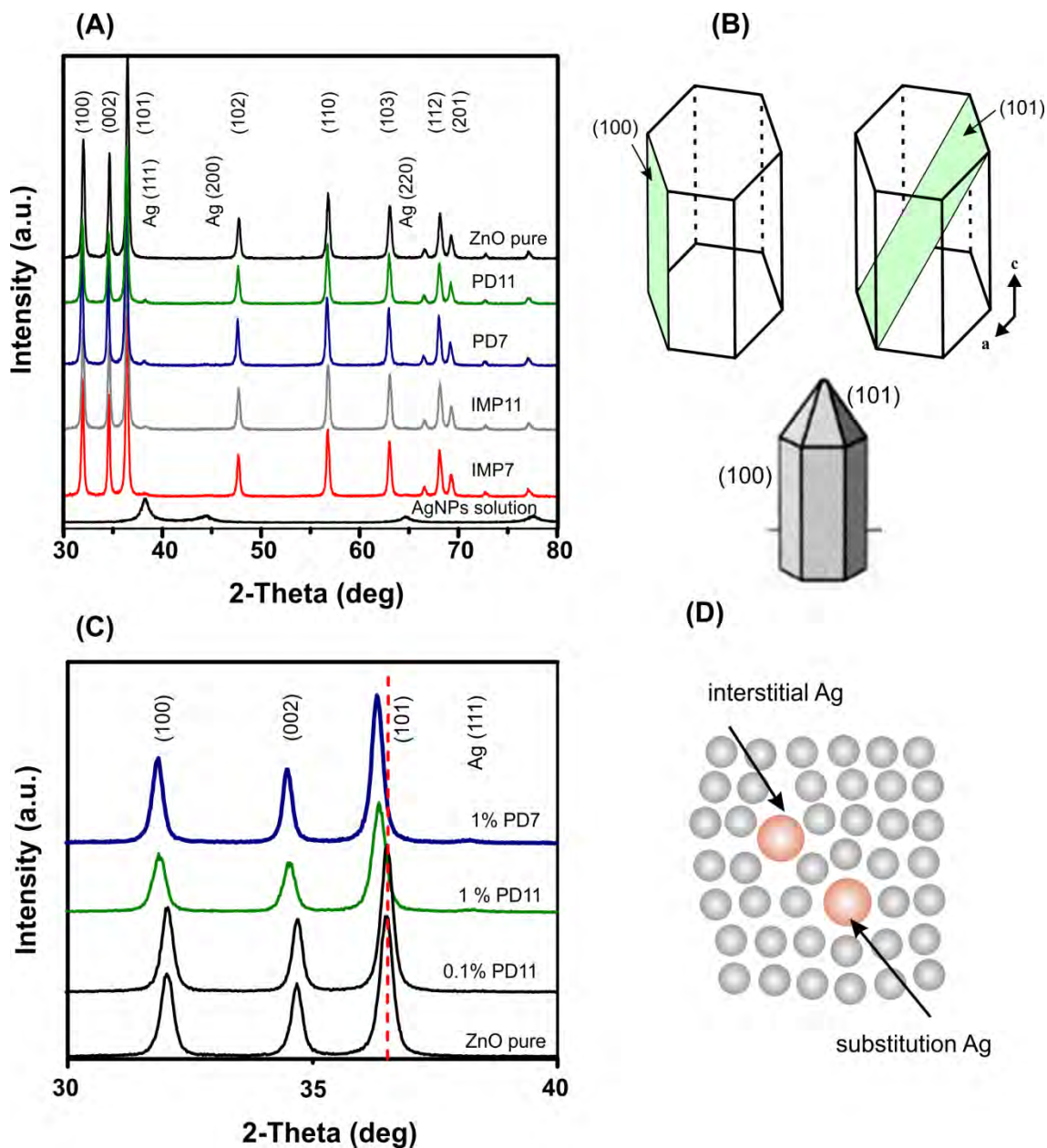
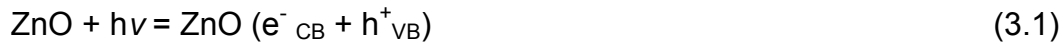


Figure 3.3. XRD pattern of 1%w/w Ag/ZnO obtained by photodeposition (PD) and impregnation (IMP) methods (A). ZnO unit cell showing (100) and (101) planes that lead the grow of nanorod with pyramidal tip (B). Zoom of Ag/ZnO XRD spectra showing the peaks shift (C) due to the insertion of Ag in ZnO crystallite (D).

Ag/ZnO photocatalyst

The calculated lattice parameters of pure ZnO ($a=3.2275 \text{ \AA}$, $c=5.1735 \text{ \AA}$) and Ag/ZnO-PD11,1 photocatalyst ($a=3.2413 \text{ \AA}$, $c=5.1896 \text{ \AA}$) using XRD data shows an increase of the lattice parameters as expected. It has been reported that insertions of metallic ions into Zn sites promotes the expansion of the lattice parameters due to different ionic radii (Ahn *et al.*, 2006).

In our study, the UV irradiation could promote interstitial insertion of Ag^+ (ionic radius $=0.122 \text{ nm}$) on ZnO (ionic radius of $\text{Zn}^{2+}=0.072 \text{ nm}$) as follows: the photogenerated holes in the valence band lead to partial oxidation of AgNPs producing ionic silver (Ag^+) and subsequent insertion on the ZnO crystalline structure (Figure 3.3D). The generation of electron-hole pair on ZnO surface and the redox reactions are described by Equation 3.1 to 3.3.



From the obtained results, we confirmed that the functionalization of ZnO by photodeposition method promotes a strong interaction between AgNPs and the ZnO surface (Zn-O-Ag bond).

It is challenging to control the particle size of metallic nanoparticles because it is the nanoparticle's nature to form agglomerates (Goebbert *et al.*, 2000). Thus, to find out whether AgNPs size was maintained after ZnO functionalization, the average particle size of AgNPs was estimated by the Scherrer formula (Kwon *et al.*, 2002). Table 3.1 shows the increase of the silver crystallite size of Ag/ZnO photocatalyst samples, which is at least twice (15 to 26 nm) that calculated for the stabilized AgNPs (7.11 nm). This result could indicate partial agglomeration of

silver nanoparticles on ZnO surface. This could be explained by the destabilization of the repelling forces between individual AgNPs at such high concentrations (> 1 % w/w) ending on the formation of agglomerates. It is well known that nanoparticles minimize their surface energy by forming agglomerates (Goebbert, C. *et al.*, 2000).

Table 3.1. Physicochemical properties of Ag/ZnO photocatalyst.

Sample	Ag (% w/w) by ICP-OES	Ag (% w/w) by EDX	Average Ag crystallite size (nm) ^a	Average Pore diameter (nm)	BET surface area (m ² /g)	ZnO surface area coated (%) ^b
ZnO	-	-	-	216.63	22.04	-
AgNPs	-	-	7.11	-	-	-
1%PD7,1	1.093	0.78	25.76	100.56	17.58	0.36
1%PD11,1	1.147	1.55	19.34	126.58	16.2	0.54
1%IMP7,2	1.203	1.39	21.97	117.23	17.45	0.46
1%IMP11,2	0.366	1.10	15.25	93.13	16.595	0.21

^aThe average corresponds to experimental values obtained by Scherrer formula from (111) plane from XRD.

^bCalculations of the ZnO surface area coated by AgNPs taking in account data from the column 2, 4 and 6, see calculations in Appendix A.

Figure 3.4 shows TEM images of stabilized AgNPs and 1 % w/w Ag/ZnO photocatalyst. Figure 3.4A shows stabilized AgNPs of spherical shape and defined boundaries. The histogram of the silver crystallite sizes shows AgNPs of 7.8 nm average size (Figure 3.4B) which is in agreement with the average crystallite size by XRD analysis (7.11 nm, see Table 3.1). Figure 3.4C and 3.4D shows the heterogeneous morphologies of ZnO (sphere, tetrapod, rod and other irregular forms). The arrows point toward both AgNPs and AgNPs agglomerates on the ZnO surface, which is in agreement with the XRD suggestions.

The high-magnification TEM image of Ag/ZnO-PD11, 1 sample (Figure 3.4E) shows AgNPs of high crystallinity and homogeneously distributed on ZnO surface. The well-defined lattice fringes and continuity confirm the strong interaction between AgNPs and ZnO.

The histogram on [Figure 3.4F](#) shows the Ag nanoparticle size distribution on both photodeposited and impregnated samples. The results indicate the functionalization of ZnO with single-anchored AgNPs of particle size smaller than the particle size on stabilized AgNPs of the precursor solution. This could be explained by the formation of new metal seeds via direct Ag oxidation by holes ([Equation 3.2](#)) or via indirect Ag oxidation by hydroxyl radicals of more positive potential than Ag^+/Ag^0 pair (Ag^+/Ag^0 , +0.799 eV vs. NHE) as explained before. The oxidation potential is different whether they are surface-bond from oxidation of hydroxyl moieties ($\text{OH}_{\text{ads}}^\bullet$, +1.6 eV vs. NHE) or diffused species from the oxidation of hydroxyl ions and water ($\text{OH}_{\text{free}}^\bullet$, +2.72 eV vs. NHE) (Teoh *et al.*, 2012).

The differences in particle size between both used methods, namely TEM and XRD, are explained in terms of the fundamentals of the analytic technique (detection limits and sensitivity). Transmission electronic microscopy lend to detect single nanoparticles of smaller size that 1 nm in a punctual analysis that become representative of the sample if the number of nanoparticles analyzed (n) is large, while X-ray diffraction is a bulk analysis limited by the silver content in the sample and the assumption of regular particle shape for the Scherrer formula. Furthermore, Sakthivel *et al.* (2004) among other authors claimed smaller size of metal nanoparticles when no peak appears in XRD spectra of metal doped TiO₂ due to the lack of sensitivity of the analysis.

In our study, we describe the presence of the peak corresponding to silver nanoparticles even when the nominal silver content is 1% w/w. However, the calculations of Scherrer formula were influenced for the nanoparticle size population of 15 nm up to 25 nm particle size. This means that XRD analysis does not discriminate between small and large nanoparticles. This does not reflect a conflict for the existence of nanoparticles of smaller size as shown TEM images ([Figure 3.3E](#) and [3.3F](#)).

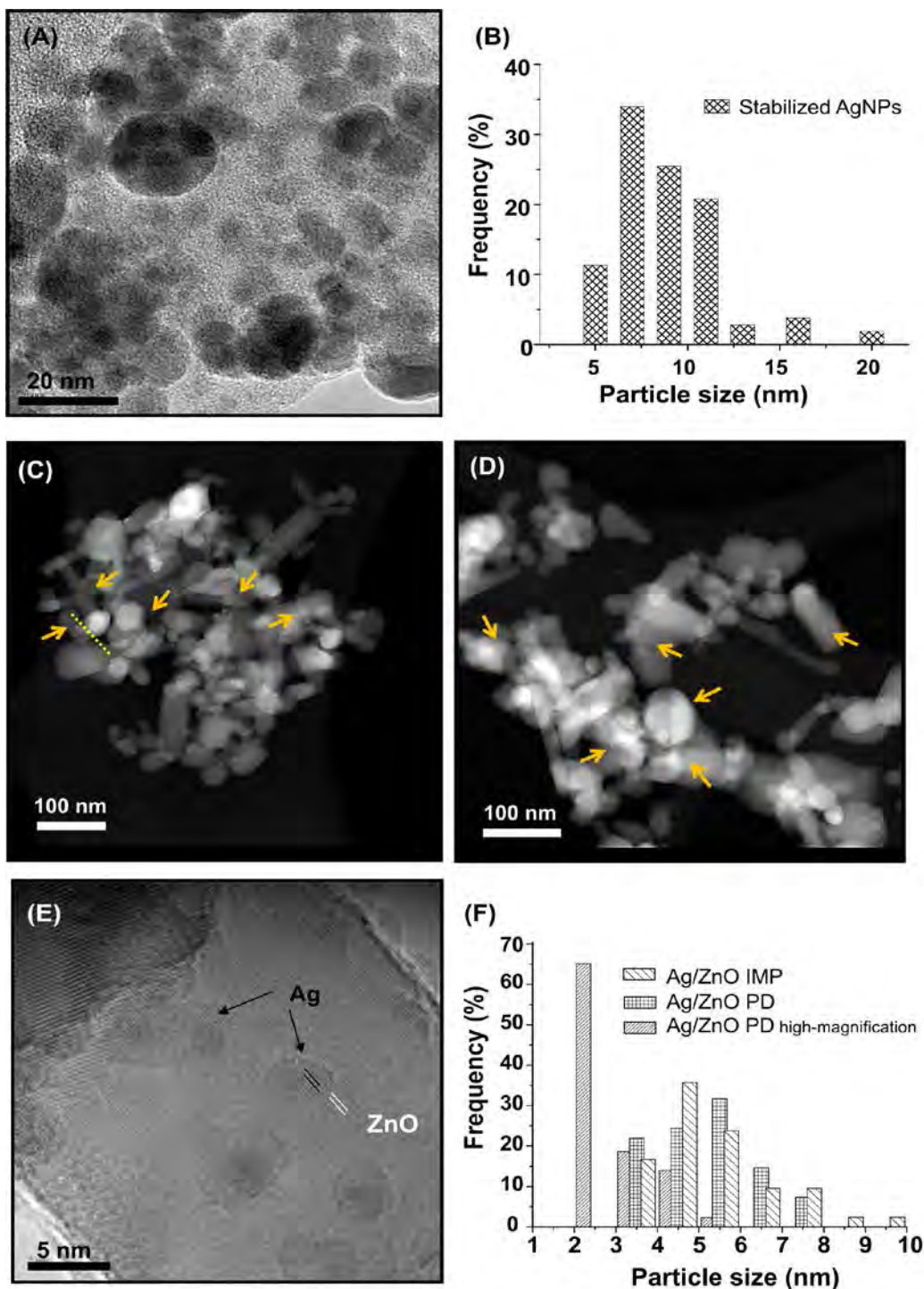


Figure 3.4. TEM images of stabilized AgNPs (A, B) and 1%w/w Ag/ZnO photocatalyst prepared by the photodeposition method (C, E: high-magnification) and impregnation method (D). Frequency histograms of AgNPs size before (B, n=106) and after (F, n=40) functionalization of ZnO.

In order to support TEM observations on homogeneous distribution of AgNPs, two methods of silver quantification were used. The first one was silver quantification in solution by ICP-OES (bulk quantification) and the second was by EDX elemental analysis coupled to TEM (surface and punctual quantification). The results in [Table 3.1](#) shows the congruence between the two quantitative analyses and confirms that the two functionalization methods, photodeposition and impregnation, did not show differences in promoting homogeneous distribution of AgNPs over ZnO.

To our knowledge, only few authors have reported the uniform deposition of metallic nanoparticles over ZnO and CeO₂ starting from pre-formed nanoparticles by high-power techniques (Salaün *et al.*, 2010; Salgueiriño-Maceira *et al.*, 2006), but *our study is the first to show the bulk modification of ZnO with stabilized AgNPs and achieve its homogeneous distribution at ambient conditions.*

The porosity profile of the samples was determined by N₂ isotherm adsorption-desorption. A Type II isotherm with an H3-type hysteresis loop was observed for pure ZnO and functionalized ZnO, which correspond to a microstructure containing macropores (Mukherjee *et al.*, 2010) or micrometric cavities around ZnO NPs ([Figure 3.5](#)). The pore diameter of ZnO samples decreased to half in Ag/ZnO samples ([Table 3.1](#)). This could be explained by two possibilities: (i) macropores obstruction and (ii) formation of agglomerates. As we discussed before, the initial amount of AgNPs and pH are key parameters to induce the agglomeration processes. [Table 3.1](#) shows that BET surface area decreases in all the Ag/ZnO photocatalysts (~ 17 m²/g); however, it was considerably larger than that reported for pure ZnO (7-12 m²/g) and comparable to that of doped ZnO/Ag (10-23 m²/g), previously reported (Mukherjee *et al.*, 2010; Zhou *et al.*, 2010).

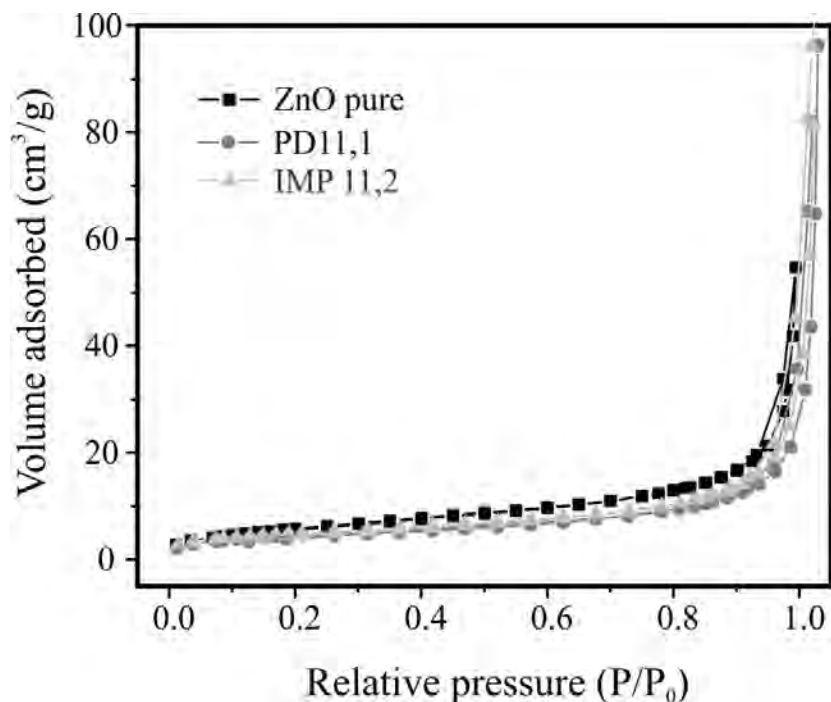


Figure 3.5. N₂ adsorption-desorption isotherm of 1% w/w Ag/ZnO photocatalyst prepared by the photodeposition (PD) and impregnation (IMP) method.

BET surface area has been related to the active surface area for the photocatalysis; however, other aspects must be considered, i.e. morphology and surface defects, crystalline orientation and ionic strength. Therefore, the decrease of BET surface area in our study surely is not a disadvantage, since the photocatalytic performance improves as shows the evidence in chapter 5.

We must point out the need for balance between AgNPs size and the coated ZnO active area as a key parameter for the highest photocatalytic activity. In order to know the nominal ZnO active area coated by 1% w/w Ag, we consider the AgNPs average diameter of the original solution, the nominal amount of AgNPs (1 % w/w=0.00008 mol Ag) and ZnO BET surface area (22 m²/g). The calculations showed that 1.62% of the ZnO surface area would be coated by 7 nm AgNPs. (Calculations are detailed in the [Appendix A](#)). The calculations for Ag/ZnO samples show less surface covered by AgNPs ([Table 3.1](#)) because silver crystallite size from XRD analysis was considered. These calculations show that a small portion of

ZnO surface area was covered with AgNPs for the electron trapping process and decrease of recombination.

The chemical interaction between AgNPs and ZnO surface was analyzed by FTIR spectra. Figure 3.6 shows the FTIR spectrum of the AgNPs solution, the peaks at 3312 and 1637 cm^{-1} can be assigned to the O-H and C=O functional groups, respectively. The weak peaks at 2830 cm^{-1} correspond to C-H bonds from the $-\text{CH}_2$ of the body of the surfactant. The characteristic peak of S-H around 2500 cm^{-1} assigned to the thiol group (Song *et al.*, 2008) was not detected because it was already bound to Ag nanoparticle surface. However, the S atom of the thiol group was detected by EDX analysis on pure AgNPs. These results indicated that the anionic surfactant contains exposed carboxylic acid groups in order to maintain water dispersion of the Ag nanoparticles.

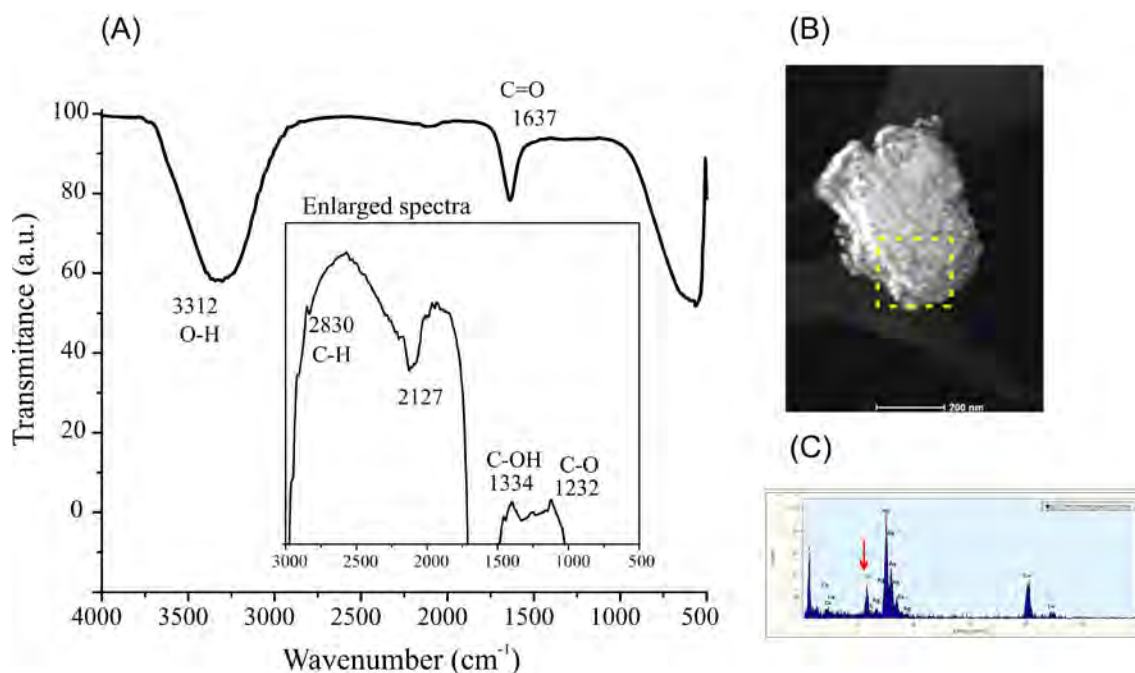


Figure 3.6. FTIR spectra (A) and TEM image (B) of stabilized AgNPs. EDX elemental analysis (C) corresponds to the squared area in B.

Figure 3.7 shows the FTIR spectra of pure ZnO, AgNPs solution and Ag/ZnO. In the spectra of Ag/ZnO, the broad peak at 3400 cm^{-1} corresponds to the O-H which could be due either to (i) water because of the humidity of the samples or (ii), the surface hydroxyl content caused by the functionalization process. The peak at 2650 cm^{-1} can be assigned to the S-H bond due to the accumulation of thiol groups on the ZnO surface. In support of the latter proposal, it should be noted that the bands at 1390 and 1256 cm^{-1} correspond to C-H group of $-\text{CH}_2$, owing to the residual molecules of the surfactant solution remaining after the functionalization processes. This suggests that the functionalization methods proposed induce the functionalization of ZnO and Ag surfaces with hydroxyl ($-\text{OH}$), S-H and C-H groups.

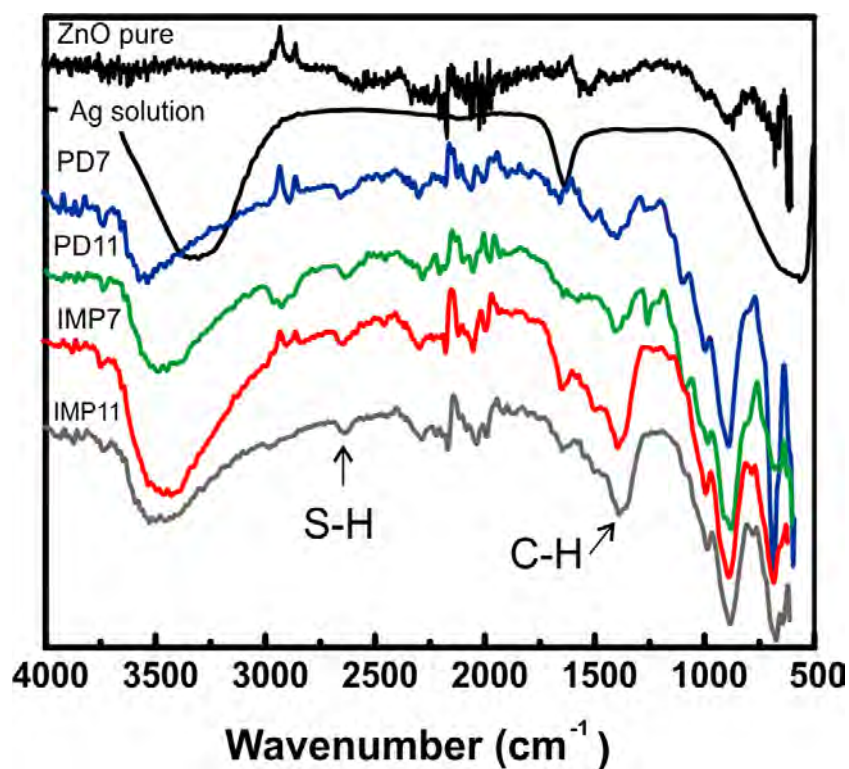


Figure 3.7. FTIR spectra of pure ZnO, AgNPs and 1%w/w Ag/ZnO.

Several authors report that the surface hydroxyl content could be increased if the surface termination of ZnO crystals allowed it, i.e. Zn-terminated polar face Zn²⁺-terminated (Kislov *et al.*, 2009; Zhang, Luyuan *et al.*, 2010). The more surface hydroxyl content there is on the ZnO surface, the more hydroxyl radicals there are for oxidation reaction and higher photocatalytic activity might have the photocatalyst.

3.3.3 Effect of synthesis conditions on optical properties

In addition to the surface properties, the interaction with light defines the photocatalyst performance, and the absorption of light needs to be considered. [Figure 3.8](#) shows the UV-Vis spectra of the samples with two peaks: 360 and 435-460 nm. The first peak at 360 nm was the absorbance corresponding to ZnO due to the optical transition of electrons from valence to conduction band. The band gap (E_g) values were estimated using using the wavelength (nm) of the intersection between the slope of the curve and the Y axis in the following [Equation 3.4](#):

$$E_g = 1240/\lambda \quad (3.4)$$

The bandgap for pure ZnO photocatalyst was estimated 3.20 eV and was increased after silver addition (3.24 eV). The second peak at 435-460 nm corresponds to the surface plasmon (SP) resonance of AgNPs. [Figure 3.8](#) shows a shift of the broader SP peak toward the visible region of the spectrum in comparison with the peak of the stabilized AgNPs solution (410 nm, [Figure 4.A Appendix A](#)). The position and width of SP have been related to the size, content and environment of the AgNPs (Emeline *et al.*, 2012; Xie, W *et al.*, 2010). In our study, this shift and narrow SP peak at 435 nm can be explained by the strong interaction between Ag and ZnO in photodeposited samples.

Despite the interaction strength between Ag and ZnO in the functionalized samples, the effect of surface-localized plasmon resonance of silver nanoparticles remains improving the spectral selectivity in the visible region and the photocatalytic activity as show bisphenol-A degradations experiments.

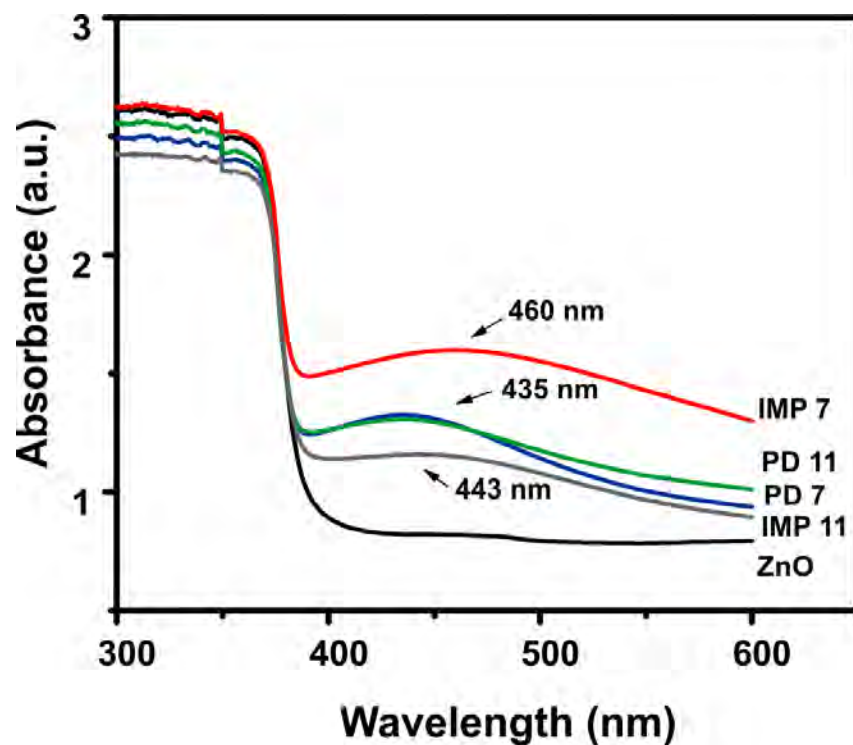


Figure 3.8. UV-Vis spectra of pure ZnO and 1%w/w Ag/ZnO.

3.4 CONCLUSION

We report two functionalization methods, photodeposition and impregnation, which promote homogeneous distribution of AgNPs on ZnO. Nevertheless, the two methods follow different mechanisms of interaction; in the case of the photodeposited photocatalyst, the UV irradiation ensures a stronger interaction between Ag and ZnO.

The 1% w/w Ag/ZnO photocatalysts by photodeposition method showed an increased in the lattice parameters due to the insertion of Ag ions into the ZnO crystalline structure. The decrease in BET surface area suggests the insertion of AgNPs between ZnO macropores. The small size of AgNPs and their homogeneous distribution on ZnO were observed by TEM images. In addition, hydroxyl (-OH) and other functional groups (-CH_2 , S-H) on the ZnO surface and the increased visible light absorption suggest an improvement of the photocatalytic activity under visible light.

Finally, our study is the first to show the bulk modification of ZnO with stabilized AgNPs and achieve its functionalization at ambient conditions

The proposed functionalization methods developed in this chapter represent a useful approach to the modification of photocatalysts with potential applications in environmental water remediation. This topic will be extensively discussed on Chapter 5.

4 Chapter 4. SYNTHESIS OF Ag/ZnO-POLY(ACRYLIC ACID) NANOCOMPOSITES

This chapter presents the synthesis of Ag/ZnO-poly(acrylic acid) nanocomposites through the polymerization of the poly(acrylic acid) in the presence of the photocatalyst. Prior to the polymerization, the surface of Ag/ZnO particles was modified owing to reaction with the epoxide functional groups of a coupling agent GLYMO®. The Ag/ZnO-poly(acrylic acid) nanocomposites were synthesized (i) by vigorously dispersing Ag/ZnO nanoparticles (5-13% wt content) in a water solution of acrylic acid, and (ii) by polymerizing the acrylic acid at 68°C under N₂ atmosphere and in the presence of two initiators (KPS and SMBS) and a crosslinker (MBA).

The objectives of this chapter concern:

- The surface modification of Ag/ZnO photocatalyst
- The synthesis of Ag/ZnO-poly(acrylic acid) nanocomposite,
- The physicochemical and thermal characterization of the nanocomposite.

4.1 BACKGROUND

Zinc oxide (ZnO) modified with Ag is a photocatalyst with an adequate efficiency for photodegradation of dyes (Georgekutty *et al.*, 2008; Wang, J *et al.*, 2011; Zheng *et al.*, 2008) and disruptor compounds in aqueous solution (Clament Sagaya Selvam *et al.*, 2013; Jasso-Salcedo *et al.*, 2014; Patil *et al.*, 2011). Moreover, in spite of Ag/ZnO advantages, like retarded charge-carriers recombination, photostability, low cost and non-toxicity; its application in pilot scale systems is not yet used. The main reason is related to the difficulty of the photocatalyst recovery, immobilization and efficiency using UV/visible light.

The state of the art regarding the ZnO photocatalyst immobilization using natural polymers, such as cellulose, and a variety of synthetic polymers has been

described in introduction (section 1.4). Note that those composites were applied as antibacterial film, conducting film, and optical coatings. This chapter will focus only on current knowledge on composites applied as photocatalyst for water treatment.

The latest results in photocatalyst immobilization, mainly TiO₂, for dyes degradation have shown high efficiencies (>90%) (Kangwansupamonkon *et al.*, 2010; Wang, SQ *et al.*, 2011) as shows Table 4.1. The polymeric matrices reported comprise polyaniline (Leng *et al.*, 2013; Li, Y *et al.*, 2013), polystyrene (Hecht, L.L. *et al.*, 2012), polypyrrole (Lu *et al.*, 2013), and acrylates (Kangwansupamonkon *et al.*, 2010; Wang, SQ *et al.*, 2011).

It is important mention that the dispersion of the photocatalyst is a key factor for the availability of reactive sites. The proper diffusion of water and quantum efficiency can be guaranteed by using hydrophilic, transparent, photochemically stable and mechanical resistant materials. For such reason the *poly (acrylates) could be a good choice for the immobilization of ZnO photocatalyst*. Acrylic polymers are hydrogels that allow effective water transport and contact with the target pollutants due to their hydrophilicity and high wettability (capacity of absorb large amount of water). Also show stimuli-responsive properties to external stimuli such as temperature, pH, solvent composition and ionic strength for novel applications such as drug delivery and agriculture. Hydrogels are generally colorless and visually transparent which permits penetration of light into the matrix. In addition, the modification of their functional groups (-COOH) could lead to selective sorption matrices (Kangwansupamonkon *et al.*, 2010).

The chemical interaction of poly(acrylic acid) and ZnO has been presented by Padilla *et al.* (1990) and Wu *et al.* (1997) in the 90's and recently studied using AFM by Kunze *et al.* (2011). The poly(acrylic acid) molecules preferentially adsorb on the non-polar facet of ZnO forming coordinative bonds between the carboxylic acid group and the Zn-atoms (Kunze *et al.*, 2011). This is important since the

photocatalytic activity of ZnO have been recently associated with polar facets (Huang *et al.*, 2014; Zhang, Luyuan *et al.*, 2010).

Those findings encourage us to hypothesize that Ag/ZnO nanoparticles-poly(acrylic acid) composites lead exposed the reactive sites of the Ag/ZnO photocatalyst for the degradation of organic compounds, i.e. bisphenol-A in aqueous solutions, while the photocatalyst is strongly bonded to the poly(acrylic acid) matrix.

Table 4.1. Photocatalytic degradation of dyes by photocatalyst-polymer composites.

Polymer or copolymer	Photocatalyst	Dye	Degradation efficiency & operating conditions	Reference
Poly(acrylamide-co-acrylic acid)	TiO ₂ 5-20% w/w	Methylene Blue 5 ppm	90% (365 nm, 40min)	Kangwansupamonkon <i>et al.</i> (2010)
Poly(N isopropylacrylamide-co-acrylic acid)	TiO ₂ 8% w/w	Methyl Orange 10 ppm	90% (365 nm, 25 min)	Wang, SQ <i>et al.</i> (2011)
Polyaniline	CoFe ₂ O ₄ -TiO ₂ 3% molar	Methylene Blue 50 ppm	0.0962 min ⁻¹ (254 nm, 60 min) 0.0011 min ⁻¹ (450 nm, 3h)	Leng <i>et al.</i> (2013)
Polyaniline on ITO ^a 0.5-3% w/w	ZnO	Methylene Blue 0.015 mM	98% (254 nm, 2 h) 86% (450 nm, 10 h)	Zhang, H <i>et al.</i> (2009)
Polyaniline on polyethylene terephthalate films	TiO ₂ (AN/Ti molar ratio is 1/1)	Methylene Blue 0.01 mM	17% (365 nm, 2h)	Li, Y <i>et al.</i> (2013)

^a Indium tin oxide glass substrates

4.2 EXPERIMENTAL METODOLOGY

4.2.1 Photocatalyst surface modification

The photocatalyst nanoagglomerates were modified with GLYMO in ethanol as follows. GLYMO is a bifunctional organosilane having a reactive organic epoxide and hydrolysable methoxysilyl groups. The role of GLYMO as surface modifier is to disperse the photocatalyst and link it to the polymer as a crosslinking agent. A total of 0.20 g of photocatalyst (Ag/ZnO or pure ZnO) and 0.3 mL of GLYMO were dissolved in ethanol (3 mL) and sonicated 40 min at 55°C. The solids were washed by centrifugation/redispersion cycles during 10 min at 3000 rpm in ethanol. Finally, the recovered solids were dried at room temperature for 16 h. The nominal weight ratio of the coupling agent used Ag/ZnO:GLYMO is equal to 1:0.13.

The photocatalyst was dried at 70°C for 16 h before used.

4.2.2 Synthesis of poly(acrylic acid) hydrogels

Acrylic acid was dissolved in deionized water and put into the triple-necked flask. The solution was stirred and heated at 68°C under N₂ atmosphere. KPS initiator was added to the above solution in order to initiate the polymerization (zero time). MBA crosslinker and SMBS second initiator were added after 9 min of polymerization time. The gelation time was 10 min and the heating maintained for 3 h (2 h at 68°C and 1 h at 77°C).

The KPS decomposes into free radicals that attack the double bonds of the monomer to initiate the polymerization. During crosslinking, the increase of viscosity is appreciable and the product stop flowing (gel point). The gel time is reached when the hydrogel is completely formed. The SMBS was used as a second source of free radicals to reduce residual monomer content in the final product.

The residual monomer, initiator and water-soluble fraction were removed by immersion of the composites into an excess of water during 48 h.

4.2.3 Synthesis of photocatalyst/poly(acrylic acid) composite

The Ag/ZnO-GLYMO photocatalyst was vigorously dispersed in de-ionized water using ultrasound (1 h) under vacuum to remove the oxygen. The degased suspensions and acrylic acid monomer dissolved in water were added to a triple-necked flask, stirred and heated at 68°C under N₂ atmosphere. KPS and SMBS initiators and MBA crosslinker were added to the polymerization reactor and heated for 3 h (2 h at 68°C and 1 h at 77°C). The residual components were removed by immersion of the final product composite into excess of water during 48 h.

Table 4.2. Composition of the solution used in polymerization.

Component	Quantity	% molar
AA monomer	2.5 mL	
Water	22.5 mL	
KPS initiator	0.01 g	
SMBS initiator	0.005 g	
MBA crosslinker	0.056 g	
PC	0.126 - 0.4 g	
Ratios:		
KPS/AA		0.101
SMBS/AA		0.131
MBA/AA		1.000
PC/AA		5.04-16 ^a

^a Ratio % w/w based in AA monomer.

Abbreviations AA: acrylic acid, PC: photocatalyst, KPS: Potassium persulfate, SMBS: Sodium metabisulfite, MBA: N, N'-Methylenbisacrylamide.

Table 4.3. Operating conditions used for the synthesis of Ag/ZnO-poly(acrylic acid) composites.

Photocatalyst content % w/w	Monomer	Initiator		Crosslinker	Sample code
		1rst	2nd		
0	AA ^a	KPS	-	-	C1-Control ^b
0	AA	KPS	SMBS	MBA	C2-Control
5	AA	KPS	SMBS	MBA	5% composite
8	AA	KPS	SMBS	MBA	8% composite
11.2	AA	KPS	SMBS	MBA	11% composite
12.8	AA	KPS	SMBS	MBA	13% composite
16	AA	KPS	SMBS	MBA	16% composite

^a Reaction total of 25 mL in water base.

^b The control without crosslinker was carried out to measure the polymerization extent and to verify the purity of acrylic acid. This product has a viscous appearance but is not an hydrogel.

4.2.4 Sample preparation for characterization

The samples were characterized in LANBAMA and LINAN national laboratories of IPICYT. The TGA and IR analysis were carried out in the Laboratoire Réactions et Genie des Procédés (LRGP) of the Lorraine University during the doctoral stage.

4.2.4.1 Inductively Coupled plasma optical emission spectroscopy

For the elemental analysis of Zn and Na, 0.01 g of dry sample was digested with 2 mL of HNO₃ 70%. The liquid sample was diluted with deionized water (1000 H₂O:120 liquid sample) and filtered (0.45 µm) prior analysis. The total Zn and Na concentration was measured at 213.9 nm and 588.99 nm wavelength, respectively. The instruments were calibrated each time with standards of 1 to 5 mg/L.

4.2.4.2 Scanning electron microscopy

Structural and textural properties of hydrogel and composites were studied by ESEM under low vacuum. The sample was hydrated overnight and then cut to obtain one small cube shape. The wet gel was placed in aluminum pin of concave shape to maintain humidity in the microscope chamber to be imaged immediately. The analysis time do not exceed half an hour since the sample get dry. Elemental analysis and mapping was carried out using EDX coupled to ESEM microscope.

4.2.4.3 Fourier transform infrared spectroscopy

For the chemical analysis, both powder sample (the enough to cover the sampler) and film samples were placed on the germanium surface, pressed with the sample press device and collect the data. The device used was ALPHA-P, Bruker in the laboratories LRGP.

4.2.4.4 X-Ray diffraction

For the X-ray analysis, the sample is dried prior analysis at 80 °C during 12 h. Approximately 1 g of powder sample was put on the sampler forming a thin layer. The spectrum was recorded at a scanning rate of 0.02°/sec in the 2-theta range of 20-80°. The sample was recovered after the analysis.

4.2.4.5 Thermogravimetric analysis

The photocatalyst content on the composites and the thermal stability were determined by thermogravimetric analysis under air and nitrogen atmosphere. Approximately 5 mg of dry sample were heated in an alumina pan with a scanning rate of 30 °C/min from 200 °C to 700°C.

4.2.4.6 Contact angle

Wetting properties of film samples were investigated by the contact angle measurements. With a syringe, a sessile drop of distilled water was formed and placed at the film surface. Image recording start before the drop touches the surface by a camera coupled to the goniometer. The contact angle was calculated by the Young-Laplace equation using the OneAttension software. Low values of contact angle (<90°) indicate that the liquid wet the solid. If it is greater than 90° it is said to be non-wetting. The reported values are the average on fourth measurements.

4.3 RESULTS AND DISCUSSION

4.3.1 Mechanism of functionalization and composites synthesis

The general mechanism for the immobilization of Ag/ZnO on poly(acrylic acid) matrix involves the use of GLYMO as coupling agent, first by formation of silane monolayers on the metal oxide surface and second by the reaction of the hydrocarbon tail with the polymeric matrix. The proposed mechanism of silanization of Ag/ZnO photocatalyst using GLYMO is shown in [Figure 4.1A](#).

1. The *first step* in the silanization process is the Ag/ZnO photocatalyst dispersion in ethanol to prevent the photocatalyst agglomeration and therefore promote hydrolysis of the metoxysilyl groups (CH_3O^-). This process gets for more reactive silanol groups.
2. The *second step* is the reaction of silane with the hydroxyl groups of ZnO surface forming hydrogen bonds.
3. The *last step* of the silanization process is the condensation of the adsorbed molecules, in which the oxygen binds with the Zn^{2+} -ZnO surface to form very stable structures. It was proposed by Petoral Jr *et al.* (2007) that the oxygen bind with the zinc surface and the condensation gives as results the formation of a self-assembled monolayer (Si-O-Si). Note that epoxy groups of GLYMO are available to perform the compatibility with the polymer.

An esterification reaction between the open ring of epoxy group of GLYMO and the carboxylic groups of the monomer occurs during the ultrasound step, just before start the polymerization process ([Figure 4.1B](#)). The free radical polymerization of acrylic acid is schematized also in [Figure 4.1B](#). The addition of MBA lead to crosslinked poly(acrylic acid) structure. Simultaneously, SMBS initiator terminates the polymerization of unreacted monomers. The purpose of add a second initiator was to reduce the non-reacted acrylic acid from the final composite and reduce the washing process time.

Two possible arrangements of the photocatalyst bonded to the polymer matrix are proposed (see Figure 4.1B):

- (i) a photocatalyst pending from the poly(acrylic acid) chain, and
- (ii) a crosslinked like structure were the photocatalyst is the bridge between two poly(acrylic acid) chains.

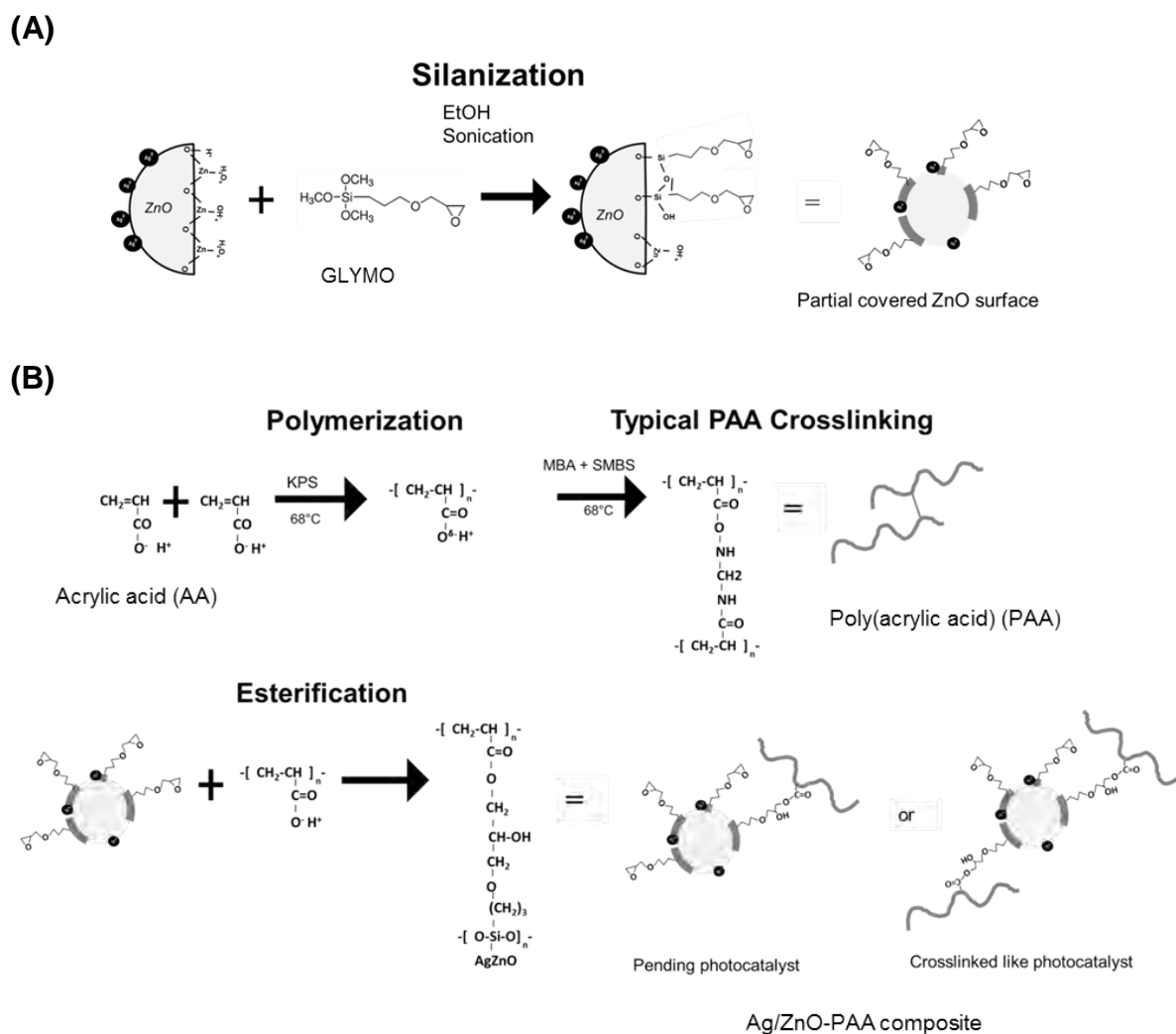


Figure 4.1. Representation of the mechanism of Ag/ZnO silanization with GLYMO (A) and the Ag/ZnO-poly(acrylic acid) composite synthesis (B).

4.3.2 Chemical interaction between Ag/ZnO photocatalyst and the matrix in the nanocomposite

Surface modification of the nanoparticles by coupling agents has been studied recently in order to synthesize polymeric composites with a broad range of applications (Abdolmaleki *et al.*, 2011; Petoral Jr *et al.*, 2007). The coupling agents guarantee both the dispersion of nanoparticles and the linkage between modified nanoparticles and polymer.

In our study, the Ag/ZnO surface modification was followed through FTIR spectroscopic analyses. GLYMO spectrum in [Figure 4.2](#) shows epoxide functional groups corresponding to 916 and 1260 cm^{-1} , such peaks remain in the spectra of modified Ag/ZnO. This means that epoxide is not reacting with ZnO surface, as expected. However, the FTIR spectrum of Ag/ZnO-GLYMO shows disappearance of peaks at 823 and 780 cm^{-1} , corresponding to C-H from the metoxysilyl groups (CH_3O^-) of GLYMO, which indicates a hydrolysis of methoxy group and the adsorption on Ag/ZnO surface by weak bond such as hydrogen bonds, as reported by Mallakpour *et al.* (2012). In addition, the peak at 1030 cm^{-1} , corresponding to the formation of Si-O-Si layer on Ag/ZnO surface, confirms the efficient silanization of the photocatalyst to prevent aggregation by means of steric hindrance.

FTIR spectra of the crosslinked poly(acrylic acid) and Ag/ZnO-poly(acrylic acid) nanocomposite (Ag/ZnO-PAA) with different photocatalyst content are shown in [Figure 4.3](#). The wide peaks in the band 3800 to 3000 cm^{-1} are assigned to hydrogen bond (O-H) probably resulting from the humidity of the sample. The broad band around 3300 cm^{-1} is due to N-H functional groups of crosslinking agent. The peaks at 1400, 1700 and 2940 cm^{-1} correspond to the characteristic carboxyl (C-O), carbonyl (C=O) and $-\text{CH}_2$ groups of pure PAA, respectively.

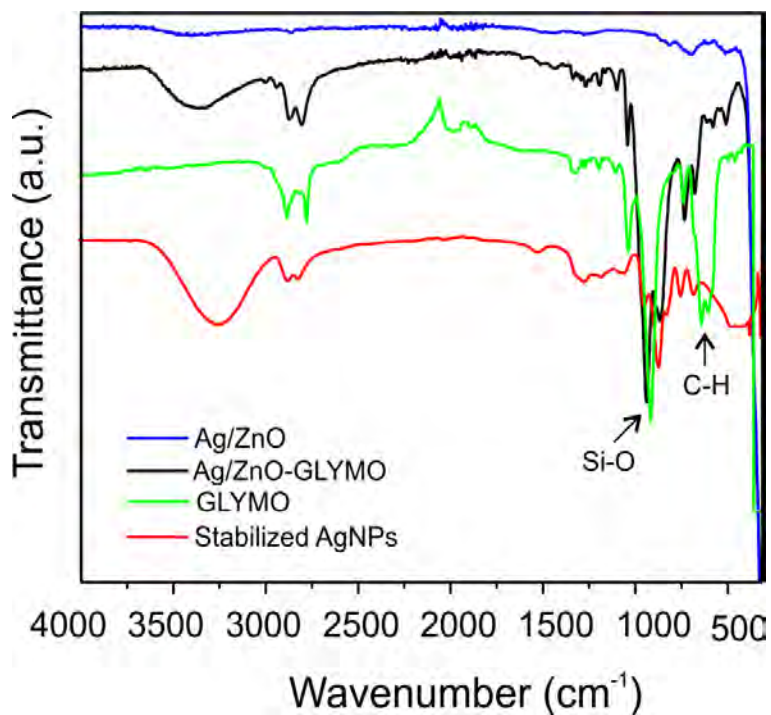


Figure 4.2. FTIR spectra of pure and surface silanized Ag/ZnO photocatalyst.

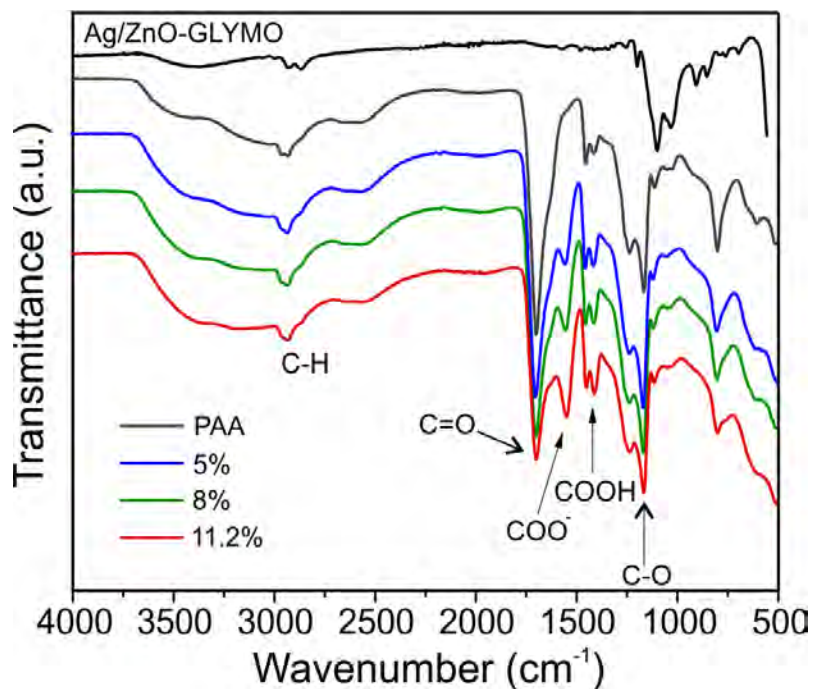


Figure 4.3. FTIR spectra of pure poly(acrylic acid) hydrogels and Ag/ZnO-poly(acrylic acid) nanocomposites. PAA: poly(acrylic acid).

Regarding the Ag/ZnO-PAA nanocomposites, the FTIR spectra show peaks similar to those of pure PAA. In addition, a new intense peak at 1540 cm^{-1} was assigned to the ionized carboxylate group (COO^-). Bejarano-Jiménez *et al.* (2014) report the ionization of carboxylate groups when the PAA was partially neutralized with NaOH since H^+ ions were irreversibly replaced by Na^+ . In our case, the cationic ions were provided by ZnO-Zn^{2+} , in such acidic medium during polymerization, to create conditions of partial neutralization.

Supporting this explanation, Wei, S *et al.* (2007) reported a new peak at 1582 cm^{-1} in spectra of PAA/ Fe_3O_4 composites obtained by impregnation coupled to ultrasound. The authors proposed the occurrence of chemical interactions between the nanoparticles surface and PAA forming a crosslinked structure. They suggest bridging between carboxyl groups of one chain and several nanoparticles. On the other side, Zou *et al.* (2009) proposed the formation of ester-like linkages with the bare ZnO surface $-(\text{C}=\text{O})-\text{O}-(\text{ZnO})$.

In our study, we supposed that direct interaction of PAA with the bare Ag/ZnO surface is more difficult due of the steric hindrance created by the attached GLYMO attached. However the interaction between the free tail of GLYMO (highly reactive epoxy groups) and the carboxylic groups of PAA chain is feasible by an esterification reaction (Sun *et al.*, 2005) (see [Figure 4.1B](#)). The esterification reactions usually lead to the point of gel, which will improve the gelation process of the composite.

4.3.3 Structural and textural properties of the Ag/ZnO-poly(acrylic acid) nanocomposite.

[Figure 4.4](#) shows SEM images of the dry and swollen poly(acrylic acid). We must to point out that the condition of low vacuum (80-130 Pa) in the Environmental SEM microscope chamber allow us for first time to obtain images of 3D network of crosslinked poly(acrylic acid) without exhausting sample preparation such as

freeze-drying procedures (Patel *et al.*, 1996). The hydrogels begin to lose water within the 30 min of the analysis and dehydrated samples are recovered at the end of the process (see [Appendix B](#)). Such condition gives us a time-window of approximately 30 minutes for the analysis.

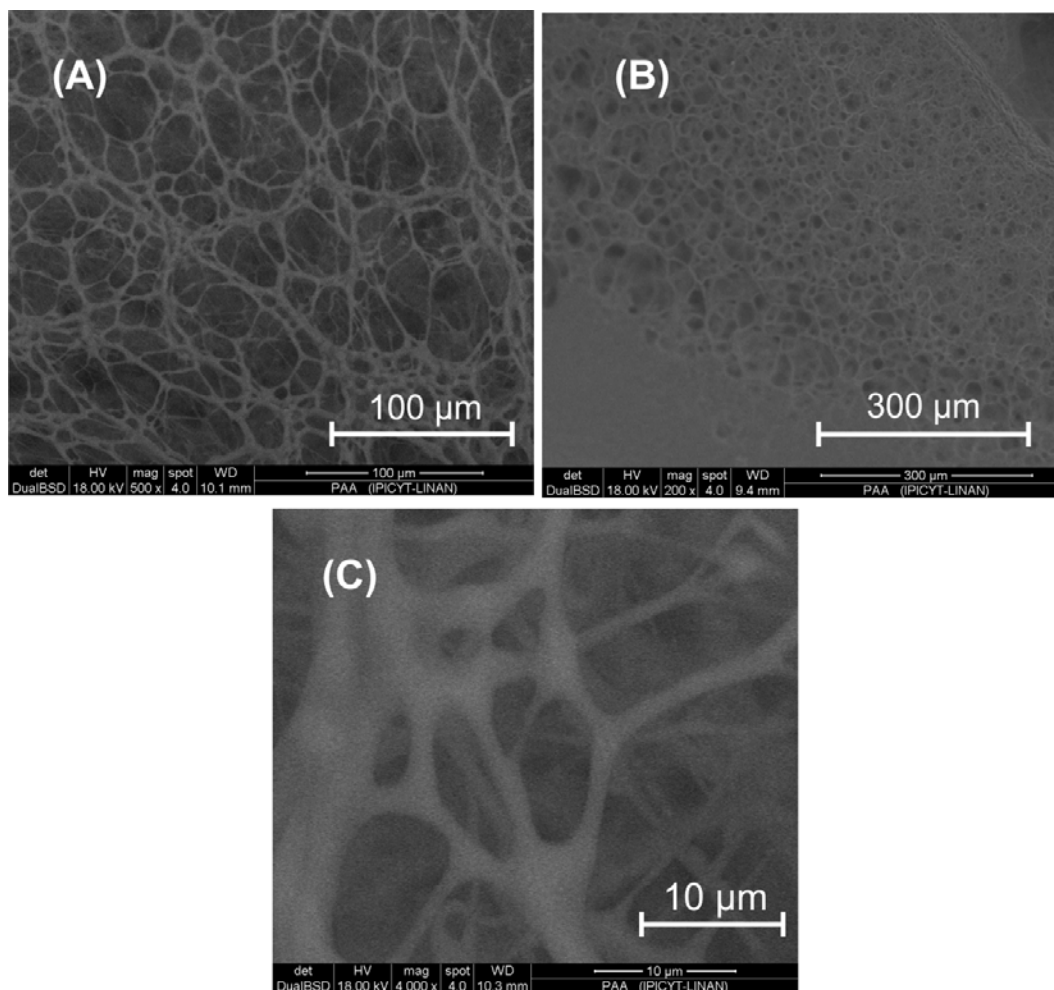


Figure 4.4. SEM images of the synthesized swollen crosslinked poly(acrylic acid).

Figure 4.4 shows the image of the swollen samples with the porous structure of the crosslinked poly(acrylic acid). The pore diameter observed in the image depends on the environmental humidity of the sample during the analysis (Figure 4.4A vs 4.4C), as explained. However based on the images, the pores on poly(acrylic acid) matrix are large enough ($> 10 \mu\text{m}$) for the diffusion of the target contaminant molecule (bisphenol-A molecular length 1.068 nm).

Ag/ZnO-poly(acrylic acid) nanocomposites

The SEM images of the composites are shown in [Figure 4.5](#). The porous structure of the crosslinked matrix is still present in the composites. Based in the images, the photocatalyst dispersion was heterogeneous, showing islands of nanoparticles on both 8% and 11.2% Ag/ZnO-poly(acrylic acid) composites. The chemical analysis by EDX coupled to ESEM of the island in 11.2% Ag/ZnO-poly(acrylic acid) composite was performed to confirm the dispersion of the photocatalyst in the sample.

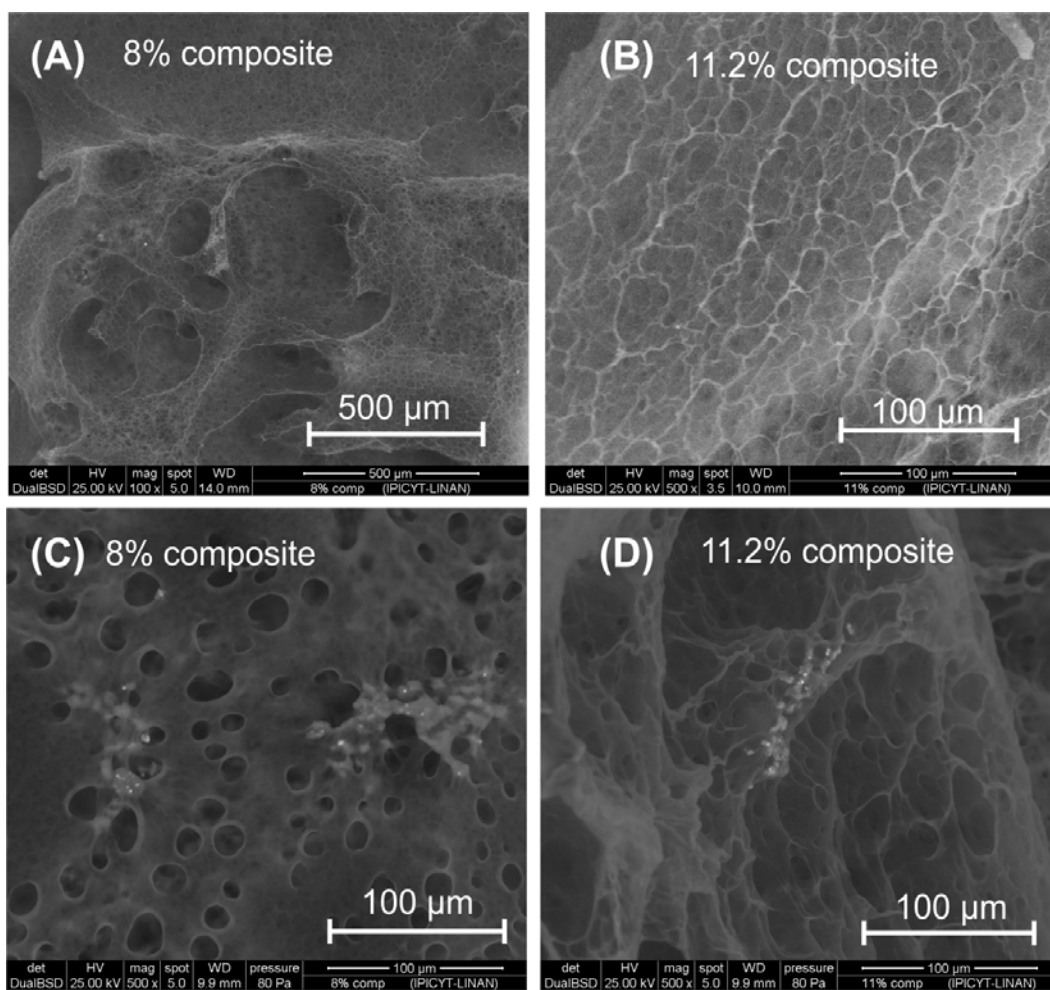


Figure 4.5. SEM images of swollen Ag/ZnO-poly(acrylic acid) nanocomposites. Low magnification (A, B) and high magnification (C, D).

Figure 4.6 shows the elemental distribution maps with a resolution of 128x100. The two elements (C and O) corresponding to the polymeric matrix are present in the complete image. On the other side, Zn is also homogeneously dispersed in the whole matrix indicating the presence of nanoparticles trapped in the polymer. The fourth element, Ag, is found mainly in the zone corresponding with the agglomerations of the photocatalyst at the left side of the image. The elemental distribution maps confirm the dispersion of the Ag/ZnO photocatalyst in the network of poly(acrylic acid). This suggests that the approach used for the synthesis of the composites promote the photocatalyst immobilization and homogeneous distribution.

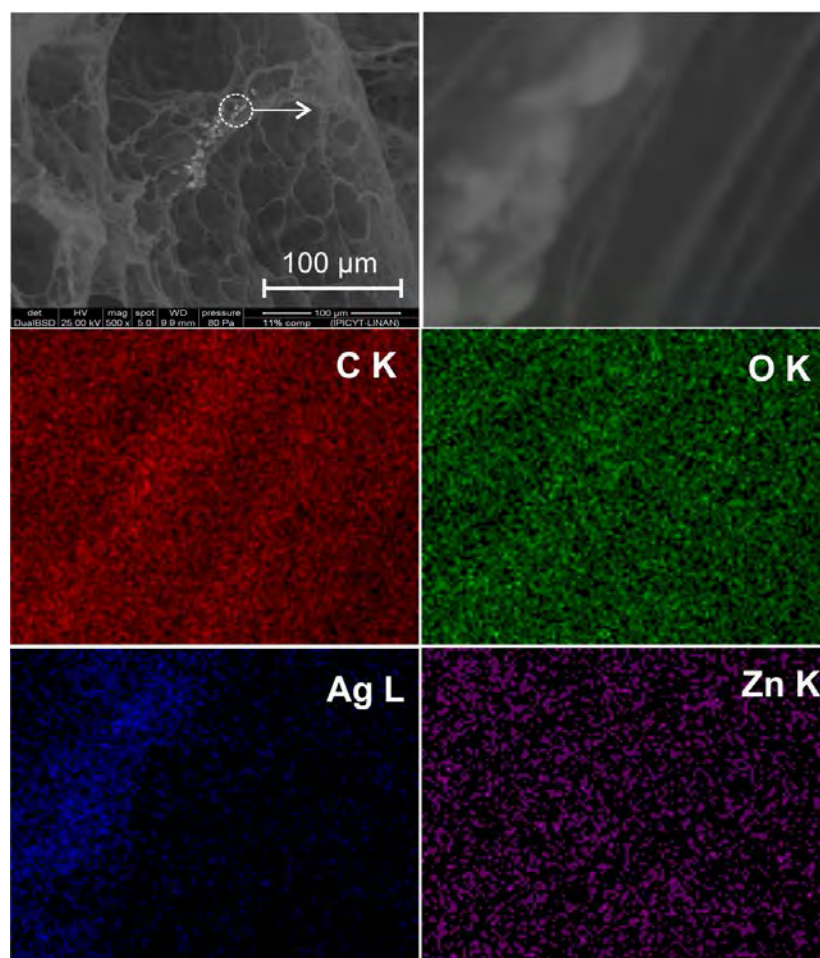


Figure 4.6. Elemental distribution maps of SEM-EDX for the 8% Ag/ZnO-poly(acrylic acid) nanocomposites.

The crystalline structure of pure Ag/ZnO, poly(acrylic acid), and 8% Ag/ZnO-poly(acrylic acid) composite was recorded in the XRD spectra and presented in [Figure 4.7](#). The peaks appearing at 32°, 34.8° and 36.5° are attributed to (100), (002), (102) diffraction patterns, respectively, correspond to hexagonal wurtzite of zinc oxide (card JCPDS 36-1451). Regarding to the crystalline structure of poly(acrylic acid) there is little information about it. Zou *et al.* (2009) report the peak at 52° corresponding to poly(acrylic acid). In our work, no peaks were found to be attributed to crystalline structure of poly(acrylic acid).

On the other hand, the nanocomposite shows an XRD pattern that exhibit a peak around 21.5°, probably due to the arrangements of the polymer chains since the modified photocatalyst is forming crosslinked structures as suggested in section 4.3.1 by FTIR results. Therefore, the interaction between ZnO and poly(acrylic acid) could result on a semi-crystalline structure of the nanocomposite.

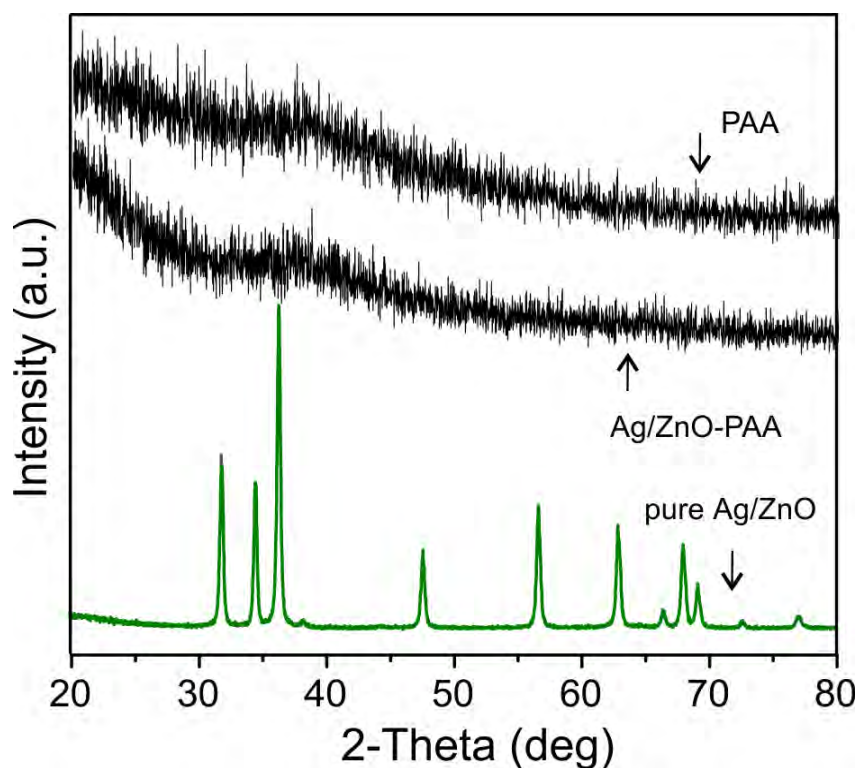


Figure 4.7. XRD pattern of poly(acrylic acid), Ag/ZnO and 8% Ag/ZnO-poly(acrylic acid) composites.

The XRD patterns in this work were obtained at a scan rate of $0.02^\circ/\text{sec}$, however the resolution could be improved at lower scan rate and could show clearly the peaks intensity of (100), (002), (102) planes of Ag/ZnO photocatalyst in the composite sample.

4.3.4 Wettability of the Ag/ZnO-poly(acrylic acid) composite

The wettability is the tendency of the fluid to coat the surface of the solid. This characteristic is determined by contact-angle measurements, and represents the interaction between the nanocomposite surface and contaminated water. Low values of the contact angle ($<90^\circ$) indicate that the liquid wet the solid. High values of contact angles ($>90^\circ$) suggest of non-wetting.

The results show different wetting capacities of the nanocomposites as a function of the photocatalyst content as follows. The contact angle values increases as the photocatalyst content increases: $104.4^\circ \pm 1.34^\circ$, $111.4^\circ \pm 3.75^\circ$, and $117.8^\circ \pm 2.51^\circ$ for 0, 5, and 8 %wt. nanocomposite, respectively. The nanocomposite with the highest photocatalyst content (i.e. 11 %wt. nanocomposite) shows the lowest contact angle: $74.9^\circ \pm 3.4^\circ$. Finally, the contact angle of pure ZnO and Ag/ZnO-PD photocatalysts was $135^\circ \pm 3.65^\circ$ and $130.42^\circ \pm 1.42^\circ$, respectively. The [Figure 4.8](#) shows the contrast on wettability of the pure ZnO and 8%wt. nanocomposite.

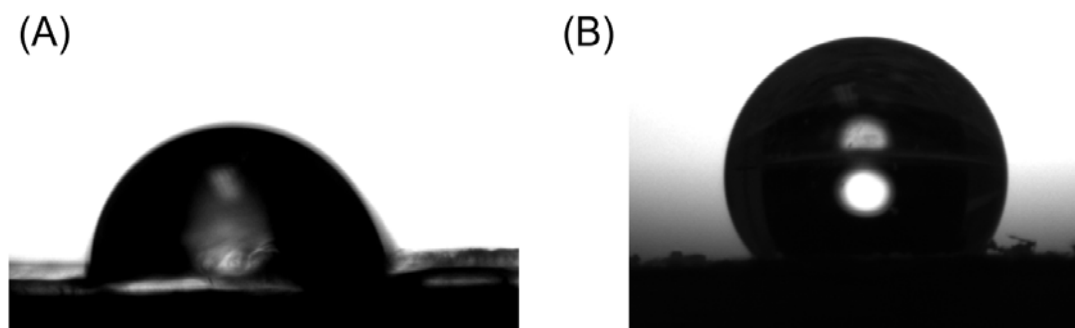


Figure 4.8. Images of water droplet on (A) 8% Ag/ZnO-poly(acrylic acid) nanocomposite (contact angle= $117.8^\circ \pm 2.51^\circ$) and (B) pure ZnO photocatalyst (contact angle= $135^\circ \pm 3.65^\circ$) placed on a glass slide.

The increment on the hydrophobicity of the nanocomposites could be explained by the high hydrophobicity of pure Ag/ZnO photocatalyst. This suggests that the surface properties of Ag/ZnO photocatalyst are exposed at the nanocomposites boundaries. Therefore the photocatalytic sites of the photocatalyst are exposed to interact with contaminant molecules.

4.3.5 Effect of Ag/ZnO photocatalyst on thermal properties of the composite

In this work, we used thermogravimetric analysis to determine the relative amount of photocatalyst inside the polymeric matrix. [Figure 4.9](#) shows the TGA traces of Ag/ZnO-GLYMO, pure PAA and 5 - 11% wt. Ag/ZnO-poly(acrylic acid) nanocomposite as obtained.

First, the estimation of Ag/ZnO silanization was possible using TGA analysis. The weight loss Ag/ZnO-GLYMO in the region 250 – 550°C (6.14% wt) is attributed to the thermal decomposition of Si-O-Si layer on Ag/ZnO surface. Similar results were reported for thermal decomposition of the monolayer on rutile grafted with GLYMO (Godnjavec *et al.*, 2012). The nominal amount of GLYMO was 13%, so the difference in the residues could be explained by the low silanization yield (47%). Low yields are obtained because of the self-condensation of silanols groups before their adsorption on metal oxide surface. Control must be made in order to avoid this undesirable step, like use of acidic media suggest by Xie, Y *et al.* (2010), or alcoholic solutions (Wang, SQ *et al.*, 2011), as in the present work. The amount of polysiloxane structures and GLYMO molecules weakly adsorbed on the surface could be quantified by termogravimetric analysis of washing solution residues. The last statement remains as a perspective of this work.

Regarding the thermal analysis of poly(acrylic acid), all the functional groups are lost at 700°C, however we decided to perform the analysis up to 900°C to assure constant weight. [Figure 4.7](#) shows three weight-loss regions, as described previously by (Dubinsky *et al.*, 2004; Godnjavec *et al.*, 2012) as follows.

- i. the dehydration and formation of anhydride-type structures (at ~100-230 °C),
- ii. the decarboxylation of free carboxylic and anhydride groups (at ~230-340 °C),
- iii. the polymer chain scission and decomposition of hydroxyethyl groups (at ~340-700 °C).

We must point out that the nature of the reactive gas is important for the total decomposition of the sample since the aim is the estimation of the photocatalyst content. We observe the formations of a carbonaceous black residue under N₂ (15.5%), meanwhile a white residue (1.458%, see [Table 4.4](#)) was obtained under air atmosphere during the decomposition of pure PAA. Dubinsky *et al.* (2004) reported that poly(acrylic acid) decomposes above 335°C under argon atmosphere to yields a carbonaceous residue (14.9 %), which match with the results obtained in this thesis (15.5%, see Appendix B), while only 1.2% of residual mass was found under air atmosphere indicating complete oxidation.

[Table 4.3](#) shows the computed values of the Ag/ZnO photocatalyst content obtained by subtraction of the PAA and Ag/ZnO-GLYMO residues from the nanocomposite residues. The nominal content is in good agreement with the calculated values if standard deviation is considered. Then thermogravimetric analysis for the calculation of the photocatalyst content gives very good approximations of both the sample homogeneity and the dispersion of Ag/ZnO particles in the matrix.

The slight differences on the calculated content of photocatalyst in the nanocomposites can be attributed to both the heterogeneity of the sample and/or formation of more stable metal oxides (e. g. silver oxides) during thermal oxidation of the sample increasing the residual mass as suggest Dubinsky, S. *et al.* (2004).

Table 4.4. Thermogravimetric analysis of Ag/ZnO-PAA composites in air atmosphere.

Sample	Residue ^a %wt.	Calculated content %wt.	T ₅₀ ^b °C
Ag/ZnO-GLYMO	93.86		
Poly(acrylic acid)	1.46		391.5
Composite:			
5%	12.71	5.11	420
8%	20.19	8.28	443.5
11.2%	20.15	10.41	447
8% (8 h UV-light exposure)	30.59	22.99	449

^a The standard deviation is ± 0.468 %, n=3.

^b Temperature of 50% weight loss.

The analysis of the TGA curve in [Figure 4.9](#) shows an increase of the thermal stability for all the composites as the Ag/ZnO photocatalyst content increases. The order of thermal stability is 11.2% wt. > 8% wt. > 5% wt. Wu *et al.* (1997) reported that among several composites of PAA-metal oxides (ZnO, CaO, CuO, etc.), PAA-ZnO composite was the most thermally stable. Similar results are reported by Luo *et al.* (2008) where the zinc oxide particles slow down the polymer chains making the composite more stable than the pure polymer matrix. Then the attachment of GLYMO modified Ag/ZnO photocatalyst to the carboxylic acid groups by ester bonds promote the crystallization of the polymer as was corroborated by XRD analysis (see [Figure 4.7](#)).

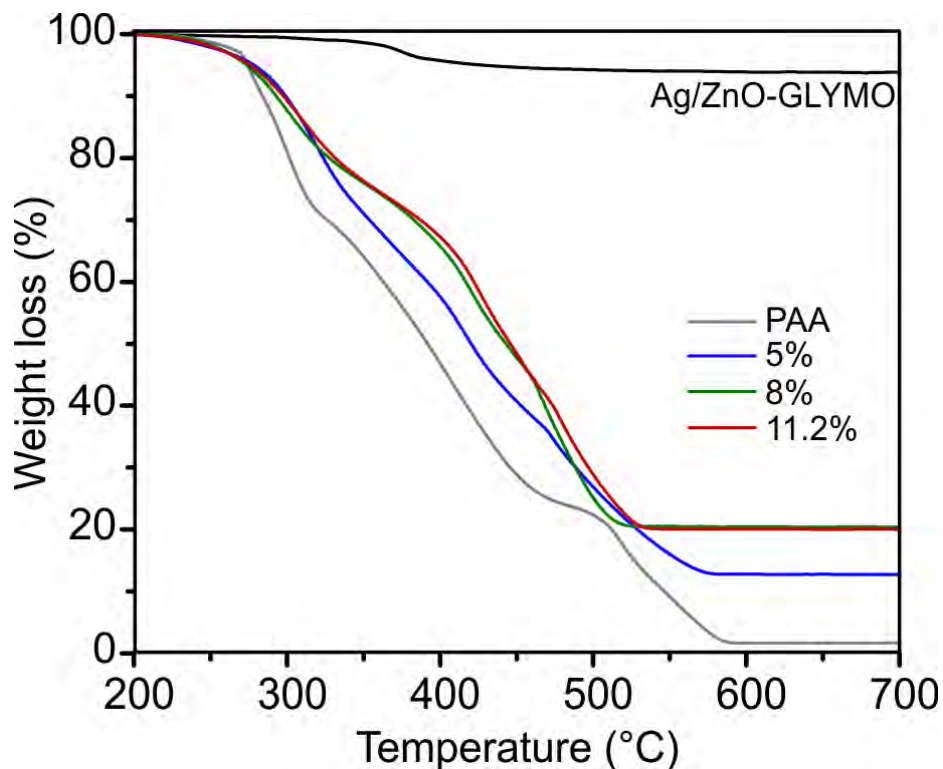


Figure 4.9. TGA curve of silanized Ag/ZnO, pure PAA and Ag/ZnO-PAA nanocomposites.

These enhanced properties give us the potential opportunity of use a resistant composite material as packing material on columns for the continuous treatment of water under UV irradiation. However this last aspect was not complete experience at the terminus of this thesis, but is an issue to be considered in the continuation of this work. Nevertheless the composites were tested in batch reactor configuration to study the degradation of bisphenol-A under UV light. The results will be given in Chapter 5. In the next lines you will find the FTIR results of the composites after being exposed to 8 h of UV light (365 nm) to probe the photostability of the material.

4.3.6 Ag/ZnO-poly(acrylic acid) nanocomposite structure photostability

In this work we must consider the possible degradation of the polymeric matrix. We observed the photodegradation phenomenon in the control composites synthesized without SMBS (data not shown) which were easily dissolved in water. The degradation of composite base on polyacrylates has been reported occurs through two possible ways: (i) degradation by photocleavage and (ii) oxidation initiated by the photocatalytic reactions.

In a *first mechanism*, the attack of C-N linkage of the MBA crosslinking molecule is highly feasible since the bond energy of C-N (305 kJ mol^{-1}) which is lower than C-C (347 kJ mol^{-1}) or C-O (358 kJ mol^{-1}). For *the second mechanism*, Kangwansupamonkon *et al.* (2010) reported the degradation of the TiO_2 /poly[acrylamide-co-(acrylic acid)] composites by free radicals attack. The authors proposed the attacking of the neighboring polymer chains by free radicals leading to carbon centered radicals, e.g. $-\text{CH}_2\cdot\text{COCOO}^-$, and cleavage of the carbon chains.

In our work, the stability of the composite obtained was superior since the hydrogel structure was visible maintained after 16 h of total exposure under UV light (365 nm). In order to corroborate this statement, the FTIR and TGA analysis of 8% wt Ag/ZnO-poly(acrylic acid) composite were carried out (see [Figure 4.10](#)). The FTIR spectra of the composite before and after 8 h of UV light exposition shows similar peaks of the carbonyl and carboxyl groups (no-ionized and ionized) ([Figure 4.10A](#)) This result indicated that the chemical structure of the composite remains unaffected after UV light exposure. On the other hand, the TGA thermogram ([Figure 4.10 B](#)) of the composite indicates 30.59% of residual mass (see [Table 4.3](#)). The differences can be assigned to the accumulation of byproducts of bisphenol-A and polymerization of bisphenol-A molecules (Lu *et al.*, 2013) during photocatalysis process. Note that free radicals are produced during UV light

irradiation and chemical interaction between functional groups of (i) bisphenol-A molecules and/or of (ii) the byproducts of bisphenol-A photodegradation and the carboxylic group of the polymer chain is feasible.

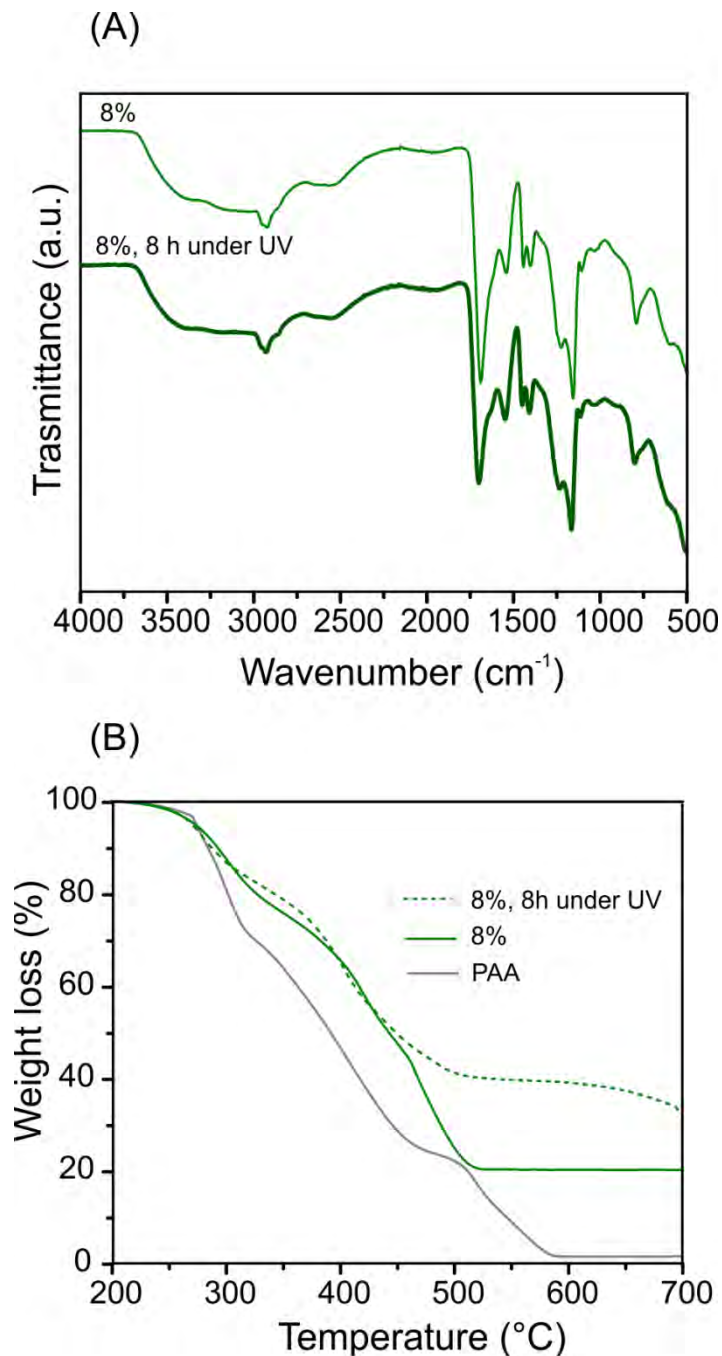


Figure 4.10. FTIR (A) and TGA spectra (B) of Ag/ZnO-poly(acrylic acid) composite under 8 h of UV irradiation exposure.

4.4 CONCLUSION

The structural, textural and thermal characterization shows that the suggested strategy of using GLYMO as coupling agent allows the chemical interaction of Ag/ZnO photocatalyst and carboxylic acid groups of the matrix by ester bonds.

The addition of the 5-11 %wt. of photocatalyst before the polymerization of crosslinked poly(acrylic acid) promotes the crystallization of the matrix as corroborated by XRD analysis. Those arrangements of the polymer chains also improve the photo and thermal stabilities.

Then the designed Ag/ZnO-poly(acrylic acid) nanocomposites gives the advantages of transparency, hydrophilicity and photostability to afford photodegradation of endocrine disruptor in aqueous solutions. Therefore the evaluation of bisphenol-A photodegradation is presented in Chapter 5.

Those enhanced properties lead the potential opportunity of use a resistant composite material as packing material on columns for the continuous treatment of water under UV irradiation.

5 Chapter 5. PHOTOCATALYTIC ACTIVITY ON DEGRADATION OF ENDOCRINE DISRUPTOR, EMERGENT COMPOUNDS AND DYES

This chapter presents the potential application of the Ag/ZnO and Ag/ZnO-poly(acrylic acid) composites on the photodegradation of endocrine disrupting compounds, emergent organic compounds and dyes, under both Visible and UV-light irradiation. It is composed of two parts.

The first part is focused on the study of the photocatalytic activity of Ag/ZnO towards the degradation of bisphenol-A, triclosan and rhodamine-B. The effect of pH, photocatalyst dosage, contaminant concentration and wavelength of light on the degradation of bisphenol-A are presented.

The second part is related to the application of the Ag/ZnO-poly(acrylic acid) composites on the degradation of bisphenol-A under UV light. The reuse and the advantages, such as the reduced photocatalyst photocorrosion, of the new composite are presented.

The mechanisms of the photocatalytic degradation of the tested organic compounds in aqueous solution are also proposed.

5.1 BACKGROUND

5.1.1 Bisphenol-A

The presence of bisphenol-A in the environment start on 30's when it came out as an estrogenic drug used for birth control. Then bisphenol-A was used as a monomer in the synthesis of polycarbonate and as an additive component in the synthesis of polyvinylchloride (PVC), polyesters, epoxy resins, lacquer coatings, etc. The extensive use of plastic containers made of polycarbonate, for food and beverages, make it possible to spread bisphenol-A worldwide. It is well known that any polymerization process is not 100% efficient then leaving bisphenol-A traces that ends in wastewater and freshwater. The quick leaching of bisphenol-A coming out from plastics (Artham *et al.*, 2009) with wrong disposal is the second source for water contamination.

According with the EPA, bisphenol-A is listed within the 146 substances with endocrine disruption properties. Then exposure to this chemical, especially in the case of infants, is undesirable. Studies have shown that bisphenol-A and sex hormones, i.e. estradiol, are equally potent at low concentrations. The potential adverse effects of this chemical in human include obesity, type-2 diabetes and breast and prostate cancer (Artham *et al.*, 2009) despite the controversy studies (vom Saal *et al.*, 2011).

Bisphenol-A has been found in fresh surface water at ppb concentrations (mean concentration 0.081 $\mu\text{g/L}$) (Klečka *et al.*, 2009). Such concentration could be higher on the wastewaters from urbanized and industrial locations. Moreover, the half-life of bisphenol-A in the environment (2.5 to 4 days), the location and time of the sampling makes difficult their detection in the real concentration. An extensive revision of the bisphenol-A concentrations reported around the world is on the reviews of Flint *et al.* (2012) and Klečka *et al.* (2009).

The biological and photochemical degradation of bisphenol-A produces byproducts more stable in the environment and sometimes toxic to marine species (Kang *et al.*, 2006). The safe concentration for aquatic organisms is 1.5 and 0.15 µg/L for freshwater and marine waters, respectively.

A total of 137 papers focuses on the photocatalytic degradation of bisphenol-A using TiO₂ (82.5% of the total papers) and ZnO (5% of the total papers) as catalysts. The number of papers increases every year, however it's represent only the 0.85% of the whole published papers on bisphenol-A that make emphasis on its harmful effects on human life. Is of concerning the amount of studies and laboratories handling this chemical around the world, and only a small portion regarding its decomposition.

5.1.2 Triclosan

Classified as emerging contaminant and endocrine disruptor, this polychlorinated binuclear aromatic compound has been present since 1970 as a powerful antibacterial agent (mean concentration 0.3-20%) in cosmetics, personal care products, textiles (i.e. wool) and a variety of plastic products (i.e. children toys and kitchen utensils).

The average half-life by photolysis is 4-7 days, and even more under anaerobic conditions. Their degradation is also affected by pH value of the water. As the pH becomes alkaline (pH > triclosan pK_a=7.9 to 8.14) the triclosan phenolate anion is susceptible to degradation. The concentration of triclosan in surface water is the ppb levels (median concentration 140 ng/L) (Yang *et al.*, 2011). However, the concentration could reach ppm concentrations on industrial wastewater plants inhibiting the anaerobic (>2 ppm) and aerobic (> 20 ppm) micro-organisms (NICNAS, 2009). In addition, the safe concentration for aquatic organisms (~1 ppm) may be exceeded.

Photocatalytic activity

The photocatalytic processes are an excellent alternative for the degradation of triclosan within minutes. A total of 8 scientific papers have been reported the mechanism of photocatalytic degradation of triclosan (100 ppm to 0.1 ppm) using TiO₂ (Behera *et al.*, 2010; Miranda-García *et al.*, 2011; Rafqah *et al.*, 2006; Yang *et al.*, 2011), which represent an opportunity to test the new photocatalyst such as ZnO.

5.1.3 Rhodamine B

Rhodamine B is the most important xanthene dye present in textile industry wastewater and a model refractory contaminant. The amphoteric characteristic of this compound due to the presence of amino (-NHR₂) and carboxyl (-COOH) groups (Nagaraja *et al.*, 2012) make its degradation pH dependent. The pK_a value for the aromatic carboxylic acid group is 4.0 (Li *et al.*, 2010). The carboxyl group is unionized and the positive charge of one of the nitrogen is present at the pH <4.0. The interesting role of rhodamine as a sensitizer allows the study of the photoactivity of ZnO and silver functionalized ZnO under visible light.

The oxidation of such compounds is feasible in terms of its redox potential as follows. The electrical potential of the photogenerated holes on the valence band of ZnO is 2.75 V, and have to be larger than the oxidation potential of the contaminant to the reaction proceed. The oxidation potential of bisphenol-A and rhodamine B are ~0.6 eV and -1.09 eV, respectively (Gao *et al.*, 2012; Zhao *et al.*, 1998), therefore direct oxidation by holes in the valence band and indirect oxidation by hydroxyl radicals of these compounds is feasible. The oxidation potential of hydroxyl radicals is different whether they are surface-bonded from oxidation of hydroxyl moieties ($\bullet\text{OH}_{\text{ads}}$, +1.6 eV vs. NHE) or diffused species from the oxidation of hydroxyl ions and water ($\bullet\text{OH}_{\text{free}}$, +2.72 eV vs. NHE) (Teoh *et al.*, 2012), however there are positive enough to carry out the oxidation reaction.

Therefore four reasons complement *the motivation on study* the photocatalytic activity of Ag/ZnO photocatalysts and nanocomposites obtained in this thesis: i) the increasing number of industrial locations contaminated by endocrine disruptor, ii) the harmful effects in aquatic organisms, and iii) the lack of literature using the ZnO photocatalysts.

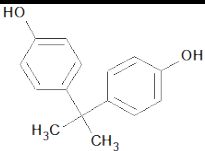
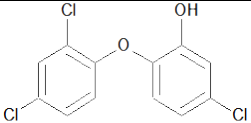
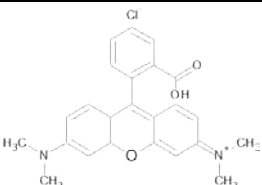
5.2 EXPERIMENTAL METHODOLOGY

5.2.1 Part 1. Ag/ZnO photocatalyst

The photocatalytic performance was evaluated following the time evolution of the contaminant concentration. Aqueous suspensions of the contaminant and the photocatalyst were placed in a glass container. Prior to irradiation, the solution was mechanically mixed for 10 min in darkness. Then the solution was irradiated by UV light using an UV lamp placed at 8 cm from the top of the solution (photoreactor 3UV, see [Figure 2.3](#) and [Table 2.5](#) in Chapter 2). The experiments were carried out at room temperature ($20\pm 1^\circ\text{C}$) without an external oxygen supply. Samples were collected at regular time intervals and centrifuged (3000 rpm, 10 min) to recover the photocatalyst powder. The samples were filtered (0.45 μm filter) before analysis.

The concentration of the contaminants was determined by HPLC or UV-Vis spectroscopy as listed in [Table 5.1](#). Only rhodamine-B degradation was performed in the reactor Oriel (see [Figure 2.4](#) and [Table 2.5](#) in Chapter 2) using an external supply of oxygen.

Table 5.1. Experimental conditions used to evaluate Ag/ZnO photocatalytic activity.

Reactant	Chemical structure	Concentration and reaction volume	Analytical technique of detection
Bisphenol-A, BPA		10-40 mg/L, 100 mL	HPLC ^a , peak at 12.1 min
Triclosan, TCS		20 mg/L, 100 mL	UV-Vis spectroscopy at 280 nm
Rhodamine-B, RB		47 mg/L, 3.5 mL	UV-Vis spectroscopy at 553 nm

^a Details of column conditions are described in Table 2.6 of Chapter 2. The standard deviation of the HPLC measurements is 0.0736 mg/L (n=5).

5.2.2 Part 2. Ag/ZnO-poly(acrylic acid) nanocomposites

An aqueous solution of bisphenol-A (80 mL, 10 ppm) and 0.27 g of dry Ag/ZnO-poly(acrylic acid) composite were placed in a glass flask, magnetically stirred and irradiated in a photoreactor Vilber (see Figure 2.5 and Table 2.5 in Chapter 2) composed of two Hg lamps at 365 nm. The measured temperature of the photoreactor was 50°C. No control over the reactor temperature was planned. The pH of the solution was monitored during the photocatalytic tests (HAch sensION+ pH31 GLP pHmeter). After a defined UV irradiation time, aliquots of the solution were filtered (0.45 µm filter) and the concentration of bisphenol-A was determined by liquid chromatography (UFLC, Shimadzu). Details of the column conditions are given in Table 2.6 of Chapter 2.

Ag/ZnO-GLYMO was used as control of photocatalysts (without poly(acrylic acid)). The calculated dose of pure photocatalyst is 0.27 g/L and 0.19 g/L for 8% and 5% nanocomposites, respectively.

Kinetic parameter calculation

The apparent rate constant, k_{app} , of the contaminant degradation was obtained considering a pseudo first-order reaction from the following mathematical calculations.

The normalized concentration C vs time (t) is plotted and the overall degradation curve is approximated by a first-order exponential decay function of the form (Equation 5.1):

$$C = a \exp^{-bt} \quad (5.1)$$

Then the degradation rate is supposed to obey a typical kinetics behavior of the type (Equation 5.2):

$$r = k_{app} C^n \quad (5.2)$$

$$dC/dt = -a b \exp^{-bt} = -k_{app} C^n \quad (5.2a)$$

The numerical values of the derivative are calculated on the basis of a simple derivation of the exponential function (Equation 5.2a).

A subsequent plot in terms of $\ln r$ vs $\ln C$ can be used for the calculation of the values of the apparent rate constant and the reaction order, n , for each experiment (see Figure 5.1). Via this treatment, the previously assumed first-order kinetics behavior is readily verified.

The normalization of k_{app} in function of the active area was using the BET surface area of the photocatalyst. TiO_2 (Degussa "Aeroxide" P25, BET surface area $50 \pm 15 \text{ m}^2/\text{g}$) was also used as a photocatalyst of reference.

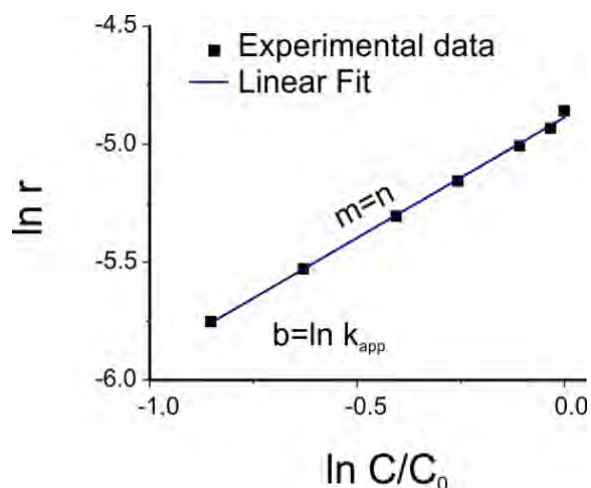


Figure 5.1. Linear plot $Y=mx + b$ to obtain the kinetics parameters (k_{app} and n).

5.3 RESULTS AND DISCUSSION

5.3.1 Part 1. Photocatalytic activity of Ag/ZnO

5.3.1.1 Bisphenol-A degradation

5.3.1.1.1 Effect of functionalization method

The effect of the functionalization method on the photocatalytic activity of the photocatalysts synthesized was studied for the bisphenol-A degradation. Figure 5.2 shows the normalized concentration versus irradiation time. The results indicate that after functionalization of ZnO nanoagglomerates with Ag nanoparticles, the samples enhanced their photoactivity compared with pure ZnO. Figure 5.2A shows that the maximum photocatalytic degradation efficiency corresponding to 1% w/w Ag/ZnO-PD11,1 photocatalyst was 86% after 120 min of irradiation time under UV light. The degradation efficiency was comparable to those reported in the literature using ZnO (Clament Sagaya Selvam *et al.*, 2013; Patil *et al.*, 2011).

The active surface area for photocatalysis has been related to the BET surface area by decades, so the normalization of the reaction rate needs could give some clues. Figure 5.2B shows the apparent rate constant normalized for surface area.

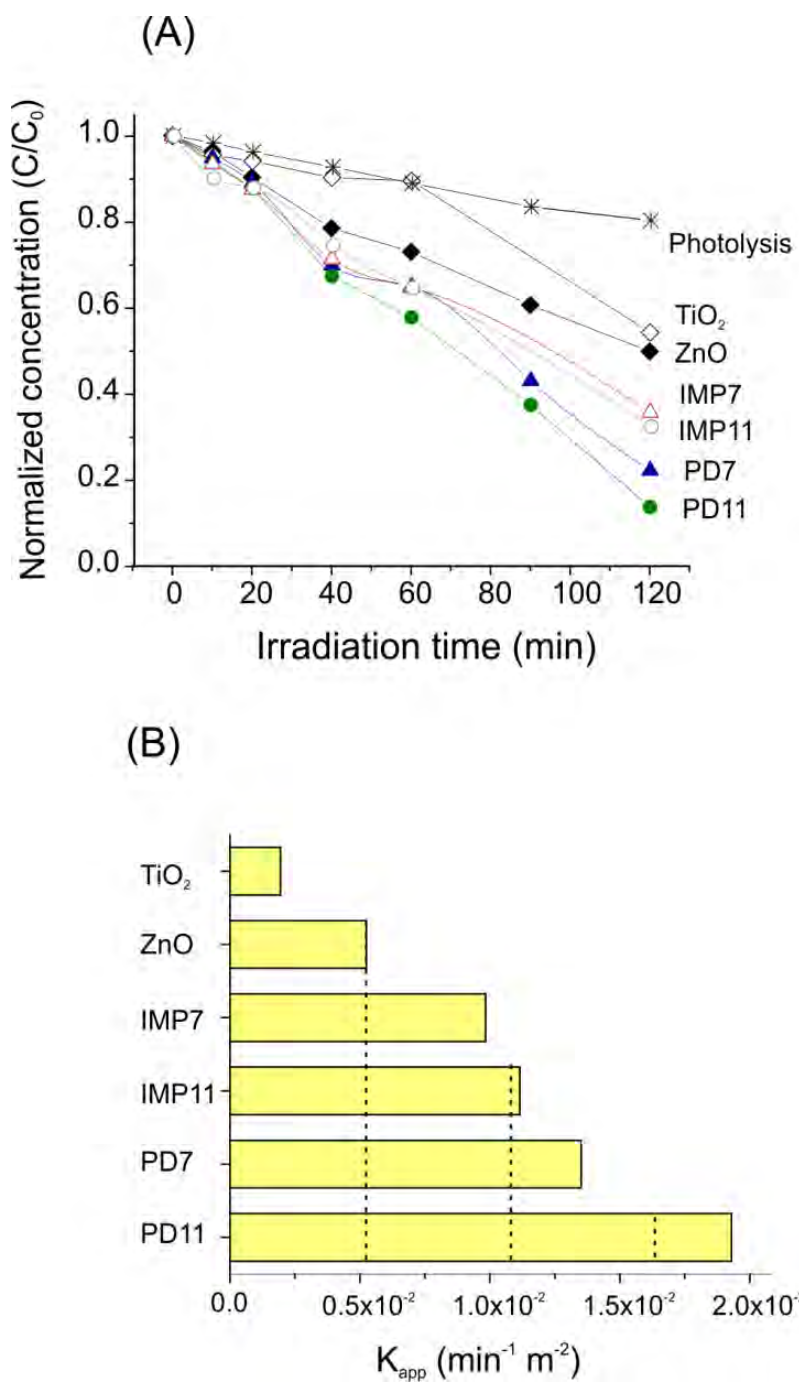


Figure 5.2. (A) Photocatalytic activity of 1%w/w Ag/ZnO and (B) surface area normalized rate constant of bisphenol-A degradation (test conditions: BPA=10 mg/L, photocatalyst= 1 g/L, pH=10.5, reaction time of 120 min for $\lambda=302$ nm).

Photocatalytic activity

The non-normalized rate constant of pure ZnO and P25-TiO₂ was found to be very close (0.00578 and 0.00484 min⁻¹, respectively). However, after k_{app} normalization, pure ZnO was three times the value of P25-TiO₂ because of the differences in specific surface area (see [Table 3.1](#)). Surface area normalized rate constants of Ag/ZnO photocatalyst were higher for photodeposited samples than for impregnated ones. The 1 % w/w Ag/ZnO-PD11,1 photocatalyst was the most active photocatalyst with a normalized k_{app} equal to 0.01929 min⁻¹ m⁻², 3.7 times the value for pure ZnO. The decreasing order of degradation apparent rate constants was Ag/ZnO-PD > Ag/ZnO-IMP > ZnO > P25-TiO₂.

The improvement in the photocatalytic performance of Ag/ZnO was attributed to the silver nanoparticles, which act to trap the photoexcited electron in the metallic bond (Georgekutty *et al.*, 2008; Zheng *et al.*, 2008). In this way, higher primary (e^{*-}-h⁺ pair) and secondary (free radicals, i.e. ·OH) active species remain on the photocatalyst surface longer to improve the photocatalytic activity for oxidation of bisphenol-A ([Figure 5.3](#)).

Note that the specific surface area of P25-TiO₂ is greater than Ag/ZnO-PD (50 vs 17 m²/g, respectively), then higher photoactivity will be expected. Contrary to the expected, the photocatalytic performance was ruled by the catalytic sites of ZnO surface and enhanced by the presence of AgNPs. In addition, the functionalization process that leads a surface chemical composition with hydroxyl ⁻OH, and S-H and C-H groups (see Chapter 3, section 3.3.1) also promotes higher photocatalytic activity.

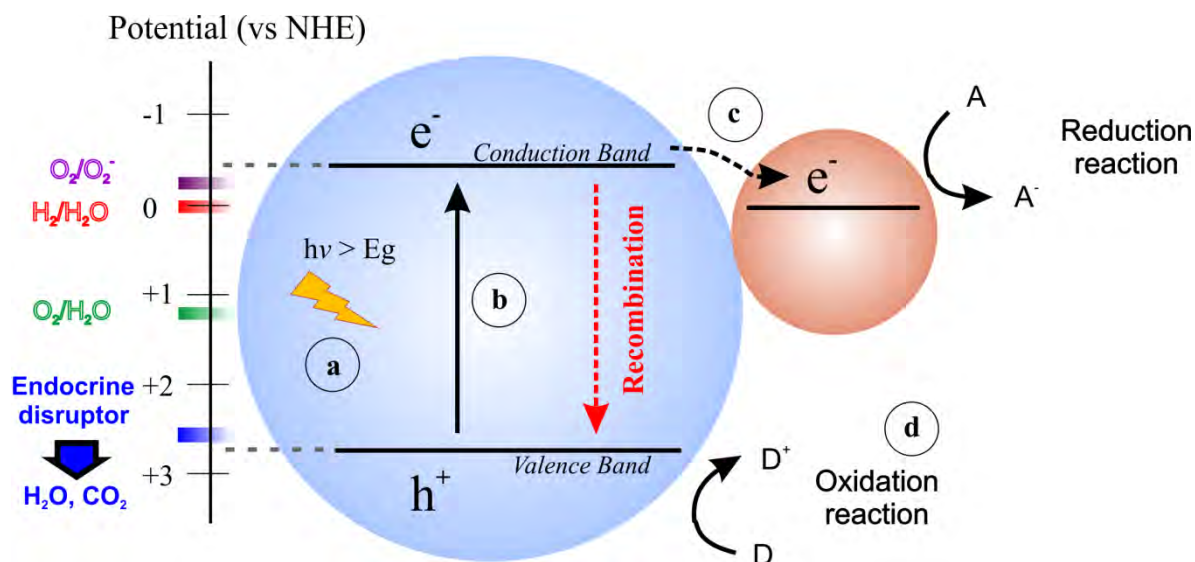


Figure 5.3. Schematic representation of the photocatalytic mechanism of Ag/ZnO where a) the photon energy greater than the bandgap energy is adsorbed by ZnO and generates electron-hole pairs, b) the photoexcited charge carriers spate and migrate to the surface, c) the photoexcited electrons are sink into the silver metal bond and d) adsorbed species are reduced and oxidized by the photogenerated electrons and holes, respectively. (A/A⁻: acceptor species, D/D⁺ donor species).

5.3.1.1.2 Effect of the wavelength

Fourth wavelengths were tested on the degradation of bisphenol-A (Figure 5.4) Three of them corresponding to the UV region of the spectra (254, 302 and 365 nm) and one to the visible region (>450 nm). The bisphenol-A degradation by photolysis (without catalyst) decreases as the intensity of the irradiation light decreases which correspond with less photons achieving the free radicals formation. In the presence of photocatalysts, the maximum degradation efficiency was achieved at 302 nm. The order of degradation efficiency was 302 nm>365 nm>254 nm that correspond with the intensity 2.8 mW/cm²> 3.8mW/cm²> 0.97 mW/cm².

Photocatalytic activity

According with Dimitroula *et al.* (2012) the excitation of the photocatalyst with a low intensity source “low photon fluxes” produces holes at such rate that can be transferred to the adsorbed molecules ($\cdot\text{OH}$ and contaminant molecules). On the other hand, at high intensity irradiation “high photon fluxes” the concentration of holes promotes the recombination process of the electron-hole pairs, reducing the photocatalytic efficiency.

Such explanation fits with observations in this study in which the optimal irradiation intensity is 2.8 mW/cm^2 (302 nm). Another reason for the low photoactivity at 254 nm is the partial sorption of light by the contaminant molecules. Bisphenol-A adsorb UV light at 230 and 280 nm, therefore decreasing the photon flux reaching the photocatalyst surface. Similar observations were reported by (Clament Sagaya Selvam *et al.*, 2013) for bisphenol-A degradation and (Venkatachalam *et al.*, 2007) for 4-chlorophenol degradation under 254 nm light. The mentioned authors compared the degradation between 254 nm and 365 nm, but we were capable to test an intermediate intensity value (302 nm) which is the optimal for the complete degradation of bisphenol-A under the tested conditions.

Regarding the degradation of bisphenol-A under visible light, the highest efficiency was achieved by Ag/ZnO-PD11 photocatalyst. Almost 25% of 10 mg/L of bisphenol-A was destroyed after 180 min i.e. two times the degradation observed with pure ZnO. The improvement is explained because of the silver deposited on ZnO surface (1.147 %w/w of actual amount AgNPs). Silver content allows the sorption of visible light due to the localized surface plasmon (435 nm, see [Figure 3.8](#)) and the storage of the photoexcited electrons because of their capacitive property (Kamat, 2012). Furthermore, the use of the visible region of the spectra provided by sunlight reduces the ZnO photocorrosion and extends their reuse (Pardeshi *et al.*, 2008).

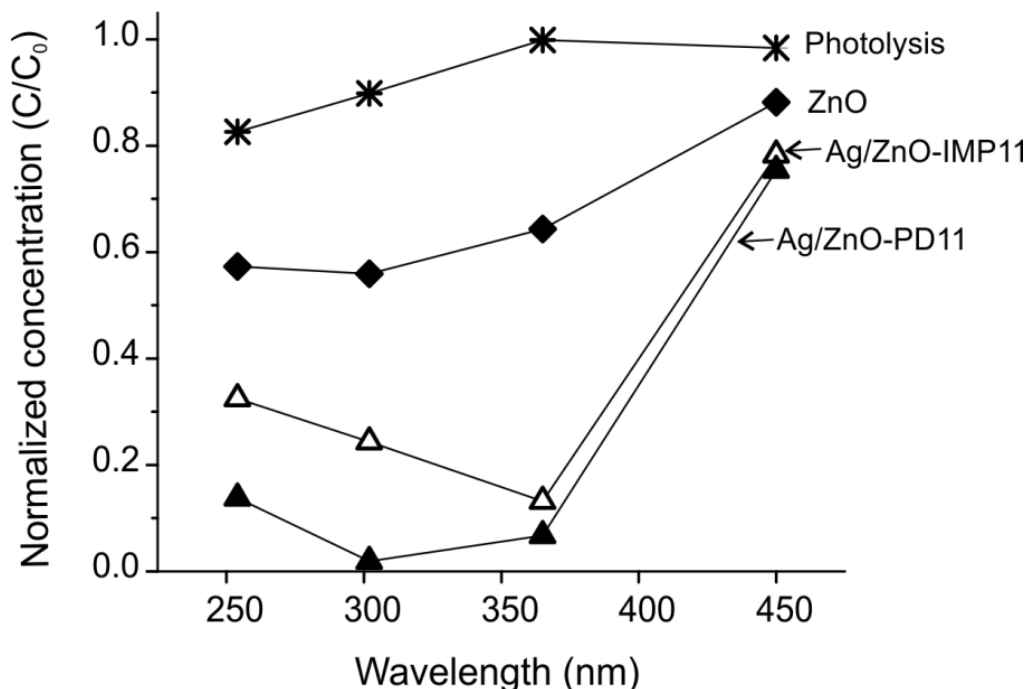


Figure 5.4. Normalized concentration of bisphenol-A at different wavelength using ZnO and Ag/ZnO photocatalyst (test conditions: BPA=10 mg/L, photocatalyst= 1 g/L, pH=10.5, reaction time of 120 min for $\lambda=254, 302, 365$ nm, and 180 min for $\lambda>450$ nm).

5.3.1.1.3 Effect of pH

The pH is an important factor in photocatalysis since it affects the surface charge of the photocatalyst and the redox potential of the contaminant. This section is divided in two sets of experiments i) the effect of initial pH on the range of 2-11 and ii) the effect of pH control during the photocatalytic reaction.

The effect of initial pH on the degradation of bisphenol-A by ZnO is shown in Figure 5.5. The pH was adjusted in the initial solution in the range of 2 to 11 using NaOH (0.05 N) or HCl (0.05 N). The pH was not controlled during the test. The final pH value of the test solution was 6.5-6.8 for ZnO and 7.2 for photolysis (without photocatalyst). The maximum degradation obtained by photolysis was 20% for alkaline pH, which corresponds with the higher concentration of hydroxyl ion (OH^-) and hydroxyl radical (OH^\bullet) in the test solution to perform the oxidation of

Photocatalytic activity

bisphenol-A. In the case of pure ZnO, the best performance was obtained at pH values of 9.4.

This can be explained considering the surface charges of both the catalyst and the contaminant as follows: the surface charges are neutral at $\text{pH}_{\text{PZC}}=8.3$ for ZnO; at $\text{pH}=9.4$ hydroxocompounds of zinc such as Zn^{+2} , ZnOH^+ and Zn(OH)_2 are formed in the solution as shown in Figure 5.5. At the same time, the undissociated bisphenol-A ($\text{HO-C}_{15}\text{H}_{14}\text{-OH}$) exists below the pK_a value of 10.1. Therefore the sorption of bisphenol-A molecules to the ZnO surface is feasible together with their subsequent oxidation.

Even at pH of 10.5, the percentage of Zn(OH)_3^- negative specie is 20% therefore not sufficient to repeal the ionized form of bisphenol-A ($\text{HO-C}_{15}\text{H}_{14}\text{-O}^-$). In addition, the concentration of hydroxyl ions is high then promoting the formation of hydroxyl radicals with high oxidant power.

The photocatalytic degradation of bisphenol-A at neutral and acidic pH is possible, however chemical dissolution of ZnO occurs (Equation 5.3). Similar situation occurs at pH higher than 12 (Equation 5.4, see Figure 5.6).



Therefore, loss of photocatalyst at extreme pH values is feasible. At pH 10.5, $\text{Zn(OH)}_{2(\text{ac})}$ predominates and the minimum solubility of ZnO exists. Thus, in order to prevent ZnO dissolution all tests will be carried out at pH 10.5.

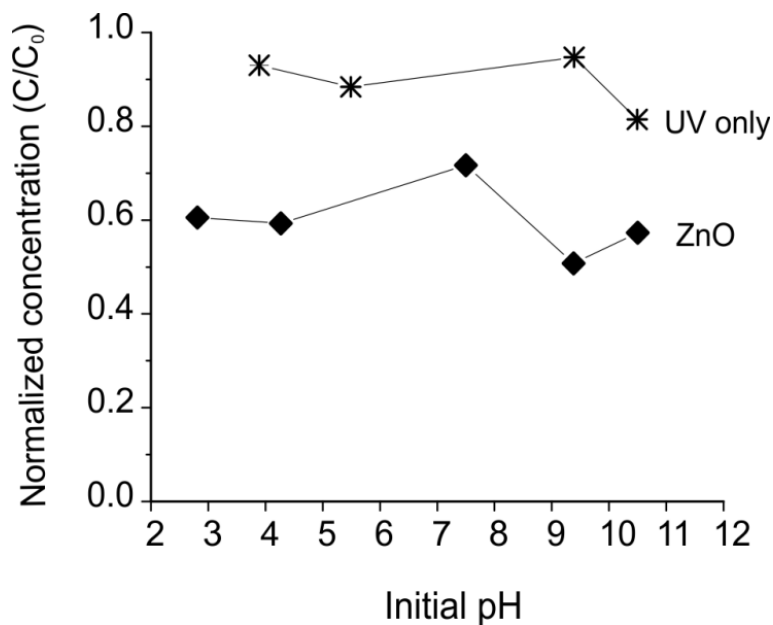


Figure 5.5. Normalized concentration of bisphenol-A at different pH using ZnO (test conditions: BPA=10 mg/L, photocatalyst= 1 g/L, $\lambda=302$ nm, reaction time=120 min).

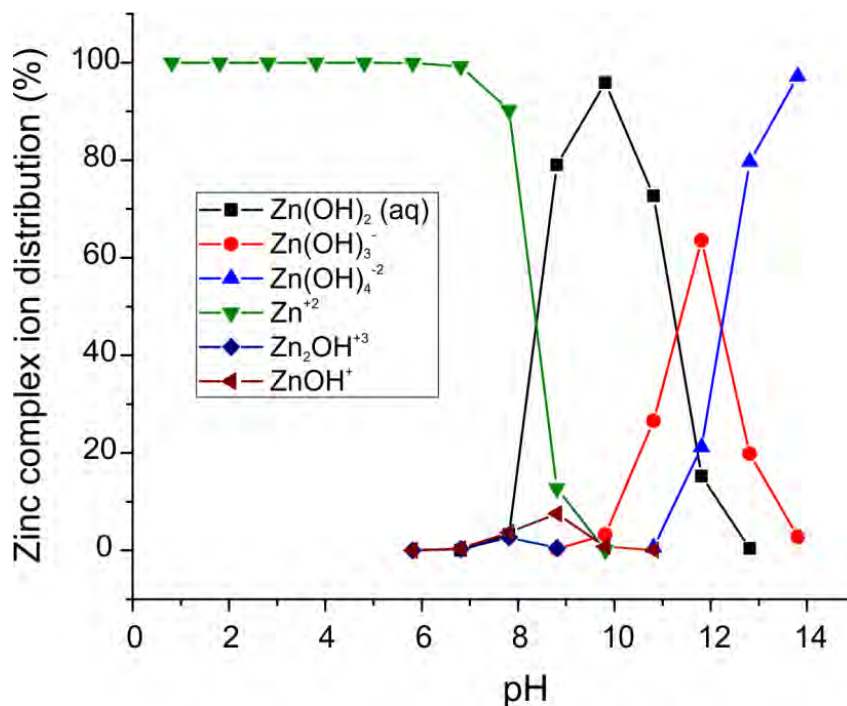


Figure 5.6. Species distribution curve of a solution containing ZnO.

Photocatalytic activity

The results of the effect of initial pH are comparable with the few ones from literature regarding the degradation of bisphenol-A by ZnO. Rahman *et al.* (2005) reported a constant degradation efficiency of 80% of 100 mg/L of bisphenol-A in the pH range of 2 to 8.5, then the degradation efficiency decreased to 60% at pH 11. Clament Sagaya Selvam *et al.* (2013) reported the complete degradation of 200 mg/L of bisphenol-A at pH 8; then, the degradation efficiency decreases at pH below and above the range of 6.5 to 9.

The pH was controlled in a second set of experiments by addition of NaOH drops to the reaction solution. Figure 5.7 shows degradation under pH control and without pH control for pure ZnO and Ag/ZnO-IMP11. Bisphenol-A degradation by photolysis was 21 and 17% under pH control and no pH control, respectively. Complete degradation was achieved for Ag/ZnO-IMP11 at 160 min under both pH control conditions. However the mineralization was not accomplished. The pH control at alkaline conditions guarantees the higher concentration of OH⁻ ions therefore the generation of hydroxyl radicals for oxidation reactions, and an improvement in the photocatalytic efficiency is expected. Contrary to the expected, no changes on photocatalytic performance were observed under pH control and no control conditions for both photocatalysts.

The detection of intermediate products could give us information on the effect of controlled pH on the photocatalytic degradation of bisphenol-A. Figure 5.8 shows the byproducts profile detected during the test. Three peaks (labeled as 1.95RT, 2.1RT and 4.7RT) were found in the chromatogram with retention times shorter than bisphenol-A peak (12.17RT). In the case of Ag/ZnO-IMP11 the major peak at 4.7RT corresponds to the intermediate product which was formed at the beginning, then accumulated, and finally started to be consumed after 120 min. The intermediate at 1.95RT start to increase at 120 min. Based on its retention time, 4.7RT peak corresponds to the decomposition of bisphenol-A, and 1.95RT is the accumulative byproduct of 4.7RT decomposition.

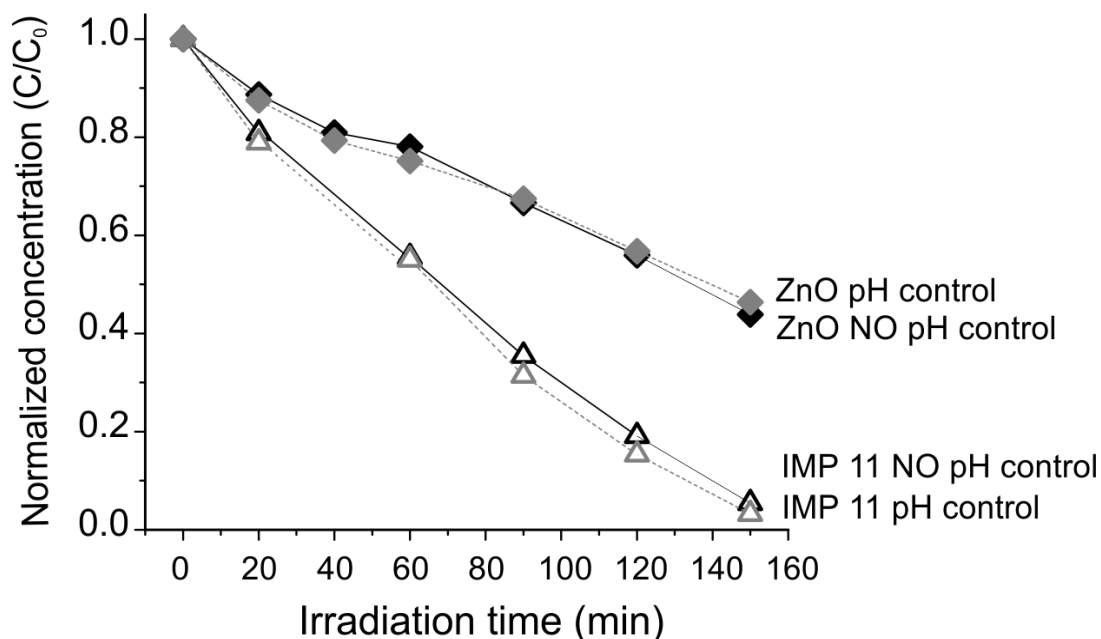


Figure 5.7. Normalized concentration of bisphenol-A at different conditions of pH control using pure ZnO and Ag/ZnO-IMP11 photocatalysts (test conditions: BPA=10 mg/L, photocatalyst= 1 g/L, $\lambda=302$ nm, pH=10.5).

Further detection techniques must be used for the identification of those intermediate products. The byproduct profiles are identical under both pH control and no pH control conditions. However, the profiles of pure ZnO versus Ag/ZnO-IMP11 show slight differences on the amount of those intermediate products. The possible explanation is related to the AgNPs deposited on ZnO surface which enhance the degradation rate of bisphenol-A and the intermediate products as follows.

The role of the silver nanoparticles in Ag/ZnO photocatalyst is to store and shuttle the photoexcited electrons to an acceptor molecule, i.e. oxygen. At the same time the holes are transferred from the excited Ag/ZnO to the adsorbed molecules (e.g. $^{\cdot}\text{OH}$, bisphenol-A, and/or intermediate products) to initiate oxidation processes. Besides the higher quantity of $^{\cdot}\text{OH}$ molecules may produces hydroxyl radicals, the

Photocatalytic activity

byproduct profiles are the same under both pH control and no pH control conditions. Then it can be suggested that the photocatalytic reaction ruled by a slower step that defines the overall reaction rate: the h^+ transference to the sorbed molecules. Kamat (2012) reported that the apparent constant rate of hole transfer is lowest, in tree order of magnitude, that the electron transference, then increasing the possibility of recombination before hole transference to the sorbed ^-OH .

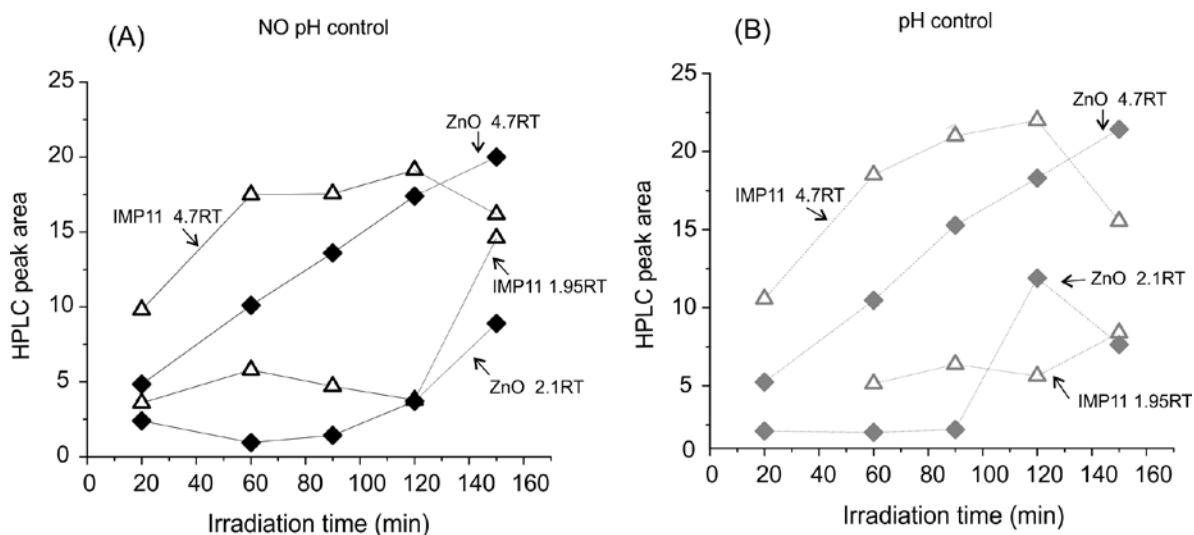


Figure 5.8. Time evolution of byproducts profile in time detected by HPLC during bisphenol-A degradation under uncontrolled pH (A) and controlled pH (B). RT: retention time (min) recorded in the chromatogram (see Appendix C). Test conditions: BPA=10 mg/L, photocatalyst= 1 g/L, $\lambda=302$ nm, pH=10.5.

5.3.1.1.4 Effect of the dose of photocatalyst

In order to determine an optimal photocatalyst dose the range of 0.5-4 g/L was tested as shown in Figure 5.9. The degradation of bisphenol-A increases as the catalyst amount increases up to 2 g/L. Increase of the catalyst doses results in a higher number of active sites for the redox reactions. Higher amount of photocatalyst than the optimal amount hinders the light penetration and the blocking of reactive sites of Ag/ZnO. Also agglomeration hinders the properties gained by the nanosized photocatalyst such as the high surface area and the light sorption selectivity by silver nanoparticles as described in Chapter 3.

Then the optimal dose of photocatalyst is 2 g/L, however in order to compare results between authors 1 g/L is further used in our study. Tsai *et al.* (2009) and Chiang *et al.* (2004) reported the destruction of bisphenol-A by 0.1 g/L of TiO₂, which correspond with a low catalyst dose compared with the dose of ZnO used (1-2.5 g/L) (Patil *et al.*, 2011; Rahman *et al.*, 2005).

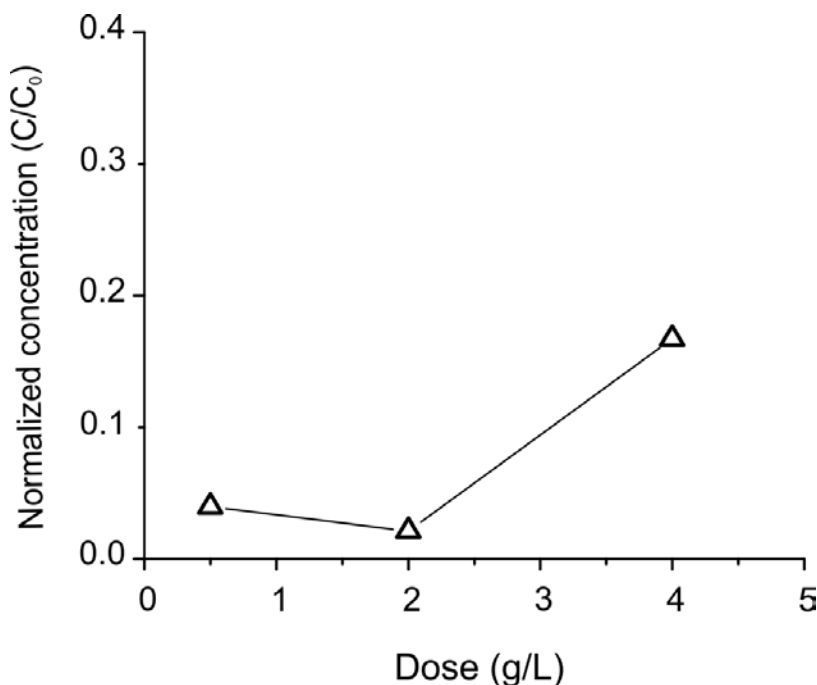


Figure 5.9. Normalized concentration of bisphenol-A at different doses of Ag/ZnO-IMP11 photocatalyst (test conditions: BPA=10 mg/L, λ =302 nm, pH=10.5, reaction time=120 min).

5.3.1.2 Triclosan degradation

Triclosan is an emergent water contaminant which degradation rate can be accelerated by the presence of photocatalysts as tested in this thesis. [Figure 5.10](#) shows the degradation of Triclosan under both visible (>450 nm) and UV light (302 nm). Almost 80% of triclosan was decomposed after 60 min and further degradation was not possible. This could be explained by the photocatalyst poisoning by the chloride ions, without distinction between pure ZnO and Ag/ZnO-IMP11 photocatalyst.

Similar results were reported by Son *et al.* (2009) were maximum 82% of triclosan was decomposed by TiO₂. The byproduct detected was dibenzo-dichloro-p-dioxin that is easily decomposed by hydroxyl radical oxidation to produce non-chlorinated dibenzo-p-dioxin, a less toxic compound (Yu *et al.*, 2006).

Regarding the degradation under visible light, 35% of triclosan was decomposed after 3 h using Ag/ZnO-IMP11. A further study on the intermediate products generated by photocatalysis under visible light is required. For example, the peaks identification using HPLC could give an evidence of the photocatalytic mechanism since the visible light slows down the degradation rate of triclosan. This is important since some the toxicity of some intermediate products is greater than triclosan itself (Sankoda *et al.*, 2011).

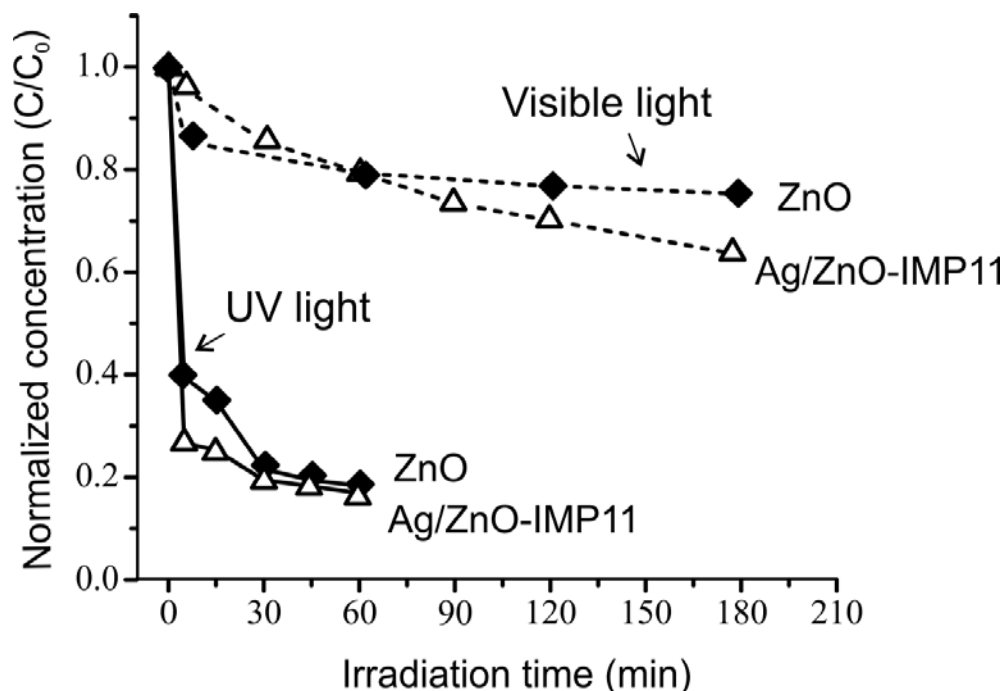


Figure 5.10. Normalized concentration of triclosan in function of time using pure ZnO and Ag/ZnO photocatalysts (test conditions: triclosan=20 mg/L, $\lambda=302$ nm, pH=8.6, photocatalyst= 0.5 g/L).

5.3.1.3 Rhodamine-B degradation

Rhodamine-B is a contaminant and the most important xanthene dye present in textile industry wastewater. It is commonly accompanied by inorganic salts used as additives in textile dyeing processes to promote the adsorption capacity of textile fibers. The photocatalytic degradation of rhodamine-B was tested under oxygen conditions with visible (>455 nm) and UV light (254 nm).

Figure 5.11 shows the degradation of rhodamine-B under UV light. Under dark conditions, the concentration of rhodamine-B did not change after 3 h in presence of pure ZnO and Ag/ZnO-PD11 photocatalysts, which means no sorption of the contaminant on the photocatalyst. UV light irradiation of rhodamine-B solution in absence of photocatalyst (photolysis) did not result in any bleaching after 1.5 h. All photocatalysts showed complete degradation after 12 min under UV light. The best performance is in the order: Ag/ZnO-PD11>Ag/ZnO-IMP11>ZnO.

Photocatalytic activity

The spectra profile of rhodamine-B degradation shows a blue shift at $\lambda_{\max} = 552$ nm (see Appendix C) which indicates the fast de-ethylation of rhodamine molecule within 12 min with simultaneous degradation of chromophore. In addition, the fast decomposition of aromatic rings (peak at 260 nm) indicates the rhodamine-B mineralization using both ZnO and Ag/ZnO. Similar results were reported by (Wilhelm *et al.*, 2007) for rhodamine-B degradation using TiO₂.

Rhodamine-B degradation under visible light is shown in [Figure 5.12](#). Photolysis under visible light is less than 10%. More than 90% of dye discoloration is obtained with Ag/ZnO-PD11 and Ag/ZnO-IMP11. The spectra of the samples show that both peaks of rhodamine-B chromophore (λ_{\max} at 552 nm) and aromatic ring (λ_{\max} at 260 nm) are still present at the end of the test (see Appendix C). This confirms the rhodamine-B chromophore decomposition under visible light but no de-ethylation and formation of aromatic byproducts. These results indicate a different pathway on RB photodegradation under visible light.

Under visible light irradiation, the Ag/ZnO-PD11 photocatalyst showed an increment of 20 % in the rhodamine-B photodegradation as compared with pure ZnO. By contrast, Ag/ZnO-PD11 increased only of 5% under UV light as compared with pure ZnO. Therefore, the AgNPs on ZnO surface were more beneficial to the photocatalytic activity under visible light than UV light. This probably results from the role of rhodamine-B on sensitization of the photocatalyst under visible light and the surface plasmon resonance of AgNPs in the visible region of the spectra, resulting in higher photocatalytic activity.

Regarding the role of rhodamine-B on their own photodegradation, the molecule contains a chromophore group that is excited by visible light (λ_{\max} at 552 nm) and transference the photoexcited electron from the visible-light sensitized rhodamine-B to the conduction band of the photocatalyst and the adsorbed O₂. The oxygen is an electron acceptor that generates superoxide ion radicals ($\cdot\text{O}_2$) and thus

hydroxyl radicals ($\cdot\text{OH}$). The oxidation of rhodamine-B by free radicals continues to produce intermediate products and complete degradation

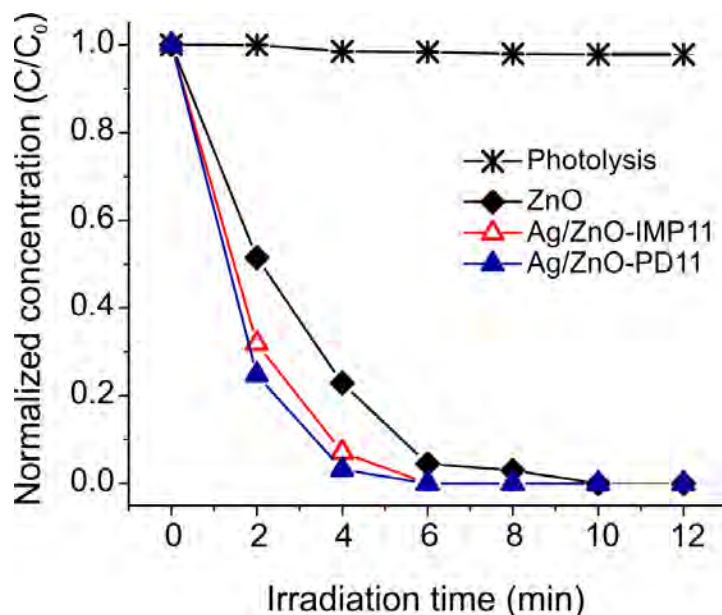


Figure 5.11. Normalized concentration of rhodamine-B in function of time using pure ZnO and Ag/ZnO photocatalysts (test conditions: rhodamine-B=47 mg/L, $\lambda=254$ nm, photocatalyst= 1 g/L).

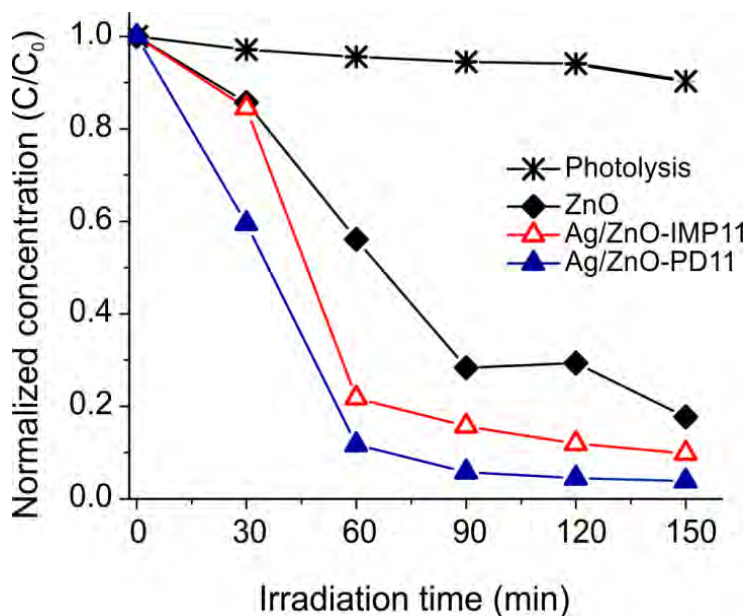


Figure 5.12. Normalized concentration of rhodamine-B in function of time using pure ZnO and Ag/ZnO photocatalysts (test conditions: rhodamine-B =47 mg/L, $\lambda>455$ nm, photocatalyst= 1 g/L).

Photocatalytic activity

The role of silver on the increase of the photocatalytic efficiency is to scavenge the photoexcited electrons of the conduction band and to transfer them to the adsorbed O_2 to produce free radicals ($\cdot O_2$) for rhodamine-B oxidation.

In more details the AgNPs role on the enhancement of the photocatalytic activity under visible is explained as follows:

- i. AgNPs act as electron sinks, enhancing the carrier-charges separation (excited electrons and holes, e^-h^+), increasing the half-life of these primary active species and the subsequent transfer of the trapped electrons to the adsorbed O_2 , an electron acceptor.
- ii. The surface plasmon resonance of AgNPs is excited by visible light, facilitating the excitation of the surface electron and interfacial electron transfer.
- iii. AgNPs creates surface changes that allows increased adsorption of dye molecules, thus leading to more passing of photoexcited electrons from rhodamine-B* radical to the conduction band of the photocatalyst.

5.3.2 Part 2. Ag/ZnO-poly(acrylic acid) composites for bisphenol-A degradation

Figure 5.13A shows the time evolution of the normalized concentration of bisphenol-A during the photodegradation. Under dark conditions the concentration of bisphenol-A change slightly within 3 h. This indicates that a small fraction of bisphenol-A is sorbed by the composite; therefore the sorption step can be avoided. Only a small fraction of bisphenol-A, equal to 8.2%, was destroyed by photolysis (i.e. UV light only), while this fraction increased to 18% when pure PAA was used. At the same time the degradation rate of bisphenol-A using 8% Ag/ZnO-PAA composite leads to an overall decomposition of 47%.

Although this percentage is inferior to the obtained using pure Ag/ZnO-GLYMO (i.e., 70%), it becomes evident that the immobilization of the photocatalyst can achieve comparable photodegradation efficiencies while providing a series of additional advantage at the same time (e.g., reduced photocatalyst loses, possibility to implement continuous systems, etc.).

The degradation of bisphenol-A increases as the Ag/ZnO content increases: 8% wt > 5% wt >> pure PAA. This result supports the findings of good dispersion of the photocatalyst inside the matrix as presented in Chapter 4 and the highly exposed catalytic sites in the composite.

In an attempt to study the deterioration of the photocatalytic efficiency of the composites, the 8% wt. Ag/ZnO-PAA composite was used in a second consecutive cycle without washing. The results show that its photocatalytic activity was kept relatively constant, corresponding to a photodegradation of bisphenol-A equal to 47% and 64%, for the 1st and 2nd cycles, respectively, as shown in Figure 5.13B. In addition, the chemical structure of the composite remains unaffected after 16 h of UV light exposure as shows the FTIR analysis (see section 4.3.6 of Chapter 4). Thus, these results suggest that the poly(acrylic acid) matrix prevent Ag/ZnO

Photocatalytic activity

photocorrosion and maintain a constant photocatalytic activity. Similar results were reported by Zhang, H *et al.* (2009) showing that PANI suppressed the ZnO photocorrosion during methylene blue degradation under UV light.

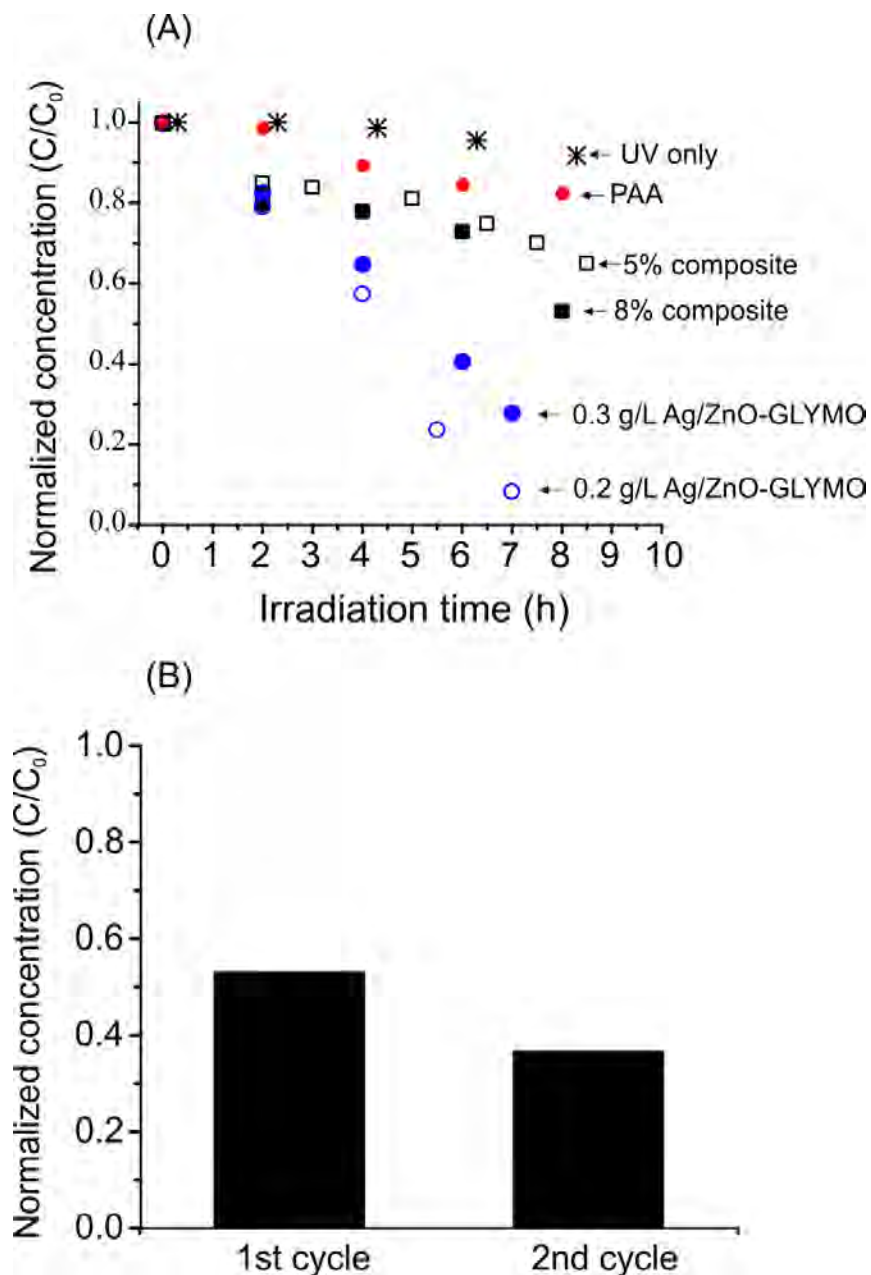


Figure 5.13. Photocatalytic performance in the degradation of bisphenol-A using pure Ag/ZnO-GLYMO photocatalyst and Ag/ZnO-poly(acrylic acid) composites (A) and overall photodegradation performance after two cycles of 8 h (B) (test conditions: bisphenol-A =10 mg/L, $\lambda=365$ nm, pH=10.5).

The general photocatalytic mechanism of bisphenol-A degradation can be described as follows. When ZnO is illuminated (light of 384 nm), the electrons of the valence band are excited to the conduction band, leaving holes behind in the valence band. The electrons are scavenged by both, the AgNPs and the adsorbed oxygen. The oxygen is usually supplied as to form superoxide ions and later hydroxyl radicals; whereas the hole in the valence band become trapped as the surface-bounded $\cdot\text{OH}$ and water molecules to form $\cdot\text{OH}$ radicals. The AgNPs role is to enhance the photocatalytic activity since they act as electron sink, improving the carrier-charges separation (excited electrons and holes, e^-h^+), and increasing the half-life time of these primary active species and the subsequent transfer of the trapped electrons to the adsorbed O_2 in order to produce more free radicals.

The degradation of the bisphenol-A was carried out by two routes. The first is by direct oxidation with holes and the second by indirect oxidation using hydroxyl and superoxide radicals. An undesirable route is the recombination of electron and hole, which dissipate the energy adsorbed as heat. Here, the charge separation (e^-h^+) and the diffusion of the pollutant are the rate-determining steps.

In addition, the oxygen restrictions to the contained in de-ionized water and the added by the mechanical stirring could slow down the catalytic performance. The oxygen supply could be another rate-determining step.

The pH of the solution is an important parameter on define the surface charges of poly(acrylic acid) and bisphenol-A. Bisphenol-A pK_a is 10.1, meaning that non-ionized molecule ($\text{HO-C}_{15}\text{H}_{14}\text{-OH}$) prevails at neutral and acid pH. On the other side, the pK_a for the carboxylic acid group is 4.0. When the pH is higher than 4.0, the carboxyl group is ionized (COO^-). Ionization of carboxyl groups of poly(acrylic acid) in aqueous media enhances their water solubility due to the anionic center that promotes interactions with water and electrostatic repulsions between chains.

Photocatalytic activity

In order to enhance the ionization and aqueous sorption, NaOH was used at the beginning of the photocatalytic activity.

According to the surface charges at the current experimental conditions, there is not repulsion forces between poly(acrylic acid) and bisphenol-A. In the swollen composite, the 3D structure of PAA allows penetration and diffusion of bisphenol-A molecules (molecular length 1.068 nm). Once into the matrix, the bisphenol-A molecules are decomposed by free radicals mostly.

The generation of intermediate products was observed in the HPLC chromatograms at lower retention times, but they were not identified. However a roughly qualitative amount of byproducts could be carried out just in order to describe apparition/desaparition versus time.

The most of the authors reported the sorption and degradation of dyes (i.e. methylene blue) using metal oxides/polymer composites (see Table 4.1 of Chapter 4). To our knowledge, this is the first study related to photocatalytic degradation of bisphenol-A using Ag/ZnO-poly(acrylic acid) composites. Thus, no comparisons of the degradation efficiency are possible. However, photodegradation of bisphenol-A is being carried out using other type of composites containing TiO₂/carbon and TiO₂/zeolite (Fukahori *et al.*, 2003; Kim, J *et al.*, 2010). Fukahori *et al.* (2003) reported the 80% of degradation of bisphenol-A (11.4 ppm) in 24 h using TiO₂/zeolite; while Kim, J *et al.* (2010) observed 75% of decomposition bisphenol-A (15 ppm) using TiO₂/carbon in 5 h. In *our study*, 47% of bisphenol-A (10 ppm) was decomposed *in 8 h using 8% Ag/ZnO-poly(acrylic acid) nanocomposite*.

We must point out that the sorption of bisphenol-A on Ag/ZnO/poly(acrylic acid) nanocomposite was not important, therefore regeneration of the composite is not necessary for the continuous treatment of water. In addition hydrogel composites

like those synthesized in this study are less sensitive to saturation in comparison to zeolites and carbon materials.

5.4 CONCLUSION

The degradation of bisphenol-A, triclosan and rhodamine-B under UV light was achieved using Ag/ZnO. Its use represents an important improvement of the photocatalytic performance of Ag/ZnO compared with that of pure ZnO (e.g. $k_{app}=0.01929 \text{ min}^{-1} \text{ m}^{-2}$, 3.7 times the value for pure ZnO for bisphenol-A degradation).

The degradation of bisphenol-A (25%, 3h), triclosan (35%, 2h) and rhodamine-B (95%, 2h) shows the potential application of the Ag/ZnO obtained by photodeposition and impregnation methods on degradation of water contaminants under visible light.

Regarding the photocatalytic performance of the Ag/ZnO-poly(acrylic acid) composites, this is the first study showing the photodegradation of bisphenol-A.

The 8% wt. Ag/ZnO-poly(acrylic acid) composite leads to an overall decomposition of 47% and 64%, for the 1st and 2nd cycles, respectively.

The immobilization of the photocatalyst can achieve comparable photodegradation efficiencies while it provides additional advantages such as hindering of the photocatalyst photocorrosion, the reuse of the composite, and reduce the photocatalyst loss.

The possibility to implement this method in continuous systems for degradation endocrine disruptor compounds dissolved in water is also another feasible possibility.

6 Chapter 6. MODELING AND OPTIMIZATION OF THE PHOTOCATALYTIC PROCESS

This chapter concerns the modeling and optimization of the photocatalytic process. The *first part* concerns the modeling of important operational conditions that influence (i) the Ag/ZnO photocatalyst synthesis (i.e. nominal amount AgNPs, pH and reaction time) and (ii) the degradation kinetics of the bisphenol-A (i.e. actual amount AgNPs, pH, wavelength and contaminant concentration) using response surface methodology and artificial neural network tools. The developed predictive models are also compared.

The *second part* presents an overall optimization study of the whole process in terms of an evolutionary algorithm, which was implemented in order to connect the input of the first model with the output of the second one and thus, to identify the optimal synthesis conditions that lead to a desired photocatalytic performance. Detailed information on the experimental design, model parameters, statistical significance and optimization process is described in the experimental section.

6.1 BACKGROUND

6.1.1 Main problems to be solved

The synthesis of the ZnO photocatalyst and the photocatalytic activity are complex processes in nature and thus difficult to model mechanistically. The review of Lam, S. et al. (2012) exposes extensively the effect of a variety of operational parameters that compromise the physical, chemical and optical properties of the ZnO semiconductor as well the photocatalytic performance in the degradation of dyes. The optimization of ZnO properties gains importance when the photocatalytic process for the environmental remediation is meant to be used at industrial scale, and the cost (\$) is the decision rule to compete with TiO₂. Therefore, the correlation between structure and performance of a photocatalyst is a non-trivial problem.

Mathematical tools like Response Surface Methodology (RSM) and Artificial Neural Networks (ANN) can perform multivariable analysis of the operational conditions and begin to draw the attention of the scientific community as shown in [Figure 6.1](#). An interesting approach to such a scientific problem is proposed in this thesis regarding the use of RSM and ANNs to correlate the synthesis parameters of the photocatalyst with the photocatalyst performance on the degradation of the contaminant. In general, this novel comprises of a two-step modeling approach on the basis of multi-layer back-propagating neural networks to solve the non-trivial scientific problem of correlating the structure-photocatalytic performance using experimental data.

A second problem addressed, which is closely related to the first one, concerns the normalization of the photocatalytic activity in the terms of the reaction rate per surface area, per photoactive surface sites or per metallic content. Such normalization will allow the comparison of the results obtained in different laboratories. Surface modification of ZnO, with silver nanoparticles (AgNPs), has received attention since it increases the half-life of both the charge carriers excited electrons and holes, e^*-h^+ (Georgekutty, R. et al., 2008) in the ZnO surface after light absorption and then secondary active species (free radicals, i.e. $\bullet\text{OH}$). The metallic bond of Ag is stated as a sink for photoexcited electrons, which reduce the recombination of the charge carriers and increase the sensitivity to visible light (Georgekutty, R. et al., 2008; Zheng, Y. et al., 2007). The dependency of photocatalytic activity on the silver particle size (Wang, J. et al., 2011) and the silver doping method (Zheng, Y. et al., 2008) have also been suggested. It is well known that doping yields are always lower than 100% despite the doping method (Gao, S. et al., 2011; Kim, M.-R. et al., 2009; Zanella, R. et al., 2002). Therefore the importance to determine the actual amount of AgNPs attached to ZnO surface and assess easily structure-photocatalytic performance associations. Thus, the actual amount AgNPs on ZnO surface as a measure of the functionalization

efficiency is proposed as one output (response) of the photocatalytic process to be modelled by RSM and ANNs, as explained earlier.

6.1.2 Modeling tools ANN and RSM

Both RSM and ANNs do not produce the explicit correlations with the physical meaning, but they develop non-parametric simulative models, which approximate the functional relationships between the output (response) and input (operational) variables based on experimental data treatment.

The RSM method is based on the fit of mathematical models (linear, square polynomial functions and others) to the experimental results generated from a design of experiments (DOE) and the verification of the model obtained by means of statistical techniques. The basic idea of DOE is to diversify all significant parameters simultaneously over a set of designed experiments and then to combine the results through the mathematical model. This leads to improving process performance, reducing the number of variables in the process by taking into account only most significant factors, and also to reducing operation costs and experimental time (Witek-Krowiak, A. et al., 2014).

The optimization by means of RSM approach could be divided into five stages (Figure 6.3): (1) selection of independent variables and possible responses, (2) selection of experimental design strategy, execution of experiments and obtaining results, (3) fitting the model response to experimental data, (4) obtaining response graphs and verification of the model, and (5) determination of optimal conditions.

The first and most important step in the whole procedure is to select the most important variables (i.e., factors) and their variation ranges from the collection of all possible candidates. Sometimes a preliminary experimental design (e.g. a two level full factorial design) may be implemented to assess the most important variables. The next crucial step is the design of the experiments to be carried out with the selection of the points where the response should be estimated. Popular

experimental design strategies are the central composite design (CCD), Box–Behnken design (BB), as well as the Plackett–Burman (PB) designs. Information on the advantages and inconveniences of each experimental design can be found elsewhere, we recommend the review of Witek-Krowiak (2014) and Sakkas, V. et al. (2010). Model fitting in RSM consists of two steps: experimental data coding and regression. The coded values are fitted to the selected model using least square methodology. Such functions are incorporated in the majority of common statistical software packages. The response can be shown as a graph, either as three-dimensional or as a contour plot. This graphical interpretation allows for the observation of the curvature of the response surface. The statistical verification of the model provides information not only on accuracy of the fit but also on its significance. To optimize the desirability function, maximize or minimize, numerical methods incorporated to the statistical software are applied. The most common implication is that the calculated model can only be used within the experimental range and cannot be used for extrapolation.

The ANNs allow for predicting the output on the basis of the input data without the need to explicitly define the relationship between them. The effect of the neural network design, training and validation is a nonlinear predictive model, which may lead to optimization and the prediction of process efficiency and in turn scaling up of the system (Witek-Krowiak, A. et al., 2014).

The procedure for the application of ANN is very similar to the previously explained one for RSM models (see Figure 6.3). Once a specific neural network structure has been chosen to solve a specific problem, a set of data (often obtained by an experimental design strategy) must be fed to the network. These data are divided to three distinct subsets used for the training, validation and testing of the produced non-linear model. Commonly, the size of the data for the network training should be 70% of the total data. Evidently, the accuracy of the model performance is directly dependent on the size of the experimental data (i.e., input). On the other

Modeling and optimization

hand, since the correlation between input and response is purely mathematical (i.e., there is no physical significance), and ANNs can be applied even to cases where few experimental data are only available.

An essential step of the ANN design is the appropriate selection of the network architecture. Currently the most popular network architecture is associated with the concept of multi-layered perception (MLP) (e.g. three-layer models with one hidden layer). A structure with feedback may be used to perform more complicated calculations and the backpropagation learning algorithm to minimize the error of the network (Antonopoulou, M. *et al.*, 2013). The selection of the number of neurons of both visible and hidden layers is often the result of empirical tests coupled with trial and error.

The last step of an artificial neural network design is the verification and validation of the prediction model which are commonly carried out in terms of a continuous error metric such as the mean absolute error (MAE), the mean squared error (MSE) or the root mean squared error (RMSE).

A major advantage of ANNs is that, despite the mathematical complexity of their structure, their implementation is quite trivial since, nowadays, most commercial mathematical or engineering software packages (e.g., Matlab) contain complete ANN toolboxes that can be easily set-up and applied to different applications.

6.1.3 Photocatalytic process modeling: state of art

Photocatalysis is a complex process that is easily affected by the nature of the photocatalyst (e.g. crystal structure, morphology, pore size, surface area and metal content) and the liquid properties (e.g. pH, contaminant concentration, light

intensity, wavelength of light and mass transport). The correlation between structure and performance of a catalyst is a non-trivial issue. RSM and ANNs have recently found application in correlating operational conditions with both the final properties of photocatalyst and the photocatalytic performance on the degradation of contaminant. It means that RSM and ANNs can sufficiently model the complex nonlinear relationships between input variables (experimental operational parameters) and the output (response) of the process using experimental data. Afterwards, the models obtained can determine the optimum settings of input variables to maximize or minimize a desired criterion.

A total of 85 papers using the keywords “photocatalysis AND response surface methodology” were found in the literature research on Web of Science in the period 1991-2014 (Figure 6.1). While the number of studies on “photocatalysis AND artificial neural network” barely reach 34. Most of them are published in the research area of engineering, chemistry and environmental science which seems logic since modeling can be extended to industry to generate engineered products and reduce the cost of the optimized design.

To the best of our knowledge, the studies dealing with the comparison of RSM and ANNs modeling methods for the optimization of photocatalytic degradation are scarce (7 papers, blue bar on Figure 6.1), and none of them have been applied for the photocatalytic degradation of endocrine disruptors such as Bisphenol-A. It should be noted that Greece, Iran, Spain and France lead the advances in this special research field.

Thus the scarce literature has encouraged us to study 1) the functionalization of ZnO with silver nanoparticles and 2) the reaction rate on the degradation of Bisphenol-A using the ANNs coupled to evolutionary algorithms to optimize the operational conditions.

Modeling and optimization

RSM and ANN represent powerful mathematical methods that can establish relationships between input variables (experimental operational parameters) and the output (response) of the process. In the last ten years, the number of papers showing the application of RSM and ANNs for the modeling and optimization of photocatalytic degradation of pollutants such as dyes, pesticides, etc., is small but increases rapidly (Figure 6.1).

Khataee and Zarei (2011b) optimized the degradation of Direct Yellow 12 (DY12) using the CCD design and RSM. They evaluated the effects of three independent variables, namely the initial dye concentration, the applied current, the initial Fe (III) concentration and the reaction time on the degradation of diazo dye by photoelectro-Fenton combined with ZnO photocatalytic process. On the basis of this CCD approach, they confirmed that time and current had a significant effect on the photoelectrocatalysis process and obtained a set of optimal conditions for DY12 degradation using surface response plots from RSM. In a parallel study, the authors show the modeling of the photocatalysis conditions on the degradation efficiency of DY12 using ANNs. A three-layered feed-forward back propagation neural network (5:14:1) was employed. The results indicated that ANNs provide a reasonable prediction ($R^2=0.98$) of the performance (Khataee, A.R. *et al.*, 2011a). However the analysis of the effect of initial pH of the solution, initial dye concentration, applied current, kind of ultraviolet (UV) light and initial Fe(III) concentration was tedious and less clear than when RSM approach is used.

Antonopoulou and Konstantinou (2013) compared RSM to ANN in the modelling of DEET (N,N-Diethyl-m-toluamide) photocatalytic degradation. A feed-forward MLP ANN model was employed to predict the disappearing of DEET from aqueous solution. The results showed that the ANN approach is more appropriate for the modelling of organic compounds photodegradation by TiO_2 than RSM based on CCD.

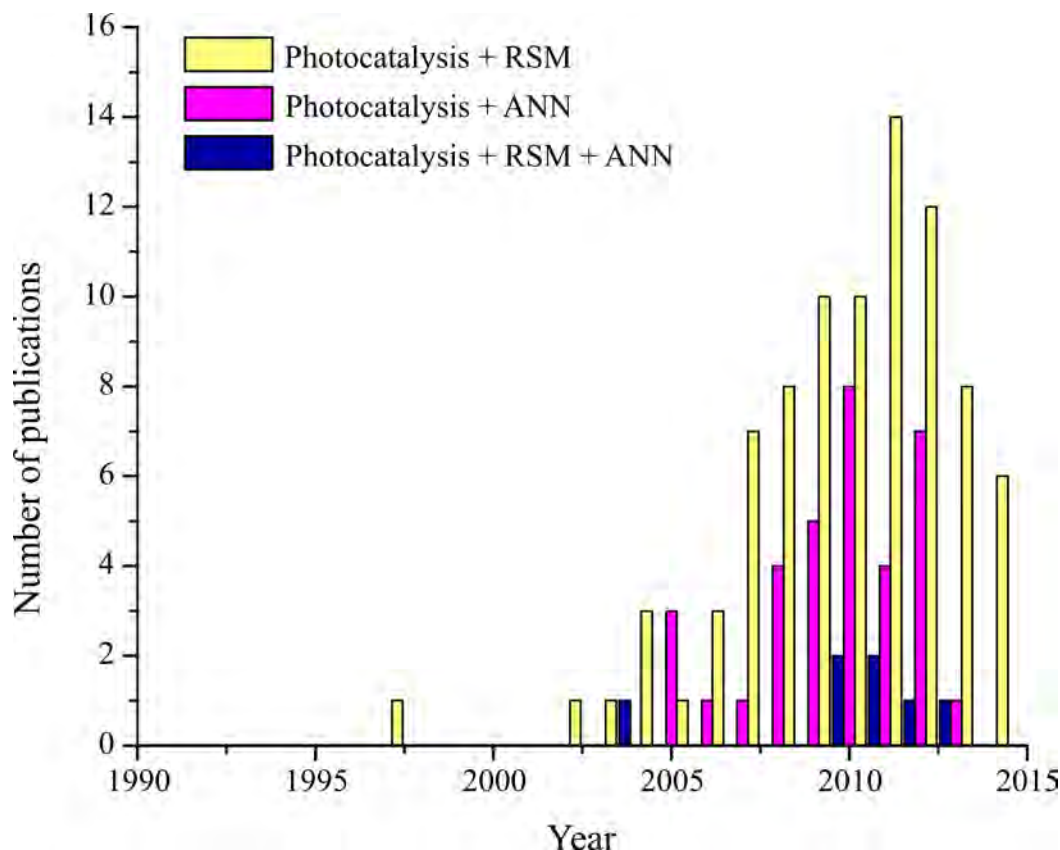


Figure 6.1. Number of papers published on photocatalysis per year in the period 1991-2014 using Web of Science database. Research results by keywords “photocatalysis AND response surface methodology” (yellow bar), “photocatalysis AND artificial neural network” (pink bar) and “photocatalysis AND response surface methodology AND artificial neural network” (blue bar).

The results of several authors have shown that the ANN is a better choice, in terms of accuracy, over the least squares method for modeling similar processes. However, having the ability of sensitivity analysis and optimization, the RSM model has advantages over the ANN model. The effects of individual variables of the process and their interactions are obvious from the coded regression equation, while the ANN is a black box model that does not give directly such information of the photocatalytic process.

6.2 METHODOLOGY

6.2.1 Define input/output parameters

6.2.1.1 Functionalization of ZnO – Model A

The independent variables, namely *nominal amount AgNPs*, *pH* and *time*, and their levels were selected based in the literature (Amadelli *et al.*, 2008; Peng *et al.*, 2007). The dependent variable (response) is the *actual amount of AgNPs attached* to ZnO surface as a measure of the *functionalization efficiency* (FE) defined by the Equation 6.1 and 6.2:

The amount of AgNPs, on dry based, is defined by Eq. (2):

$$\text{Ag \% w/w} = \frac{\text{weight Ag}}{\text{weight Ag} + \text{weight Zn}} * 100 \quad (6.1)$$

$$\text{FE} = \frac{\text{actual amount Ag}}{\text{nominal amount Ag}} * 100 \quad (6.2)$$

6.2.1.2 Photocatalytic activity: apparent rate constant – Model B

The independent variables are *pH*, *bisphenol-A concentration*, *actual amount of Ag* and *wavelength*. The dependent variable (response) chosen is the apparent rate constant (k_{app}). Notice that bisphenol-A degradation by ZnO is a pseudo-first order reaction, therefore the reaction order was set constant and equal to 1. The apparent rate constant of bisphenol-A degradation is obtained from the following mathematical calculations.

The normalized concentration C vs time (t) is plotted and the overall degradation curve is approximated by a first-order exponential decay function of the form (Equation 6.3 and 6.3a):

$$Y = a \exp^{bx} \quad (6.3)$$

$$C = a \exp^{bt} \quad (6.3a)$$

The implementation of a regression technique to describe the complete degradation curve provides a more global approach to the characterization of the

photodegradation performance of the synthesized catalyst without including time in the factors of the experiment. In order to provide a more “physical sense” to this regression, the degradation rate is supposed to obey a typical kinetics behavior of the type (Equation 6.4):

$$r = k_{app} C^n \quad (6.4)$$

$$\ln r = \ln k_{app} + n \ln C \quad (6.4a)$$

The numerical values of the derivation of the exponential regression function are equal to degradation rate r (Equation 6.4a). A subsequent plot in terms of $\ln r$ vs $\ln C$ can be used for the calculation of the values of the apparent rate constant, k_{app} , and the reaction order, n , for each experiment (see Figure 6.2). Via this treatment, the previously assumed first-order kinetics behavior is readily verified, thus reducing the model response to one (i.e., k_{app}).

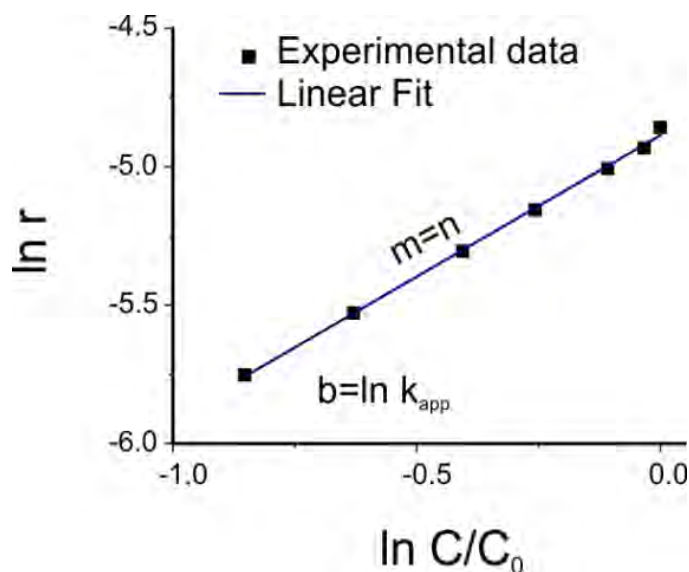


Figure 6.2. Linear plot $Y=mx + b$ to obtain the kinetics parameters (k_{app} and n).

6.2.2 Experimental design

6.2.2.1 Full factorial

Previous knowledge of the effect of the independent variables, individually or in combination, was obtained from a preliminary experimental design. Eight experimental runs, produced by a 2^3 full factorial design, were carried out for this purpose. The two factors - three levels design was analyzed through main effects plots and interaction plots.

Table 6.1. Experimental range of the independent variables on the 2^3 factorial design

Variables	Coded	PD	IMP
Nominal amount AgNPs (% w/w)	x_1	0.1-1	1-5
Initial pH	x_2	7-11	7-11
Time (h)	x_3	0.5-1	2-5

PD: photodeposition method, IMP: impregnation method

6.2.2.2 Central composite design

The central composite design (CCD) with a smaller number of experimental runs provides high quality predictions of linear and quadratic interaction effects of parameters affecting the process. The CCD contains the full factorial or fractional factorial design at two levels (2^n), center points (cp), which corresponds to the middle level of the factors, and axial points ($2n$).

Therefore in this thesis was used a CCD experimental design for the functionalization of ZnO. A 2^3 full factorial CCD, 6 center points and 6 axial points which give a total of 20 experiments was chosen. The experimental range of the independent variables is shown in [Table 6.2](#).

Table 6.2. Experimental range of the independent variables on the CCD design

Variables		PD			IMP		
Nominal amount AgNPs (% w/w)	x_1	0.1	0.3	1	0.1	1	5
Initial pH	x_2	7	9	11	7	9	11
Time (h)	x_3	0.5	0.75	1	1	2	5

PD: photodeposition method, IMP: impregnation method

On the other hand, no experimental design was followed for the photocatalytic tests. The range of variation of the independent variables were pH (2.8 to 10.5), actual amount AgNPs (0-1.2 %w/w), bisphenol-A (10-40 mg/L) and wavelength (254 to 450 nm). The data were collected of a variety of experiments. A total of 27 experiments were used for the ANNs model. All the experimental data used for the calculations of this chapter are presented in [Tables 6.3, 6.4 and 6.5](#).

Table 6.3. Experimental data of the functionalization of ZnO with AgNPs by the photodeposition method of CCD design.

Sample	Input			Output		Predicted RSM		Predicted ANN	
	Nominal amount Ag %w/w	pH	Reaction time (min)	Actual amount Ag %w/w	FE (%)	Actual amount Ag %w/w	Actual amount Ag %w/w	FE (%)	
1	0.1073	7	30	0.082	76.301	0.105	0.0444	76.720	
2	0.1073	7	60	0.107	99.867	0.131	0.0903	99.879	
3	1.0623	7	30	0.991	93.298	1.039	0.9895	93.108	
4	1.0623	7	60	1.093	102.892	1.065	1.1805	83.064	
5	0.3573	9	30	0.358	100.331	0.388	0.3384	72.760	
6	0.3573	9	60	0.375	105.062	0.414	0.3939	106.134	
7	0.1073	11	30	0.091	84.570	0.04	0.1534	84.636	
8	0.1073	11	60	0.116	107.876	0.066	0.1254	107.463	
9	1.0623	11	30	1.186	111.689	1.137	0.9318	111.497	
10	1.0623	11	60	1.147	108.012	1.163	1.0979	107.876	
Table 6.3 continuation									
11	0.3573	7	45	0.320	89.636	0.254	0.3272	83.832	
12	0.3573	11	45	0.097	27.185	0.232	0.1009	27.206	
13	0.1073	9	45	0.074	68.938	0.13	-0.1070	60.279	
14	1.0623	9	45	1.132	106.560	1.146	0.8704	106.540	
15	0.3573	9	45	0.362	101.401	0.344	0.3583	102.645	
16	0.3573	9	45	0.371	103.922	0.344	0.3583	102.645	
17	0.3573	9	45	0.368	103.081	0.344	0.3583	102.645	
18	0.3573	9	45	0.385	107.700	0.344	0.3583	102.645	
19	0.3573	9	45	0.357	100.000	0.344	0.3583	102.645	
20	0.3573	9	45	0.362	101.300	0.344	0.3583	102.645	

FE: Functionalization efficiency

Table 6.4. Experimental data of the functionalization of ZnO with AgNPs by the impregnation method of CCD design.

Sample	Input			Output		Predicted RSM	Predicted ANN	
	Nominal amount Ag %w/w	pH	Reaction time (min)	Actual amount Ag %w/w	FE (%)	Actual amount Ag %w/w	Actual amount Ag %w/w	FE (%)
1	0.1072	7	60	0.10	92.948	0.147	0.1037	97.345
2	0.1072	7	300	0.094	87.861	0.244	0.0942	127.405
3	1.0623	7	120	1.203	113.248	0.996	1.1942	129.718
4	5.095	7	60	0.521	10.23	0.55	0.5015	15.548
5	5.095	7	300	0.668	13.117	0.648	0.6873	10.522
6	0.1072	9	120	0.11	102.155	0.2	0.7751	117.305
7	1.0623	9	60	0.97	91.341	1.133	0.9748	96.138
8	1.0623	9	120	1.192	112.23	1.092	1.1336	112.978
9	1.0623	9	300	1.194	112.385	1.231	0.7631	107.958
10	5.095	9	120	0.494	9.7	0.604	0.4805	-30.031
11	0.1072	11	60	0.116	107.878	-0.077	0.1819	98.649
12	0.1072	11	300	0.116	108.278	0.021	-0.0074	70.565
13	1.0623	11	120	0.366	34.441	0.773	0.3653	39.801
14	5.095	11	60	0.374	7.34	0.327	0.4139	9.549
15	5.095	11	300	0.498	9.78	0.425	0.5169	1.339
16	1.0623	9	120	1.169	110	1.092	1.1336	112.978
17	1.0623	9	120	1.223	115.105	1.092	1.1336	112.978
18	1.0623	9	120	1.023	96.318	1.092	1.1336	112.978
19	1.0623	9	120	1.179	111	1.092	1.1336	112.978
20	1.0623	9	120	1.167	109.85	1.092	1.1336	112.978

FE: Functionalization efficiency

Table 6.5. Experimental data of the photocatalytic degradation of bisphenol-A.

Sample	Input		Output		Predicted ANN			
	pHi	Actual amount Ag (%w/w)	BPA (mg/L)	Wavelength (nm)	^a R ²	k _{app}	n	k _{app}
ZnO	10.5	0	10	302	0.993	0.00453367	0.8874	0.0066745
	10.5	0	10	450	0.9745	0.00062311	0.9986	0.00012785
	7.5	0	10	254	0.9835	0.00255049	1.1615	0.00384502
	2.81	0	10	254	0.9868	0.00382683	1.0192	0.00389089
	4.27	0	10	254	0.9887	0.00389177	0.9991	0.00394836
	9.38	0	10	254	0.9878	0.00496742	1.0007	0.00559822
	10.5	0	10	254	0.9878	0.00754838	1.0218	0.00814319
	7.25	0	20	254	0.9677	0.00174637	1.0309	0.00184683
	8.53	0	20	302	0.9531	0.00109969	1.0133	0.00230427
	8.53	0	20	365	0.98	0.00231113	0.9923	0.00237865
(1.06% Ag/ZnO-PD7,1)	10.5	1.093	10	254	0.9817	0.01017078	1.0176	0.01115039
	10.5	1.093	10	302	0.9887	0.01864457	1.0056	0.01689106
	10.5	1.093	10	365	0.9963	0.01538319	1.0018	0.01545645
	10.5	1.093	20	254	0.9892	0.00497232	1.0220	0.00530728
	7.51	1.093	40	254	0.9894	0.00173134	0.9702	0.00165973
(1.06% Ag/ZnO-PD11,1)	10.5	1.147	10	254	0.977	0.0121439	1.0240	0.01256046
	10.5	1.147	10	302	0.9795	0.01850155	1.0112	0.01873602
	10.5	1.147	10	365	0.9937	0.01675167	1.0083	0.01691386
	10.5	1.147	10	450	0.9891	0.00145351	1.0457	0.00113776
	7.2	1.147	40	254	0.9816	0.00117506	0.9557	0.00114764
(1.06% Ag/ZnO-IMP7,2)	10.5	1.203	10	254	0.9962	0.00828052	1.0069	0.00828052
	10.5	1.203	10	302	0.9962	0.00936462	0.9948	0.00759062

Modeling and optimization

(1.06% Ag/ZnO- IMP11,2)	10.5	1.203	10	365	0.992	0.0109531 4	0.993 4	0.0109531 4
	10.5	0.366	10	254	0.991	0.0084165 3	1.006 4	0.0084165 3
	10.5	0.366	10	302	0.993	0.0122333 9	0.992 2	0.0122333 9
	10.5	0.366	10	365	0.993	0.0137491 9	1.005 5	0.0112574 2
	10.5	0.366	10	450	0.991	0.0012794 7	1.009 5	0.0059302

^a Correlation value of the exponential fit $y=a \exp^{bx}$ of the experimental data.
 k_{app} : kinetic constant rate (min^{-1}), n : calculated reaction order.

6.2.3 Mathematical tools for model and optimization

6.2.3.1 Response surface methodology

After running a total of 20 experiments, a second order (quadratic) model was used to fit the experimental data that express the functionalization efficiency as a function of the independent variables (see **Equation 6.5**).

$$Y=b_0 + b_1x_1 + b_2x_2 + b_3x_3 + b_{11}x_1^2 + b_{22}x_2^2 + b_{33}x_3^2 + b_{12} x_1x_2 + b_{13} x_1x_3 + b_{23} x_2x_3 + \varepsilon \quad (6.5)$$

Where Y is the response, b_0 is the constant coefficient; b_1 , b_2 , b_3 are the linear coefficients; b_{11} , b_{22} , b_{33} are quadratic coefficients, and b_{12} , b_{13} , b_{23} the second order coefficients of x_1 , x_2 , and x_3 independent variables, and ε is the random error. The accuracy and applicability of the model was evaluated by the R^2 , R^2_{adj} , and p -values in the analysis of variance (ANOVA). Statistical analysis was performed using the software package Minitab 14.

6.2.3.2 Artificial neural networks

In this study a feed-forward multilayered perceptron network was used, the structure of which can be denoted as a (In:Hid:Out) network corresponding to the numbers of neurons in the inputs, hidden and output layers, respectively. Log-sigmoidal and linear transfer functions were used for the neurons of the hidden and output layers, respectively (Xi, J. et al., 2013). Typically, 70% of the experimental data are used within the training set and 30% of the data are used for the

verification and testing of the model. The optimal architecture of the ANN model was determined based on the minimum value of the mean square error and maximum correlation coefficient value (R^2) of the training and validation sets. For this part of the study, the Neural Network Toolbox of the commercial software package MATLAB 7.11.0 (academic license) was used.

6.2.3.3 Evolutionary algorithm for optimization

Evolutionary algorithms (EA) are based on the principle of evolution of biological systems and have become quite popular as probabilistic tools for various optimization studies. Recently, EAs have been applied for the study of the operational conditions in the extraction of industrial relevant compounds (Xi, J. *et al.*, 2013) and in polymerization processes (Camargo, M. *et al.*, 2011), at both laboratory and pilot scale. EAs can solve linear and nonlinear problems using concepts as selection, crossover and mutation ruling the evolution to get a population with optimal individuals. Detailed information on the theoretical basis of EAs for mono- and multi-objective optimization, applied in the field of polymers, can be found in the relevant literature (Camargo, M. *et al.*, 2011; Deb, K. *et al.*, 2001; Viennet, R. *et al.*, 1996).

In general, an EA is based on the principle of the continuous improvement of a characteristic or criterion (i.e., the optimization criterion) of the individuals of a population. Such a population may, for example, be composed of a large set of randomly generated possible experimental conditions (i.e., the individuals) which are characterized by a measured property or model response (e.g., the functionalization efficiency) corresponding to each of these experiments. The population is classified from the *best* individual (i.e., the one with the minimum or maximum value of the criterion, depending on whether the problem is a minimization or maximization one) to the *worst* and is subjected to a series of cycles of improvement of this criterion. In this respect, some of the best individuals are combined to generate new ones that might perform better. A predefined

Modeling and optimization

number of the worst individuals are removed from the population after each cycle and the procedure continues until the population has “evolved” to such a point where the desired convergence to an optimal has been achieved. (Xi, J. *et al.*, 2013).

In this study, the previously developed ANN models were coupled with an EA approach in order to define the optimal synthesis conditions of the Ag/ZnO photocatalyst that lead to the optimal photodegradation performance.

More precisely, this optimization study was carried out in two consecutive steps. Initially, the model of the photodegradation process was used within an optimization run, in terms of an EA, in order to define the actual amount of AgNPs that maximize the apparent rate constant of bisphenol-A degradation (i.e., objective function B). This optimized amount of AgNPs was subsequently introduced as the new objective function (i.e., objective function A). In a second optimization study it was used to identify the optimal Ag/ZnO synthesis conditions (i.e., nominal amount, pH and reaction time) that lead to desired final photocatalytic performance.

In this work, we carried out *mono-objective optimization* which leads for a desired optimal value of the response, i.e. maximize the apparent rate constant.

However multi-objective optimization is feasible, particularly by adding another output criteria (response), i.e. the cost of the whole process, which must be minimized. In this case a compromise has to be proposed by a decision-maker among the numerous solutions resulting using, for example, Pareto’s methodology. The participation of the decision-maker will be required for affecting the weights of the new two objective functions: maximize the apparent rate constant and minimize the cost of the whole process.

The general diagram of the approach that was used in this thesis to model and optimize the functionalization of ZnO and their photocatalytic performance on the degradation of bisphenol-A is shown in [Figure 6.3](#).

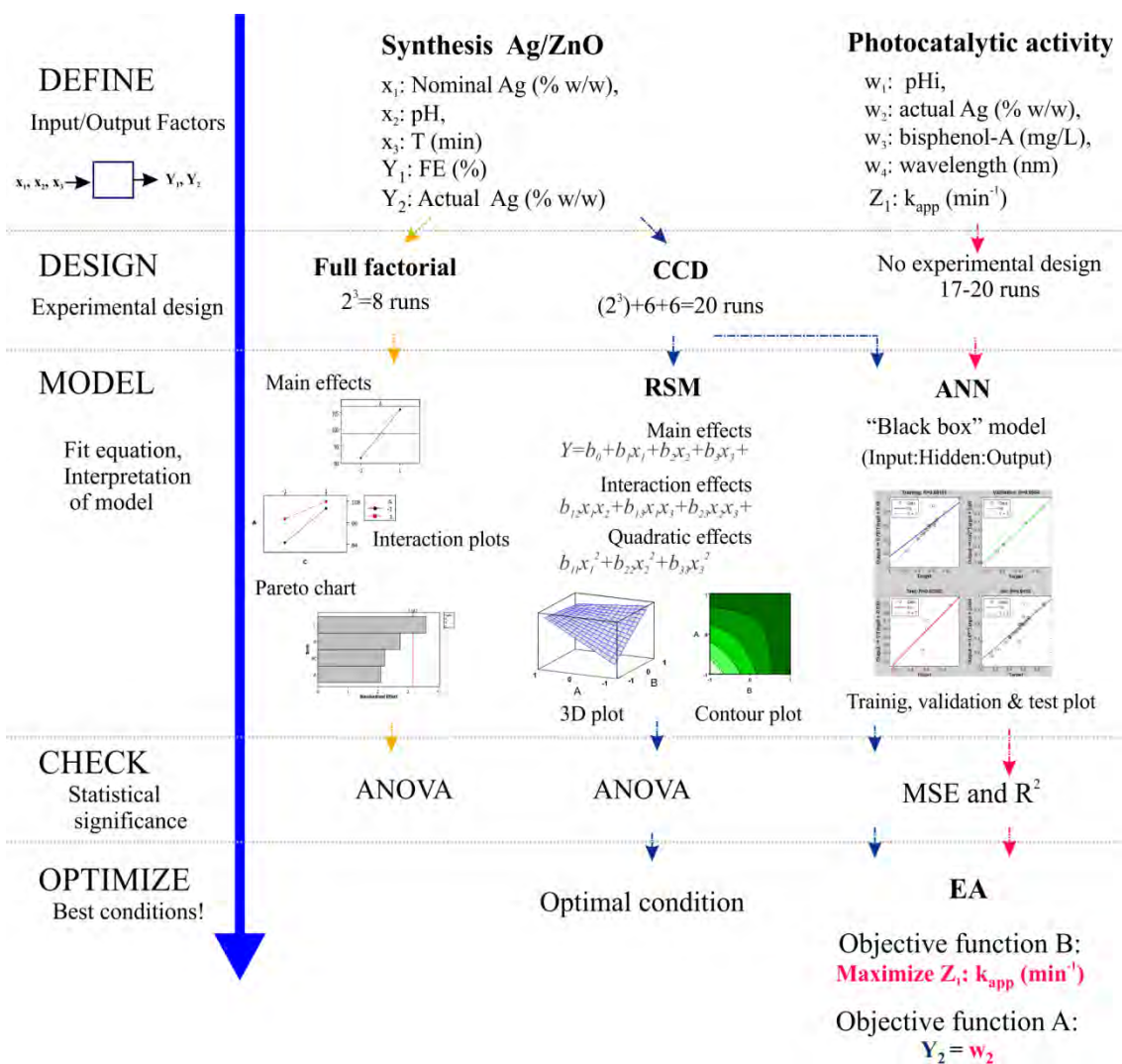


Figure 6.3. Scheme of the experimental design, model and optimization setting used to study the synthesis of Ag/ZnO photocatalyst and their photocatalytic behavior. The abbreviations FE: functionalization efficiency, CCD: central composite design, RSM: response surface methodology, ANN: artificial neural network, MSE: mean square error, EA: evolutionary algorithm.

6.3 RESULTS AND DISCUSSION

6.3.1 Preliminary experiments

The purpose of a first experimental design was to know the influence of the functionalization conditions. A total of 8 experiments were analyzed through the effect of variables individually and interactions plots. The Pareto chart in [Figure 6.4](#) and the p-values of the regression model show that the effect of the independent variable *nominal amount of AgNPs* is statistically significant ($p < 0.05$), suggesting a strong influence on the actual amount AgNPs as a measure of the functionalization efficiency.

Interaction of the independent variables increases the actual amount AgNPs attached to ZnO surface: nominal amount AgNPs vs reaction time, in case of the photodeposition method and nominal amount AgNPs vs pH for the impregnation method. Thus, interaction between pH and AgNPs is relevant for the impregnation method, meanwhile photodeposition is greatly influenced just for AgNPs.

Based on the results of the preliminary experiments, new experimental range values were set for the second experimental design, namely a central composite design and the regression coefficients are in [Table 6.6](#).

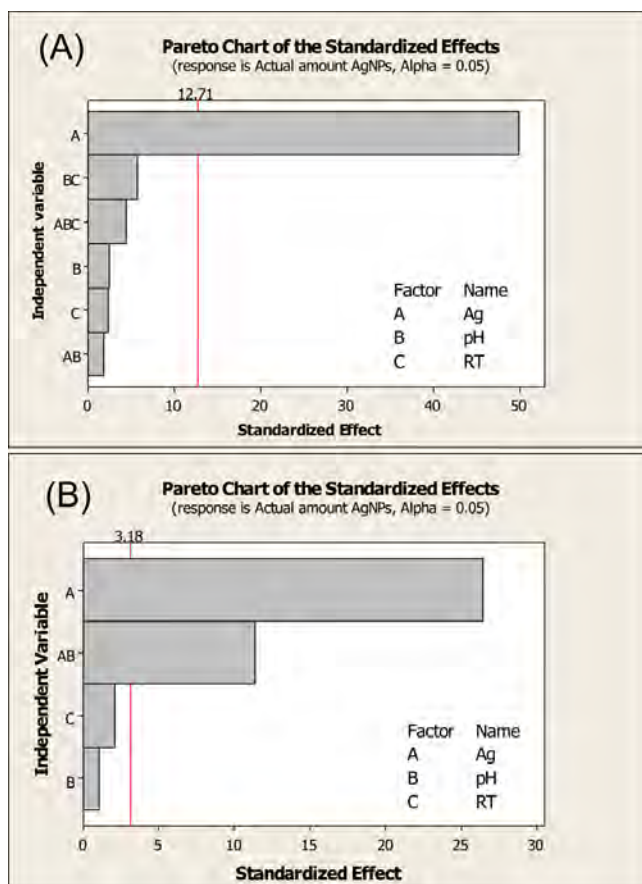


Figure 6.4. Pareto chart of the standardized effects on the functionalization of ZnO by the (A) photodeposition and (B) impregnation method.

Table 6.6. Estimated regression coefficients and p -values of the factorial fit.

Coded	Coefficient		p -value	
	PD	IMP	PD	IMP
Constant	0.5438	0.8023	0.011*	<0.001**
x_1	0.4639	-0.2636	0.013*	<0.001**
x_2	0.0231	-0.0103	0.243	0.379
x_3	0.0217	0.0210	0.257	0.126
$x_1 x_2$	0.0166	-0.1135	0.323	0.001*
$x_2 x_3$	-0.0526		0.111	
$x_1 x_2 x_3$	-0.0414		0.141	
R^2	0.9996	0.9964		
R^2_{adj}	0.9973	0.9916		

* Statistically significant $p < 0.05$, ** Statistically highly significant $p < 0.001$
PD: photodeposition method, IMP: impregnation method

6.3.2 Modeling step

6.3.2.1 Functionalization of ZnO-Model A

6.3.2.1.1 RSM modeling of ZnO functionalization-Model A

The ANOVA test (Table 6.7) shows that the model is highly statistically significant for the functionalization of ZnO by both the photodeposition and impregnation methods ($p < 0.001$) since it explains 98.5% and 90.2% of the experimental data, respectively. Based on p -values, the most important operational condition is the nominal amount of AgNPs. The significance of the nominal amount of AgNPs on the functionalization efficiency resulted from the poor dispersion of the stabilized AgNPs in the bulk of the solution; the lower the initial quantity of AgNPs (e.g. 0.1 % w/w), the higher the time to reach the ZnO surface due to diffusion problems. On the other hand, the higher the initial amount of AgNPs, the higher AgNPs agglomeration due to destabilization of the repelling forces. Nanoparticles minimize their surface energy by forming agglomerates (Goebbert *et al.*, 2000), which ends in poorly attached AgNPs agglomerates that are easily washed-out from the ZnO surface and in low functionalization efficiency. This phenomenon was observed in our study for the case of the samples obtained by impregnation method because of the experimental range tested (0.1 to 5%w/w). Zanella *et al.* (2002) reported Au deposition onto TiO₂ by incipient wetness impregnation method with low yields. When the gold amount was increased from 1 to 4 % wt., the yield decreased from 100% to 15%.

The importance of pH, the second important variable, is attributed to the minimal repulsion forces between stabilized AgNPs and the ZnO surface at pH of point zero charge ($\text{pH}_{\text{PZC}}=8.2$, see Appendix A). In other words, the neutralized charges of ZnO surface allow the interaction with a non-ionized surfactant-AgNPs. Highest sorption of non-ionized organic molecules on ZnO surface at the pH_{PZC} values was also reported by Clament Sagaya Selvam *et al.* (2013).

Note that our study employed stabilized AgNPs as metal source, while silver salts (AgNO_3 and CH_3COOAg) are commonly used for the ZnO modification in the literature (Peng *et al.*, 2007; Wang, J *et al.*, 2011; Zheng *et al.*, 2007). Therefore, the operating conditions influence the interaction between the ZnO surface and the surfactant-AgNPs in such different way. Then, our results demonstrate for the first time the importance of the operating conditions, namely initial amount of AgNPs and pH on the functionalization efficiency of ZnO using RSM based on CCD.

The visualization of the interactive effect of the two most significant variables is shown in the 3D response surface plots (Figure 6.5). The results of quadratic regression model that describe the functionalization of ZnO using CCD coupled to RSM are shown in Table 6.8. The regression equation (see Equation 6.5) describes the Y_2 actual amount AgNPs by x_1 , the nominal amount of AgNPs, x_2 , the pH and x_3 , the reaction time with high correlation coefficient.

Note that the robustness of the RSM model is dependent on the quality of the experimental data used. We must point out that the functionalization efficiency higher than 100% has no physical sense and it could imply that all the added silver nanoparticles were attached to ZnO surface. The probable reasons for a functionalization efficiency value higher than 100% could be attributed to the following facts: a non-linear signal in such concentration range, a low accuracy of the equipment or an experimental error in the silver solution added. All those reasons combined or individually, could contribute to an overestimation of the functionalization efficiency.

The model of Y_1 functionalization efficiency shows a very low correlation value ($R^2=0.439$) with the experimental data obtained from the photodeposition method. In other words, pure error is highly significant and the experimental data are not predicted by the model (ANOVA test non-shown). On the other hand, the

Modeling and optimization

correlation coefficient for impregnation method was $R^2=0.881$. Therefore the model of Y_1 was not used for the optimization step.

The predicted values by the model for Y_2 response are listed in [Table 6.3](#) for the photodeposition method and in [Table 6.4](#) for the impregnation method.

Table 6.7. ANOVA test of the quadratic model for the response Y_2

Source	Sum of squares	Degree of freedom	Mean square	F-value	p-value
PD					
Model	2.979	7	0.425	116.26	<0.001**
Residual	0.044	12	0.003		
Lack of fit	0.043	7	0.006	63.4	<0.001**
Pure error	0.0005	5	0.0001		
IMP					
Model	3.558	6	0.593	19.89	<0.001**
Residual	0.387	13	0.029		
Lack of fit	0.363	8	0.045	9.37	0.012*
Pure error	0.024	5	0.005		

* Statistically significant $p < 0.05$, ** Statistically highly significant $p < 0.001$
 PD: photodeposition method, IMP: impregnation method

Table 6.8. Estimated regression coefficients and p-values of the quadratic model for the response Y_2

Coded	Coefficient		p-value	
	PD	IMP	PD	IMP
Constant	0.574	1.719	<0.001**	<0.001**
x_1	0.508	0.202	<0.001**	0.003*
x_2	0.008	-0.112	0.674	0.062
x_3	0.013	0.049	0.510	0.387
$x_1 x_1$	0.066	-1.315	0.198	<0.001**
$x_2 x_2$	-0.101	-0.207	0.017*	0.068
$x_3 x_3$	-0.057	0.088	0.146	0.550
$x_1 x_2$	0.041		0.075	NS
R^2	0.985	0.902		
R^2_{adj}	0.977	0.856		

* Statistically significant $p < 0.05$, ** Statistically highly significant $p < 0.001$, NS: No statistically significant.
 PD: photodeposition method, IMP: impregnation method

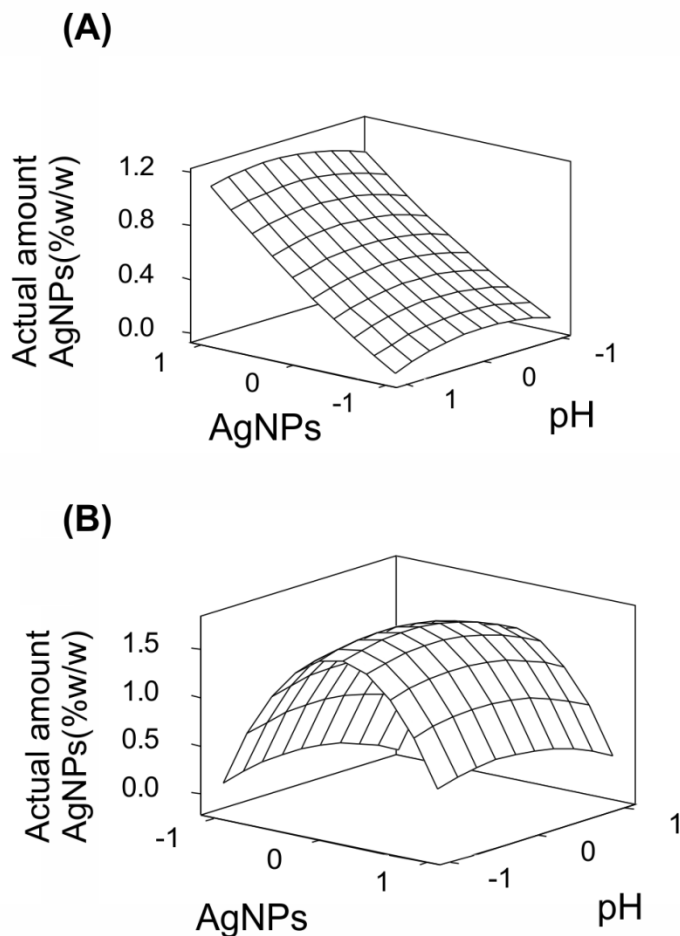


Figure 6.5. 3D surface plot of the effect of actual amount AgNPs and pH on the response of the RSM model of the functionalization of ZnO by the (A) photodeposition and (B) impregnation method.

6.3.2.1.2 ANN modeling of ZnO functionalization – Model A

A three-layered feed-forward back propagation neural network was used for the modeling of the functionalization of ZnO by both photodeposition and impregnation methods. The experimental data from the CCD design were divided into training, validation and test subsets (70%, 15% and 15%, respectively). We must point out that the data were randomly selected to proceed with the model. Several configurations of the network (In:Hid:Out) were tested to determine the best

Modeling and optimization

number of neurons in the hidden layer based on R^2 value (data not shown). The best network for each functionalization method is (3:16:1) for photodeposition method and (3:18:1) for impregnation method.

Figure 6.6 shows the correlation of the experimental and predicted data by ANN. The plot shows the correlation coefficient for the photodeposition method (0.974) and for the impregnation method (0.909), which indicated a good agreement of the ANN model with the experimental data. The results confirm that ANN can adequately model the functionalization process of ZnO by both methods, within the experimental range used in this work.

Note that the elimination of experimental data with higher error could improve the model correlation coefficient. For example, by taking away the data#12 from Table 6.3, the model reaches $R^2=0.995$, which further increases the robustness of the optimization study.

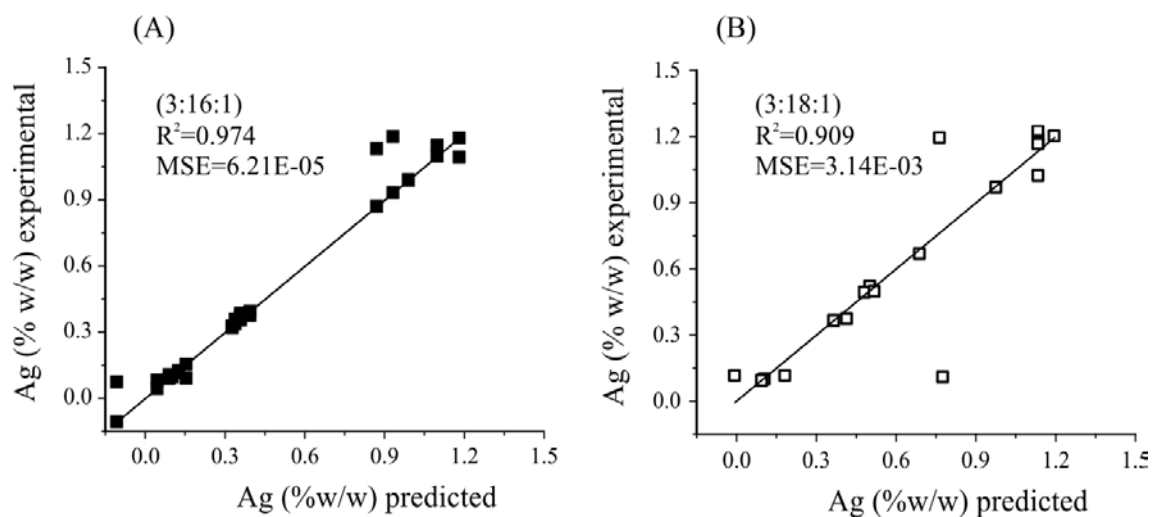


Figure 6.6. Plot of the experimental data against predicted data by ANN model for Y_2 actual amount AgNPs response prepared by the (A) photodeposition and (B) impregnation methods.

6.3.2.1.3 Comparison of RSM and ANN models

The predictive capacity of RSM and ANN models are compared in [Table 6.9](#) in function of the correlation coefficients obtained for both functionalization methods. Regarding RSM, a good model fit is considered when R^2 and R^2_{adj} are close to 1.0. In this study, very low values of R^2 and R^2_{adj} imply poor predictive capacity to model, which is the case of Y_1 for photodeposition method. In general, the model obtained by RSM for Y_1 and Y_2 shows acceptable correlation coefficients, with exception of Y_1 of photodeposition method.

Concerning the ANN models, the MSE value close to zero indicates a good model. Large R^2 value and small MSE values obtained shown that ANN allows a good fitting and high prediction of the functionalization process for both functionalization methods (see [Table 6.9](#)).

In our study, ANN models show a better agreement with experimental data than RSM models. The better performance of ANNs versus RSM model can be explained by the ability to approximate the non-linearity of the system and to the fact that RSM is restricted to second order equation (quadratic model) (Antonopoulou, M. *et al.*, 2012). However, the information given by RSM on the effect of operational conditions over the response allows the understanding of the mechanism for ZnO functionalization with AgNPs. Then ANN model is recommended to be used to optimize as well as predict complex process as the case of functionalization by photodeposition method were other parameters such as irradiation intensity are involved.

Table 6.9. Comparison of the predictive capacity of the models for the functionalization of ZnO.

Functionalization method	RSM R^2	R^2_{adj}	NN R^2	MSE
Y_1^a				
PD	0.439	0.180	0.929	1.49E-03
IMP	0.881	0.826	0.943	5.11E-03
Y_2^b				
PD	0.985	0.997	0.974	6.21E-05
IMP	0.902	0.856	0.909	3.14E-03

PD: photodeposition method, IMP: impregnation method

^a Y_1 : functionalization efficiency

^b Y_2 : actual amount AgNPs

6.3.2.2 Photocatalytic activity: apparent rate constant-Model B

A four-layered feed-forward back propagation neural network is used for the modeling of the kinetic parameter k_{app} for the degradation of bisphenol-A using Ag/ZnO photocatalyst. The experimental data were divided into training, validation and test subsets (70%, 15% and 15%, respectively). Several configurations (4:Hid:1) of the network were tested in order to determine the best number of neurons in the hidden layer on the basis of the R^2 value. The best network for each functionalization method is given in Table 6.10. Figure 6.7 shows the experimental data and the predicted data of ANN. The correlation coefficient and MSE value for the photodeposition method (0.992 and 1.25E-22, respectively) and for the impregnation method (0.912 and 2.40E-21, respectively) shows the very good agreement of the model with the experimental data.

Khataee, A.R. *et al.* (2011a) and Antonopoulou, M. *et al.* (2013; 2012) concluded that ANNs allows a better capacity for the modelling of degradation efficiency of different organic compounds than RSM. Besides, ANN models do not require prior knowledge of the photocatalytic process and can be used for limited number of

experimental data. Then ANNs correlate good enough the initial conditions such as pH, AgNPs content, bisphenol-A concentration and wavelength with the k_{app} for the degradation of bisphenol-A by Ag/ZnO photocatalyst.

To our knowledge, this is the first time that k_{app} is used to model the photocatalytic performance instead of photocatalytic efficiency (%) usually reported. k_{app} takes into account the whole degradation curve and not a single value corresponding to a specific degradation time, thus making it possible to predict the overall degradation curve of bisphenol-A of each experiment.

The predicted values of ANN model are listed in [Table 6.5](#).

Table 6.10. Structure and R^2 optimum values of ANN model of k_{app} .

Functionalization method	Structure	Training	Validation	Test	All ^a
PD	4:23:1	0.9989	0.9957	0.9913	0.9923
IMP	4:17:1	0.8618	1	1	0.9117

^a The general performance of the model.

PD: photodeposition method, IMP: impregnation method

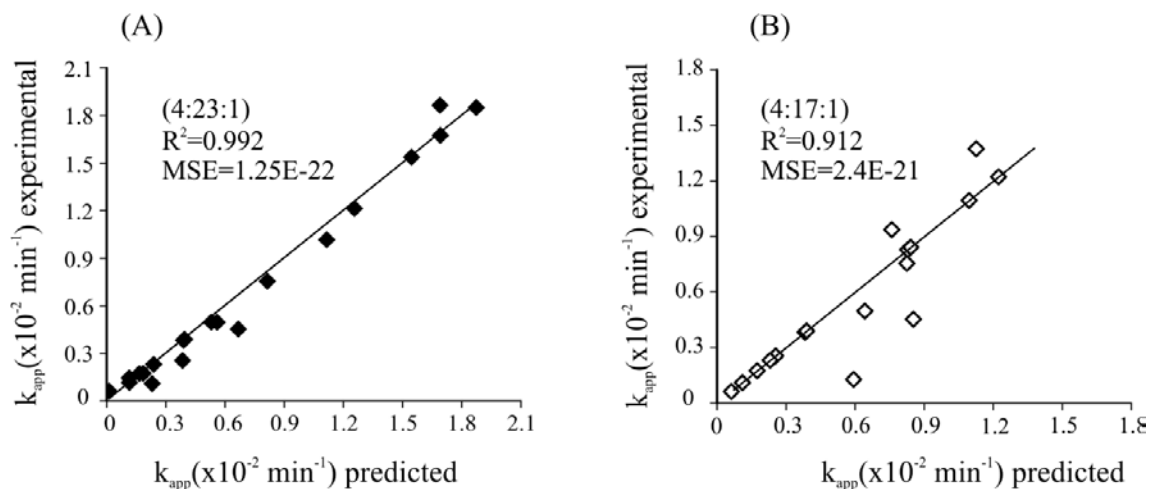


Figure 6.7 Plot of the experimental data against predicted data by ANN model for apparent rate constant (k_{app}) of the bisphenol-A degradation using Ag/ZnO photocatalysts obtained by the (A) photodeposition and (B) impregnation methods.

6.3.3 Optimization step

The implementation of an EA optimization technique, on the basis of the developed ANN model B and in terms of the previously defined objective function B, resulted in the identification of the maximum k_{app} value (i.e., corresponding to the optimal bisphenol-A degradation curve).

The results of the optimization, presented in [Table 6.11](#), show (i) that lower silver content on the Ag/ZnO photocatalyst and (ii) pH values near the point of zero charge of ZnO ($pH_{PZC}=8.2$) maximize the k_{app} value and allow the fastest photodegradation of bisphenol-A. It can be explained because of the minimal repulsion forces between the non-ionized bisphenol-A and the Ag/ZnO photocatalyst surface lead to high degradation rates (see Chapter 5: effect of pH for further detail). Also the concentration of hydroxyl radicals ($\cdot OH$) is enough to lead for generation of free radical formation with high oxidation potential to decompose bisphenol-A molecules. Similar result was reported by Clament Sagaya Selvam *et al.* (2013) for the photocatalytic degradation of 200 mg/L bisphenol-A at pH= 8 using La-ZnO.

In the second optimization step, the objective function A was used to get a specific amount of AgNPs attached to ZnO surface as calculated by the first optimization study. The ANN Y_2 model was used to find the target functionalization condition (nominal amount of Ag, pH, and reaction time). The predicted preparation conditions are shown in [Table 6.12](#).

The results indicated, for example, that pH=9 and reaction time of 42 min lead to a functionalization efficiency of 88% using the photodeposition method. Again the importance of pH come out from the minimal repulsion forces between stabilized AgNPs and the neutralized charges of ZnO surface at pH of point zero charge.

Note that, in the present study, stabilized AgNPs were used as metal source in contrast to silver salts (AgNO_3 and CH_3COOAg) that are commonly used for the ZnO modification (Peng *et al.*, 2007; Wang, J *et al.*, 2011; Zheng *et al.*, 2007).

Then the optimization using the approach of ANN-EA demonstrate the importance the operating conditions, i.e. pH, on the functionalization of ZnO with stabilized AgNPs.

Table 6.11. Optimal conditions for bisphenol-A degradation

Photocatalyst	pH	Actual amount AgNPs (% w/w)	BPA concentration (g/L)	Wavelength (nm)	k_{app}
Ag/ZnO-PD	10.46	0.3062	19.14	315.42	0.02021
Ag/ZnO-IMP	8.09	0.4402	19.93	266.61	0.01529

Table 6.12. Optimal conditions for the target amount AgNPs.

Functionalization method	Nominal amount AgNPs (% w/w)	pH	Reaction time (min)	Actual amount AgNPs (% w/w)
PD	0.3485	9.06	41.97	0.3062
IMP	0.5335	9.71	145.08	0.4387

Since the predicted optimal conditions were allowed to vary freely within the predefined range for each condition, this resulted in non-standardized values of the wavelength that will be difficult to reproduce experimentally. Hence, the optimization study has been repeated while keeping the value of this condition constant and equal to the closest standardized value (i.e., equal to 302nm and 254nm for the photodeposition and impregnation methods, respectively). The results of this second optimization are shown in [Table 6.13](#).

Modeling and optimization

The optimal photocatalytic conditions show that the amount AgNPs close to 1%w/w increases the apparent rate constant. The only coincidence with the previous results is the initial pH of the bisphenol-A solution. This is expected as since the number of free radical increases as the pH increases. The larger the quantity of free radicals, the higher the apparent rate constant value.

The optimal functionalization conditions that lead to the target amount of AgNPs are listed in [Table 6.14](#). The predicted preparation conditions also need to be validated by performing the experimentation.

Table 6.13. Optimal conditions for bisphenol-A degradation at fixed wavelength.

Photocatalyst	pH	<i>Actual amount AgNPs (% w/w)</i>	BPA concentration (g/L)	Wavelength (nm)	K_{app}
Ag/ZnO-PD	9.83	1.03	10.41	302	0.01752
Ag/ZnO-IMP	10.13	1.16	19.22	254	0.02034

Table 6.14. Optimal conditions for the target amount AgNPs.

Functionalization method	Nominal amount AgNPs (% w/w)	pH	Reaction time (min)	<i>Actual amount AgNPs (% w/w)</i>
PD	1.0299	9.4	50.86	1.0281
IMP	1.1595	7.69	207.32	1.16

6.4 CONCLUSION

We report the model for the functionalization of ZnO with AgNPs by Response Surface Methodology (RSM) and Artificial Neural Network (ANN) based in central composite design. In general ANN has a higher predictive capacity than RSM. Furthermore, ANN model allows a better description of the photocatalyst functionalization process by photodeposition method than RSM.

We were able to model the complete photodegradation of bisphenol-A using data from multiple experiences, without using an experimental design, showing high predictive capacity and a good correlation between the experimental data and the predicted values.

The optimization results using the ANN coupled to evolutionary algorithm (EA) show that low silver content ($\sim 0.35 - 0.5$ %w/w) and an alkaline pH, during both the functionalization of ZnO and the photodegradation, maximized the apparent rate constant of bisphenol-A degradation.

Furthermore, the approach of ANN-EA was able to predict that Ag/ZnO nanoparticles functionalized by the photodeposition showed higher photocatalytic activity than the ones the functionalized by impregnation method.

Finally, the correlation between the structure-photocatalytic performance was established using the metal content (AgNPs) as the convergence point.

This study open the possibility to come out with engineered photocatalysts that lead with a desired performance on the degradation of endocrine disruptor compounds.

Modeling and optimization

As perspective for future work, we propose the use of the cost as a second response to be optimized. The mathematical tools ANN coupled to EA with the capacity to carry out multi-objective optimization could be applied to compromise a highest photocatalytic performance with the lowest cost of the process. This approach will predict the feasibility of ZnO to be used as photocatalyst for treatment of water contaminated with endocrine disruptor compounds.

7 Chapter 7. GENERAL CONCLUSION

7.1 Recall to the objectives

The development and the understanding of relationships between catalysts properties and performance in the context of heterogeneous catalysis is an important challenge. Indeed, catalysis processes are generally affected by several different operating parameters.

In this thesis ZnO was chosen as the photocatalyst to be studied. It is a cheap non-toxic compound with an interesting photocatalytic potential. However, its application is not much developed because of its low efficiency, its photocorrosion and the difficulties for its recovery.

So, the **main objective** of this work is to **improve its photocatalytic efficiency** over the photodegradation, in batch and continuous systems, of water contaminants, particularly endocrine disrupting compounds (i.e. bisphenol-A), emergent contaminants (i.e. triclosan) and dyes (i.e. rhodamine-B).

The main goal will then be to try to answer to the objectives of this work through the development of a methodology that allows:

- (i) studying the functionalization process and understanding the mechanisms involved,
- (ii) finding how the physical, chemical and optical properties of the catalyst system are affected by the operating conditions,
- (iii) evaluating the performance of the new photocatalyst towards the degradation of the contaminants under UV and visible light,
- (iv) optimizing the whole process using adapted mathematical tools,
- (v) developing a method for immobilizing advantageously the photocatalyst in a polymeric matrix in order to extend its use on continuous systems.

7.2 General conclusions

In the first chapter a literature overview showed the state of the art about ZnO photocatalytic properties and the methods proposed for their improvement. It gave a summary of the current trends on the third generation of semiconductor materials based on ZnO, i.e. (i) the use of nanostructured materials, (ii) the doping with metals and (iii) the most used polymeric modifiers. Special attention was given to ZnO semiconductor-conducting polymer composites and their synthesis to understand (i) the chemical interactions between the polymer and ZnO surface and (ii) how ZnO can be used to design new engineered composites with high photocatalytic potential.

Chapter 2 presents the reactants, the devices used for the synthesis and the characterization of Ag/ZnO nanoparticles and Ag/ZnO-poly(acrylic acid) nanocomposites.

The methods related to (i) the photodegradation and the evaluation of the photocatalytic activity of those catalysts, (ii) the experimental strategy and the mathematical tools used to develop the models and the optimization, i.e. response surface methodology and artificial neural network coupled to evolutionary algorithm, are also described.

Chapter 3 proposes two methods (photodeposition and impregnation of silver nanoparticles) that were used for the functionalization of ZnO nanoagglomerates.

The effect of the synthesis parameters on the structural, textural and optical properties of the nanoparticles is presented. In fact, each method follows different mechanisms for the interaction between AgNPs and ZnO surface. The interesting results indicate that the photodeposited photocatalyst promotes (i) the oxidation of AgNPs to form new Ag⁺ seeds and their insertion on the ZnO crystalline structure

to lead a stronger interaction that enhances the electron transport, (ii) reduce recombination and (iii) promotes homogeneous distribution of AgNPs on ZnO surface, which was corroborated by XRD and TEM. The increased lattice parameters indicate that and the insertion of Ag⁺ ions into the crystalline structure of ZnO. It was found that the macropores obstruction of ZnO by AgNPs decreased the BET surface area and pore diameters. Finally, the absorption in the visible region of the spectra (435 nm), improved by the presence of the 1%w/w of AgNPs, suggests a higher efficiency towards the degradation of water contaminants under both UV and visible light.

Therefore **the first part of chapter 5** shows the evidence of the increased photocatalytic efficiency of silver modified ZnO towards the degradation of endocrine disruptors (e.g. bisphenol-A), emergent contaminants (e.g. triclosan) and dyes (e.g. rhodamine-B). It was found that Ag/ZnO obtained by photodeposition and impregnation methods showed higher reaction rates for the complete degradation of bisphenol-A than pure ZnO, under UV light at 302 nm ($k_{app}=0.01929 \text{ min}^{-1} \text{ m}^{-2}$ i.e. 3.7 times the value for pure ZnO). The degradation of bisphenol-A (25% after 3h), triclosan (35% after 2h) and rhodamine-B (95% after 2h) was successfully carried out under visible light, which represents an important achievement in the use of solar driven Ag/ZnO photocatalysts. The effect of pH, photocatalyst dosage, contaminant concentration and wavelength of light on the degradation efficiency of bisphenol-A and the kinetic rate constant were also studied.

Chapter 4 presents first an overview of the state of the art on photocatalyst-polymer composites used for the adsorption and degradation of dyes. The designed Ag/ZnO-poly(acrylic acid) composites gives the advantages of

transparency, hydrophilicity and photostability to afford photodegradation of contaminants dissolved in aqueous solutions.

The structural, textural and thermal characterization shows that the suggested strategy of using GLYMO as coupling agent allows the chemical interaction of Ag/ZnO photocatalyst and carboxylic acid groups of the matrix by ester bonds. The addition of the photocatalyst before the polymerization of crosslinked poly(acrylic acid) promotes the crystallization of the matrix as corroborated by XRD analysis. The arrangements of the polymer chains because of the 5-11 %wt. of photocatalyst content also improve the photo and thermal stabilities. The composites were tested in batch reactor configuration for degradation of bisphenol-A under UV light (365 nm) as shown **chapter 5**.

Moreover, using the 8% wt. composite, two successive cycles led to an overall degradation of 47% and 64%, for the 1st and 2nd cycles, respectively. In addition, the chemical structure of the composite remains unaffected after 16 h of UV light exposure as corroborated by FTIR analysis. Thus, these results suggest that the poly(acrylic acid) matrix prevent from Ag/ZnO photocorrosion maintaining their photocatalytic activity as expected.

Furthermore, the Ag/ZnO-poly(acrylic acid) composites can achieve photodegradation efficiencies comparable to the ones obtained by pure Ag/ZnO. It also provides additional advantages such reduction of photocatalyst loss and reuse of the composite on the degradation of endocrine disrupting compounds. The possibility to implement this new photocatalysts in continuous systems for the degradation endocrine disruptors dissolved in water is also another feasible possibility.

Further, the **chapter 6** has presented an overview of the mathematical tools used to model and optimize a complete photocatalytic process, namely response surface methodology (RSM) and artificial neural networks (ANNs). The correlation

between structure and performance of a photocatalyst is a non-trivial problem. Then an interesting approach is proposed in this thesis.

This novel two-step modeling approach, on the basis of multi-layer back-propagating neural networks, describes (i) the operating conditions effects on the synthesis of Ag/ZnO (i.e. pH, silver concentration, and reaction time) and (ii) the photocatalysis parameters effects (i.e. contaminant concentration, catalyst concentration, pH and source of light) on the apparent rate constant of the degradation bisphenol-A in aqueous solutions. The two models were coupled to evolutionary algorithm to carry-out an optimization of the synthesis conditions that lead to the best photocatalytic performance.

The results of the optimization shows that a low silver content ($\sim 0.35 - 0.5$ %w/w) and alkaline pH values, during both the synthesis of Ag/ZnO and the photodegradation, maximizes the apparent rate constant of bisphenol-A degradation. The models predict that Ag/ZnO photocatalyst obtained by photodeposition method show higher photocatalytic activity that the ones obtained by impregnation as corroborated.

Furthermore, the coupling of the developed models to an evolutionary algorithm resulted in the successful correlation between the catalyst structure and its photocatalytic performance in terms of its metal content (AgNPs) as the convergence point.

In addition, RSM methodology was used to describe the importance of the operating conditions effects, individually and by pairs, on the synthesis of the Ag/ZnO on basis of a central composite experimental design. It was compared with the system description provided by ANNs model. The results indicated that ANN model shows a displayed increased accuracy and sufficient predictive capacity

than the RSM model, even in the case where no experimental design study was used for the experimentation.

This study opens the possibility to come out with engineered photocatalysts that lead with a desired performance on the degradation of endocrine disruptor compounds.

7.3 Final remarks

The contributions of this thesis:

Proposal of two methodologies to carry out the Ag-functionalization of ZnO that promotes the homogeneous distribution of small size AgNPs which are bonded strongly to ZnO surface. The mechanisms are proposed.

Bulk functionalization of ZnO with stabilized AgNPs and achieves its homogeneous distribution at ambient conditions.

Demonstrate the improvement of photocatalytic activity of Ag/ZnO for the degradation of an endocrine disruptor, an emergent contaminant and dye in water.

Use of actual amount of Ag attached to ZnO (functionalization degree) and K_{app} as responses on the RSM and ANN models.

The correlation of structure of the photocatalyst-photocatalytic performance was studied using the metal content (AgNPs) as the convergence point.

Selection of a matrix and design of nanocomposite (Ag/ZnO-poly(acrylic acid)) with photocatalytic activity for the degradation of endocrine disruptors in water.

7.4 Challenges and recommendations

This section describes various limitations found during the course of this investigation. It is divided in four sections regarding chapters 3, 4, 5 and 6.

(i) Ag/ZnO photocatalyst

- *Wettability*

The water contact angle is related to the wettability of the material, which is becomes important when the material is a photocatalyst dissolved in water. The most adequate method to measure such property in powders is sessile drop. Nowak *et al.* (2013) reported that powder catalyst deposited in glass slide provides consistent results after multiple measures. In this thesis we prepared samples for contact angle by dispersing powder onto an adhesive slide. The resulting values were unreproducible.

Then some considerations should be taken into account during sample preparation. This means that the either the method to disperse the powder and the thick of the powder films need to be optimized. But also the time at which the measure is taken: (i) when the droplet made contact with the powder or (ii) when the drop is completely stable.

Overcoming this limitation more questions could be answer like if Ag/ZnO shows a lower water contact angle (i.e. higher wettability) than ZnO due to the functional groups (-OH, -SH, CH₂) that remain after the functionalization process. Other conditions could be tested like ionic strength, concentrations of water contaminant, time of UV exposure, etc.

(ii) Ag/ZnO-poly(acrylic acid) composite

- *Molecular weight.*

The average molecular weight of crosslinked poly(acrylic acid) and composites was not determined in this study due to the limitations to dissolve it. The closest approximation could be done using non-crosslinked poly(acrylic acid). The determination of the average molecular weight before and after the immobilization of the photocatalyst will gives a clue about the mechanism of the chains growth. In

other words, could answer the questions: the photocatalyst make shorter polymer chains?, it is a growing center?, act as a crosslinker?.

- *Crystalline structure.*

The interaction between ZnO and poly(acrylic acid) could result on a semi-crystalline structure on the composite. However the XRD patterns of the composites show high noise and no defined peaks. The XRD patterns in this work were obtained at a scan rate of 0.02°/seg, then resolution could be improved at lower scan rate and show clearly the peaks intensity of (100), (002), (102) planes of Ag/ZnO photocatalyst in the composite sample.

- *Matrix nature.*

The challenge on the immobilization of photocatalyst remains in the photostability of the organic matrix. This limits the options of material polymers that can be effectively used. The present thesis choose poly(acrylic acid) but other hydrogels materials and their combination could be feasible matrices.

- *Methodology of immobilization*

Finally, we suggest exploring other approaches for the immobilization of Ag/ZnO, for example, the incorporation of the photocatalyst using ultrasound during the polymerization to lead a better dispersion.

- *Continuous configuration*

Finally, the degradation of contaminants in a continuous reactor configuration is also encouraged.

(iii) Photocatalytic activity

- *Byproducts identification.*

The byproducts identification and determination of the mineralization degree by total organic carbon was a limitation to propose a detailed mechanism of the studied contaminants decomposition by Ag/ZnO. The approach to identify byproduct by the retention time in the HPLC spectra and the absorption peak position in UV-Vis spectra allowed us to propose a general mechanism but the mineralization process is unknown.

- *Diffusion of contaminants.*

A measure of the contaminant diffusion was made by following the time evolution of the bisphenol-A concentration in the solution. Two approaches can be used: (1) the swelling by pure water until reaching the maximal swelling, followed by the addition of the contaminant and (2) the swelling by the contaminant solution.

- *Re-hydration of composites.*

We observed that the re-hydration of the composites lead to the loss of photocatalyst dispersion. It means that the photocatalyst particles remain in the center of composite sample while the transparent hydrogel growth. We proposed to use the fresh composite (without dry process) in order to avoid the re-hydration process by keeping the material in the refrigerator.

- *Low pH during photodegradation.*

The pH of the bisphenol-A solution was very low after being in contact with the composite. This can be explained by the pK_a of PAA, which is approximately 4, and the presence of residual acrylic acid monomer that decreases the pH values drastically. The dissolution of Ag/ZnO occurs at acidic pH, therefore the photocatalyst is destroyed and unable to be reused. In order to avoid this process we apply:

- a. Intense washing of the composite using distilled water in order to remove the residual monomer and the raw materials used. This also leads to the elimination of the photocatalyst that is not attached to the polymer matrix.
- b. Decrease the residual monomer by using a second initiator (i.e. SMBS).

The second approach allows diminishment of the residual acrylic acid, as measured by HPLC, and higher pH values of the solution media are obtained (pH= 3.7 before vs 5 after).

An unexplored approach is the use of a buffer solution to maintain alkaline pH that could promote higher degradation efficiencies. This option also shows a disadvantage: the higher ionic strength and ions competition for the active sites of the photocatalyst.

(iv) Modeling and optimization

The results of this work can be extended further opening windows for a broader range of applications.

- *Multi-objective optimization*

This is the case for the optimization, particularly by adding another output criteria e.g. the cost of the whole process, which must be minimized while the photocatalyst performance must be maximized.

In this case a compromise has to be proposed by a decision-maker among the numerous solutions resulting from the multicriteria optimization using, for example, Pareto's methodology. The participation of the decision-maker will be required for affecting the weights of the two objective functions.

- *Convergence point of two ANN model*

The mathematical models of the experimental data of Ag-functionalization of ZnO (model 1) and the photocatalytic degradation of bisphenol-A (model 2) can be connected through other variables like the silver size, plasmon of resonance, specific surface area, etc.

- *Modeling and optimization of photocatalytic process on continuous configuration*

The application of ANN model coupled to EA to study the photocatalytic activity of the nanocomposite over the degradation of rhodamine-B. This suggestion comes out from the fact that dyes discoloration, under UV light, is a faster process as corroborated in this thesis. .

7.5 SCIENTIFIC PRODUCTS

7.5.1 List of publications

Jasso-Salcedo AB, Palestino G, Escobar-Barrios VA. (2014). Effect of Ag, pH and time on preparation of Ag-functionalized zinc oxide nanoagglomerates as photocatalysts. *Journal of Catalysis (accepted)* doi: 10.1016/j.jcat.2014.06.008

Jasso- Salcedo AB, Escobar-Barrios V. (2014). Photodegradation of bisphenol-A in aqueous solutions using functionalized zinc oxide as photocatalyst. *Applied catalysis B: Environmental* (in preparation).

Jasso-Salcedo AB, Meimaroglou D, Camargo M, Hoppe S, Pla F, Escobar-Barrios VA. (2014). Photocatalytic degradation of endocrinal disruptors using Ag/ZnO nanoparticles immobilized in a polyacrylic matrix. (in preparation)

Jasso-Salcedo AB, Hoppe S, Escobar-Barrios VA, Pla F, Camargo M, Meimaroglou D. (2014). Artificial neural network modeling and optimization of the synthesis and performance of a functionalized ZnO photocatalyst. (in preparation)

7.5.2 Extended abstracts

Jasso-Salcedo AB, Hoppe S, Pla F, Escobar-Barrios VA, Camargo M, Meimaroglou D. Artificial neural network modeling and optimization of the synthesis and performance of a functionalized ZnO photocatalyst. *XXVII Interamerican and Colombian Chemical Engineering Congress*, Cartagena de Indias, Colombia, October 6-8, 2014. Paper 6 pages.

Jasso-Salcedo AB, Meimaroglou D, Camargo M, Hoppe S, Pla F, Escobar-Barrios VA. Immobilized AgZnO photocatalyst in Poly(acrylic acid) matrix synthesized in water suspension and their photocatalytic activity. *TechConnect World Conference 2014/Nanotech*, Washington, U.S.A., June 16-18, 2014. Paper 4 pages.

Jasso-Salcedo AB, Meimaroglou D, Camargo M, Hoppe S, Pla F, Escobar-Barrios VA. Photodegradation of Endocrine Disruptor Compounds using AgZnO: Pure vs immobilized in polyacrylic matrix. *Annual Seminar RP2E 2014, Lorraine University*, Nancy, France. January 16th, 2014. Paper 4 pages ISBN *pending*

7.5.3 Attendance at conferences

Accepted for oral presentation

Jasso-Salcedo AB, Hoppe S, Pla F, Escobar-Barrios VA, Camargo M, Meimaroglou D. ANN modeling and optimization of synthesis-performance of ZnO photocatalyst. *XXVII Interamerican and Colombian Chemical Engineering Congress*, October 6-8, 2014 in Cartagena de Indias, Colombia.

Jasso Salcedo AB, Remita H, Escobar Barrios VA. Photodegradation of emergent organic compounds in water under visible and UV light by using modified nanoagglomerates of ZnO as photocatalyst. *XIth European Congress on Catalysis*, September 1-6, 2013 in Lyon, France.

Jasso Salcedo AB, Palestino G, Rangel-Mendez R, Escobar Barrios VA. Functionalization of ZnO with Ag-nanoparticles for photodegradation of Bisphenol-A in aqueous solutions. *7th International Conference on Environmental Catalysis (ICEC)*, September 2012 in Lyon, France.

Jasso Salcedo AB, Palestino G, Escobar Barrios V. Functionalization of ZnO nanoagglomerates with silver nanoparticles obtained by photoreduction and impregnation methods. *XX International Materials Research Congress (IMRC)*, August 2011 in Cancun, Mexico

Accepted for poster presentation

Jasso-Salcedo AB, Meimaroglou D, Camargo M, Hoppe S, Pla F, Escobar-Barrios VA. Photocatalytic degradation of endocrinal disruptors using AgZnO nanoparticles immobilized in a polyacrylic matrix. *13th International Conferences on MicroREaction Technology (IMRET 13)*, June 23-25, 2014 in Budapest, Hungary.

Jasso-Salcedo AB, Meimaroglou D, Camargo M, Hoppe S, Pla F, Escobar-Barrios VA. Immobilization of AgZnO photocatalyst in Poly(acrylic acid) matrix and their photocatalytic activity evaluation. *TechConnect World Conference 2014/Nanotech*, June 16-18, 2014 in Washington, D.C., U.S.A.

Jasso-Salcedo AB, Meimaroglou D, Camargo M, Hoppe S, Pla F, Escobar-Barrios VA.. Photodegradation of Endocrine Disruptor Compounds using AgZnO: Pure vs immobilized in polyacrylic matrix. *Annual Seminar RP2E 2014, Lorraine University*, January 16th, 2014 in Nancy, France.

Jasso Salcedo AB, Remita H, Escobar Barrios VA. Photodegradation of emergent organic compounds in water under visible and UV light by using modified nanoagglomerates of ZnO as photocatalyst. *XIth European Congress on Catalysis*, September 1-6, 2013 in Lyon, France.

Jasso Salcedo AB, Palestino G, Escobar Barrios V. Photodegradation of Bisphenol-A in aqueous solutions using functionalized ZnO as Photocatalyst. *9th Topical Meeting on Nanostructured Materials and Nanotechnology*, May 20-23, 2012 in San Luis Potosi, Mexico.

8 REFERENCES

- Abdolmaleki A, Mallakpour, S, Borandeh, S. (2011). Preparation, characterization and surface morphology of novel optically active poly (ester-amide)/functionalized ZnO bionanocomposites via ultrasonication assisted process. *Applied Surface Science*, 257(15), 6725-6733.
- Ahn BD, Kang, HS, Kim, JH, Gun Hee, K, Chang, HW, Lee, SY. (2006). Synthesis and analysis of Ag-doped ZnO. *Journal of Applied Physics*, 100(9), 093701-093701-093706. doi: 10.1063/1.2364041
- Amadelli R, Samiolo, L, Maldotti, A, Molinari, A, Valigi, M, Gazzoli, D. (2008). Preparation, Characterisation, and Photocatalytic Behaviour of C o-T i O 2 with Visible Light Response. *International Journal of Photoenergy*, 2008. doi: 10.1155/2008/853753
- Angappane S, Selvi, NR, Kulkarni, GU. (2009). ZnO(101) films by pulsed reactive crossed-beam laser ablation. *Bulletin of Materials Science*, 32(3), 253-258. doi: 10.1007/s12034-009-0038-4
- Artham T, Doble, M. (2009). Fouling and degradation of polycarbonate in seawater: field and lab studies. *Journal of Polymers and the Environment*, 17(3), 170-180.
- Azizi S, Ahmad, M, Mahdavi, M, Abdolmohammadi, S. (2013). Preparation, Characterization, and Antimicrobial Activities of ZnO Nanoparticles/Cellulose Nanocrystal Nanocomposites. *BioResources*, 8(2).
- Bangun J, Adesina, AA. (1998). The photodegradation kinetics of aqueous sodium oxalate solution using TiO₂ catalyst. *Applied Catalysis A: General*, 175(1-2), 221-235. doi: [http://dx.doi.org/10.1016/S0926-860X\(98\)00223-3](http://dx.doi.org/10.1016/S0926-860X(98)00223-3)
- Behera SK, Oh, S-Y, Park, H-S. (2010). Sorption of triclosan onto activated carbon, kaolinite and montmorillonite: effects of pH, ionic strength, and humic acid. *Journal of Hazardous Materials*, 179(1), 684-691.
- Bejarano-Jiménez A, Escobar-Barrios, VA, Kleijn, JM, Ortíz-Ledón, CA, Cházaro-Ruiz, LF. (2014). Electroactive behavior assessment of poly(acrylic acid)-graphene oxide composite hydrogel in the detection of cadmium. *Journal of applied polymer science*. doi: 10.1002/app.40846
- Carey JHL, J.; Tosine, H.M. (1976). Photocatalytic treatment of polychlorinated biphenyls on TiO₂. *Bull. Environ. Contam. Toxicol.*, 16, 696-701.
- Clament Sagaya Selvam N, Judith Vijaya, J, John Kennedy, L. (2013). Comparative studies on influence of morphology and La doping on structural, optical, and photocatalytic properties of zinc oxide nanostructures. *Journal of Colloid and Interface Science*, 407(0), 215-224. doi: <http://dx.doi.org/10.1016/j.jcis.2013.06.004>
- Colbeau-Justin C, Valenzuela, M. (2013). Time-resolved microwave conductivity (TRMC) a useful characterization tool for charge carrier transfer in photocatalysis: a short review. *Revista mexicana de física*, 59(3), 191-200.
- Chang J, Ahmed, R, Wang, H, Liu, H, Li, R, Wang, P, et al. (2013). ZnO Nanocones with High-Index {10 $\bar{1}\bar{1}$ } Facets for Enhanced Energy Conversion

- Efficiency of Dye-Sensitized Solar Cells. *The Journal of Physical Chemistry C*, 117(27), 13836-13844. doi: 10.1021/jp402742n
- Chiang K, Lim, TM, Tsen, L, Lee, CC. (2004). Photocatalytic degradation and mineralization of bisphenol A by TiO₂ and platinumized TiO₂. *Applied Catalysis A: General*, 261(2), 225-237.
- Chu D, Masuda, Y, Ohji, T, Kato, K. (2009). Formation and Photocatalytic Application of ZnO Nanotubes Using Aqueous Solution. *Langmuir*, 26(4), 2811-2815. doi: 10.1021/la902866a
- Daneshvar N, Aber, S, Seyed Dorraji, M, Khataee, A, Rasoulifard, M. (2007). Photocatalytic degradation of the insecticide diazinon in the presence of prepared nanocrystalline ZnO powders under irradiation of UV-C light. *Separation and purification Technology*, 58(1), 91-98.
- Di Paola A, García-López, E, Marci, G, Palmisano, L. (2012). A survey of photocatalytic materials for environmental remediation. *Journal of Hazardous Materials*, 211, 3-29.
- Dimitroula H, Daskalaki, VM, Frontistis, Z, Kondarides, DI, Panagiotopoulou, P, Xekoukoulotakis, NP, *et al.* (2012). Solar photocatalysis for the abatement of emerging micro-contaminants in wastewater: Synthesis, characterization and testing of various TiO₂ samples. *Applied Catalysis B: Environmental*, 117, 283-291.
- Dubinsky S, Grader, GS, Shter, GE, Silverstein, MS. (2004). Thermal degradation of poly (acrylic acid) containing copper nitrate. *Polymer Degradation and Stability*, 86(1), 171-178.
- Emeline AV, Kuznetsov, VN, Ryabchuk, VK, Serpone, N. (2012). On the way to the creation of next generation photoactive materials. *Environmental Science and Pollution Research*, 19(9), 3666-3675. doi: 10.1007/s11356-011-0665-3
- Fan Z, Lu, JG. (2005). Zinc oxide nanostructures: synthesis and properties. *Journal of nanoscience and nanotechnology*, 5(10), 1561-1573.
- Flint S, Markle, T, Thompson, S, Wallace, E. (2012). Bisphenol A exposure, effects, and policy: A wildlife perspective. *Journal of environmental management*, 104, 19-34.
- Fujishima A. (1972). Electrochemical photolysis of water at a semiconductor electrode. *Nature*, 238, 37-38.
- Fujishima A, Zhang, X, Tryk, DA. (2008). TiO₂ photocatalysis and related surface phenomena. *Surface Science Reports*, 63(12), 515-582. doi: <http://dx.doi.org/10.1016/j.surfrep.2008.10.001>
- Fukahori S, Ichiura, H, Kitaoka, T, Tanaka, H. (2003). Photocatalytic decomposition of bisphenol A in water using composite TiO₂-zeolite sheets prepared by a papermaking technique. *Environmental Science & Technology*, 37(5), 1048-1051.
- Gao S, Jia, X, Yang, S, Li, Z, Jiang, K. (2011). Hierarchical Ag/ZnO micro/nanostructure: Green synthesis and enhanced photocatalytic performance. *Journal of Solid State Chemistry*, 184(4), 764-769. doi: <http://dx.doi.org/10.1016/j.jssc.2011.01.025>

- Gao Y, Cao, Y, Yang, D, Luo, X, Tang, Y, Li, H. (2012). Sensitivity and selectivity determination of bisphenol A using SWCNT-CD conjugate modified glassy carbon electrode. *Journal of Hazardous Materials*, 199, 111-118.
- Georgekutty R, Seery, MK, Pillai, SC. (2008). A Highly Efficient Ag-ZnO Photocatalyst: Synthesis, Properties, and Mechanism. *The Journal of Physical Chemistry C*, 112(35), 13563-13570. doi: 10.1021/jp802729a
- Gimenez AJ, Yáñez-Limón, JM, Seminario, JM. (2010). ZnO-Paper Based Photoconductive UV Sensor. *The Journal of Physical Chemistry C*, 115(1), 282-287. doi: 10.1021/jp107812w
- Godnjavec J, Znoj, B, Vince, J, Steinbacher, M, Venturini, P. (2012). STABILIZATION OF RUTILE TiO₂ NANOPARTICLES WITH GLYMO IN POLYACRYLIC CLEAR COATING. *Materiali in tehnologije*, 46(1), 19-24.
- Goebbert C, Bisht, H, Al-Dahoudi, N, Nonninger, R, Aegerter, MA, Schmidt, H. (2000). Wet Chemical Deposition of Crystalline, Redispersable ATO and ITO Nanoparticles. *Journal of Sol-Gel Science and Technology*, 19(1-3), 201-204. doi: 10.1023/a:1008728103512
- Hahn Y-B. (2011). Zinc oxide nanostructures and their applications. *Korean Journal of Chemical Engineering*, 28(9), 1797-1813.
- He J, Shao, W, Zhang, L, Deng, C, Li, C. (2009). Crystallization behavior and UV-protection property of PET-ZnO nanocomposites prepared by in situ polymerization. *Journal of applied polymer science*, 114(2), 1303-1311.
- Huang M, Yan, Y, Feng, W, Weng, S, Zheng, Z, Fu, X, et al. (2014). Controllable Tuning Various Ratios of ZnO Polar Facets by Crystal Seed-Assisted Growth and Their Photocatalytic Activity. *Crystal Growth & Design*, 14(5), 2179-2186. doi: 10.1021/cg401676r
- Irzh A, Gedanken, A. (2009). A microwave-assisted process for coating polymer and glass surfaces with semiconducting ZnO submicron particles. *Journal of applied polymer science*, 113(3), 1773-1780.
- Jasso-Salcedo AB, Palestino, G, Escobar-Barrios, VA. (2014). Effect of Ag, pH and time on preparation of Ag functionalized Zinc Oxide Nanoagglomerates as photocatalyst. *Journal of Catalysis*, In press.
- Jeng J, Chen, T-Y, Lee, C-F, Liang, N-Y, Chiu, W-Y. (2008). Growth mechanism and pH-regulation characteristics of composite latex particles prepared from Pickering emulsion polymerization of aniline/ZnO using different hydrophilicities of oil phases. *Polymer*, 49(15), 3265-3271.
- Kamat PV. (2012). Manipulation of charge transfer across semiconductor interface. A criterion that cannot be ignored in photocatalyst design. *The Journal of Physical Chemistry Letters*, 3(5), 663-672.
- Kang J-H, Katayama, Y, Kondo, F. (2006). Biodegradation or metabolism of bisphenol A: from microorganisms to mammals. *Toxicology*, 217(2), 81-90.
- Kangwansupamonkon W, Jitbunpot, W, Kiatkamjornwong, S. (2010). Photocatalytic efficiency of TiO₂/poly [acrylamide-co-(acrylic acid)] composite for textile dye degradation. *Polymer Degradation and Stability*, 95(9), 1894-1902.

- Kawano K, Komatsu, M, Yajima, Y, Haneda, H, Maki, H, Yamamoto, T. (2002). Photoreduction of Ag ion on ZnO single crystal. *Applied Surface Science*, 189(3), 265-270.
- Kim J, Kwak, BS, Kang, M. (2010). TiO₂/carbon composites prepared from rice husk and the removal of bisphenol A in photocatalytic liquid system. *Bulletin of the Korean Chemical Society*, 31(2), 344-350.
- Kim M-R, Choi, S-H. (2009). One-step synthesis of Pd-M/ZnO (M=Ag, Cu, and Ni) catalysts by γ -irradiation and their use in hydrogenation and Suzuki reaction. *Journal of Nanomaterials*, 2009(Article ID 302919), 1-7. doi: 10.1155/2009/302919
- Kislov N, Lahiri, J, Verma, H, Goswami, DY, Stefanakos, E, Batzill, M. (2009). Photocatalytic Degradation of Methyl Orange over Single Crystalline ZnO: Orientation Dependence of Photoactivity and Photostability of ZnO. *Langmuir*, 25(5), 3310-3315. doi: 10.1021/la803845f
- Klečka GM, Staples, CA, Clark, KE, van der Hoeven, N, Thomas, DE, Hentges, SG. (2009). Exposure analysis of bisphenol A in surface water systems in North America and Europe. *Environmental Science & Technology*, 43(16), 6145-6150.
- Kunze C, Valtiner, M, Michels, R, Huber, K, Grundmeier, G. (2011). Self-localization of polyacrylic acid molecules on polar ZnO (0001)–Zn surfaces. *Physical Chemistry Chemical Physics*, 13(28), 12959-12967.
- Kwon YJ, Kim, KH, Lim, CS, Shim, KB. (2002). Characterization of ZnO nanopowders by the polymerized complex method via an organochemical route. *Journal of ceramic processing research*, 3(3/2), 146-149.
- Leng C, Wei, J, Liu, Z, Xiong, R, Pan, C, Shi, J. (2013). Facile synthesis of PANI-modified CoFe₂O₄–TiO₂ hierarchical flower-like nanoarchitectures with high photocatalytic activity. *Journal of Nanoparticle Research*, 15(5), 1-11.
- Li B, Cao, H. (2011). ZnO@graphene composite with enhanced performance for the removal of dye from water. [10.1039/C0JM03253K]. *Journal of Materials Chemistry*, 21(10), 3346-3349. doi: 10.1039/c0jm03253k
- Li D, Haneda, H. (2003). Morphologies of zinc oxide particles and their effects on photocatalysis. *Chemosphere*, 51(2), 129-137. doi: [http://dx.doi.org/10.1016/S0045-6535\(02\)00787-7](http://dx.doi.org/10.1016/S0045-6535(02)00787-7)
- Li L, Liu, S, Zhu, T. (2010). Application of activated carbon derived from scrap tires for adsorption of Rhodamine B. *Journal of Environmental Sciences*, 22(8), 1273-1280.
- Li SC, Li, YN. (2010). Mechanical and antibacterial properties of modified nano-ZnO/high-density polyethylene composite films with a low doped content of nano-ZnO. *Journal of applied polymer science*, 116(5), 2965-2969.
- Li Y, Yu, Y, Wu, L, Zhi, J. (2013). Processable polyaniline/titania nanocomposites with good photocatalytic and conductivity properties prepared via peroxo-titanium complex catalyzed emulsion polymerization approach. *Applied Surface Science*, 273, 135-143.
- Lu B, Liu, M, Shi, H, Huang, X, Zhao, G. (2013). A Novel Photoelectrochemical Sensor for Bisphenol A with High Sensitivity and Selectivity Based on

- Surface Molecularly Imprinted Polypyrrole Modified TiO₂ Nanotubes. *Electroanalysis*, 25(3), 771-779.
- Lü N, Lü, X, Jin, X, Lü, C. (2007). Preparation and characterization of UV-curable ZnO/polymer nanocomposite films. *Polymer international*, 56(1), 138-143.
- Luo Y-D, Dai, C-A, Chiu, W-Y. (2008). Synthesis of P(AA-SA)/ZnO composite latex particles via inverse miniemulsion polymerization and its application in pH regulation and UV shielding. *Journal of Polymer Science Part A: Polymer Chemistry*, 46(24), 8081-8090. doi: 10.1002/pola.23105
- Ma CCM, Chen, YJ, Kuan, HC. (2005). Polystyrene nanocomposite materials: Preparation, morphology, and mechanical, electrical, and thermal properties. *Journal of applied polymer science*, 98(5), 2266-2273.
- Mallakpour S, Madani, M. (2012). Use of silane coupling agent for surface modification of zinc oxide as inorganic filler and preparation of poly (amide-imide)/zinc oxide nanocomposite containing phenylalanine moieties. *Bulletin of Materials Science*, 35(3), 333-339.
- Marschall R, Wang, L. (2013). Non-metal doping of transition metal oxides for visible-light photocatalysis. *Catalysis Today*.
- Maschmeyer T, Che, M. (2010). Catalytic Aspects of Light-Induced Hydrogen Generation in Water with TiO₂ and Other Photocatalysts: A Simple and Practical Way Towards a Normalization? *Angewandte Chemie International Edition*, 49(9), 1536-1539. doi: 10.1002/anie.200903921
- Matsumoto K, Saito, N, Mitate, T, Hojo, J, Inada, M, Haneda, H. (2009). Surface polarity determination of ZnO spherical particles synthesized via solvothermal route. *Crystal Growth & Design*, 9(12), 5014-5016.
- Miranda-García N, Suárez, S, Sánchez, B, Coronado, J, Malato, S, Maldonado, MI. (2011). Photocatalytic degradation of emerging contaminants in municipal wastewater treatment plant effluents using immobilized TiO₂ in a solar pilot plant. *Applied Catalysis B: Environmental*, 103(3), 294-301.
- Mukherjee B, Viswanath, B, Ravishankar, N. (2010). Functional nanoporous structures by partial sintering of nanorod assemblies. *Journal of Physics D: Applied Physics*, 43(45), 455301-455306. doi: 10.1088/0022-3727/43/45/455301
- Nagaraja R, Kottam, N, Girija, C, Nagabhushana, B. (2012). Photocatalytic degradation of Rhodamine B dye under UV/solar light using ZnO nanopowder synthesized by solution combustion route. *Powder Technology*, 215, 91-97.
- Narayanan KB, Sakthivel, N. (2010). Biological synthesis of metal nanoparticles by microbes. *Advances in Colloid and Interface Science*, 156(1-2), 1-13. doi: <http://dx.doi.org/10.1016/j.cis.2010.02.001>
- NICNAS. (2009). Triclosan Priority existing chemical assessment report no. 30. Sydney: Australian Government
- Nowak E, Combes, G, Stitt, EH, Pacek, AW. (2013). A comparison of contact angle measurement techniques applied to highly porous catalyst supports. *Powder Technology*, 233, 52-64.

- Padilla A, Vazquez, A, Vazquez-Polo, G, Acosta, D, Castaño, V. (1990). Porosimetry studies on polyacrylic acid-ZnO cements. *Journal of Materials Science: Materials in Medicine*, 1(3), 154-156.
- Pardeshi S, Patil, A. (2008). A simple route for photocatalytic degradation of phenol in aqueous zinc oxide suspension using solar energy. *Solar Energy*, 82(8), 700-705.
- Patel VR, Amiji, MM. (1996). Preparation and characterization of freeze-dried chitosan-poly (ethylene oxide) hydrogels for site-specific antibiotic delivery in the stomach. *Pharmaceutical research*, 13(4), 588-593.
- Patil AB, Patil, KR, Pardeshi, SK. (2011). Enhancement of oxygen vacancies and solar photocatalytic activity of zinc oxide by incorporation of nonmetal. *Journal of Solid State Chemistry*, 184(12), 3273-3279. doi: <http://dx.doi.org/10.1016/j.jssc.2011.10.016>
- Patole S, Islam, M, Aiyer, R, Mahamuni, S. (2006). Optical studies of ZnO/Ag nanojunctions. *Journal of materials science*, 41(17), 5602-5607.
- Peng F, Zhu, H, Wang, H, Yu, H. (2007). Preparation of Ag-sensitized ZnO and its photocatalytic performance under simulated solar light. *Korean Journal of Chemical Engineering*, 24(6), 1022-1026. doi: 10.1007/s11814-007-0114-7
- Petoral Jr RM, Yazdi, GR, Spetz, AL, Yakimova, R, Uvdal, K. (2007). Organosilane-functionalized wide band gap semiconductor surfaces. *Applied physics letters*, 90(22), 223904.
- Rahman MA, Kaneco, S, Suzuki, T, Katsumata, H, Ohta, K. (2005). Optimized Conditions for the Solar Photocatalytic Degradation of Bisphenol a in Water Using Zinc Oxide. *Annali di chimica*, 95(9-10), 715-719.
- Rafqah S, Wong-Wah-Chung, P, Nelieu, S, Einhorn, J, Sarakha, M. (2006). Phototransformation of triclosan in the presence of TiO₂ in aqueous suspension: Mechanistic approach. *Applied Catalysis B: Environmental*, 66(1), 119-125.
- Rajeshwar K. (2011). Solar energy conversion and environmental remediation using inorganic semiconductor-liquid interfaces: The road traveled and the way forward. *The Journal of Physical Chemistry Letters*, 2(11), 1301-1309.
- Reddy KM, Feris, K, Bell, J, Wingett, DG, Hanley, C, Punnoose, A. (2007). Selective toxicity of zinc oxide nanoparticles to prokaryotic and eukaryotic systems. *Applied physics letters*, 90(21), 213902.
- Sakthivel S, Neppolian, B, Shankar, M, Arabindoo, B, Palanichamy, M, Murugesan, V. (2003). Solar photocatalytic degradation of azo dye: comparison of photocatalytic efficiency of ZnO and TiO₂. *Solar Energy Materials and Solar Cells*, 77(1), 65-82.
- Sakthivel S, Shankar, M, Palanichamy, M, Arabindoo, B, Bahnemann, D, Murugesan, V. (2004). Enhancement of photocatalytic activity by metal deposition: characterisation and photonic efficiency of Pt, Au and Pd deposited on TiO₂ catalyst. *Water Research*, 38(13), 3001-3008.
- Salaün A, Hamilton, JA, Iacopino, D, Newcomb, SB, Nolan, MG, Padmanabhan, SC, *et al.* (2010). The incorporation of preformed metal nanoparticles in zinc

- oxide thin films using aerosol assisted chemical vapour deposition. *Thin Solid Films*, 518(23), 6921-6926. doi: <http://dx.doi.org/10.1016/j.tsf.2010.07.051>
- Salgueiriño-Maceira V, Correa-Duarte, MA, Farle, M, López-Quintela, A, Sieradzki, K, Diaz, R. (2006). Bifunctional Gold-Coated Magnetic Silica Spheres. *Chemistry of Materials*, 18(11), 2701-2706. doi: 10.1021/cm0603001
- Sankoda K, Matsuo, H, Ito, M, Nomiyama, K, Arizono, K, Shinohara, R. (2011). Identification of triclosan intermediates produced by oxidative degradation using TiO₂ in pure water and their endocrine disrupting activities. *Bulletin of environmental contamination and toxicology*, 86(5), 470-475.
- Shewale V, Joshi, P, Mukhopadhyay, S, Deshpande, M, Pandey, R, Hussain, S, et al. (2011). First-Principles Study of Nanoparticle–Biomolecular Interactions: Anchoring of a (ZnO) 12 Cluster on Nucleobases. *The Journal of Physical Chemistry C*, 115(21), 10426-10430.
- Shvalagin VV, Stroyuk, AL, Kuchmii, SY. (2007). Photochemical synthesis of ZnO/Ag nanocomposites. *Journal of Nanoparticle Research*, 9(3), 427-440. doi: 10.1007/s11051-006-9086-5
- Son H-S, Ko, G, Zoh, K-D. (2009). Kinetics and mechanism of photolysis and TiO₂ photocatalysis of triclosan. *Journal of Hazardous Materials*, 166(2–3), 954-960. doi: <http://dx.doi.org/10.1016/j.jhazmat.2008.11.107>
- Song R, Liu, Y, He, L. (2008). Synthesis and characterization of mercaptoacetic acid-modified ZnO nanoparticles. *Solid State Sciences*, 10(11), 1563-1567. doi: <http://dx.doi.org/10.1016/j.solidstatesciences.2008.02.006>
- Sun S, Sun, P, Liu, D. (2005). The study of esterifying reaction between epoxy resins and carboxyl acrylic polymers in the presence of tertiary amine. *European Polymer Journal*, 41(5), 913-922. doi: <http://dx.doi.org/10.1016/j.eurpolymj.2004.11.024>
- Teoh WY, Scott, JA, Amal, R. (2012). Progress in heterogeneous photocatalysis: from classical radical chemistry to engineering nanomaterials and solar reactors. *The Journal of Physical Chemistry Letters*, 3(5), 629-639.
- Tsai W-T, Lee, M-K, Su, T-Y, Chang, Y-M. (2009). Photodegradation of bisphenol-A in a batch TiO₂ suspension reactor. *Journal of Hazardous Materials*, 168(1), 269-275.
- Van Dijken A, Meulen Kamp, E, Vanmaekelbergh, D, Meijerink, A. (2000). The luminescence of nanocrystalline ZnO particles: the mechanism of the ultraviolet and visible emission. *Journal of Luminescence*, 87, 454-456.
- Venkatachalam N, Palanichamy, M, Murugesan, V. (2007). Sol–gel preparation and characterization of alkaline earth metal doped nano TiO₂: Efficient photocatalytic degradation of 4-chlorophenol. *Journal of Molecular Catalysis A: Chemical*, 273(1), 177-185.
- vom Saal FS, Taylor, JA. (2011). Adverse Health Effects of Bisphenol A (BPA): Implications for the Use of BPA in Hemodialyzers and Other Medical Equipment. *Spektrum der Dialyse & Apherese*(12).
- Wachs IE, Phivilay, SP, Roberts, CA. (2013). Reporting of Reactivity for Heterogeneous Photocatalysis. *ACS Catalysis*, 3(11), 2606-2611.

- Wang J, Fan, XM, Tian, K, Zhou, ZW, Wang, Y. (2011). Largely improved photocatalytic properties of Ag/tetrapod-like ZnO nanocompounds prepared with different PEG contents. *Applied Surface Science*, 257(17), 7763-7770. doi: <http://dx.doi.org/10.1016/j.apsusc.2011.04.026>
- Wang SQ, Liu, QL, Zhu, AM. (2011). Preparation of multisensitive poly (N-isopropylacrylamide-co-acrylic acid)/TiO₂ composites for degradation of methyl orange. *European Polymer Journal*, 47(5), 1168-1175.
- Wang ZL. (2004a). Nanostructures of zinc oxide. *Materials today*, 7(6), 26-33.
- Wang ZL. (2004b). Zinc oxide nanostructures: growth, properties and applications. *Journal of Physics: Condensed Matter*, 16(25), R829.
- Wang ZL, Kong, XY, Ding, Y, Gao, P, Hughes, WL, Yang, R, et al. (2004). Semiconducting and Piezoelectric Oxide Nanostructures Induced by Polar Surfaces. *Advanced Functional Materials*, 14(10), 943-956. doi: 10.1002/adfm.200400180
- Wei S-H, Li, J, Yan, Y. (2008). *Design of Shallow p-type dopants in ZnO*. Paper presented at the Photovoltaic Specialists Conference, 2008. PVSC'08. 33rd IEEE.
- Wei S, Zhang, Y, Xu, J. (2007). Preparation and property characterization of PAA/Fe₃O₄ nanocomposite. *Frontiers of Chemical Engineering in China*, 1(3), 233-237.
- Wilcoxon JP, Abrams, BL. (2006). Synthesis, structure and properties of metal nanoclusters. [10.1039/B517312B]. *Chemical Society Reviews*, 35(11), 1162-1194. doi: 10.1039/b517312b
- Wilhelm P, Stephan, D. (2007). Photodegradation of rhodamine B in aqueous solution via SiO₂@ TiO₂ nano-spheres. *Journal of Photochemistry and Photobiology A: Chemistry*, 185(1), 19-25.
- Wu HS, Jone, HC, Hwang, Jw. (1997). Reaction of polyacrylic acid and metal oxides: Infrared spectroscopic kinetic study and solvent effect. *Journal of applied polymer science*, 63(1), 89-101.
- Xie W, Li, Y, Sun, W, Huang, J, Xie, H, Zhao, X. (2010). Surface modification of ZnO with Ag improves its photocatalytic efficiency and photostability. *Journal of Photochemistry and Photobiology A: Chemistry*, 216(2-3), 149-155. doi: <http://dx.doi.org/10.1016/j.jphotochem.2010.06.032>
- Xie Y, Hill, CA, Xiao, Z, Militz, H, Mai, C. (2010). Silane coupling agents used for natural fiber/polymer composites: A review. *Composites Part A: Applied Science and Manufacturing*, 41(7), 806-819.
- Xiong Z, Zhang, LL, Ma, J, Zhao, XS. (2010). Photocatalytic degradation of dyes over graphene-gold nanocomposites under visible light irradiation. [10.1039/C0CC01259A]. *Chemical Communications*, 46(33), 6099-6101. doi: 10.1039/c0cc01259a
- Yang B, Ying, G-G, Zhao, J-L, Zhang, L-J, Fang, Y-X, Nghiem, LD. (2011). Oxidation of triclosan by ferrate: Reaction kinetics, products identification and toxicity evaluation. *Journal of Hazardous Materials*, 186(1), 227-235.

- Yan Y, Al-Jassim, M, Wei, S-H. (2006). Doping of ZnO by group-IB elements. *Applied physics letters*, 89(18), 181912-181912-181913.
- Ye C, Fang, X, Hao, Y, Teng, X, Zhang, L. (2005). Zinc oxide nanostructures: morphology derivation and evolution. *The Journal of Physical Chemistry B*, 109(42), 19758-19765.
- Yu JC, Kwong, TY, Luo, Q, Cai, Z. (2006). Photocatalytic oxidation of triclosan. *Chemosphere*, 65(3), 390-399. doi: <http://dx.doi.org/10.1016/j.chemosphere.2006.02.011>
- Zanella R, Giorgio, S, Henry, CR, Louis, C. (2002). Alternative Methods for the Preparation of Gold Nanoparticles Supported on TiO₂. *The Journal of Physical Chemistry B*, 106(31), 7634-7642. doi: 10.1021/jp0144810
- Zhang H, Zong, R, Zhu, Y. (2009). Photocorrosion inhibition and photoactivity enhancement for zinc oxide via hybridization with monolayer polyaniline. *The Journal of Physical Chemistry C*, 113(11), 4605-4611.
- Zhang L, Yin, L, Wang, C, Lun, N, Qi, Y. (2010). Sol-Gel Growth of Hexagonal Faceted ZnO Prism Quantum Dots with Polar Surfaces for Enhanced Photocatalytic Activity. *ACS Applied Materials & Interfaces*, 2(6), 1769-1773. doi: 10.1021/am100274d
- Zhang L, Yu, JC, Yip, HY, Li, Q, Kwong, KW, Xu, A-W, *et al.* (2003). Ambient Light Reduction Strategy to Synthesize Silver Nanoparticles and Silver-Coated TiO₂ with Enhanced Photocatalytic and Bactericidal Activities. *Langmuir*, 19(24), 10372-10380. doi: 10.1021/la035330m
- Zhao J, Wu, T, Wu, K, Oikawa, K, Hidaka, H, Serpone, N. (1998). Photoassisted degradation of dye pollutants. 3. Degradation of the cationic dye rhodamine B in aqueous anionic surfactant/TiO₂ dispersions under visible light irradiation: evidence for the need of substrate adsorption on TiO₂ particles. *Environmental Science & Technology*, 32(16), 2394-2400.
- Zheng Y, Chen, C, Zhan, Y, Lin, X, Zheng, Q, Wei, K, *et al.* (2008). Photocatalytic Activity of Ag/ZnO Heterostructure Nanocatalyst: Correlation between Structure and Property. *The Journal of Physical Chemistry C*, 112(29), 10773-10777. doi: 10.1021/jp8027275
- Zheng Y, Zheng, L, Zhan, Y, Lin, X, Zheng, Q, Wei, K. (2007). Ag/ZnO Heterostructure Nanocrystals: Synthesis, Characterization, and Photocatalysis. *Inorganic Chemistry*, 46(17), 6980-6986. doi: 10.1021/ic700688f
- Zhou D, Keller, AA. (2010). Role of morphology in the aggregation kinetics of ZnO nanoparticles. *Water Research*, 44(9), 2948-2956. doi: <http://dx.doi.org/10.1016/j.watres.2010.02.025>
- Zou S, Bai, H, Yang, P, Yang, W. (2009). A Biomimetic Chemical Approach to Facile Preparation of Large-Area, Patterned, ZnO Quantum Dot/Polymer Nanocomposites on Flexible Plastics. *Macromolecular Chemistry and Physics*, 210(18), 1519-1527.

9 SUPPORTING INFORMATION

9.1 APPENDIX A

pH point of zero charge

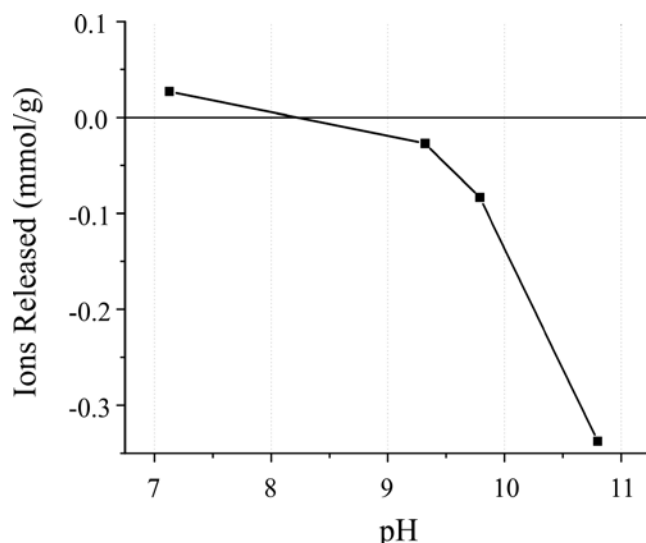


Figure 1.A Surface charge of pure ZnO.

Surface charge was determined as follows: First, 74 mg of ZnO were dispersed in 15 mL of 0.1 M NaCl to keep constant ionic strength. Initial pH values were obtained by adding HCl or NaOH 0.1 N and N₂ was bubbled for 5 min before sealing the vials. After 5 days in stirring, final pH was measured and surface charge obtained from mass balance (expressed as ions released, mmol/g).

Following pH during photocatalyst synthesis

Table 1.A Change of pH in reaction solution

Sample 1 %w/w Ag/ZnO	Initial pH	Final pH
PD7,1	7	6.90
PD11,1	11	8.32
IMP7,2	7	6.84
IMP11,2	11	10.55

Surface plasmon resonance of AgNPs

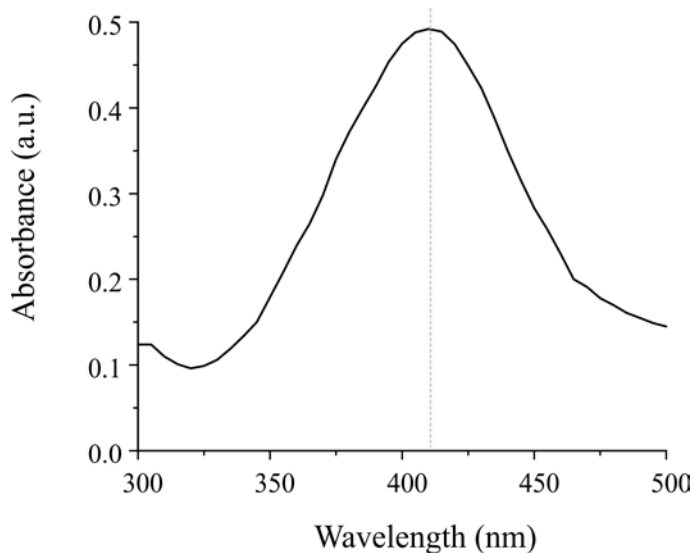


Figure 2.A. UV-Vis spectra of fresh solution of stabilized silver nanoparticles (OM20030601907)

Calculations of the ZnO surface area coated by AgNPs

AgNPs average diameter is 7 nm in the original solution. By considering that the ZnO surface area would be covered by one layer of AgNPs, then the covered area by a single AgNP (7 nm x 7 nm) is equal to 49 nm². The theoretical quantity of AgNPs necessary to coat 1 gram of ZnO nanoagglomerates (total surface area 22x10¹⁸ nm²) is calculated by Equation (A.1).

$$(22 \times 10^{18} \text{ nm}^2) / (49 \text{ nm}^2) = 4.49 \times 10^{17} \quad (\text{A.1})$$

Now the conversion of amount of AgNPs per gram of ZnO (1%w/w Ag=8x10⁻⁵ mol Ag) to number of NPs is obtained by equations (A.2) to (A. 4) taking in consideration molecular weight, density and circular shape of Ag.

$$(8 \times 10^{-5} \text{ mol}) (107.86 \text{ g mol}^{-1}) = 8.63 \times 10^{-3} \text{ g} \quad (\text{A.2})$$

$$(8.63 \times 10^{-3} \text{ g}) / (10.501 \text{ g cm}^{-3}) = 8.22 \times 10^{-4} \text{ cm}^3 \quad (\text{A.3})$$

$$(8.22 \times 10^{-4} \text{ cm}^3) / ((4/3) * \pi * (3.5 \times 10^{-7})^3) = 7.26 \times 10^{15} \quad (\text{A.4})$$

Finally the percentage of ZnO surface area coated by 1% w/w AgNPs is obtained of Equation (A.5)

$$(7.26 \times 10^{15} / 4.49 \times 10^{17}) \times 100 = 1.62\% \quad (\text{A.5})$$

9.2 APPENDIX B

ESEM image of swollen and dehydrated composite sample

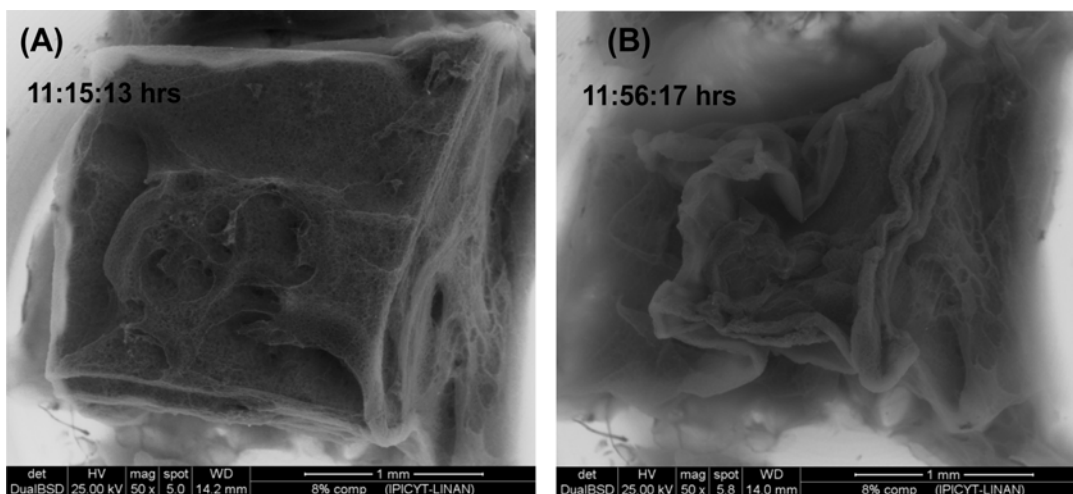


Figure 1.B Low vacuum ESEM images of 8% Ag/ZnO-poly(acrylic acid) composite in taken in different times. Note the porosity of the fresh swollen (A) and dehydrated-collapsed sample (B). The time-window of the analysis is 40 min.

TGA of pure poly(acrylic acid) under nitrogen and air atmosphere

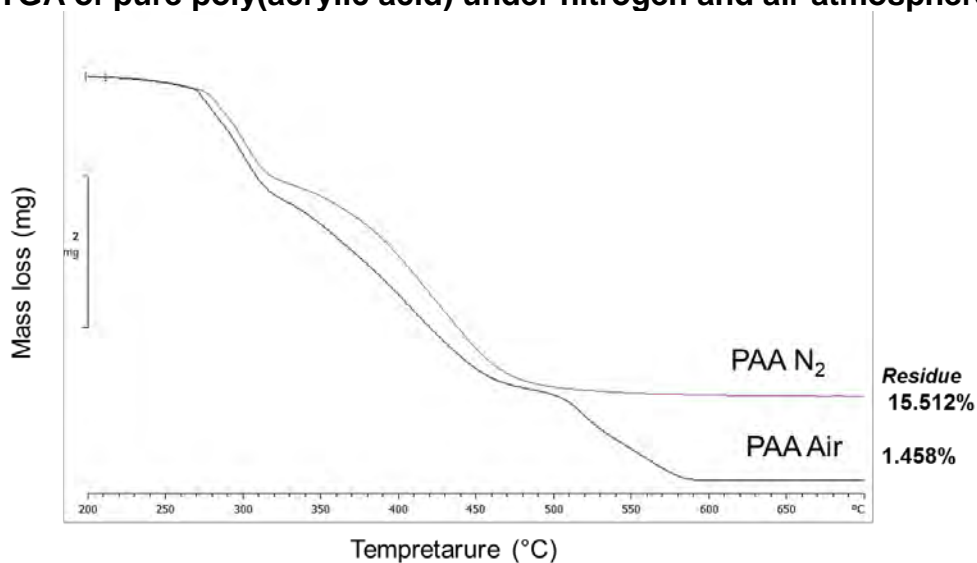


Figure 2.B Thermal analysis of pure poly(acrylic acid).

APPENDIX C

Profile of the intermediate products compared with a standard profile

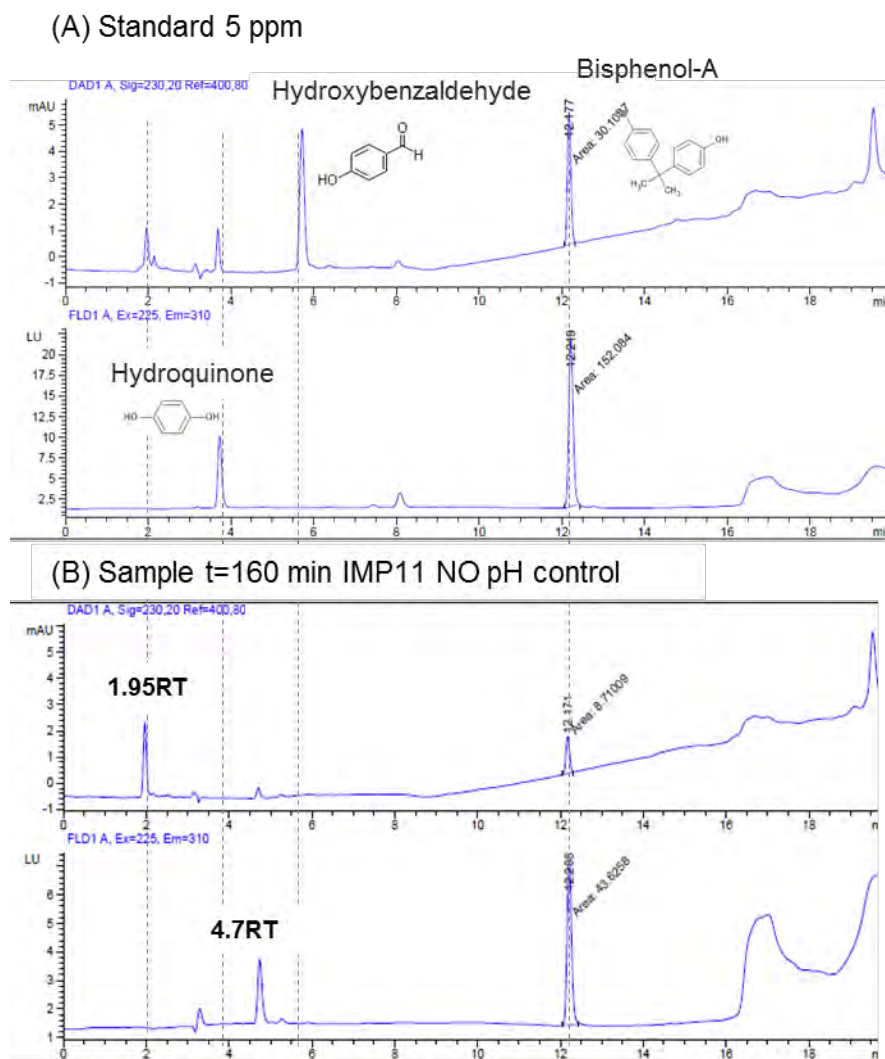


Figure 1.C HPLC chromatogram of the 5 ppm standard (A) and IMP11 samples at t=160 min (test conditions: BPA=10 mg/L, photocatalyst= 1 g/L, $\lambda=302$ nm, pH=10.5, no controlled pH).

Profile of the photocatalytic degradation of rhodamine-B under UV light (254 nm)

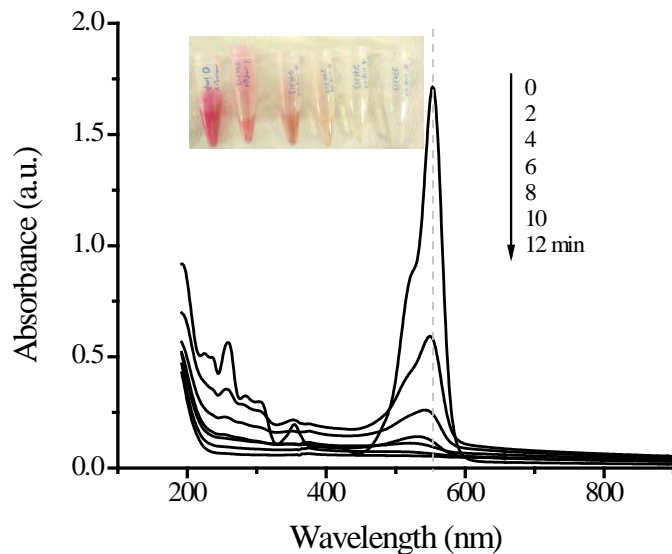


Figure 2.C. Evolution of the UV-Vis spectra of rhodamine-B degradation using Ag/ZnO-PD11 photocatalyst under UV light (test conditions: rhodamine-B =47 mg/L, photocatalyst= 1 g/L, $\lambda=254$ nm). Photograph of rhodamine-B discoloration in function of time.

Profile of the photocatalytic degradation of rhodamine-B under Visible light (>455 nm)

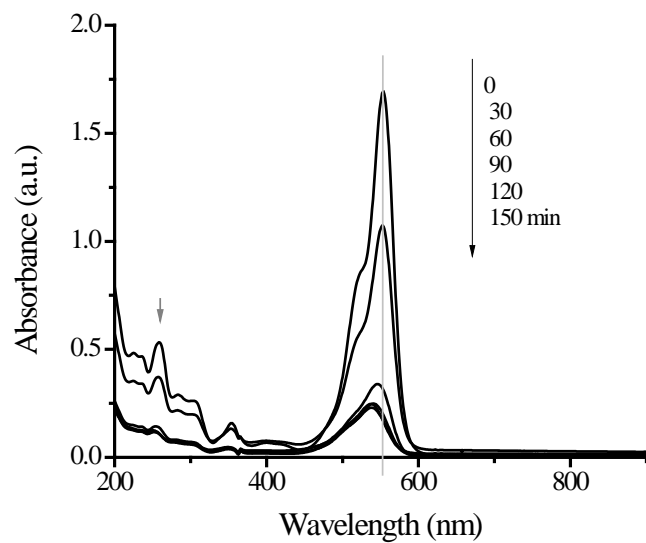


Figure 3.C. Evolution of the UV-Vis spectra of rhodamine-B degradation using Ag/ZnO-PD11 photocatalyst under Visible light (test conditions: rhodamine-B =47 mg/L, photocatalyst= 1 g/L, $\lambda > 455$ nm).

9.3 APPENDIX D

Experimental design 2³ to define the independent variables range

Table 1.D. Experimental data of the functionalization of ZnO by photodeposition method.

Sample	Input			Output	
	Nominal amount Ag %w/w	pH	Reaction time (min)	Actual amount Ag %w/w	FE (%)
1	7	0.1073	60	0.097	90.550
2	11	0.1073	30	0.843	785.573
3	7	1.0623	60	0.088	8.249
4	11	1.0623	30	1.111	104.542
5	11	0.1073	60	1.093	1018.658
6	7	0.1073	30	0.050	46.459
7	7	1.0623	30	0.085	8.012
8	11	1.0623	60	0.985	92.689

FE: Functionalization efficiency

Table 2.D. Experimental data of the functionalization of ZnO by impregnation method.

Sample	Input			Output	
	Nominal amount Ag %w/w	pH	Reaction time (min)	Actual amount Ag %w/w	FE (%)
1	11	1.0623	2	0.650	0.612
2	7	1.0623	2	0.962	0.906
3	7	5.095	2	1.145	0.225
4	7	1.0623	5	0.963	0.907
5	11	1.0623	5	0.675	0.635
6	11	5.095	2	0.368	0.072
7	11	5.095	5	0.462	0.091
8	7	5.095	5	1.193	0.234

FE: Functionalization efficiency

Main effects and Interaction plot of the 2³ design

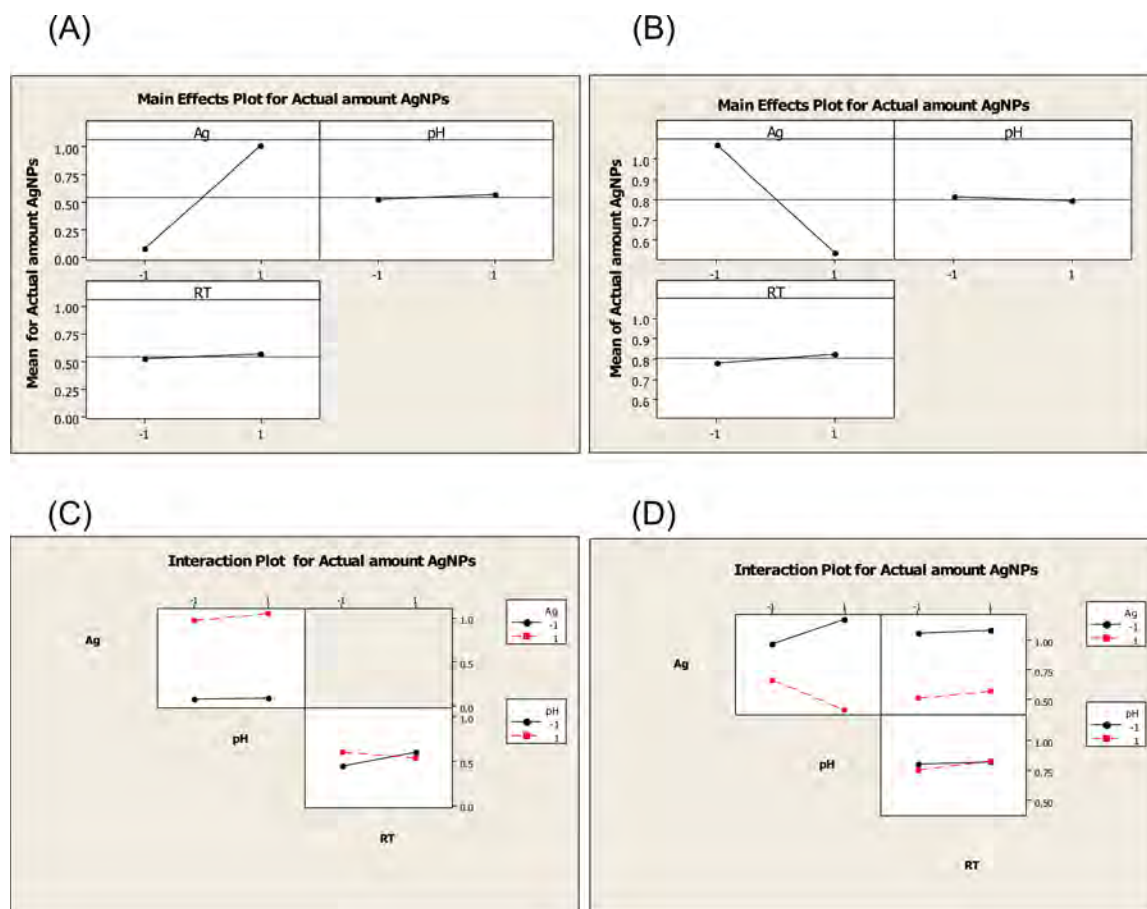


Figure 1.D. Plot of the effect of the operating conditions on the actual amount AgNPs on ZnO surface prepared by the (A, C) photodeposition and (B, D) impregnation methods.